

NAG-254-62

UNPUBLISHED PRELIMINARY DATA

N 64 26866

Code 1

222p

NASA Co. 51827 Cat 29

MASSACHUSETTS INSTITUTE OF TECHNOLOGY

VOLUME I

INTERPLANETARY MIDCOURSE GUIDANCE ANALYSIS

by

Robert Gottlieb Stern

B.S., Lehigh University, 1941

M.S., Stevens Institute of Technology, 1950

Doctor of Science

OTS PRICE

XEROX

\$ 15.00 ph

MICROFILM

\$

TE-5  
EXPERIMENTAL ASTRONOMY LABORATORY

MASSACHUSETTS INSTITUTE OF TECHNOLOGY

CAMBRIDGE 39, MASSACHUSETTS

VOLUME I  
INTERPLANETARY MIDCOURSE GUIDANCE ANALYSIS

by

ROBERT GOTTLIEB STERN

B.S., Lehigh University, 1941  
M.S., Stevens Institute of Technology, 1950

SUBMITTED IN PARTIAL FULFILLMENT  
OF THE REQUIREMENTS FOR THE  
DEGREE OF DOCTOR OF SCIENCE

at the

MASSACHUSETTS INSTITUTE OF TECHNOLOGY

Signature of Author Robert G. Stern  
Department of Aeronautics and Astronautics,  
May 10, 1963

Certified by Richard H. Battin  
Thesis Supervisor

Certified by Walter Wrigley  
Thesis Supervisor

Certified by Walter McKee  
Thesis Supervisor

Accepted by Walter Wrigley  
Chairman, Departmental Committee  
on Graduate Students

# INTERPLANETARY MIDCOURSE GUIDANCE ANALYSIS

by

Robert G. Stern

Submitted to the Department of Aeronautics and Astronautics on May 10, 1963 in partial fulfillment of the requirements for the degree of Doctor of Science.

## ABSTRACT

The problem studied in this thesis is the midcourse correction of the path of an interplanetary vehicle by means of several intermittent thrust impulses. The analysis is linearized by assuming that the vehicle's actual path differs only slightly from a known pre-computed reference path. The difference between the actual path and the reference path is known as the variant path. The linearized equations of motion are those in which the dependent variables are the position and velocity components of the variant path.

The emphasis in the thesis is placed on the analytic solution of the linearized equations of motion. Two distinct methods are developed for obtaining an analytic solution when the reference trajectory is an ellipse. The first method involves the separation of the sixth-order system into two independent systems, one of fourth order and the other of second order. Although the two independent systems have variable coefficients, both are integrated directly in closed form. The second method of solution utilizes variational techniques to determine the effect on the path of small variations in a set of six orbital elements. The two solutions are shown to be mathematically equivalent.

The analytic solution is used to obtain closed-form expressions for the elements of all the matrices appearing in the guidance equations.

Both fixed-time-of-arrival and variable-time-of-arrival guidance schemes are discussed. In fixed-time-of-arrival guidance the three-dimensional velocity correction vector is expressed as a linear function of the three-dimensional predicted position variation at the destination. In variable-time-of-arrival guidance both the correction vector and the position variation vector to be corrected are expressed as two-dimensional vectors in a special coordinate system known as the critical-plane coordinate system.

In the case of variable-time-of-arrival guidance an empirical technique is developed for determining the optimum time to apply a midcourse correction. The optimum correction time is a function of a single characteristic of the vehicle's variant path.

There are three types of singularities that appear in the fixed-time-of-arrival guidance equations for elliptical reference trajectories. Two of the types are readily explained physically. The third type, no previous mention of which has been found in the literature, is shown to be related to the minima of the time-of-flight curves obtained from Lambert's theorem. No finite fixed-time-of-arrival correction can be computed at a correction time corresponding to any one of the three types of singularity. If variable-time-of-arrival guidance is used, two of the singularity types are effectively cancelled out, but the third type still remains.

Both Earth-based and self-contained navigation systems are described. The function of the navigation system is to determine the vehicle's variant path from measurements made during the flight. The six parameters selected to define the variant path are the components of position variation and velocity variation at the nominal time of arrival at the destination.

In the self-contained navigation system vehicle position is determined from the optical sighting of the angles between pairs of celestial bodies, and the variant path is computed after several position determinations have been made. A survey is made of all first-magnitude stars to determine which are most useful for position determination. A graphical technique is evolved for selecting the angular sightings which result in the greatest accuracy of position determination.

The guidance theory is illustrated by a numerical example of a long-duration Earth-Mars trajectory.

A midcourse guidance system is outlined which utilizes the analytic results of the theoretical investigation.

Thesis Supervisors:

Professor Walter Wrigley

Title: Professor of Instrumentation and Astronautics

Professor Walter McKay

Title: Associate Professor of Aeronautics  
and Astronautics

Dr. Richard H. Battin

Title: Assistant Director, M. I. T. Instrumentation  
Laboratory



## ACKNOWLEDGMENTS

The author wishes to thank Professor Walter Wrigley and Professor Walter McKay, faculty supervisors of this thesis. Their sympathetic understanding and encouragement are deeply appreciated.

He also wishes to acknowledge the helpful suggestions of Dr. Richard H. Battin, research supervisor, whose work provided the original motivation for this investigation.

He is indebted to the M. I. T. Instrumentation Laboratory, under the directorship of Dr. C. Stark Draper, for supplying facilities and financial support during the course of the study.

Thanks are due to Captain Mack Mauldin, Jr. and Captain Robert G. Millard, of the United States Air Force, who programmed the computations and supervised the plotting of the curves contained in Chapter 4.

There are many members of the M. I. T. community, both students at the Institute and colleagues at the Instrumentation Laboratory, with whom the author has engaged in stimulating critical discussion that has led to a clearer understanding of the physical phenomena that are treated. The author takes this opportunity to express his gratitude to all these people.

Finally, he wishes to thank Miss Kelly Brouillette, Miss Theo Coughlin, and Miss Mimi Ganem, who typed early drafts of this thesis; Mr. Ray Parks, who made some of the sketches; and the staff of Jackson & Moreland, Inc., under the supervision of Messrs. Gardner Pope, Chester Brimblecom, and Frank Cross, who prepared the final draft for publication.

This research was sponsored in part by DSR Project 52-156 through USAF Contract AF 04(647)-303 and in part by DSR Project 55-191 through NASA Contract NAS 9-153. The costs of preparing the final draft for publication were underwritten by DSR Project 9406 through NASA Contract NsG 254-62.

# TABLE OF CONTENTS

## VOLUME I

### Chapter

<b>1</b>	<b>INTRODUCTION . . . . .</b>	<b>1</b>
1.1	Object . . . . .	1
1.2	Summary of Chapter 1 . . . . .	1
1.3	Phases of an Interplanetary Mission. . . . .	1
1.4	The Reference Trajectory . . . . .	2
1.5	Sequence of Operations. . . . .	2
1.6	Midcourse Guidance Development at the M. I. T. Instrumentation Laboratory . . . . .	2
1.7	Midcourse Guidance Development at the C. I. T. Jet Propulsion Laboratory . . . . .	5
1.8	Midcourse Guidance Development at Ames Re- search Center . . . . .	7
1.9	Additional Literature Related to Midcourse Guidance . . . . .	8
1.10	Relation of Present Study to Previous Work in the Field . . . . .	11
1.11	Synopsis . . . . .	13
<b>2</b>	<b>LINEAR GUIDANCE THEORY FOR AN N-BODY GRAVI- TATIONAL FIELD . . . . .</b>	<b>16</b>
2.1	Summary . . . . .	16
2.2	Introduction . . . . .	16
2.3	Clarification of the Term "Perturbation" . . . . .	16
2.4	Mathematical Model . . . . .	18
2.5	Equations of Motion . . . . .	18
2.6	State Vector . . . . .	20
2.7	Transition Matrix. . . . .	21
2.8	Numerical Solution of Variant Equations of Motion . . . . .	22
2.9	Choice of Coordinate System. . . . .	23
2.10	State Vector at Destination . . . . .	24
2.11	Two-Position Path Deviation Vector. . . . .	25
2.12	Midcourse Velocity Correction. . . . .	26
2.13	Fixed-Time-of-Arrival Guidance . . . . .	27

TABLE OF CONTENTS (Cont.)  
VOLUME I

Chapter

2.14	Variable-Time-of-Arrival Guidance . . . . .	28
2.15	Critical-Plane Coordinate System . . . . .	30
2.16	Optimum Time of Correction . . . . .	31
2.17	Multiple Corrections . . . . .	32
2.18	Applicability of Linear Theory . . . . .	33
3	LINEAR GUIDANCE THEORY FOR ELLIPTICAL REFERENCE TRAJECTORIES . . . . .	36
3.1	Summary. . . . .	36
3.2	Introduction . . . . .	36
3.3	Coordinate Systems . . . . .	38
3.4	Equations of Motion . . . . .	39
3.5	Variant Motion Normal to the Reference Trajectory Plane . . . . .	41
3.6	Integration of the Variant Equations for Elliptical Reference Trajectories . . . . .	42
3.7	Solution by Variation of the Orbital Elements of the Elliptical Reference Trajectory . . . . .	45
3.8	Variation in Position, Velocity, and Acceleration . . . . .	52
3.9	Discussion of Effects of Variations in Orbital Elements . . . . .	53
3.10	Transition Matrix . . . . .	70
3.11	Fixed-Time-of-Arrival Guidance . . . . .	74
3.12	Variable-Time-of-Arrival Guidance . . . . .	77
3.13	General Discussion of Singularities in the Matrix Solution . . . . .	79
3.14	Singularities at $(t_j - t_i) = NP$ . . . . .	81
3.15	Singularities at $(f_j - f_i) = (2N - 1)\pi$ . . . . .	83
3.16	Singularities at $X = 0$ . . . . .	84
3.17	The Noncritical Vector . . . . .	87
3.18	Low-Eccentricity Reference Trajectories . . . . .	87
3.19	The Destination Point . . . . .	89

# TABLE OF CONTENTS (Cont.)

## VOLUME I

### Chapter

4	ILLUSTRATIVE CALCULATIONS . . . . .	91
4.1	Summary. . . . .	91
4.2	Introduction . . . . .	91
4.3	Characteristics of the Reference Trajectory . . . . .	93
4.4	Description of Data and Graphs . . . . .	95
4.5	Analysis of Graphical Results. . . . .	98
4.6	Concluding Remarks . . . . .	108
5	NAVIGATION THEORY . . . . .	125
5.1	Summary. . . . .	125
5.2	Introduction . . . . .	125
5.3	Earth-Based Radio-Command System. . . . .	126
5.4	Estimate of the State Vector from Earth-Based Measurements . . . . .	128
5.5	Self-Contained Optical System . . . . .	130
5.6	The Effect of Clock Error . . . . .	132
5.7	Estimate of the State Vector from Optical Measurements. . . . .	134
5.8	The Initial Estimate . . . . .	140
5.9	The Estimate Immediately Following a Mid-course Correction . . . . .	141
5.10	Physical Considerations in the Selection of Optical Sightings. . . . .	144
5.11	Mathematical Criterion for the Selection of Optical Sightings. . . . .	150
5.12	Survey of First Magnitude Stars . . . . .	153
5.13	Illustration of Procedure for Selection of Angular Measurements. . . . .	157
5.14	Physical Considerations . . . . .	160
6	APPLICATIONS OF THE THEORY. . . . .	163
6.1	Summary. . . . .	163
6.2	Introduction . . . . .	163
6.3	Reference Trajectory . . . . .	163

TABLE OF CONTENTS (Cont.)  
VOLUME I

Chapter

6.4	Injection Guidance . . . . .	164
6.5	Midcourse Guidance . . . . .	164
6.6	Radio-Command Guidance . . . . .	164
6.7	Self-Contained Guidance . . . . .	165
6.8	Strategy for Determining Whether to Make a Correction . . . . .	167
6.9	Other Applications . . . . .	170
6.10	Concluding Remarks . . . . .	171
7	CONCLUSIONS AND RECOMMENDATIONS . . . . .	172
7.1	Summary. . . . .	172
7.2	Résumé of Guidance Theory . . . . .	172
7.3	Résumé of Navigation Theory . . . . .	174
7.4	Novel Features of the Analysis . . . . .	175
7.5	The Analytic Approach . . . . .	176
7.6	Recommendations for Further Study . . . . .	177
	List of References . . . . .	179
	Biographical Sketch . . . . .	184

# LIST OF ILLUSTRATIONS

## VOLUME I

Figure		
3.1	Effect of $\delta a$ , Variation in Length of Semi-Major Axis. .	55
3.2	Effect of $\delta M_0$ , Variation in Mean Anomaly at Epoch . .	58
3.3	Effect of $\delta e$ , Variation in Eccentricity . . . . .	63
3.4	Effect of $\delta \phi$ , Variation in Longitude of Perihelion . . .	67
3.5	Effect of $\delta \Omega$ , Variation in Longitude of Ascending Node,, and $\delta i$ , Variation in Inclination . . . . .	69
4.1	Outbound Leg of Trajectory No. 1034 . . . . .	92
4.2	Reciprocal of Magnitude of VTA Velocity Correction, $1/c_V$ , vs. Difference in True Anomaly, $(f_2 - f_1)$ , for Constant Values of Phase Angle $\psi$ . . . . .	109
4.3	Optimum Value of True Anomaly Difference for Applica- tion of VTA Velocity Correction . . . . .	110
4.4	Reciprocal of Minimum Value of Magnitude of VTA Vel- ocity Correction, $1/c_V \min$ , as a Function of Phase Angle $\psi$ . . . . .	111
4.5	Reciprocal of Magnitude of FTA Velocity Correction, $1/c_F$ , vs. Difference in True Anomaly, $(f_2 - f_1)$ , for Constant Values of Phase Angle $\psi$ between $0^\circ$ and $90^\circ$ . .	112
4.6	Reciprocal of Magnitude of FTA Velocity Correction, $1/c_F$ , vs. Difference in True Anomaly, $(f_2 - f_1)$ , for Constant Values of Phase Angle $\psi$ between $130^\circ$ and $170^\circ$ . .	113
4.7	Comparison of FTA and VTA Velocity Corrections When Position Variation at Destination is Normal to Reference Trajectory Plane. . . . .	114
4.8	Reciprocal of Magnitude of VTA Velocity Correction, $1/c_V$ , vs. Difference in True Anomaly, $(f_2 - f_1)$ , for Constant Values of Phase Angle $\mu_2$ between $0^\circ$ and $90^\circ$ .	115
4.9	Reciprocal of Magnitude of VTA Velocity Correction, $1/c_V$ , vs. Difference in True Anomaly, $(f_2 - f_1)$ , for Constant Values of Phase Angle $\mu_2$ between $100^\circ$ and $170^\circ$ . . . . .	116

# LIST OF ILLUSTRATIONS (Cont.)

## VOLUME I

### Figure

4.10	Reciprocal of Magnitude of FTA Velocity Correction, $1/c_F$ , vs. Difference in True Anomaly, $(f_2 - f_1)$ , for Constant Values of Phase Angle $\mu_2$ between $0^\circ$ and $90^\circ$ .	117
4.11	Reciprocal of Magnitude of FTA Velocity Correction, $1/c_F$ , vs. Difference in True Anomaly, $(f_2 - f_1)$ , for Constant Values of Phase Angle $\mu_2$ between $100^\circ$ and $170^\circ$ . . . . .	118
4.12	Effect of Position Variation Normal to Reference Trajectory Plane at Time $t_1$ on Position Variation and Velocity Variation at Time $t_2$ . . . . .	119
4.13	Effect of Velocity Variation Normal to Reference Trajectory Plane at Time $t_1$ on Position Variation and Velocity Variation at Time $t_2$ . . . . .	120
4.14	Effect of Position Variation in Reference Trajectory Plane at Time $t_1$ on Position Variation at Time $t_2$ . . .	121
4.15	Effect of Position Variation in Reference Trajectory Plane at Time $t_1$ on Velocity Variation at Time $t_2$ . . .	122
4.16	Effect of Velocity Variation in Reference Trajectory Plane at Time $t_1$ on Position Variation at Time $t_2$ . . .	123
4.17	Effect of Velocity Variation in Reference Trajectory Plane at Time $t_1$ on Velocity Variation at Time $t_2$ . . .	124
5.1	Geometry of Angular Measurement. . . . .	146
5.2	Celestial Longitude and Latitude of First Magnitude Stars	156
5.3	Selection of Measurement Angles . . . . .	158

LIST OF TABLES  
VOLUME I

<u>Table No.</u>		
3-1	Planetary Data . . . . .	90
4-1	Effect of Fixed Correction Time on Magnitude of VTA Correction . . . . .	107
5-1	Characteristics of First Magnitude Stars. . . . .	154



# TABLE OF CONTENTS

## VOLUME II

### Appendix

A	COORDINATE SYSTEMS . . . . .	1
A.1	Summary. . . . .	1
A.2	Heliocentric Ecliptic Coordinate System. . . . .	1
A.3	Reference Trajectory Stationary Coordinate System . . . . .	2
A.4	Reference Trajectory Local Vertical Coordinate System . . . . .	4
A.5	Reference Trajectory Flight Path Coordinate System . . . . .	4
B	CELESTIAL MECHANICS . . . . .	7
B.1	Summary . . . . .	7
B.2	Motion of a Small Mass in a Many-Body Gravitational Field . . . . .	7
B.3	Equations of Motion in Reference Trajectory Coordinate Systems . . . . .	9
B.4	Two-Body Motion . . . . .	14
B.5	Integration of Equations of Two-Body Motion. . . . .	15
B.6	Orbital Elements . . . . .	16
B.7	Geometric Properties of the Ellipse . . . . .	18
B.8	The Anomalies . . . . .	19
B.9	Dynamic Relations for Elliptical Trajectories . . . . .	23
C	GRAPHICAL CONSTRUCTIONS. . . . .	29
C.1	Summary . . . . .	29
C.2	Graphical Representation of Mean Anomaly . . . . .	29
C.3	Graphical Solution for Orbital Velocity and Its Components . . . . .	32
D	ELLIPTICAL CYLINDRICAL COORDINATES . . . . .	36
D.1	Summary . . . . .	36
D.2	Basic Coordinates in the Elliptical System . . . . .	36

TABLE OF CONTENTS (Cont.)  
VOLUME II

Appendix

D. 3	Coordinate Curves and Tangent Vectors. . . . .	39
D. 4	Evaluation of the Elliptical Cylindrical Coordinate System . . . . .	43
E	VARIANT EQUATIONS OF MOTION . . . . .	45
E. 1	Summary . . . . .	45
E. 2	The Variant Equation in Vector Form . . . . .	45
E. 3	Variant Equations in the Reference Trajectory Coordinate Systems . . . . .	46
E. 4	Symmetry of Matrix $\overset{*}{G}$ . . . . .	49
F	GENERAL MATRIX FORMULATIONS . . . . .	51
F. 1	Summary . . . . .	51
F. 2	Path Deviation . . . . .	51
F. 3	Variation in Position . . . . .	53
F. 4	Variation in Velocity . . . . .	55
F. 5	Matrix Differential Equations . . . . .	58
F. 6	Numerical Integration . . . . .	64
F. 7	Matrix Symmetry . . . . .	66
F. 8	Method of Adjoints . . . . .	73
F. 9	Symplectic Matrices . . . . .	78
G	INTEGRATION OF THE VARIANT EQUATIONS OF MOTION FOR ELLIPTICAL REFERENCE TRAJECTORIES . . . . .	81
G. 1	Summary . . . . .	81
G. 2	Variant Equations for Two-Body Motion . . . . .	81
G. 3	Three Solutions for Motion in Reference Trajectory Plane . . . . .	83
G. 4	Fourth Solution for Motion in Reference Trajectory Plane . . . . .	88
G. 5	Solutions for Motion Normal to Reference Trajectory Plane . . . . .	95
G. 6	Complete Solution for Position Variation . . . . .	97

# TABLE OF CONTENTS (Cont.) VOLUME II

## Appendix

H	DETERMINATION OF VARIANT MOTION FROM FIRST VARIATIONS OF ORBITAL ELEMENTS . . . . .	99
H.1	Summary . . . . .	99
H.2	Introduction . . . . .	99
H.3	Effect of Variation in Euler Angles . . . . .	100
H.4	Variation in Eccentric Anomaly . . . . .	103
H.5	General Equations for Components of Position Variation . . . . .	105
H.6	Position Deviation for Trajectories of Moderate Eccentricity . . . . .	107
H.7	Relation Between Solution of Appendix G and Solution of Appendix H. . . . .	109
I	VARIATION IN POSITION, VELOCITY, AND ACCELERATION . . . . .	112
I.1	Summary . . . . .	112
I.2	Vector Forms . . . . .	112
I.3	Component Equations in Matrix Form . . . . .	115
I.4	Variation in Acceleration . . . . .	118
J	LOW-ECCENTRICITY REFERENCE TRAJECTORIES . . . . .	124
J.1	Summary . . . . .	124
J.2	Introduction . . . . .	124
J.3	Position Variation and Velocity Variation . . . . .	124
J.4	Variation in Acceleration . . . . .	128
J.5	Comparison with Differential Equation Solution of Appendix G . . . . .	128
K	MATRICES FOR ELLIPTICAL TRAJECTORIES . . . . .	132
K.1	Summary . . . . .	132
K.2	Selection of a Coordinate System . . . . .	132
K.3	Selection of an Independent Variable . . . . .	134
K.4	Selection of a Grouping of Orbital Elements . . . . .	134

# TABLE OF CONTENTS (Cont.)

## VOLUME II

### Appendix

K. 5	The Use of Position Variation and Velocity Variation to Describe the Motion in the Reference Trajectory Plane . . . . .	135
K. 6	The Use of Two Position Variations to Describe the Motion in the Reference Trajectory Plane . .	141
K. 7	Motion Normal to the Reference Trajectory Plane	143
K. 8	The Transition Matrix $\dot{C}_{ji}^*$ . . . . .	146
K. 9	Matrices Associated with Position Variation at Two Different Times . . . . .	155
K. 10	Checks of the Matrix Elements . . . . .	161
L	FIXED-TIME-OF-ARRIVAL GUIDANCE . . . . .	163
L. 1	Summary . . . . .	163
L. 2	The Velocity Correction . . . . .	163
L. 3	The Velocity Correction for FTA Guidance . . .	165
L. 4	Velocity Variation at the Destination . . . . .	166
L. 5	Change in the Orbital Elements . . . . .	168
L. 6	Method of Numerical Evaluation . . . . .	170
M	VARIABLE-TIME-OF-ARRIVAL GUIDANCE . . . . .	173
M. 1	Summary . . . . .	173
M. 2	Design Philosophy of VTA Guidance . . . . .	173
M. 3	Basic Guidance Equations for VTA Guidance . . .	174
M. 4	Variation in Time of Arrival . . . . .	178
M. 5	Velocity Correction in VTA Guidance . . . . .	178
M. 6	Position Variation and Velocity Variation at the Destination . . . . .	179
M. 7	Change in the Orbital Elements . . . . .	182
M. 8	Numerical Evaluation . . . . .	183
N	OPTIMIZATION OF TIME OF CORRECTION . . . . .	184
N. 1	Summary . . . . .	184
N. 2	Introduction . . . . .	184

# TABLE OF CONTENTS (Cont.)

## VOLUME II

### Appendix

N. 3	Critical-Plane Coordinate System . . . . .	184
N. 4	Critical-Plane System Coordinate Axes at Nominal Time of Arrival . . . . .	185
N. 5	Transformation Relations . . . . .	187
N. 6	Velocity Correction . . . . .	192
N. 7	Selection of Time of Correction . . . . .	194
N. 8	Application to Two-Body Reference Trajectories . . . . .	195
N. 9	Evaluation of Parameters . . . . .	199
O	SINGULARITIES IN THE MATRIX SOLUTION FOR ELLIPTICAL TRAJECTORIES . . . . .	203
O. 1	Summary . . . . .	203
O. 2	Preliminary Remarks . . . . .	204
O. 3	The Singular Matrix . . . . .	204
O. 4	Mathematical Study of Singularities at $(t_j - t_i) = NP$ . . . . .	205
O. 5	Physical Interpretation of Singularities at $(t_j - t_i) = NP$ . . . . .	208
O. 6	Mathematical Study of Singularities at $(f_j - f_i) = (2N - 1)\pi$ . . . . .	211
O. 7	Physical Interpretation of Singularities at $(f_j - f_i) = (2N - 1)\pi$ . . . . .	213
O. 8	Numerical Example of Singularities at $X = 0$ . . . . .	215
O. 9	Mathematical Study of Singularities at $X = 0$ . . . . .	220
O. 10	Lambert's Theorem . . . . .	223
O. 11	Minimum Time of Flight . . . . .	230
O. 12	Physical Interpretation of Singularities at $X = 0$ . . . . .	235
O. 13	Analytic Formulation of the VTA Velocity Correction . . . . .	238
O. 14	Effect on VTA Guidance of Singularities at $(t_D - t_C) = NP$ . . . . .	242
O. 15	Effect on VTA Guidance of Singularities at $(f_D - f_C) = (2N - 1)\pi$ . . . . .	248
O. 16	Effect on VTA Guidance of Singularities at $X = 0$ . . . . .	250
O. 17	Physical Interpretation of the Effect of the Singularities on VTA Guidance . . . . .	252

# TABLE OF CONTENTS (Cont.)

## VOLUME II

### Appendix

P	STATISTICAL THEORY . . . . .	258
P.1	Summary . . . . .	258
P.2	Introduction . . . . .	258
P.3	Mathematical Preliminaries . . . . .	258
P.4	Conditional Probability Density . . . . .	260
P.5	The Maximum Likelihood Estimate . . . . .	260
P.6	Uncertainty in the Maximum Likelihood Estimate . . . . .	263
P.7	The Equi-Probability Ellipsoid . . . . .	263
P.8	Circular Probable Error and Spherical Probable Error . . . . .	265

# LIST OF ILLUSTRATIONS

## VOLUME II

<u>Figure</u>		
A. 1	Euler Angles $\Omega_E, i_E, \omega_E$ . . . . .	3
A. 2	Orientations of Reference Trajectory Coordinate Systems	6
B. 1	Vector Diagram for the Three-Body Problem . . . . .	8
B. 2	The Ellipse . . . . .	20
B. 3	Graphical Construction of Eccentric Anomaly . . . . .	21
C. 1	Graphical Approximation of Mean Anomaly . . . . .	30
C. 2	Graphical Determination of Orbital Velocity and Its Components . . . . .	33
H. 1	Orientation of Actual Trajectory Relative to Reference Trajectory . . . . .	101
L. 1	Fixed-Time-of-Arrival Guidance . . . . .	167
M. 1	Relative Velocity Vector . . . . .	175
M. 2	Miss Distance Vector and VTA Guidance . . . . .	177
M. 3	Vector Relation Between Velocity Corrections in FTA and VTA Guidance . . . . .	180
O. 1	Special Cases of Vehicle Position at Time of Correction for Singularities at $t_D - t_C = NP$ . . . . .	212
O. 2	Effect of z-Component of Position Variation when $f_D - f_C = (2N - 1) \pi$ . . . . .	214
O. 3	A Typical Plot of the Singularity Factor X . . . . .	217
O. 4	Positions of the Singularities at $X = 0$ . . . . .	219
O. 5	Special Case for which Velocity Correction Can Be Computed at $X = 0$ . . . . .	222
O. 6	Illustration for Lambert's Theorem . . . . .	225
O. 7	The Two Ellipses for a Given Space Triangle and a Given Length of the Major Axis . . . . .	229

# LIST OF ILLUSTRATIONS (Cont.)

## VOLUME II

### Figure

O. 8	Time of Flight for One-Way Trip from Earth to Mars .	231
O. 9	VTA Guidance for Singularities at $t_D - t_C = NP$ . . .	254
O. 10	VTA Guidance for Singularities at $f_D - f_C = (2N - 1)\pi$ .	256



LIST OF TABLES  
VOLUME II

O-1	The Singularity Points $X = 0$ for $e = 0.25$ and $E_j = 210^\circ$ . . . . .	220
O-2	Angles $\mu_C$ and $\mu_D$ at $X = 0$ Singularity Points . . .	223

## LIST OF SYMBOLS

### General Notation Rules

An asterisk over a capital letter indicates a matrix.

An underlined lower-case letter indicates a vector, which is equivalent to a one-column matrix. A vector symbol without the underlining indicates the magnitude of the vector.

A bar over a symbol signifies the average value of the quantity represented by the symbol. A bar over a group of symbols signifies the average value of the product of the quantities represented by the symbols.

A single dot over a symbol indicates the first derivative with respect to time of the quantity represented by the symbol. Two dots indicate the second derivative with respect to time. Time derivatives of vectors are taken with respect to an inertial coordinate system unless noted otherwise.

### English Symbols

$a$	semi-major axis of reference trajectory
$a_i$	i-component of acceleration vector
$\underline{a}$	acceleration vector on reference trajectory
a. u.	astronomical unit
$A$	area of equi-probability ellipse (See Section P. 8.)
$A$	parameter used in development of expression for $\dot{Y}^*$ (See Section N.8.)
$\delta A_{SR}$	variation of R-th angular measurement made at time $t_S$ (See Section 5.7.)
$\dot{A}^*$	typical square matrix (See Section F.9.)
$\dot{A}_1^*, \dots, \dot{A}_4^*$	2-by-2 sub-matrices of the 4-by-4 matrix relating in-plane variations in position and velocity to variations in the orbital elements (See Section K.5.)
$\dot{A}_{ij}^*$	6-by-6 matrix relating $\delta \underline{r}_i$ and $\delta \underline{r}_j$ to $\delta \underline{e}$ (See Section O.3.)

b	semi-minor axis of reference trajectory
B	parameter used in development of expression for $\dot{\mathbf{Y}}$ (See Section O.13.)
$\mathbf{\hat{B}}_S$	covariance matrix of components of uncertainty in position at time $t_S$ (See Section 5.7.)
$ \mathbf{\hat{B}}_S $	determinant of $\mathbf{\hat{B}}_S$ (See Section 5.11.)
c	linear eccentricity of reference trajectory
$\underline{c}$	midcourse velocity correction vector
$\underline{c}_F$	midcourse velocity correction vector for FTA guidance
$\underline{c}_V$	midcourse velocity correction vector for VTA guidance
$\underline{c}_W$	two-dimensional midcourse velocity correction vector for VTA guidance (See Section N.6.)
C	constant of integration (See Section G.4.)
C	parameter used in development of expression for $\dot{\mathbf{Y}}$ (See Section O.13.)
$\mathbf{\hat{C}}_{ji}$	transition matrix; 6-by-6 matrix relating components of $\delta \underline{x}_j$ to components of $\delta \underline{x}_i$
CPE	circular probable error (See Section P.8.)
d	distance between initial position and final position (See Section O.10 and Figure O.6.)
d	distance between near bodies P and Q (See Section 5.10.)
det	determinant of a square matrix
$(\det)_{pq}$	determinant of 4-by-4 matrix of Equation (K-13)
$(\det)_z$	determinant of 2-by-2 matrix of Equation (K-24)
$\underline{d}_i$	position vector of space vehicle relative to i-th disturbing body (See Section B.2)
D	operator representing first derivative with respect to time (See Section G.3.)

D	parameter used in development of expression for $\dot{\underline{Y}}$ (See Section O.13.)
$\dot{D}_{ji}$	6-by-6 vector relating $\underline{\lambda}_j$ to $\underline{\lambda}_i$ (See Section F.8.)
e	eccentricity of reference trajectory
$\delta \underline{e}$	variation in grouping of six orbital elements
E	eccentric anomaly on reference trajectory
$E_M$	one half the difference between $E_j$ and $E_i$ (See Section K.6.)
$E_P$	one half the sum of $E_j$ and $E_i$ (See Section K.6.)
$\delta E$	variation in eccentric anomaly
$\dot{\underline{E}}$	covariance matrix of the uncertainty vector $\underline{\epsilon}$ (See Section P.6.)
$ \dot{\underline{E}} $	determinant of $\dot{\underline{E}}$ (See Section P.7.)
$\dot{\underline{E}}_p$	covariance matrix of the uncertainty in $\hat{\delta \underline{p}}$ (See Section 6.8.)
f	true anomaly on reference trajectory (See Figure A.2.)
f'	true anomaly on actual trajectory (See Figure H.1.)
$\dot{f}$	rate of change of true anomaly; angular velocity of r s z coordinate system
$\delta f$	variation in true anomaly
F	operator representing first derivative with respect to true anomaly (See Section G.3.)
$\dot{F}_m$	3-by-6 matrix relating components of $\delta \underline{r}_m$ to components of $\delta \underline{e}$ (See Section F.3.)
FTA	fixed-time-of-arrival
g	angle between velocity vector on reference trajectory and y-axis (See Figure A.2.)
$\dot{g}$	angular velocity of p q z coordinate system

$\underline{g}_{SR}^T$	four-component row vector relating $\delta A_{SR}$ to $\delta \underline{s}_S$ (See Section 5.7.)
$G$	constant of gravitation
$\underline{G}^*$	3-by-3 matrix relating components of $\delta \underline{\dot{r}}$ to elements of $\delta \underline{r}$ (See Section E.3.)
$\underline{G}_S^*{}^T$	$(K+1)$ -by-4 matrix relating $\delta \underline{m}_S$ to $\delta \underline{s}_S$ (See Section 5.7.)
$h$	orbital angular momentum per unit mass of space vehicle
$H$	total energy per unit mass of space vehicle
$\underline{H}_{ij}^*$	6-by-3 matrix relating components of $\delta \underline{e}$ to components of $\delta \underline{r}_i$ when $\delta \underline{r}_j$ is constant (See Section F.2.)
$i$	inclination angle of reference trajectory plane
$i_C$	angle between positive $z$ -axis and positive $\zeta_C$ -axis (See Section N.3.)
$i_E$	inclination angle of reference trajectory plane relative to axes of heliocentric ecliptic coordinate system (See Section A.3.)
$\delta i$	angle between $z'$ -axis and $z$ -axis (See Figure H.1.)
$\underline{I}_N^*$	$N$ -by- $N$ identity matrix
$j$	clock drift rate (See Section 5.6.)
$J$	operator representing first derivative with respect to eccentric anomaly (See Section G.5.)
$\underline{J}_{ij}^*$	3-by-3 matrix relating components of $\delta \underline{v}_i$ to components $\delta \underline{r}_i$ when $\delta \underline{r}_j$ is constant (See Section F.4.)
$k$	arbitrary constant (See Section D.2.)
$k$	constant in definition of equi-probability ellipsoid (See Section P.7.)
$k_1, \dots, k_6$	constants of integration (See Section G.6.)

$k_{i\xi}, k_{i\eta}, k_{i\zeta}$	components of $\underline{k}_i$ along $\xi_D$ , $\eta_D$ , and $\zeta_D$ axes, respectively (See Section N.5.)
$k_{rs}$	element in r-th row and s-th column of $\overset{*}{K}_{ij}$ (See Section K.9.)
$\underline{k}_i$	three-dimensional vector composed of elements in i-th row of $\overset{*}{K}_{CD}$ (See Section N.5.)
$K$	number of measurements made at $t_S$ (See Section 5.4.)
$K_1, K_2$	constants of integration (See Section 3.5.)
$K_{mn}$	adjusted element in m-th row and n-th column of $\overset{*}{K}_{CD}$ (See Section O.13.)
$\overset{*}{K}_{CD}$	3-by-3 correction matrix
$\overset{*}{K}_{ij}$	3-by-3 matrix relating components of $\delta \underline{v}_i$ to components $\delta \underline{r}_j$ when $\delta \underline{r}_i$ is constant (See Section F.4.)
$\ell$	semi-latus rectum of reference trajectory
$\log$	Napierian logarithm (to base $e = 2.71828$ )
$L(\delta \underline{x})$	likelihood function of $\delta \underline{x}$ (See Section P.4.)
$\overset{*}{L}_m$	3-by-6 matrix relating components of $\delta \underline{v}_m$ to components of $\delta \underline{e}$ (See Section F.4.)
$m$	mass of space vehicle
$m_o$	mass of sun
$m_i$	mass of i-th disturbing body (See Section B.2)
$m_i$	i-th measurement (See Section P.3.)
$\delta m_i$	variation in i-th measurement (See Section P.3.)
$\underline{m}$	measurement vector (See Section P.3.)
$\underline{m}_P, \underline{m}_Q$	line-of-sight unit vectors (See Section 5.10.)
$\delta m_{SR}$	variation in R-th measurement at time $t_S$ (See Section 5.4.)

$\delta \underline{m}$	variation in measurement vector (See Section P.3.)
$\delta \underline{m}_S$	measurement variation vector for measurements made at time $t_S$ (See Section 5.4.)
$M$	mean anomaly on reference trajectory
$M$	total number of measurements (See Section P.3.)
$M_0$	value of mean anomaly at $t = 0$
$\tilde{M}$	graphical approximation of mean anomaly (See Section C.2.)
$\delta M$	variation in mean anomaly
$\delta M_0$	variation in mean anomaly at epoch
$\Delta M$	error in graphical approximation of mean anomaly (See Section C.2.)
$\overset{*}{M}_{ji}$	two-dimensional version of $\overset{*}{M}_{ji}$ (See Section K.5.)
$\overset{*}{M}_{mk}$	3-by-3 matrix relating components of $\delta \underline{r}_m$ to components of $\delta \underline{r}_k$ when $\delta \underline{v}_k$ is constant (See Section F.3.)
$ML$	maximum likelihood
$n$	number of disturbing bodies (See Section B.2.)
$n$	mean angular motion (See Section B.8.)
$\underline{n}_P$	unit vector normal to $\underline{m}_P$ and in the plane containing $\underline{m}_P$ and $\underline{m}_Q$ (See Section 5.10.)
$N$	positive integer
$N$	number of complete circuits of the attractive focus (See Section O.10.)
$N$	number of components of generalized vector $\delta \underline{x}$ (See Section P.3.)
$\overset{*}{N}_{ji}$	two-dimensional version of $\overset{*}{N}_{ji}$ (See Section K.5.)
$\overset{*}{N}_{mk}$	3-by-3 matrix relating components of $\delta \underline{r}_m$ to components of $\delta \underline{v}_k$ when $\delta \underline{r}_k$ is constant (See Section F.3.)

$\mathbf{O}_N^*$	N-by-N zero matrix
$p$	distance along first axis of reference trajectory flight path coordinate system (See Section A.5.)
$p(\underline{u})$	joint probability density of the components of the vector $\underline{u}$ (See Section P.5.)
$p(\delta \underline{x}   \delta \underline{\tilde{m}})$	conditional probability density of $\delta \underline{x}$ , given $\delta \underline{\tilde{m}}$ (See Section P.4.)
$p(\delta \underline{\tilde{m}}   \delta \underline{x})$	likelihood function of $\delta \underline{x}$ ; conditional probability density of $\delta \underline{\tilde{m}}$ , given $\delta \underline{x}$ (See Section P.4.)
$\delta p$	variation in distance parallel to p-axis
$\underline{p}_{SR}^T$	six-component row vector relating $\delta m_{SR}$ to $\delta \underline{x}_S$ (See Section 5.4.)
$P$	period of reference trajectory
$\delta P$	variation in reference period
$\mathbf{P}^*$	6-by-6 matrix relating $\underline{\lambda}'$ to $\underline{\lambda}$ (See Section F.8.)
$q$	distance along second axis of reference trajectory flight path coordinate system (See Section A.5.)
$\delta q$	variation in distance parallel to q-axis
$\underline{q}_i$	vector relating $\delta m_i$ to $\delta \underline{x}$ (See Section P.3.)
$\underline{q}_{SR}^T$	six-component row vector relating $\delta m_{SR}$ to $\delta \underline{x}_D$ (See Section 5.4.)
$\mathbf{Q}^*$	N-by-M matrix whose transpose relates $\delta \underline{m}$ to $\delta \underline{x}$ (See Section P.3.)
$\mathbf{Q}_S^{*T}$	K-by-N matrix relating $\delta \underline{m}_S$ to $\delta \underline{x}_D$ (See Section 5.4.)
$r$	distance along first axis of reference trajectory local vertical coordinate system (See Section A.4.)
$\delta r$	variation in radial distance (See Section H.3.)
$\underline{r}$	position vector on reference trajectory



$\underline{r}'$	position vector on actual trajectory
$\delta \underline{r}$	variation in position vector
$\delta \underline{r}_S$	position variation at time $t_S$ inferred from measurements made at time $t_S$ (See Section 5.5.)
$(\delta \underline{r}_D)_R$	vehicle's position variation relative to destination point at time $t_D$ (See Section 5.6.)
$R$	disturbing function (See Section 2.5.)
$\mathbf{R}_k^*$	6-by-3 matrix relating components of $\delta \underline{e}$ to components of $\delta \underline{r}_k$ when $\delta \underline{v}_k$ is constant (See Section F.2.)
$s$	distance along second axis of reference trajectory local vertical coordinate system (See Section A.4.)
$\delta s$	variation in transverse distance (See Section H.3.)
$\delta \underline{s}_S$	four-component vector composed of $\delta t_S$ and $\delta \underline{r}_S$ (See Section 5.7.)
$S$	sensitivity factor (See Section 5.10.)
$\mathbf{S}_{ji}^*$	two-dimensional version of $\mathbf{S}_{ji}^*$ (See Section K.5.)
$\mathbf{S}_{mk}^*$	3-by-3 matrix relating components of $\delta \underline{v}_m$ to components of $\delta \underline{r}_k$ when $\delta \underline{v}_k$ is constant (See Section F.4.)
$\text{sgn}$	signum (See Equation (O-51))
$\text{SPE}$	spherical probable error (See Section P.8.)
$t$	time
$t_o$	time of perihelion passage for reference trajectory (See Section B.6.)
$\delta t_o$	variation in time of perihelion passage
$t_{C_{\text{opt}}}$	optimum time of midcourse correction in VTA guidance (See Section N.7.)
$\Delta t_D$	change in time of arrival due to VTA guidance (See Section M.3.)
$t_F$	time of flight (See Section O.10.)

$\tilde{t}_F$	alternate time of flight (See Section O.10.)
$t_L$	time of last measurement (See Section 5.4.)
$\delta \tilde{t}_S$	clock error at time $t_S$ inferred from measurements made at time $t_S$ (See Section 5.5.)
$\delta t_{SR}$	time interval between nominal measurement time $t_S$ and actual time of R-th measurement (See Section 5.7.)
$T$	kinetic energy per unit mass of space vehicle
$T_{ji}'$	two-dimensional version of $\overset{*}{T}_{ji}$ (See Section K.5.)
$\overset{*}{T}_{mk}$	3-by-3 matrix relating components of $\delta \underline{v}_m$ to components of $\delta \underline{v}_k$ when $\delta \underline{r}_k$ is constant (See Section F.4.)
$u$	reciprocal of radial distance $r$ (See Section B.5.)
$u$	integration variable (See Section G.4.)
$u$	difference between observed value and true value of measured quantity (See Section 5.4.)
$\underline{u}$	measurement uncertainty vector (See Section P.3.)
$\underline{u}_i$	unit vector in direction of i-axis
$U$	potential energy per unit mass of space vehicle
$\overset{*}{U}$	covariance matrix of measurement uncertainties (See Section P.3.)
$ \overset{*}{U} $	determinant of $\overset{*}{U}$ (See Section P.5.)
$v$	integration variable (See Section G.4.)
$v_i$	i-component of velocity vector
$\underline{v}$	velocity vector on reference trajectory
$\underline{v}_P$	velocity of destination planet at nominal time of arrival (See Section M.2.)
$\underline{v}_R$	velocity of space vehicle relative to destination planet at nominal time of arrival (See Section M.2.)
$\underline{v}_S$	velocity of space vehicle on its reference trajectory at nominal time of arrival (See Section M.2.)

$\delta \underline{v}$	variation in velocity vector
$V$	volume of equi-probability ellipsoid (See Section P.8.)
${}^*V_k$	6-by-3 matrix relating components of $\delta \underline{e}$ to components of $\delta \underline{v}_k$ when $\delta \underline{r}_k$ is constant (See Section F.2.)
VTA	variable-time-of-arrival
$\underline{w}$	vector in noncritical direction (See Section M.3. and Figure M.3.)
$\underline{w}_i$	tangent vector in direction of i-axis (See Section D.3.)
${}^*W$	angular velocity matrix (See Section F.5.)
$x$	distance along first axis of reference trajectory stationary coordinate system (See Section A.3.)
$x$	integration variable (See Section G.4.)
$x'$	distance along first axis of actual trajectory stationary coordinate system (See Section H.3.)
$x_o$	distance from center of ellipse, measured parallel to x-axis (See Section D.2.)
$x_E$	distance along first axis of heliocentric ecliptic coordinate system (See Section Q.2.)
$\delta x$	variation in distance parallel to x-axis
$(\delta x_m)_u$	u-th component of $\delta \underline{x}_m$ (See Section 2.18.)
$\underline{x}$	six-component vector consisting of $\underline{r}$ and $\underline{v}$
$\underline{x}$	generalized parameter vector (See Section P.3.)
$\delta \underline{x}$	six-component vector consisting of $\delta \underline{r}$ and $\delta \underline{v}$
$\delta \underline{x}$	variation in generalized parameter vector (See Section P.3.)
$X$	singularity factor (See Section K.6.)
${}^*X$	transformation matrix for transforming a three-dimensional vector from one of the reference trajectory coordinate systems to the critical-plane coordinate system (See Section N.5.)

$y$	distance along second axis of reference trajectory stationary coordinate system (See Section A.3.)
$y'$	distance along second axis of actual trajectory stationary coordinate system (See Section H.3.)
$y_E$	distance along second axis of heliocentric ecliptic coordinate system (See Section A.2.)
$y_{ij}$	element in i-th row and j-th column of $\overset{*}{Y}$ (See Section N.8.)
$\delta y$	variation in distance parallel to y-axis
$\overset{*}{Y}$	2-by-2 matrix relating $\underline{c}_W$ to $(\delta \underline{\rho}^-)_W$ (See Section N.6.)
$\overset{*}{Y}_D$	transformation matrix for transforming the state vector $\delta \underline{x}_D$ from one of the reference trajectory coordinate systems to the critical-plane coordinate system (See Section 6.8.)
$z$	distance normal to reference trajectory plane
$z'$	distance normal to actual trajectory plane
$z_E$	distance normal to ecliptic plane
$\delta z$	variation in distance normal to reference trajectory plane (See Section H.3.)
$z_P$	distance of space vehicle from near body P (See Section 5.10)
$\overset{*}{Z}$	6-by-6 matrix relating $\delta \dot{\underline{x}}$ to $\delta \underline{x}$ (See Section F.8.)

### Greek Symbols

$\alpha$	coordinate in elliptical cylindrical coordinate system (See Section D.2.)
$\alpha$	variable in development of simplified expression for $\overset{*}{Y}$ (See Section N.6.)
$\alpha$	angle used in development of Lambert's theorem (See Section O.10.)
$\alpha$	right ascension (See Section 5.12.)

$(\alpha, x)$	angle between $\underline{u}_\alpha$ and $\underline{u}_x$ (See Section D.3.)
$(\alpha, y)$	angle between $\underline{u}_\alpha$ and $\underline{u}_y$ (See Section D.3.)
$\beta$	coordinate in elliptical cylindrical coordinate system (See Section D.2.)
$\beta$	variable in development of simplified expression for $\ddot{Y}^*$ (See Section N.6.)
$\beta$	angle used in development of Lambert's theorem (See Section O.10.)
$\beta$	celestial latitude
$\beta_S$	difference between inferred position variation vector and true position variation vector (See Section 5.7.)
$\gamma$	flight path angle of reference trajectory (See Figure A.2.)
$\gamma$	first point of Aries (See Figure 5.3.)
$\Gamma ( \ )$	gamma function of the argument (See Section P.8.)
$\delta$	operator signifying first variation
$\delta$	declination (See Section 5.12.)
$\delta_{ij}$	Kronecker delta (See Section 5.4.)
$\nabla$	gradient of a scalar quantity
$\epsilon$	infinitesimal quantity (See Section O.14.)
$\epsilon$	obliquity of the ecliptic (See Section 5.12.)
$\underline{\epsilon}$	uncertainty vector associated with the maximum likelihood estimate $\hat{\delta \underline{x}}$ (See Section P.6.)
$\zeta$	distance normal to the critical plane (See Section N.3.)
$\eta$	distance along second axis of critical-plane coordinate system (See Section N.3.)
$\eta$	angle used in development of Lambert's theorem (See Section O.10.)
$\eta$	difference between desired midcourse correction vector and midcourse correction vector actually applied (See Section 5.9.)

$\theta$	angle subtended at attractive focus by initial position and final position on elliptical trajectory (See Section O.10.)
$\lambda$	celestial longitude
$\underline{\lambda}$	adjoint vector to $\delta \underline{x}$ (See Section F.8.)
$\underline{\lambda}'$	modified adjoint vector (See Section F.8.)
$\mu$	gravitational invariant in sun's gravitational field
$\mu_C, \mu_D$	angles used in analysis of $X = 0$ singularity (See Section O.9.)
$\mu_i$	angle between $\delta \underline{r}_i$ and $p_i$ - axis (See curves of Chapter 4.)
$\underline{\mu}$	three-component vector constituting upper half of adjoint vector $\underline{\lambda}$ (See Section F.8.)
$\nu_S$	difference between inferred time variation and true time variation (See Section 5.7.)
$\nu_1$	angle between $\delta \underline{v}_1$ and $p_1$ - axis (See Figures 4.16 and 4.17.)
$\underline{\nu}$	three-component vector constituting lower half of adjoint vector $\underline{\lambda}$ (See Section F.8.)
$\xi$	distance along first axis of critical-plane coordinate system (See Section N.3.)
$\underline{\xi}_S$	difference between $\delta \underline{\tilde{s}}_S$ and $\delta \underline{s}_S$ (See Section 5.7.)
$\rho$	projection of $\underline{r}$ in reference trajectory plane (See Section B.3.)
$\delta \underline{\rho}$	miss distance vector (See Section M.2.)
$\sigma$	standard deviation of angular measurement (See Section 5.11.)
$\sigma_c^2$	variance in clock drift rate (See Section 5.7.)
$\sigma_i^2$	variance of $u_i$ (See Section 5.4.)
$\Sigma$	summation symbol

$\phi$	longitude of perihelion of reference trajectory
$\phi$	angle subtended at vacant focus by initial position and final position on elliptical trajectory (See Section O.10.)
$\phi_E$	longitude of perihelion of reference trajectory relative to axes of heliocentric ecliptic coordinate system (See Section A.3.)
$\delta\phi$	longitude of perihelion of actual trajectory relative to perihelion of reference trajectory (See Section H.3.)
$\psi$	phase angle of miss distance vector in critical-plane coordinate system (See Section N.7.)
$\omega$	latitude of perihelion of reference trajectory
$\omega_E$	latitude of perihelion of reference trajectory relative to axes of heliocentric ecliptic coordinate system (See Section A.3.)
$\delta\omega$	angle, in actual trajectory plane, between positive half of line of nodes and $x'$ - axis (See Figure H.1.)
$\underline{\omega}$	angular velocity vector of rotating coordinate system (See Section F.5.)
$\Omega$	longitude of ascending node of reference trajectory
$\Omega_C$	angle between positive $r_1$ - axis and positive $\xi_C$ - axis (See Section N.3.)
$\Omega_E$	longitude of ascending node of reference trajectory relative to axes of heliocentric ecliptic coordinate system (See Section A.3.)
$\delta\Omega$	angle, in reference trajectory plane, between $x$ -axis and positive half of line of nodes (See Figure H.1.)

### Superscripts

T	transpose of a vector or matrix
-1	inverse of a square matrix
'	pertaining to actual trajectory as opposed to reference trajectory (See Section H.3.)

-	pertaining to variant path before application of midcourse correction
+	pertaining to variant path after application of midcourse correction
~	observed value of measurement, as distinguished from true value (See Section P.3.)
^	maximum likelihood estimate (See Section P.4.)

### Subscripts

C	corresponding to time of midcourse velocity correction
D	corresponding to nominal time of arrival at destination
i	general index; $i = 1, \dots, n$ (See Section B.2.)
$i$	corresponding to time $t_i$
I	corresponding to time of injection into heliocentric orbit
j	corresponding to time $t_j$
k	corresponding to time $t_k$
min	minimum
NR	relative to non-rotating coordinate system
o	pertaining to low-eccentricity reference trajectories (See Section J.3.)
opt	corresponding to optimum time of midcourse correction
p	component along p-axis
q	component along q-axis
r	component along r-axis
R	relative to rotating coordinate system
s	component along s-axis
S	corresponding to time $t_S$
SR	corresponding to R-th measurement at $t_S$ (See Section 5.4.)
W	vector expressed in critical-plane coordinate system (See Section N.5.)



$x$	component along $x$ -axis
$x_E$	component along $x_E$ -axis
$y$	component along $y$ -axis
$y_E$	component along $y_E$ -axis
$z$	component along $z$ -axis
$z_E$	component along $z_E$ -axis
1	corresponding to an intermediate point of the trajectory, usually the point at which a midcourse correction is applied (See Section 4.4.)
2	corresponding to nominal time of arrival at destination (See Section 4.4.)
1 2 3	components along axes of an arbitrary reference trajectory coordinate system (See Section F.5 and N.3.)
1	
2	
1 2	corresponding to initial point and final point, respectively, in development of Lambert's theorem (See Section O.10.)
$\zeta$	component along $\zeta$ -axis
$\eta$	component along $\eta$ -axis
$\xi$	component along $\xi$ -axis

# CHAPTER 1

## INTRODUCTION

### 1.1 Object

The object of this thesis is to utilize the techniques of linear perturbation theory and the characteristics of elliptical motion in making an intensive analytical study of interplanetary midcourse guidance. Possible applications of the results of the academic study in the design of a guidance system are to be considered.

### 1.2 Summary of Chapter 1

This introductory chapter contains a general discussion of the midcourse guidance problem and indicates the relationship between the present study and previous work in the field. There is also a synopsis of the material in succeeding chapters and in the appendices.

### 1.3 Phases of an Interplanetary Mission

A one-way interplanetary journey from one planet to the vicinity of a second planet may be divided into three phases – the launch phase, the midcourse phase, and the terminal phase. In the launch phase sufficient thrust is imparted to the vehicle so that it escapes the gravitational field of the launch planet and is injected into a heliocentric ballistic trajectory which carries it toward the desired destination. The midcourse phase is the phase in which the vehicle is traversing the heliocentric ballistic trajectory. The terminal phase involves any final maneuvering required to achieve the specific objectives of the mission.

The purpose of guidance during the launch phase is to inject the vehicle into the proper heliocentric trajectory. Because the launch guidance system is not ideal, the velocity of the vehicle at injection is subject to uncertainties which cause the actual heliocentric trajectory to differ from the desired trajectory. The function of the midcourse guidance system is to make measurements from which the differences between the two trajectories can be ascertained and then to compute a correction which can be applied to the vehicle so that it will reach its destination.

#### 1.4 The Reference Trajectory

The desired heliocentric ballistic trajectory is known as the reference trajectory. The determination of a suitable reference trajectory for a given mission is a separate field in itself which falls beyond the scope of the present paper. Battin<sup>(1)\*</sup> presents a technique for generating three-dimensional reference trajectories.

For the purposes of this study it is assumed that a reference trajectory has been pre-computed and that its characteristics are known to the designer of the midcourse guidance system.

#### 1.5 Sequence of Operations

In a typical midcourse guidance system the sequence of operations is as follows:

1. A series of measurements is made. The measured values are compared with the computed values, i. e., those values that would be measured if the vehicle were on the reference trajectory and if there were no errors in making the measurements themselves.
2. The differences between the measured values and the ideal values are processed by a computer, usually a digital computer, to determine the difference between the vehicle's actual ballistic trajectory and the reference trajectory.
3. The required midcourse correction is computed as a function of the difference between actual and reference trajectories and of the time at which the correction is to be applied.

The signals representing the midcourse correction constitute the output of the guidance system and the input to the control system. The operation of the control system in actually applying the computed correction is not considered in this analysis.

#### 1.6 Midcourse Guidance Development at the M. I. T. Instrumentation Laboratory

Of the various midcourse guidance systems that have been suggested during recent years, three, all apparently developed independently, are

---

\* When not otherwise identified, single-digit or two-digit numbers indicate correspondingly numbered items listed in the References.

considered by the author to be representative of current thinking in the midcourse guidance field in this country. The first of the three is the work of the M.I.T. Instrumentation Laboratory, the second is the system proposed by the Jet Propulsion Laboratory of the California Institute of Technology, and the third comes from the Ames Research Center of NASA.

Reference (2), the first report in the M.I.T. series, discusses the technical feasibility of an unmanned round-trip reconnaissance of Mars. It is estimated that, if no midcourse corrections are made, the position error of the vehicle at its nominal time of arrival at Mars will be of the order of several hundred thousand miles. The weight break-down of a vehicle whose total weight is 300 lb. allots 80 lb. for the midcourse propulsion device and propellant and 60 lb. for guidance and control equipment, including the central computer.

An analysis of the proposed midcourse guidance system is presented in Reference (3). Unlike most studies that preceded it, this report uses a three-dimensional mathematical model. The system is completely self-contained within the space vehicle. The measurements consist of the angles subtended at the vehicle between the lines of sight to pairs of celestial bodies. A group of four or more angular measurements made within a relatively short time interval is used to estimate the difference between the vehicle's position on the actual trajectory at the nominal time of the measurements and the corresponding position on the reference trajectory; an estimate of the error in the vehicle's clock is also obtained. The groups of angular measurements are made at several pre-determined times during the journey.

Position estimates at two distinct times are sufficient to compute a midcourse correction. After each set of measurements has been completed, a correction is made, based on the position estimate just determined and the position estimate at the immediately preceding time of measurement.

Each correction is treated as a thrust impulse, which causes a step change in the vehicle's velocity vector. The computation of the correction is in terms of the required velocity step. Linear perturbation theory, based on the known reference trajectory, is used in all computations.

The report also contains an error analysis, including the effects of uncertainties in launch velocity, uncertainties in angular measurements, uncertainty in the measurement of elapsed time, and uncertainties in the application of the computed midcourse corrections.

In Reference (3) the midcourse correction is computed under the assumption that the destination is a point that is fixed both in heliocentric space and in time. Computation of the correction on this basis is known as fixed-time-of-arrival (FTA) guidance. For many space missions small variations in the time of arrival at the destination can be tolerated. In Reference (4) Battin develops the theory for a navigation concept in which the time of arrival is permitted to vary slightly, so that the magnitude of the required step change in velocity can be minimized. This type of computation is called variable-time-of-arrival (VTA) guidance.

A digital computer study in Reference (4) indicates that a saving of as much as 50% in weight of propellant can be realized by the use of VTA guidance. In a typical one-way trip to Mars in which four VTA midcourse corrections are applied, the first correction, made soon after launch, is by far the largest; the magnitude of the velocity step is 126 ft./sec. The sum of the magnitudes of the four corrections, which is directly proportional to the weight of propellant consumed, is 179 ft./sec. The rms value of the predicted position error at the destination is 26 miles.

The analysis in (3) and (4), as well as that in (1), is contained in the appendices of a four-volume proposal<sup>(5)</sup> for a recoverable interplanetary space probe. Chapter 5 of the proposal contains the results of an extensive computer study of the guidance system. There are also chapters describing the on-board digital computer, the communications system, and the propulsion system for supplying the corrective thrust impulses.

References (6), (7), and (8) are additional contributions by Battin. All three are concerned with the problem of optimizing particular phases of the guidance system. In (6) the problem of selecting angular sightings to be used in determining position is considered. Optimum combinations of three sightings are found for the case when there is

no clock error. When errors in both the clock and the sightings are taken into consideration, the maximum likelihood method is applied to estimate position from a redundant set of measurements.

The first part of (7) uses the filter theory approach to determine the best estimate of the actual path of the vehicle when more than two position fixes have been made. In the second part of (7) clock errors are neglected; individual angular measurements are used directly to estimate the actual path without the intermediate step of computing a position fix. An optimizing procedure is developed for selecting the particular angular measurement which provides the maximum reduction in the uncertainty of the estimate of the actual path.

Reference (8) is a continuation of the development of a method for selecting the best angular measurement. It also describes a decision-making procedure for determining when a measurement should be made and when a correction should be applied. There are tables of numerical results obtained from a computer study in which the recommended decision-making procedure is used in the midcourse guidance system of a lunar probe.

### 1.7 Midcourse Guidance Development at the C. I. T. Jet Propulsion Laboratory

The Jet Propulsion Laboratory's approach to midcourse guidance is described in References (9), (10), and (11).

In (9) Noton discusses "post-injection" guidance, which includes both midcourse guidance and terminal guidance. The mission is a one-way journey from Earth to either Venus or Mars. The analysis is three-dimensional, and it makes use of perturbation theory based on the pre-computed reference trajectory.

Noton considers the possibility of using either a radio-command system or a self-contained system for midcourse guidance. He makes a strong case for the use of the radio-command system for relatively simple missions, and he recommends the development of self-contained systems to be used in conjunction with the radio-command system for more sophisticated missions.

In the radio-command system several tracking stations on the surface of the earth make measurements of the angular orientation of the line of sight to the vehicle, of the vehicle's radial velocity (range rate), and possibly of range. The observed data are read into ground-based digital computers to determine the vehicle's actual trajectory. The maximum likelihood technique is used in the data processing. The required mid-course velocity correction is then computed and is transmitted to the vehicle as a radio-command signal from one of the tracking stations.

For a one-way interplanetary journey, one midcourse correction, made within ten days after launch, is deemed to be adequate to achieve the mission objective.

Both fixed-time-of-arrival and variable-time-of-arrival guidance concepts are described. It is pointed out that the fixed-time-of-arrival midcourse correction can be expressed as a linear function of the three components of the estimated position error at the nominal time of arrival at the destination. The variable-time-of-arrival correction can be expressed as a linear function of only two components of the estimated position error at the destination, these two components comprising the estimated miss distance vector.

Several types of variable-time-of-arrival guidance systems are listed. The "optimum" type is that which minimizes the magnitude of the velocity correction. The "nonoptimum" types are all intended to simplify the control system. In one such system the total impulse of the propulsion system supplying the correction is assumed to be fixed; in another the magnitude of the thrust impulse is variable, but its direction is constrained to a particular plane (either the plane perpendicular to the vehicle-sun line or the plane perpendicular to the vehicle-earth line).

Reference (10) is an extension of the work in (9). An iterative process is developed for improving the accuracy of the computation of the midcourse correction beyond that which is obtained from the initial value given by linear perturbation theory. A statistical estimate is made of the magnitude of the velocity correction and hence of the weight of propellant required. Statistical theory is also used to estimate errors at the destination.

There is a detailed discussion of the method of determining the vehicle's actual trajectory from radio measurements. During the interval that the vehicle is visible to a particular tracking station, samples of each type of measurement are taken once every ten seconds. Range rate information, obtained from doppler data, is shown to be the most effective type of measurement for reducing the uncertainty in the estimate of miss distance at the destination.

It is pointed out that all the guidance systems under consideration are characterized by the fact that the two components of miss distance are controlled. Thus, fixed-time-of-arrival guidance may be regarded as a special case of nonoptimum variable-time-of-arrival guidance in which time of arrival is the third controlled quantity. The magnitude of the velocity vector at arrival is also suggested as a possible third controlled quantity for a nonoptimum system.

Gates, Scull, and Watkins<sup>(11)</sup> present a general survey of the space guidance problem, based on the work done at the Jet Propulsion Laboratory. The guidance phase defined as midcourse guidance in Section 1.3 is sub-divided by these authors into Earth-based midcourse guidance and planetary-approach guidance. The former is the radio-command system already described; the latter, which is used only during the last one or two million miles of the interplanetary voyage, utilizes optical measurements involving the line of sight to the destination planet. It is stated that a single velocity correction derived from the earth-based midcourse system reduces the probable position error at the destination from several hundred thousand miles to several thousand miles, and the planetary-approach system causes a further reduction to a few tens or hundreds of miles.

### 1.8 Midcourse Guidance Development at Ames Research Center

The Ames contribution to midcourse guidance is contained in References (12) and (13). Both are concerned with guidance on a circumlunar mission, but the techniques developed are applicable to interplanetary missions as well.



Smith, Schmidt, and McGee<sup>(12)</sup> obtain an optimal estimate of a space vehicle's actual position and velocity relative to the reference trajectory by means of statistical filter theory. Whenever a set of measurements is made, the old optimal estimate is up-dated by including the effect of the new data in formulating a new optimal estimate. The key to applying the method is the determination of the weighting matrix to be applied to each new set of data; it is in the derivation of the equation for the weighting matrix that linear filter theory is utilized.

McLean, Schmidt, and McGee<sup>(13)</sup> describe a fixed-time-of-arrival guidance system. The adjoint method is used in deriving the guidance equations. The analysis is three-dimensional and is based on linear perturbation theory. The effect of neglecting nonlinear terms is discussed.

A computer study of the effects of uncertainties in the input variables shows that the total weight of propellant required for midcourse corrections is primarily a function of the accuracy of the launch guidance system. Increasing the uncertainties in the measurements made during the journey or increasing the uncertainties in the application of midcourse corrections has little effect on propellant weight but materially increases the magnitude of the predicted position and velocity errors at the destination.

### 1.9 Additional Literature Related to Midcourse Guidance

In this section additional papers pertinent to the study of midcourse guidance are briefly summarized.

Porter<sup>(14)</sup> is one of the first to point out the necessity for midcourse guidance on interplanetary flights because of the extreme sensitivity of position at the destination to errors in launch velocity. He also states that the determination of realistic three-dimensional reference trajectories for interplanetary journeys is considerably more complex than is indicated by a two-dimensional approach based on the assumption of coplanar planetary orbits.

Lawden<sup>(15)</sup> presents one of the first analytic treatments of midcourse guidance. He develops analytic expressions for the required midcourse velocity correction for a two-dimensional two-body model.

Baker<sup>(16)</sup> points out that the fundamental problem in interplanetary guidance is how to get the vehicle to the proper destination; a knowledge of the vehicle's position and velocity in transit may not be necessary to solve the fundamental problem. He also indicates the computational advantages of working with the differences between observed measurements and precomputed ideal values of the measurements in determining the corrections to be applied.

Wheelon<sup>(17)</sup> makes a survey of the problems of midcourse and terminal guidance. This paper was prepared as one of a group of papers which constitute a lecture course with the title Space Technology. The emphasis is on physical reasoning, with some analytic expressions being derived to illustrate the techniques involved.

The work of Magness, McGuire, and Smith<sup>(18)</sup> is not directly related to midcourse guidance, but its conclusions are relevant to a midcourse guidance study. A two-dimensional two-body analysis is made of the sensitivity of miss distance at the destination to errors in launch velocity. It is shown that this sensitivity varies widely for different reference trajectories, and certain desirable trajectories, called "guidance minimum" trajectories, are defined.

Gunkel, Lascody, and Merrilees<sup>(19)</sup> determine permissible errors in launch guidance if a Martian impact is to be achieved without the use of midcourse corrections. They devise "preferred" reference trajectories which are similar to the "guidance minimum" trajectories described in (18). Launch accuracy requirements obtained from a two-dimensional analysis are shown to be less stringent but generally of the same order of magnitude as those obtained from a more elaborate three-dimensional analysis. In order to relax the launch requirements, a single midcourse correction is recommended.

Kierstead<sup>(20), (21)</sup> extends the sensitivity analysis of (18) to three dimensions. He points out that the component of the vehicle's actual motion in the ecliptic plane, which in his simplified model is also the plane of the reference trajectory, is only loosely coupled with the component of actual motion normal to the ecliptic plane. Thus, as a first approximation for guidance studies, a considerable saving in computation is effected by studying the two types of motion independently. A

simple analytic expression is obtained for the out-of-plane motion; the in-plane motion is handled numerically. The effect of midcourse corrections on guidance requirements is treated for both Earth-based and self-contained guidance systems.

Breakwell<sup>(22)</sup> attacks the problem of determining the times at which midcourse corrections should be made in order to satisfy the criterion that the total fuel expenditure be minimized. The analysis is statistical, based on a priori knowledge of the variances in the launch velocity, the measurements, and the applied corrections. The basic mathematical model is two-dimensional, with the reference trajectory being a Hohmann-type ellipse. With these assumptions Breakwell's analysis leads to the following simple rule: After a correction has been made, wait until two thirds of the remaining transit time has elapsed before applying the next correction.

In a more recent paper<sup>(23)</sup> by Breakwell the analysis is extended to several special cases which include the effect of position error in the direction normal to the reference trajectory plane. This paper points out that a considerable saving in fuel can be achieved if a procedure is developed for utilizing all measurements made since launch in computing the next correction to be applied, rather than using only those measurements made subsequent to the immediately preceding correction.

Bock and Mundo,<sup>(24)</sup> in a survey of interplanetary guidance problems, discuss the choice of a reference trajectory and the various types of measurement systems that may be used. Measurement systems are classified as active electromagnetic, passive electromagnetic, or inertial. The physical equipment associated with each system is described, and some indication is given of performance characteristics and limitations.

Safren<sup>(25)</sup> introduces the concept of a six-component vector, consisting of three components of position variation and three components of velocity variation between actual trajectory and reference trajectory at a specified time, to define the space vehicle's actual path. It is shown that the matrix equation for the midcourse velocity correction is simplified if the specified time for which the elements of the six-component vector are evaluated is the time of arrival at the destination.

Haake and Welch<sup>(26)</sup> discuss several types of self-contained space guidance systems. The discussion includes a summary of the linearized guidance equations and a description of the required physical equipment. The problem of position determination from optical sightings of celestial angles is analyzed, and a qualitative method is proposed for the selection of angles to be measured. The advantages and disadvantages of large-angle optical trackers and small-field optical trackers are weighed; performance specifications are proposed for the design of a small-field tracker.

The method of adjoints has already been mentioned in connection with the work at Ames Research Center.<sup>(13)</sup> The application of this method to the midcourse guidance problem was suggested earlier by Dunn and Giannetto,<sup>(27)</sup> who point out that a considerable saving in computation time can be achieved by its use in generating the matrix coefficients of the linearized guidance equations.

#### 1.10 Relation of Present Study to Previous Work in the Field

The development of midcourse guidance theory has involved the linearization of a fundamentally nonlinear set of differential equations by means of small perturbation theory. The solution of the linearized equations is manipulated to yield a matrix equation expressing the components of the midcourse velocity correction vector as a time-varying function of a set of constants which define the difference between the vehicle's actual trajectory and its reference trajectory.

Even after the differential equations are linearized, they cannot in general be solved analytically in closed form because the coefficients are time-varying. The usual procedure is to perform the necessary integrations numerically on digital computers.

The problem of determining when to apply a correction has received only cursory treatment in the literature, most investigators contenting themselves by drawing inferences from the numerical results of their computer programs. The single exception to this generalization is the work of Breakwell,<sup>(22), (23)</sup> who has performed a statistical optimization of the time of correction for several special types of reference trajectories.

The present paper extends the linear theory and develops a simple deterministic method of computing the optimum correction time as a function of one of the parameters which characterize the difference between actual and reference trajectories. The method is applicable to all types of reference trajectories.

In order to provide a deeper insight into the physics of the problem, this paper presents a complete analytic solution of the guidance equations for a mathematical model in which the reference trajectory is an ellipse. This solution materially reduces computation time required for preliminary guidance studies, and it may be applicable in the final guidance mechanization for some missions.

The determination of the six independent parameters needed to specify completely the vehicle's actual trajectory relative to the reference trajectory is the navigation problem. The parameters are evaluated from measurements made during the journey. Usually a redundant number of measurements is made, and statistical theory is used in obtaining an estimate of the parameters.

Estimation techniques for this application are discussed in References (10) and (12). Each individual measurement, when properly weighted, reduces the uncertainty in the computed values of the six parameters. Implicit in the development of the procedures in these references is the assumption that errors in the clock, if they exist at all, are so small that their effect on the numerical values of the parameters is insignificant. This assumption is undoubtedly justified when the measurements are made from Earth, as in (10), or when the duration of the voyage is relatively short, as in the case of the circumlunar trajectories considered in (12). However, for interplanetary trajectories, extending over an interval of months or possibly years, neglect of clock errors may have a significant effect.

The clock error is taken into account in Reference (3), in which the measurements are processed not singly but in groups, each group being related to a single nominal time of measurement. From each group an estimate is obtained of clock error and position variation at the nominal measurement time.

This paper extends the procedure of (3). The maximum likelihood method of estimation is used to compute position variation at the nominal measurement time and also to compute the six orbital parameters from several position variations. A simple practical technique is developed for selecting the optical measurements to be made in a self-contained guidance system.

The choice of the set of six parameters which define the actual trajectory can have a material effect on the amount of computation required. This paper exploits the suggestion of Safren<sup>(25)</sup> by selecting the six-component vector consisting of the three components of position variation and the three components of velocity variation at the nominal time of arrival at the destination.

### 1.11 Synopsis

An attempt has been made in the format of this thesis to emphasize in the main text the physical principles underlying guidance theory. Detailed mathematical derivations and some background material are relegated to the appendices. Each chapter and each appendix opens with a brief summary of its salient features.

The remainder of this section describes the inter-relationships among the various chapters and appendices.

Appendix A and Appendix B provide background material. They provide some of the mathematical tools that are useful in succeeding appendices.

Appendix C is parenthetical; it does not contribute to the development of guidance theory. It presents two simple and illuminating graphical constructions, not previously known to the author, which were suggested by the formulation of the equations of elliptical motion in Appendix B.

Appendix D is also parenthetical. It investigates the possibility of using elliptical cylindrical coordinates for developing the guidance theory for elliptical reference trajectories and concludes that there is no significant advantage in using this system.

Appendix E develops the variant equations of motion of the space vehicle in several coordinate systems.

Appendix F expresses the variant equations of motion and their solution in matrix form. Some special symmetry properties of the matrices are derived.

Appendices G and H present two distinct methods of solving the variant equations of motion of Appendix E for the special case when the reference trajectory is an ellipse.

Appendix I and Appendix J express the analytic solution of Appendix H as a matrix equation in several coordinate systems, the difference between the two appendices being that Appendix I treats reference trajectories for which the eccentricity is significantly greater than zero but less than unity, while Appendix J is concerned only with low-eccentricity reference trajectories.

Appendix K utilizes the results of Appendix I to obtain analytic expressions for the terms in the matrices of Appendix F.

Appendices L and M formulate the basic matrix equations of midcourse guidance, the former for FTA guidance and the latter for VTA guidance.

Appendix N develops the method of selecting the optimum time at which to apply a midcourse VTA velocity correction.

Appendix O analyzes the singularities occurring in some of the matrices of Appendix K.

Chapter 2 describes the linear approach to midcourse guidance of a vehicle in an  $n$ -body gravitational field. It makes use of the mathematical developments in Appendices E, F, L, M, and N.

Chapter 3 applies the results of Chapter 2 to missions for which the reference trajectory is an ellipse. It utilizes the material in Appendices E, G, H, I, K, L, M, N, and O.

Chapter 4 contains a numerical example which illustrates the theory developed in Chapters 2 and 3.

Appendix P is a mathematical development of the equations for the maximum likelihood estimate of a multi-dimensional random variable.

Chapter 5 discusses linear navigation theory for both Earth-based radio-command systems and self-contained optical systems. It utilizes the results of the statistical theory in Appendix P.

Chapter 6 represents an attempt to utilize the novel features of this analysis in conjunction with the best features of previous proposals in the synthesis of a simple and effective midcourse guidance system.

Chapter 7 summarizes the salient points of the study and suggests the areas in which additional work may be desirable.



## CHAPTER 2

### LINEAR GUIDANCE THEORY FOR AN N-BODY GRAVITATIONAL FIELD

#### 2.1 Summary

The guidance equations for both fixed-time-of-arrival guidance and variable-time-of-arrival guidance are developed from the solution of the linearized equations of motion of a space vehicle in an n-body gravitational field. A method is outlined for determining the optimum time at which to apply a midcourse correction.

#### 2.2 Introduction

The literature reviewed in Chapter 1 contains several papers which develop methods of computing the midcourse velocity correction as a function of the time of correction and the parameters which define the difference between the space vehicle's actual trajectory and its reference trajectory. The first part of the present chapter collates much of this material, the primary sources being References (5), (9), (13), (22), and (25).

The latter portion of the chapter extends the previously known theory by developing a relatively simple deterministic method of specifying the optimum time to apply a VTA velocity correction as a function of a single parameter of the vehicle's variant path.

#### 2.3 Clarification of the Term "Perturbation"

In the study of guidance theory a certain amount of confusion is caused by the fact that investigators with different backgrounds sometimes use the same technical term to describe similar but not identical situations. In particular, this problem in semantics arises in the use of the word perturbation.

In the development of planetary theory astronomers start with a two-body orbit of the planet about the focus at the sun, then refine the

computation by taking into account the gravitational effects of the other planets. Smart\* refers to these planets as "disturbing" planets, and the relatively small changes they cause in the two-body orbit are known as "perturbations."

A similar approach is currently used to develop desirable reference trajectories for space vehicles on interplanetary missions. The differences between the numerically computed trajectories, which include such effects as earth oblateness and gravitation due to the planets, and the corresponding two-body heliocentric trajectories are again called "perturbations." This usage is consistent with the older use of the term by astronomers.

The primary concern of the guidance analyst is the difference between the actual trajectory traversed by a space vehicle and the pre-computed reference trajectory. This difference, due to imperfect instrumentation and inexact guidance equations, is also referred to in some of the literature as a "perturbation." The mathematical technique of expressing the actual trajectory as a series expansion of certain measured or inferred deviations between the two trajectories is an application of "perturbation theory." If no terms higher than first-order are retained in the series expansion, the process is "linear perturbation theory."

Thus, the term perturbation describes two similar, but nevertheless distinct, phenomena. The older astronomical usage indicates the small deviations from a two-body orbit due to the effect of forces that have not previously been considered; the more recent space guidance usage refers to deviations from a pre-computed reference trajectory caused primarily by a change in initial conditions and to a lesser extent by a lack of precise knowledge of the required astronomical constants.

To resolve this dilemma, "perturbation" in this analysis will be used only in the sense that it is used by astronomers. The differences between the vehicle's actual trajectory and the reference trajectory will be referred to as "variations" or "deviations." The differential equations describing the motion of the vehicle relative to the reference trajectory will be called the "variant" equations of motion.

---

\*Page 9 of (28).

## 2.4 Mathematical Model

For the purposes of this analysis the space vehicle is regarded as a small mass point moving in a three-dimensional gravitational field dominated by the sun. The masses of the planets cause disturbances which produce perturbations of the two-body motion of the vehicle in the sun's field.

All motions are referred to an origin at the center of mass of the sun. The positions of the planets as a function of time are obtained from an ephemeris; no simplifying assumptions are necessary, such as the assumption that the planetary orbits are exact conic sections or that they are exactly planar.

During the midcourse phase the vehicle's distance from any of the planets is large enough so that the effect of planetary oblateness can be neglected; therefore, the planets are treated as mass points.

Non-gravitational forces, such as those due to aerodynamic, electromagnetic, or solar radiation effects, are not considered.

Although oblateness is neglected in the variational analysis to be presented, the effect of earth oblateness should certainly be included in the computation of the reference trajectory for a trip from the earth to another planet. The reference trajectory is obtained by numerical integration of all significant gravitational forces.

The departure of the vehicle's actual trajectory from the reference trajectory is assumed to be small enough so that a linear variational analysis is acceptable.

Midcourse corrections take the form of small thrust impulses applied at several distinct times during the midcourse phase of the journey.

## 2.5 Equations of Motion

In vector form, the motion of the space vehicle in the gravitational field can be expressed by one compact equation.

$$\ddot{\underline{r}} + \frac{\mu}{r^3} \underline{r} = \nabla R \quad (2-1)$$

where

$$R = G \sum_{i=1}^n m_i \left( \frac{1}{d_i} - \frac{\underline{r} \cdot \underline{r}_i}{r_i^3} \right) \quad (2-2)$$

These equations are adapted from Page 9 of Smart. <sup>(28)</sup> They are equivalent to Equation (B-3) of Appendix B.

The function  $R$  is known as the disturbing function. It represents the effect of the  $n$  disturbing planets on the vehicle's motion.

The notation used in this thesis includes the following: Underlining a lower-case letter indicates that the letter represents a vector. The same symbol used without underlining signifies the magnitude of the vector quantity. A single dot over a symbol indicates the first derivative with respect to time of the variable represented by the symbol; similarly, two dots indicate the second time derivative, etc. Time derivatives of vectors are taken with respect to inertial space unless specified otherwise.

In Equation (2-1),  $\underline{r}$  is the position vector of the vehicle on the reference trajectory with respect to the origin at the center of the sun, and  $\ddot{\underline{r}}$  is the acceleration of the vehicle on the reference trajectory relative to the origin.  $\nabla R$  is the gradient of the scalar function  $R$ .

The gravitational symbols  $G$  and  $\mu$  are defined in Section B. 2 of Appendix B.  $d_i$  is the distance of the  $i$ -th disturbing planet, whose mass is  $m_i$ , from the space vehicle.  $\underline{r}_i$  is the position vector of the  $i$ -th disturbing planet. Vectors  $\underline{r}$ ,  $\underline{r}_i$ , and  $\underline{d}_i$  are illustrated in Figure B. 1 of Appendix B for the case  $i = 1$ .

The component equations represented by (2-1), modified to include the effect of earth oblateness, are the equations that are integrated numerically (with the proper initial conditions) to obtain the vehicle's reference trajectory.

The variant equations of motion are obtained from the variations in the terms of (2-1) due to variations in the components of  $\underline{r}$  at some arbitrary time  $t$ . In matrix form the variant equations can be written as follows:

$$\delta \ddot{\underline{r}} = \dot{\underline{G}}^* \delta \underline{r} \quad (2-3)$$

where

$$\dot{\underline{G}}^* = \frac{\mu}{r^5} (3 \underline{r} \underline{r}^T - \underline{r}^T \underline{r} \underline{I}_3^*) + \dot{\underline{G}} \sum_{i=1}^n \frac{m_i}{d_i^5} (3 \underline{d}_i \underline{d}_i^T - \underline{d}_i^T \underline{d}_i \underline{I}_3^*) \quad (2-4)$$

An asterisk over a capital letter indicates a matrix.  $\underline{I}_3^*$  is a 3-by-3 identity matrix. The superscript T signifies the transpose of a vector or matrix. The symbol  $\delta$  denotes the first variation of the quantity immediately following it. The product  $\underline{r} \underline{r}^T$ , unlike the conventional dot product or cross product of vector analysis, is a 3-by-3 symmetric matrix.

It is evident from (2-4) that  $\dot{\underline{G}}^*$  is a symmetric 3-by-3 matrix. It is shown in Section E.4 that  $\dot{\underline{G}}^*$  remains symmetric even when oblateness effects are taken into consideration.

The elements of  $\dot{\underline{G}}^*$  are time-varying because  $\underline{r}$  and  $\underline{d}_i$  are time-varying. It may be noted that these elements are functions of vehicle position on the reference trajectory and do not depend on vehicle velocity. Once the reference trajectory has been determined, the elements of  $\dot{\underline{G}}^*$  can be computed directly.

The derivation of (2-3) and (2-4) is given in Appendix E.

## 2.6 State Vector

Equation (2-3) represents three coupled second-order linear differential equations. The solution of these equations for the components of  $\delta \underline{r}$  as a function of time contains six arbitrary constants, which can be regarded as the elements of a six-component column vector; such a vector is designated a path deviation vector.

In Section F.2 several types of path deviation vectors are defined, and linear relations among the types are presented. The most useful type is that which consists of the three components of position variation and the three components of velocity variation at some specified time  $t_k$ . This particular path deviation vector is known as the state vector and is symbolized by  $\delta \underline{x}_k$ . The subscript k indicates that the vector refers to conditions existing at time  $t_k$ . In matrix notation,

$$\delta \underline{x}_k = \begin{Bmatrix} \delta \underline{r}_k \\ \delta \underline{v}_k \end{Bmatrix} \quad (2-5)$$

The state vector defines the difference between the vehicle's actual trajectory and the reference trajectory in terms of its position and velocity variations (i. e., its "state") at time  $t_k$ . For an initial condition problem,  $t_k$  becomes  $t_I$ , the time of injection into the heliocentric orbit; for a final condition problem,  $t_k$  becomes  $t_D$ , the time of arrival at the destination.

## 2.7 Transition Matrix

The solution of (2-3) has the form

$$\begin{aligned} \delta \underline{r}_m &= \underline{M}_{mk}^* \delta \underline{r}_k + \underline{N}_{mk}^* \delta \underline{v}_k \\ &= \begin{Bmatrix} \underline{M}_{mk}^* & \underline{N}_{mk}^* \end{Bmatrix} \delta \underline{x}_k \end{aligned} \quad (2-6)$$

$\delta \underline{r}_m$  is the position variation at any arbitrary time  $t_m$ . The elements of the 3-by-3 matrices  $\underline{M}_{mk}^*$  and  $\underline{N}_{mk}^*$  depend on  $t_m$  and  $t_k$  and also on the characteristics of the reference trajectory.

By differentiating (2-6) with respect to the variable time  $t_m$ , an expression is obtained for the velocity variation  $\delta \underline{v}_m$ .

$$\delta \underline{v}_m = \begin{Bmatrix} \underline{S}_{mk}^* & \underline{T}_{mk}^* \end{Bmatrix} \delta \underline{x}_k \quad (2-7)$$

$\underline{S}_{mk}^*$  and  $\underline{T}_{mk}^*$  are 3-by-3 time-varying matrices.

Equations (2-6) and (2-7) can be combined into a single equation.

$$\delta \underline{x}_m = \underline{C}_{mk}^* \delta \underline{x}_k \quad (2-8)$$

where

$$\underline{C}_{mk}^* = \begin{Bmatrix} \underline{M}_{mk}^* & \underline{N}_{mk}^* \\ \underline{S}_{mk}^* & \underline{T}_{mk}^* \end{Bmatrix} \quad (2-9)$$

The 6-by-6 matrix  $\underline{C}_{mk}^*$  is known as the transition matrix; it is the means by which the state at time  $t_m$  is determined from a specified

state at time  $t_k$ . The transition matrix has some interesting mathematical properties which are discussed in detail in Appendix F and are summarized here. First, when  $t_m = t_k$ , it is obvious that the transition matrix must reduce to the 6-by-6 identity matrix.

$$\bar{C}_{kk}^* = \bar{I}_6 \quad (2-10)$$

Secondly, the transition matrix relating  $\delta \underline{x}_k$  to  $\delta \underline{x}_m$  is the inverse of the transition matrix relating  $\delta \underline{x}_m$  to  $\delta \underline{x}_k$ .

$$\bar{C}_{km}^* = \bar{C}_{mk}^{*-1} \quad (2-11)$$

The third property also is concerned with the inverse of the transition matrix. It is shown in Appendix F that the elements of  $\bar{C}_{mk}^{*-1}$  are the elements of  $\bar{C}_{mk}^*$  arranged in different order.

$$\bar{C}_{mk}^{*-1} = \begin{Bmatrix} \bar{T}_{mk}^* & -\bar{N}_{mk}^* \\ -\bar{S}_{mk}^* & \bar{M}_{mk}^* \end{Bmatrix} \quad (2-12)$$

Thus, if the elements of  $\bar{C}_{mk}^*$  have been determined, the elements of its inverse are available without need for the tedious numerical computations normally associated with inverting a 6-by-6 matrix.

Finally, despite the fact that the elements of  $\bar{C}_{mk}^*$  are time-varying, its determinant is always equal to +1.

$$\det \bar{C}_{mk}^* = +1 \quad (2-13)$$

## 2.8 Numerical Solution of Variant Equations of Motion

The numerical integration of (2-3) to yield a solution of the form (2-8) is facilitated if the three second-order equations comprising (2-3) are re-arranged as six first-order equations.

$$\delta \dot{\underline{r}} = \delta \underline{v} \quad (2-14)$$

$$\delta \dot{\underline{v}} = \bar{G}^* \delta \underline{r} \quad (2-15)$$

In terms of the state vector,

$$\delta \dot{\underline{x}} = \bar{Z}^* \delta \underline{x} \quad (2-16)$$

where

$$\overset{*}{Z} = \begin{Bmatrix} \overset{*}{0}_3 & \overset{*}{I}_3 \\ \overset{*}{G} & \overset{*}{0}_3 \end{Bmatrix} \quad (2-17)$$

The subscript 3 on the zero and identity sub-matrices of (2-17) indicates the order of these matrices.

Since (2-8) is the solution of (2-16), it follows that

$$\frac{\partial \overset{*}{C}_{mk}}{\partial t_m} \delta \underline{x}_k = \overset{*}{Z}_m \overset{*}{C}_{mk} \delta \underline{x}_k \quad (2-18)$$

For an arbitrary  $\delta \underline{x}_k$ ,

$$\frac{\partial \overset{*}{C}_{mk}}{\partial t_m} = \overset{*}{Z}_m \overset{*}{C}_{mk} \quad (2-19)$$

(2-19) represents thirty-six first-order equations which can be integrated numerically from  $t_m = t_k$  to any other value of  $t_m$ . The initial conditions are given by the fact that  $\overset{*}{C}_{kk}$  is the identity matrix. As a result of the integration the terms of  $\overset{*}{C}_{mk}$  are obtained as a function of  $t_m$  for the specified value of  $t_k$ , and consequently  $\delta \underline{x}_m$  is determined as a function of  $\delta \underline{x}_k$ .

## 2.9 Choice of Coordinate System

In choosing a coordinate system in which to carry out the numerical integration, there are two important considerations. First, it is desirable to use an inertially non-rotating system so that Coriolis effects do not complicate the problem. Secondly, it is advisable to choose the fixed axes such that two of them lie in the plane of the two-body motion that would occur ideally if there were no disturbing forces, and the third axis is perpendicular to that plane. With these axes the only coupling between the variant motion in the plane and the variant motion normal to the plane is due to the effect of the disturbing forces, and this effect is usually quite small. Thus, the sixth-order system can be sub-divided into two systems, one of fourth order and the other of second order, with weak coupling between the two.

Then in each of the four 3-by-3 matrices  $\overset{*}{M}_{mk}$ ,  $\overset{*}{N}_{mk}$ ,  $\overset{*}{S}_{mk}$ , and  $\overset{*}{T}_{mk}$ , the first two terms of the third row and the first two terms of the third column will, in general, be numerically small compared to the other five terms of the matrix, and round-off errors in the integration procedure will be materially reduced.



The two orthogonal in-plane axes may have any desired orientation; a convenient choice is that in which the positive x-axis is in the direction of perihelion from the origin at the center of the sun; then the positive y-axis is in the direction of the positive semi-latus rectum; this axis system is described in Appendix A as the "reference trajectory stationary coordinate system."

In the non-rotating coordinate system the thirty-six equations of (2-19) may be re-written as follows:

$$\frac{\partial M_{mk}^*}{\partial t_m} = S_{mk}^* \quad (2-20)$$

$$\frac{\partial N_{mk}^*}{\partial t_m} = T_{mk}^* \quad (2-21)$$

$$\frac{\partial S_{mk}^*}{\partial t_m} = G_m^* M_{mk}^* \quad (2-22)$$

$$\frac{\partial T_{mk}^*}{\partial t_m} = G_m^* N_{mk}^* \quad (2-23)$$

It is evident from these equations that  $M_{mk}^*$  and  $S_{mk}^*$  are inter-related, and  $N_{mk}^*$  and  $T_{mk}^*$  are inter-related, but there is no coupling between  $M_{mk}^*$  and  $S_{mk}^*$  on one hand and  $N_{mk}^*$  and  $T_{mk}^*$  on the other. Therefore, the thirty-six equations consist of two independent sets, each containing eighteen coupled equations.

## 2.10 State Vector at Destination

The most important state vector to the guidance analyst is  $\delta \underline{x}_D$ , the state vector at the nominal time of arrival at the destination. It is useful to be able to ascertain the effect of small variations in position and velocity at time  $t_C$ , the time of a midcourse correction, on the corresponding variations at  $t_D$ . From Equation (2-8) the effect is determined from the equation

$$\delta \underline{x}_D = \dot{C}_{DC}^* \delta \underline{x}_C \quad (2-24)$$

Although  $t_D$  is a fixed time for a specified reference trajectory,  $t_C$  can take on any value between  $t_I$  and  $t_D$ . It is of interest to find the effect of varying  $t_C$  on the transition matrix  $\dot{C}_{DC}^*$ . If normal forward integration is used, the thirty-six equations comprising (2-19) must be integrated from the initial values at  $t = t_C$  to the end point at  $t = t_D$  for each separate value of  $t_C$ . If many values of  $t_C$  are to be investigated, the amount of computing required quickly becomes prohibitive.

By making use of (2-12) and integrating backward in time from an "initial" condition at  $t = t_D$ , the integration process need be carried out only once. The result of the integration is a relation between  $\dot{C}_{CD}^*$  and  $t_C$  for the known fixed value of  $t_D$ . Then  $\dot{C}_{DC}^*$ , the desired matrix, is obtained from  $\dot{C}_{CD}^*$  for any  $t_C$  by a simple re-arrangement of terms.

$$\dot{C}_{DC}^* = \dot{C}_{CD}^{*-1} = \begin{Bmatrix} \dot{M}_{DC}^* & \dot{N}_{DC}^* \\ \dot{S}_{DC}^* & \dot{T}_{DC}^* \end{Bmatrix} = \begin{Bmatrix} \dot{T}_{CD}^{*T} & -\dot{N}_{CD}^{*T} \\ -\dot{S}_{CD}^{*T} & \dot{M}_{CD}^{*T} \end{Bmatrix} \quad (2-25)$$

## 2.11 Two-Position Path Deviation Vector

The only type of path deviation vector that has been discussed thus far is the state vector  $\delta \underline{x}$ . Another type of path deviation vector that is useful in the analysis of midcourse guidance is the two-position vector, which consists of the position variation vectors at two different times. If the two times are  $t_i$  and  $t_j$ , the two-position vector is

$$\begin{Bmatrix} \delta \underline{r}_i \\ \delta \underline{r}_j \end{Bmatrix}$$

The velocity variation at time  $t_i$  can be written in terms of the two-position vector.

$$\delta \underline{v}_i = \dot{J}_{ij}^* \delta \underline{r}_i + \dot{K}_{ij}^* \delta \underline{r}_j \quad (2-26)$$

where  $\dot{J}_{ij}^*$  and  $\dot{K}_{ij}^*$  are 3-by-3 matrices. From the results obtained in Appendix F,  $\dot{J}_{ij}^*$  and  $\dot{K}_{ij}^*$  can be related to the 3-by-3 sub-matrices of  $\dot{C}_{ji}^*$  and  $\dot{C}_{ij}^*$ .

$$\mathbf{J}_{ij}^* = - \mathbf{N}_{ji}^{*-1} \mathbf{M}_{ji} = (\mathbf{N}_{ij}^* \mathbf{T})^{-1} \mathbf{T}_{ij}^* \mathbf{T} \quad (2-27)$$

$$\mathbf{K}_{ij}^* = \mathbf{N}_{ji}^{*-1} = - (\mathbf{N}_{ij}^* \mathbf{T})^{-1} \quad (2-28)$$

It is also shown in Appendix F that  $\mathbf{J}_{ij}^*$  is a symmetric matrix.

Equations (2-27) and (2-28) will be used in the analysis of the midcourse correction.

## 2.12 Midcourse Velocity Correction

The preceding sections describe the variant motion of a space vehicle in a gravitational field. Once the variant motion is known, the problem is to alter this motion by means of a midcourse correction so that the objective of the mission can be achieved.

The means of altering the motion is a short application of thrust from a reaction-type engine. Because the thrust application is so short in duration relative to the time required for the space voyage, it is treated mathematically as a thrust impulse. At the time of the correction,  $t_C$ , there is a step change in vehicle velocity but no instantaneous change in vehicle position.

Obviously, the correction causes a change in the state vector  $\delta \underline{x}_k$  which characterizes the variant motion. The superscripts - and + will be used to distinguish conditions applicable before the correction from those applicable after the correction. The change in the state vector  $\delta \underline{x}_C$  is given by

$$\delta \underline{x}_C^+ - \delta \underline{x}_C^- = \left\{ \begin{array}{c} \underline{0}_3 \\ \underline{c} \end{array} \right\} \quad (2-29)$$

where  $\underline{0}_3$  is the three-dimensional zero vector and  $\underline{c}$  is the velocity correction vector. The three components of  $\underline{c}$  are to be computed in such a manner that three specified design conditions are satisfied.

It is apparent that a single correction cannot cause the vehicle to return immediately to its reference trajectory, because accomplishing this would require that six conditions be met (i. e.,  $\delta \underline{r} = \underline{0}_3$ ,  $\delta \underline{v} = \underline{0}_3$ ). The three design conditions that are to be satisfied are generally associated with the vehicle's state vector when it arrives at the destination.

Thus, the correction is intended to establish a new variant path which modifies  $\delta \underline{x}_D$  in some desired fashion. The difference between the corrected and the original state vectors at time  $t_D$  is related to the corresponding difference in state vectors at  $t_C$  by the equation

$$\begin{aligned}\delta \underline{x}_D^+ - \delta \underline{x}_D^- &= \tilde{C}_{DC}^* (\delta \underline{x}_C^+ - \delta \underline{x}_C^-) \\ &= \tilde{C}_{DC}^* \begin{Bmatrix} 0 \\ -3 \\ \underline{c} \end{Bmatrix} = \begin{Bmatrix} \tilde{N}_{DC}^* \\ \tilde{T}_{DC}^* \end{Bmatrix} \underline{c}\end{aligned}\quad (2-30)$$

In the two types of guidance system to be analyzed, all three design conditions are related to the desired position variation at the destination,  $\delta \underline{r}_D^+$ . Then the velocity correction can be found in terms of  $(\delta \underline{r}_D^+ - \delta \underline{r}_D^-)$ .

$$\begin{aligned}\underline{c} &= \tilde{N}_{DC}^{*-1} (\delta \underline{r}_D^+ - \delta \underline{r}_D^-) \\ &= \tilde{K}_{CD}^* (\delta \underline{r}_D^+ - \delta \underline{r}_D^-)\end{aligned}\quad (2-31)$$

When the elements of  $\tilde{C}_{CD}^*$  have been computed by backward integration, the elements of  $\tilde{K}_{CD}^*$  are obtained from the sub-matrix  $\tilde{N}_{CD}^*$  by means of (2-28). It may be noted that evaluation of  $\tilde{K}_{CD}^*$  requires the integration of only eighteen of the thirty-six first-order equations comprising (2-19).

### 2.13 Fixed-Time-of-Arrival Guidance

In fixed-time-of-arrival guidance it is stipulated that the space vehicle arrive at the destination at the exact time specified by the reference trajectory. Thus, the three mathematical conditions to be satisfied by the midcourse correction are contained in the simple equation

$$\delta \underline{r}_D^+ = \underline{0}_3 \quad (2-32)$$

With the subscript F used to denote fixed-time-of-arrival guidance, the equation for the correction is

$$\underline{c}_F = - \tilde{K}_{CD}^* \delta \underline{r}_D^- \quad (2-33)$$

The resulting velocity variation  $\delta \underline{v}_D^+$  can be determined from (2-30), with the aid of the relations given by (2-27) and (2-28).

$$\begin{aligned}\delta \underline{v}_D^+ &= \delta \underline{v}_D^- + \underline{T}_{DC}^* \underline{c}_F \\ &= \delta \underline{v}_D^- - \underline{T}_{DC}^* \underline{K}_{CD}^* \delta \underline{r}_D^- \\ &= \left\{ \begin{array}{cc} \underline{0}_3 & \underline{0}_3 \\ -\underline{J}_{DC}^* & \underline{I}_3 \end{array} \right\} \delta \underline{x}_D^- \end{aligned} \quad (2-34)$$

From (2-32) and (2-34), the new and the old state vectors at  $t_D$  are related by the equation

$$\delta \underline{x}_D^+ = \left\{ \begin{array}{cc} \underline{0}_3 & \underline{0}_3 \\ -\underline{J}_{DC}^* & \underline{I}_3 \end{array} \right\} \delta \underline{x}_D^- \quad (2-35)$$

A more detailed analysis of fixed-time-of-arrival guidance is presented in Appendix L.

#### 2.14 Variable-Time-of-Arrival Guidance

In variable-time-of-arrival guidance it is required that the vehicle reach its proper destination point relative to the destination planet, but it is not required that the actual time of arrival coincide with the nominal arrival time indicated by the reference trajectory. The problem then is analogous to a simple fire-control problem, in which the motion of the "target" (i. e., the destination planet) is completely predictable.

Instead of arriving at  $t = t_D$ , the vehicle actually arrives at  $t = t_D + \Delta t_D$ , the increment  $\Delta t_D$  being small relative to the period of the orbital motion. At  $t = t_D$  the deviation of the vehicle's actual position from the destination point on the reference trajectory is

$$\delta \underline{r}_D^+ = -\underline{v}_R \Delta t_D \quad (2-36)$$

where  $\underline{v}_R$  is the velocity of the vehicle relative to the destination planet at  $t = t_D$ . It is assumed in the linear theory that  $\underline{v}_R$  remains constant in the time interval between  $t_D$  and  $(t_D + \Delta t_D)$ . Clearly, at  $t = t_D$  the vehicle's position must lie on the line through the nominal destination point and parallel to  $\underline{v}_R$ ; this is illustrated by Figure M. 2 of Appendix M.

The variable-time-of-arrival guidance concept requires that the component of  $\delta \underline{r}_D^-$  lying in the plane normal to  $\underline{v}_R$  be reduced to zero by the midcourse correction. This component is designated  $\delta \underline{\rho}^-$ , the miss distance vector. Since  $\delta \underline{\rho}$  can be considered a two-dimensional vector, only two of the three conditions that can be satisfied by the correction are contained in the equation

$$\delta \underline{\rho}^+ = \underline{0} \quad (2-37)$$

The third condition, which uniquely determines  $\delta \underline{r}_D^+$  and  $\Delta t_D$ , is that the magnitude of the correction be a minimum.

From Eq. (2-31), the VTA correction, designated  $\underline{c}_v$ , is

$$\begin{aligned} \underline{c}_v &= \underline{K}_{CD}^* (-\underline{v}_R \Delta t_D - \delta \underline{r}_D^-) \\ &= \underline{c}_F - \underline{w} \Delta t_D \end{aligned} \quad (2-38)$$

where the vector  $\underline{w}$  is defined by

$$\underline{w} = \underline{K}_{CD}^* \underline{v}_R \quad (2-39)$$

In Section M. 4 it is shown that the magnitude of  $\underline{c}_v$  is a minimum when

$$\Delta t_D = \frac{\underline{w}^T \underline{c}_F}{\underline{w}^T \underline{w}} \quad (2-40)$$

When (2-40) is substituted into (2-38), the correction becomes

$$\underline{c}_v = \left( \underline{I}_3 - \frac{\underline{w} \underline{w}^T}{\underline{w}^T \underline{w}} \right) \underline{c}_F = - \left( \underline{I}_3 - \frac{\underline{w} \underline{w}^T}{\underline{w}^T \underline{w}} \right) \underline{K}_{CD}^* \delta \underline{r}_D^- \quad (2-41)$$

In Section M. 5  $\underline{c}_v$  is proved to be perpendicular to  $\underline{w}$ . Thus, Eq. (2-38) represents a vector right triangle whose hypotenuse is  $\underline{c}_F$ . The direction of  $\underline{w}$  is known as the "noncritical direction," and the plane perpendicular to  $\underline{w}$  is the "critical plane."  $\underline{c}_v$  is the component of  $\underline{c}_F$  in the critical plane.

The expected position and velocity variations at  $t = t_D$  after the VTA correction is applied may be written as

$$\delta \underline{r}_D^+ = - \underline{v}_R \Delta t_D = \frac{\underline{v}_R \underline{w}^T}{\underline{w}^T \underline{w}} \underline{K}_{CD}^* \delta \underline{r}_D^- \quad (2-42)$$

$$\begin{aligned} \delta \underline{v}_D^+ &= \delta \underline{v}_D^- + \underline{T}_{DC}^* \underline{c}_v \\ &= \delta \underline{v}_D^- - \underline{T}_{DC}^* \left( \underline{I}_3 - \frac{\underline{w} \underline{w}^T}{\underline{w}^T \underline{w}} \right) \underline{K}_{CD}^* \delta \underline{r}_D^- \\ &= \delta \underline{v}_D^- - \underline{J}_{DC}^* \left( \underline{I}_3 - \frac{\underline{v}_R \underline{w}^T}{\underline{w}^T \underline{w}} \underline{K}_{CD}^* \right) \delta \underline{r}_D^- \end{aligned} \quad (2-43)$$

The matrix relationship between  $\delta \underline{x}_D^+$  and  $\delta \underline{x}_D^-$  is

$$\delta \underline{x}_D^+ = \begin{Bmatrix} \frac{\underline{v}_R \underline{w}^T}{\underline{w}^T \underline{w}} \underline{K}_{CD}^* & \underline{0}_3^* \\ -\underline{J}_{DC}^* \left( \underline{I}_3 - \frac{\underline{v}_R \underline{w}^T}{\underline{w}^T \underline{w}} \underline{K}_{CD}^* \right) & \underline{I}_3^* \end{Bmatrix} \delta \underline{x}_D^- \quad (2-44)$$

A more detailed discussion of the material in this section will be found in Appendix M.

## 2.15 Critical-Plane Coordinate System

The fact that the VTA correction lies in a plane perpendicular to  $\underline{w}$  and the miss distance lies in a plane perpendicular to  $\underline{v}_R$  suggests the possibility of simplifying the guidance equations by the use of a rotating coordinate system in which one axis, the noncritical axis, is parallel to  $\underline{w}$  for any given  $t_C$ , and the other two axes lie in the critical plane. At  $t = t_D$  the noncritical axis is parallel to  $\underline{v}_R$ , and the other two axes lie in the plane containing  $\delta \underline{\rho}^-$ .

The axis system incorporating these characteristics is designated the critical-plane coordinate system, with axes  $\xi$ ,  $\eta$ , and  $\zeta$ . The  $\xi$ - $\eta$

plane is the critical plane, and the  $\xi$ -axis is the noncritical axis. The  $\xi$ -axis lies along the line of nodes between the critical plane and the reference trajectory plane.

As  $t_C$  varies, the coordinate system rotates about the z-axis. The  $\xi$ -axis is always in the reference trajectory plane; the z-axis is always in the  $\eta$ - $\xi$  plane.

In the new coordinate system the miss distance vector is

$$(\delta \underline{\rho}^-)_W = \begin{Bmatrix} \delta \xi_D^- \\ \delta \eta_D^- \end{Bmatrix} = (\delta \underline{\rho}^-) \begin{Bmatrix} \cos \psi \\ \sin \psi \end{Bmatrix} \quad (2-45)$$

where the subscript W indicates that the miss distance vector is expressed in terms of its two components in the  $\xi_D$  -  $\eta_D$  plane.  $\psi$  is the angle between  $\delta \underline{\rho}^-$  and the positive  $\xi_D$ -axis.

The VTA correction vector, designated  $\underline{c}_W$  in the critical-plane system, is given by

$$\underline{c}_W = \bar{Y}^* (\delta \underline{\rho}^-)_W \quad (2-46)$$

Equation (N-30) expresses the elements of the 2-by-2 matrix  $\bar{Y}^*$  as functions of the elements of  $\bar{K}_{CD}^*$  and the orientation of  $\underline{v}_R$ .

Comparison of (2-46) with (2-41) indicates the conceptual simplicity achieved by use of the new coordinate system.

## 2.16 Optimum Time of Correction

Either (2-41) or (2-46) defines the VTA velocity correction as a function of  $\delta \underline{\rho}^-$  and  $t_C$ . On an actual space mission the value of  $\delta \underline{\rho}^-$  is estimated from measurements made during the voyage. The value of  $t_C$  can be chosen as any time after the last measurement and prior to  $t_D$ , the nominal time of arrival. The problem to be considered in this section is the determination of the value of  $t_C$  which, for the given  $\delta \underline{\rho}^-$ , minimizes the magnitude of  $\underline{c}_V$ .



From (2-45) and (2-46),

$$\underline{c}_W = \underline{\dot{Y}}^* \begin{Bmatrix} \delta \xi_D^- \\ \delta \eta_D^- \end{Bmatrix} = (\delta \rho^-) \underline{\dot{Y}}^* \begin{Bmatrix} \cos \psi \\ \sin \psi \end{Bmatrix} \quad (2-47)$$

The magnitude of  $\underline{c}_W$  varies linearly with  $\delta \rho^-$  but in a nonlinear fashion with  $\psi$  and, through  $\underline{\dot{Y}}^*$ , with  $t_C$ . The procedure to be followed now is to find that value of  $t_C$  which minimizes  $c_W^2 = c_V^2$  for the known estimate of  $\psi$ .

$$c_V^2 = \underline{c}_W^T \underline{c}_W = (\delta \rho^-)^2 \begin{Bmatrix} \cos \psi & \sin \psi \end{Bmatrix} \underline{\dot{Y}}^{*T} \underline{\dot{Y}}^* \begin{Bmatrix} \cos \psi \\ \sin \psi \end{Bmatrix} \quad (2-48)$$

For each of several values of  $\psi$ , Equation (2-48) is used to compute and plot  $c_V/\delta \rho^-$  as a function of  $t_C$ . The minimum value of  $c_V/\delta \rho^-$  for each curve occurs at the optimum correction time,  $t_{C_{opt}}$ , for the  $\psi$  corresponding to that curve. A cross-plot can then be made of  $t_{C_{opt}}$  versus  $\psi$ . This single design curve serves to define the optimum correction time as a function of the angular orientation of the predicted miss distance vector.

A second cross-plot,  $(c_V/\delta \rho^-)_{min}$  versus  $\psi$ , can be drawn if desired, to indicate the magnitude of the minimum correction for a given  $\delta \rho^-$ .

Although  $\psi$ , as defined, can vary from  $0^\circ$  to  $360^\circ$ , only angles between  $0^\circ$  and  $180^\circ$  need be used in the plots and the cross-plots, since an increase of  $180^\circ$  in  $\psi$  reverses the direction of  $\underline{c}_V$  but has no effect on its magnitude.

## 2.17 Multiple Corrections

The analysis of the past few sections relates to the determination of a single velocity correction, applied at  $t = t_C$ , which under ideal conditions enables the space vehicle to achieve the desired objective at

$t = t_D$  without the need for any further corrections. In any practical situation conditions are not ideal. The estimated position variation at the destination,  $\delta \underline{r}_D$ , is inaccurate due to inaccuracies in the measurements made during the voyage, and also there are inaccuracies in the application of the computed velocity correction.

The consequence of these inaccuracies is that, after a midcourse correction has been applied, additional measurements indicate a new non-zero value of the vector that is to be nulled ( $\delta \underline{r}_D$  in FTA navigation,  $\delta \underline{\rho}$  in VTA navigation), and a new correction vector can be computed. The guidance theory that has been presented is applicable to each individual correction in turn, irrespective of the number of corrections that have preceded.

For VTA corrections made late in the flight, it is likely that the optimum  $t_C$  will have occurred before the time of the last measurement; in that case the determination of  $t_{C_{opt}}$  has no practical significance.

## 2.18 Applicability of Linear Theory

The basic vector equation of motion of a space vehicle in a gravitational field is (2-1), which is nonlinear. Once a reference trajectory has been established, the general solution for the actual motion can be expressed as an equation relating the state vector  $\delta \underline{x}_m$  at any arbitrary time  $t_m$  to the characteristics of the reference trajectory and the components of the state vector  $\delta \underline{x}_k$  at some specified time  $t_k$ .

$$\delta \underline{x}_m = \delta \underline{x}_m(\underline{x}_k, \delta \underline{x}_k, t_k, t_m) \quad (2-49)$$

In this equation the characteristics of the reference trajectory are contained in  $\underline{x}_k$ , which represents the components of position and velocity on the reference trajectory at  $t_k$ .

The components of  $\delta \underline{x}_m$  can be written as a Taylor series expansion in the components of  $\delta \underline{x}_k$ . Let  $(\delta x_m)_u$  represent the u-th component of  $\delta \underline{x}_m$ . Also let  $(\delta x_k)_i$  and  $(\delta x_k)_j$  represent the i-th and j-th components of  $\delta \underline{x}_k$ . The series expansion for  $(\delta x_m)_u$  is

$$\begin{aligned}
(\delta x_m)_u &= \sum_{i=1}^6 \frac{\partial (x_m)_u}{\partial (x_k)_i} (\delta x_k)_i \\
&+ \frac{1}{2} \sum_{i=1}^6 \sum_{j=1}^6 \frac{\partial^2 (x_m)_u}{\partial (x_k)_i \partial (x_k)_j} (\delta x_k)_i (\delta x_k)_j + \dots \quad (2-50)
\end{aligned}$$

The six partial derivatives in the first term on the right-hand side of (2-50) are the elements of the  $u$ -th row of the transition matrix  $\tilde{C}_{mk}^*$ .

In the linear theory  $(\delta x_m)_u$  is equated to the first term on the right-hand side; the remaining terms on the right-hand side constitute the truncation error, the lead term of which appears on the second line of (2-50). The magnitude of the truncation error is a function of the magnitudes of the higher-order partial derivatives in (2-50) and also of the magnitudes of the components of  $\delta \underline{x}_k$ . The applicability of linear theory is determined by the magnitude of the truncation error in relation to the permissible error in the components of  $\delta \underline{x}_D$ , the state vector at the destination.

The magnitudes of the components of  $\delta \underline{x}_k$  are determined primarily by the accuracy with which the vehicle is injected into its heliocentric orbit. The more accurate the injection guidance system, the greater is the likelihood that linear theory is acceptable for midcourse guidance.

The magnitudes of the higher-order partial derivatives depend on the reference trajectory and on the times  $t_k$  and  $t_m$ . For interplanetary missions the magnitudes are relatively high in regions close to a planet, where the nonlinear gravitational force field is strong. If times  $t_k$  and  $t_m$  are such that at neither time is the vehicle close to a planet, the truncation error is materially reduced.

The fundamental state vector in midcourse guidance is  $\delta \underline{x}_D$ . Equation (2-50) is used to determine the components of  $\delta \underline{x}_D$ . For missions in which the vehicle at its point of closest approach to the destination planet is within several planet radii of the surface of the planet, the truncation error in computing  $\delta \underline{x}_D$  by linear analysis may be reduced by selecting as the

destination point for the midcourse guidance system an earlier point on the reference trajectory, such as the point at which the reference trajectory intersects the planet's sphere of influence, and then using a separate terminal guidance scheme for final maneuvering. (The sphere of influence is that region surrounding the surface of a planet in which the planet itself, rather than the sun, should be used as the main body in Equation (2-1). A mathematical derivation of the expression for the radius of the sphere appears on Pages 234 and 235 of Plummer<sup>(29)</sup> and also on Pages 478 and 479 of Ehricke, Vol. I.<sup>(30)</sup> Ehricke refers to the sphere as the "activity sphere" rather than the "sphere of influence".)

A quantitative study of the truncation error has been reported by McLean, Schmidt, and McGee.<sup>(13)</sup> In this work the FTA correction was computed at several points on both the outbound and the inbound legs of a circumlunar trajectory. For the outbound leg the destination point is the perilune, at a lunar altitude of 2960 miles; the inbound destination point is at vacuum perigee. It is shown that the truncation error in position at the destination due to the neglect of second-order variational terms in computing the midcourse velocity correction is proportional to the square of the magnitude of the position variation  $\delta \underline{r}_C$  at the time of the correction, the proportionality factor being a function of the range  $\underline{r}_C$  (in a geocentric coordinate system). The proportionality factor is of the order of  $10^{-4}$  mi./mi.<sup>2</sup> near the two ends of either leg of the reference trajectory and is smaller in the middle, the minimum value of  $10^{-6}$  mi./mi.<sup>2</sup> occurring about two-thirds of the way out on the outbound leg. Thus, if at two-thirds of the way out, the position variation is 10,000 miles and a velocity correction is applied in accordance with linear theory, the position variation at perilune due to truncation error is approximately 100 miles. The author is not aware of any similar quantitative study of truncation error for interplanetary trajectories.

## CHAPTER 3

### LINEAR GUIDANCE THEORY FOR ELLIPTICAL REFERENCE TRAJECTORIES

#### 3.1 Summary

For the special case of two-body motion the variant motion in the plane of the reference trajectory is uncoupled from the variant motion normal to that plane. Therefore, with the proper choice of a coordinate system, each of the 3-by-3 matrices defined in the linear theory of Chapter 2 contains four elements which are identically zero for all values of time.

Two different methods are presented for solving analytically the variant equations of motion when the reference trajectory is an ellipse. The solution is used to obtain analytic expressions for the five non-zero elements of each of the 3-by-3 matrices of Chapter 2. Singularities occurring in some of the matrix elements are discussed.

#### 3.2 Introduction

The linear theory of Chapter 2 enables the solution of the variant equations of motion to be expressed by the simple matrix equation (2-8). However, the time-varying elements of the transition matrix  $\dot{C}_{mk}^*$  cannot be found analytically; numerical integration is required to evaluate the elements. In this chapter an analytic solution is obtained by imposing a limitation on the mathematical model of Chapter 2. The new limitation is the assumption that the perturbations due to the disturbing planets are negligible and therefore the resulting motion of the vehicle is two-body motion in the sun's gravitational field. This two-body approximation is deemed to be reasonably realistic for the midcourse phase of an interplanetary flight, when the vehicle's distance from the nearest planet is relatively large.

Utilization of the two-body assumption in the guidance analysis does not require that the same assumption be used in obtaining the reference trajectory. The reference trajectory is still to be obtained accurately by the numerical integration of the basic vector equation (2-1). The midcourse phase of the trajectory is then approximated by a conic section with one focus at the center of the sun, and the orbital elements

of this conic section are computed for use in the guidance analysis. However, variations measured or inferred from the analysis are variations of the actual trajectory from the numerically computed reference trajectory, not variations from the conic approximation. Thus, the primary effects of the disturbing forces are included in the analysis, but the changes in the disturbing forces due to the fact that the vehicle is not on the reference trajectory are ignored.

The assumption of two-body motion gives rise to two interesting conditions, each of which can be used to obtain an analytic solution of the variant equations of motion. The first condition is that the variant motion in the plane of the reference trajectory is independent of the variant motion normal to that plane. Because of this condition, the sixth-order system represented by Equation (2-3) can be replaced by two uncoupled systems, one of fourth order and one of second order, and both systems can be integrated analytically. The second condition is that, inasmuch as the reference trajectory is approximated by a conic section, the actual trajectory, which differs from the reference trajectory only due to a change in initial conditions, can also be approximated by a conic section, and the relation between the two trajectories can be expressed in terms of the variations of six orbital elements.

The first condition was recognized by Kierstead, (20), (21) who solved the second-order system describing the out-of-plane motion but apparently made no attempt to obtain a similar solution for the fourth-order system describing in-plane motion. The second condition was utilized by Battin in Appendix G of (5) in developing analytic expressions for an elaborate set of matrices which can be combined to yield a solution for the variant motion without the use of integration. However, the author is not aware of any previously published literature which carries out the two-body analysis, as in the succeeding sections of this chapter, to derive relatively straightforward analytic expressions for all the elements in the basic matrices of Chapter 2.

In performing the detailed analysis, only elliptical reference trajectories are considered, since these are deemed to be the only conic sections of practical importance in the midcourse phase of interplanetary transfers.

### 3.3 Coordinate Systems

The problem of selecting a coordinate system has already been discussed in Section 2.9 in connection with the numerical integration of the equations of the many-body problem. It was pointed out in that section that there is an advantage to selecting a system in which two of the three axes lie in the reference trajectory plane. This advantage is even more pronounced in the analysis of two-body motion, for now the uncoupling between in-plane and out-of-plane motion is complete, and consequently the two types of motion may be treated independently.

Appendix A describes three reference trajectory coordinate systems, each of which has been found to be useful in one phase of the development. The three are the stationary system with axes  $x y z$ , the local vertical system with axes  $r s z$ , and the flight path system with axes  $p q z$ . In all three the origin is at the center of the sun, and all have the same  $z$ -axis. In the  $x y z$  system the  $x$ -axis is in the direction of perihelion of the reference trajectory; the axes are non-rotating. In the  $r s z$  system the  $r$ -axis is in the direction of the vehicle's position vector on the reference trajectory; the  $r$  and  $s$  axes are rotating in the reference trajectory plane with angular velocity  $f$ , where  $f$  is the true anomaly (the angle between the position vector on the reference trajectory and the  $x$ -axis). In the  $p q z$  system the  $q$ -axis is parallel to the instantaneous velocity vector of the vehicle in its motion on the reference trajectory; the  $p$  and  $q$  axes rotate with angular velocity  $g$ , where  $g$  is the angle between the velocity vector and the  $y$ -axis. It may be noted that when the vehicle is at perihelion of its reference trajectory all three coordinate systems instantaneously coincide.

The  $x y z$  system is most appropriate when the problem is to be solved numerically, as in Chapter 2. The  $r s z$  system is used to obtain an analytic solution of the variant equations of motion of the two-body problem. The  $p q z$  system yields the simplest form for the analytic expressions for the elements of the basic matrices of Chapter 2.

A fourth coordinate system that might at first glance appear useful is the elliptical cylindrical coordinate system. There are some striking similarities between this system and the p q z system. Appendix D is an analysis of the elliptical system and its applicability to the guidance problem. It is concluded that this curvilinear coordinate system offers no significant advantages over the three rectilinear systems that have already been discussed.

### 3.4 Equations of Motion

For the two-body problem, the vector equation of motion, (2-1), simplifies to

$$\ddot{\underline{r}} + \frac{\mu}{r^3} \underline{r} = \underline{0}_3 \quad (3-1)$$

where  $\underline{0}_3$  is the three-dimensional zero vector. If (3-1) is regarded as describing motion along the reference trajectory, the component equations in the x y z coordinate system are

$$\begin{pmatrix} \ddot{x} \\ \ddot{y} \end{pmatrix} + \frac{\mu}{r^3} \begin{pmatrix} x \\ y \end{pmatrix} = \begin{pmatrix} 0 \\ 0 \end{pmatrix} \quad (3-2)$$

where

$$x^2 + y^2 = (r^2 \cos^2 f + r^2 \sin^2 f) = r^2 \quad (3-3)$$

In the r s z coordinate system the component equations are

$$\begin{pmatrix} \ddot{r} - r \dot{f}^2 \\ r \ddot{f} + 2 \dot{r} \dot{f} \end{pmatrix} + \frac{\mu}{r^3} \begin{pmatrix} r \\ 0 \end{pmatrix} = \begin{pmatrix} 0 \\ 0 \end{pmatrix} \quad (3-4)$$

No z-axis equation is required because the coordinate systems have been defined in such a manner that the motion is confined to the plane perpendicular to the z-axis; i.e., z is identically zero for all values of t.



Equations (3-4) can be integrated directly. A single integration of the lower equation yields

$$r^2 \dot{f} = h \quad (3-5)$$

The constant  $h$  is the orbital angular momentum of the space vehicle per unit mass. (3-5) is used in integrating the upper equation of (3-4). The result is

$$r = \frac{h^2/\mu}{1 + e \cos f} \quad (3-6)$$

(3-5) and (3-6) constitute the familiar solution of two-body motion. (3-6) is the general equation of a conic section with the origin at one focus and the line  $f = 0$  coinciding with the major axis of the conic.

These relations, as well as many more that are useful in celestial mechanics, are discussed in Appendix B. Appendix C, which has no direct bearing on the main subject matter of this thesis, describes two interesting graphical constructions which evolved from the formulations for elliptical motion in Appendix B.

The vector form of the variant equations of motion for the two-body problem, corresponding to (2-3) and (2-4) for the  $n$ -body problem, is

$$\ddot{\underline{r}} = \overset{*}{G} \underline{r} \quad (3-7)$$

with

$$\overset{*}{G} = \frac{\mu}{r^5} (3 \underline{r} \underline{r}^T - \underline{r}^T \underline{r} \overset{*}{I}_3) \quad (3-8)$$

Equation (3-7), like (3-1), is most easily integrated when the component equations are expressed in the  $r$   $s$   $z$  coordinate system. In this system  $\overset{*}{G}$  is a diagonal matrix.

$$\ddot{\mathbf{G}}^* = \frac{\mu}{r^3} \begin{pmatrix} 2 & 0 & 0 \\ 0 & -1 & 0 \\ 0 & 0 & -1 \end{pmatrix} \quad (3-9)$$

The component equations are simplified if  $\delta f$  is used in place of  $\delta s$ .

$$\delta s = r \delta f \quad (3-10)$$

Then the three equations to be integrated are

$$\begin{pmatrix} \delta \ddot{r} - \dot{f}^2 \delta r - 2r\dot{f}\delta \dot{f} \\ 2\dot{f}\delta \dot{r} + \ddot{f}\delta r + r\delta \ddot{f} + 2\dot{r}\delta \dot{f} \\ \delta \ddot{z} \end{pmatrix} = \frac{\mu}{r^3} \begin{pmatrix} 2\delta r \\ 0 \\ -\delta z \end{pmatrix} \quad (3-11)$$

The detailed derivation of (3-11) is presented in Appendix E and Section G.2 of Appendix G.

The uncoupling effect mentioned previously is brought out by (3-11). The first two equations, involving the dependent variables  $\delta r$  and  $\delta f$ , are not coupled to the third equation, in which  $\delta z$  is the only dependent variable.

### 3.5 Variant Motion Normal to the Reference Trajectory Plane

The z-axis equation of (3-11) may be written as

$$\delta \ddot{z} + \frac{\mu}{r^3} \delta z = 0 \quad (3-12)$$

Comparison of (3-12) with (3-2) indicates that  $x$  and  $y$  are independent solutions for  $\delta z$ .

$$\delta z = K_1 x + K_2 y \quad (3-13)$$

$$= r (K_1 \cos f + K_2 \sin f) \quad (3-14)$$

$$= (K_1^2 + K_2^2)^{1/2} r \sin \left( f + \tan^{-1} \frac{K_1}{K_2} \right) \quad (3-15)$$

where  $K_1$  and  $K_2$  are arbitrary constants.

This simple solution for the variant motion normal to the reference trajectory plane is independent of the nature of the two-body reference trajectory; the reference trajectory may be elliptical, parabolic, or hyperbolic.

### 3.6 Integration of the Variant Equations for Elliptical Reference Trajectories

The integration of the first two equations of (3-11) is carried out in Sections G.3 and G.4. The two equations constitute a fourth-order system in  $\delta r$  and  $\delta f$ . The first of the four independent solutions can be obtained directly by virtue of the fact that  $\delta f$  does not appear explicitly in either equation. It is apparent that both equations are satisfied if  $\delta f$  is a constant and  $\delta r$  is identically zero. Thus, the first solution is

$$\delta r = 0 \quad \delta f = k_1 \quad (3-16)$$

where  $k_1$  is an arbitrary constant.

If the independent variable in the two equations is changed from the time  $t$  to the true anomaly  $f$  and the two equations are combined, the following third-order equation is obtained:

$$[(1 + e \cos f) F - (3 e \sin f)] (F^2 + 1) \delta r = 0 \quad (3-17)$$

where  $F$  represents the operator  $d/df$  and  $e$  is the eccentricity of the reference trajectory. Two more solutions for  $\delta r$  follow immediately from

$$(F^2 + 1) \delta r = 0 \quad (3-18)$$

These are

$$\delta r = k_2 \cos f \quad (3-19)$$

$$\delta r = k_3 \sin f \quad (3-20)$$

The corresponding solutions for  $\delta f$  are

$$\delta f = - \frac{k_2}{a(1-e^2)} (2 + e \cos f) \sin f \quad (3-21)$$

$$\delta f = \frac{k_3}{a(1-e^2)} (2 + e \cos f) \cos f \quad (3-22)$$

To obtain the fourth solution, the new variable  $x$  is introduced, where

$$x = (F^2 + 1) \delta r \quad (3-23)$$

Then, Equation (3-17) becomes

$$(1 + e \cos f) \frac{dx}{df} - (3 e \sin f) x = 0 \quad (3-24)$$

After the variables  $x$  and  $f$  are separated, the equation is integrated, with the result

$$x = \frac{C}{(1 + e \cos f)^3} \quad (3-25)$$

$C$  is another integration constant. The method of variation of parameters is used to solve (3-25) for the fourth solution of  $\delta r$ . After considerable mathematical manipulation, all of which is explained in

Section G.4, the solution is

$$\delta r = k_4 \left[ -\frac{3 e M \sin f}{2 (1 - e^2)^{3/2}} + \frac{1}{1 + e \cos f} \right] \quad (3-26)$$

where M is the mean anomaly. For this value of  $\delta r$ ,  $\delta f$  is

$$\delta f = -\frac{3 k_4}{2 a (1 - e^2)^{5/2}} M (1 + e \cos f)^2 \quad (3-27)$$

Section G.5 presents a method of solution of the z-axis equation of (3-11) which is less direct than that given in Section 3.5. The solution in G.5 involves the substitution of the eccentric anomaly E for the time t as the independent variable. The differential equation becomes

$$[(1 - e \cos E) J^2 - (e \sin E) J + 1] \delta z = 0 \quad (3-28)$$

where J signifies the operator  $d/dE$ . The two independent solutions for  $\delta z$  are

$$\delta z = \frac{k_5}{(1 - e^2)^{1/2}} \sin E = k_5 \frac{\sin f}{1 + e \cos f} \quad (3-29)$$

$$\delta z = \frac{k_6}{(1 - e^2)} (\cos E - e) = k_6 \frac{\cos f}{1 + e \cos f} \quad (3-30)$$

Since the radius r is proportional to  $1/(1 + e \cos f)$ , it is apparent that the second forms of (3-29) and (3-30) are consistent with the solution of (3-14).

The results of this section may be combined to give the complete homogeneous solution of the equations of (3-11), the dependent variables  $\delta r$ ,  $\delta s$ , and  $\delta z$  being expressed in terms of the anomalies f and M.

$$\begin{aligned} \delta r = & k_2 \cos f + k_3 \sin f \\ & + k_4 \left[ -\frac{3 e M \sin f}{2 (1 - e^2)^{3/2}} + \frac{1}{1 + e \cos f} \right] \end{aligned} \quad (3-31)$$

$$\delta s = \frac{k_1 a (1 - e^2)}{1 + e \cos f} - \frac{k_2 (2 + e \cos f) \sin f}{1 + e \cos f} + \frac{k_3 (2 + e \cos f) \cos f}{1 + e \cos f} - \frac{3 k_4 M (1 + e \cos f)}{2 (1 - e^2)^{3/2}} \quad (3-32)$$

$$\delta z = \frac{k_5 \sin f}{1 + e \cos f} + \frac{k_6 \cos f}{1 + e \cos f} \quad (3-33)$$

### 3.7 Solution by Variation of the Orbital Elements of the Elliptical Reference Trajectory

The past few sections have presented a method of determining position along the actual trajectory by formulating and then integrating the differential equations of the variant motion. A second method, to be presented in this section, follows a different procedure. The basic vector equation of two-body motion, (3-1), is integrated, the result being the familiar conic section. The solution for position on the actual trajectory is obtained by finding the effect on position at any given time of small variations in each of the six orbital elements characterizing the basic conic section. Whereas the first method involves taking variations and then integrating, the second method involves integrating and then taking variations. A detailed analysis of the second method appears in Appendix H.

The fundamental premise of the second method is that the actual trajectory, like the reference trajectory, is an ellipse and that the two ellipses lie close to each other in space. To distinguish quantities on the actual trajectory from the corresponding quantities on the reference trajectory, a prime will be added to each symbol referring to the actual trajectory. Thus, the position variation  $\delta \underline{r}$  is

$$\delta \underline{r} = \underline{r}' - \underline{r} \quad (3-34)$$

The six orbital elements whose variations are to be investigated are the semi-major axis length  $a$ , the eccentricity  $e$ , the longitude of the ascending node  $\Omega$ , the inclination  $i$ , the latitude of perihelion  $\omega$ , and the time of perihelion passage  $t_0$ . These elements are discussed in Section B.6. Later the longitude of perihelion  $\phi$  is substituted for  $\omega$ , and the mean anomaly  $M_0$  at epoch is substituted for  $t_0$ .

$$\phi = \Omega + \omega \quad (3-35)$$

$$M_0 = -n t_0 \quad (3-36)$$

where  $n$  is the mean angular motion, i.e., the mean angular velocity of the space vehicle in its elliptical orbit about the sun.

The basic analysis is applicable to all elliptical reference trajectories for which the eccentricity is not very close to either zero or one.

As shown in Figure H.1, the orientation of the actual trajectory with respect to the reference trajectory is defined by the three angles  $\delta \Omega$ ,  $\delta i$ , and  $\delta \omega$ . The angles  $\delta \Omega$  and  $\delta \omega$  need not be small, but their sum, which is equal to  $\delta \phi$ , is a small angle. The angle  $\delta i$  is always small. The variation in true anomaly,  $\delta f$ , although time-varying, is also small.

The components of  $\underline{r}'$  along the  $r$ ,  $s$ , and  $z$  axes are designated  $r'_r$ ,  $r'_s$ , and  $r'_z$ , respectively. The components of  $\underline{r}$  along these axes are, by definition,  $r$ , 0, and 0. From Figure H.1, the effect of variations in the orientation angles on the components of  $\delta \underline{r}$  are

$$\begin{aligned} \delta r &= r'_r - r \\ &= r' [\cos (f' + \delta \omega) \cos (f - \delta \Omega) \\ &\quad + \sin (f' + \delta \omega) \cos \delta i \sin (f - \delta \Omega)] - r \\ &= r' \cos (\delta f + \delta \phi) - r \\ &= r' - r \end{aligned} \quad (3-37)$$

$$\delta s = r'_s - 0$$

$$\begin{aligned}
 &= r' [-\cos(f' + \delta\omega) \sin(f - \delta\Omega) \\
 &\quad + \sin(f' + \delta\omega) \cos\delta i \cos(f - \delta\Omega)] \\
 &= r' \sin(\delta f + \delta\phi) \\
 &= r(\delta f + \delta\phi)
 \end{aligned} \tag{3-38}$$

$$\delta z = r'_z - 0$$

$$\begin{aligned}
 &= r' \sin(f' + \delta\omega) \sin\delta i \\
 &= r \delta i \sin(f - \delta\Omega)
 \end{aligned} \tag{3-39}$$

In these relations the usual small-angle approximations have been applied to  $\delta\phi$ ,  $\delta i$ , and  $\delta f$ . Also, second-order terms in the small variational quantities have been neglected, the small quantities consisting of  $(\delta r/r)$  in addition to the angles just cited.

Comparison of (3-39) with (3-15) indicates that

$$(K_1^2 + K_2^2)^{1/2} = \delta i \tag{3-40}$$

$$\tan^{-1} \frac{K_1}{K_2} = -\delta\Omega \tag{3-41}$$

The analysis presented below for determining the effects of  $\delta a$ ,  $\delta e$ , and  $\delta t_0$  on  $\delta \underline{r}$  differs from the basic presentation in Appendix H in that the former is applicable only to ellipses of "moderate" eccentricity (the only practical ones for interplanetary transfers to neighboring planets), while the latter can be used in the circular or nearly circular case as well as in the case of moderate eccentricity. The restriction to moderate eccentricity simplifies the analysis considerably.



For ellipses of moderate eccentricity, linear theory requires that the angular variations  $\delta E$ ,  $\delta M$ , and  $\delta M_0$ , like  $\delta f$ , be small angles.

The analysis proceeds as follows:

1.  $\delta r$  is expressed as a function of  $\delta a$ ,  $\delta e$ , and  $\delta f$ .
2.  $\delta r$  is expressed as a function of  $\delta a$ ,  $\delta e$ , and  $\delta E$ .
3. By equating the two expressions for  $\delta r$ , a relation is found between  $\delta f$  and  $\delta E$ .
4. Kepler's equation and Kepler's third law are used to find  $\delta E$  as a function of  $\delta a$ ,  $\delta e$ , and  $\delta t_0$ .
5. The expression for  $\delta E$  is substituted into the expressions for  $\delta r$  and  $\delta f$  to obtain final relations for  $\delta r$  and  $\delta s$  in terms of variations in the orbital elements.

From the basic equation

$$r = \frac{a(1 - e^2)}{1 + e \cos f} \quad (3-42)$$

$\delta r$  becomes

$$\delta r = r' - r$$

$$\begin{aligned} &= \frac{(a + \delta a) [1 - (e + \delta e)^2]}{1 + (e + \delta e) \cos (f + \delta f)} - \frac{a(1 - e^2)}{1 + e \cos f} \\ &= a \left[ \frac{(1 - e^2 - 2e\delta e) + (1 - e^2) \frac{\delta a}{a}}{1 + e \cos f - e \sin f \delta f + \cos f \delta e} - \frac{1 - e^2}{1 + e \cos f} \right] \end{aligned}$$

(equation continued on next page)

$$\begin{aligned}
&= \frac{a}{1+e \cos f} \left\{ \left[ (1-e^2 - 2e \delta e) + (1-e^2) \frac{\delta a}{a} \right] \right. \\
&\quad \left. , \left[ 1 + \frac{e \sin f \delta f - \cos f \delta e}{1+e \cos f} \right] - (1-e^2) \right\} \\
&= \frac{a}{1+e \cos f} \left[ (1-e^2) \frac{\delta a}{a} - \left( e + \frac{\cos f + e}{1+e \cos f} \right) \delta e \right. \\
&\quad \left. + \frac{(1-e^2) e \sin f}{1+e \cos f} \delta f \right] \tag{3-43}
\end{aligned}$$

The expression for  $r$  in terms of  $E$  is

$$r = a (1 - e \cos E) \tag{3-44}$$

Then  $\delta r$  is

$$\begin{aligned}
\delta r &= (a + \delta a) [1 - (e + \delta e) \cos (E + \delta E)] \\
&\quad - a (1 - e \cos E) \\
&= (a + \delta a) (1 - e \cos E + e \sin E \delta E - \cos E \delta e) \\
&\quad - a (1 - e \cos E) \\
&= a \left[ (1 - e \cos E) \frac{\delta a}{a} - \cos E \delta e + e \sin E \delta E \right] \\
&= \frac{a}{1+e \cos f} \left[ (1-e^2) \frac{\delta a}{a} - (\cos f + e) \delta e \right. \\
&\quad \left. + (1-e^2)^{1/2} e \sin f \delta E \right] \tag{3-45}
\end{aligned}$$

When (3-43) is equated to (3-45),

$$\begin{aligned}
\delta f &= \frac{1+e \cos f}{(1-e^2) e \sin f} \left[ \left( e + \frac{\cos f + e}{1+e \cos f} - \cos f - e \right) \delta e \right. \\
&\quad \left. + (1-e^2)^{1/2} e \sin f \delta E \right] \\
&= \frac{\sin f}{1-e^2} \delta e + \frac{1+e \cos f}{(1-e^2)^{1/2}} \delta E \tag{3-46}
\end{aligned}$$

Two expressions for the mean anomaly can be obtained from the definition of mean anomaly and from Kepler's equation.

$$M = n (t - t_0) = E - e \sin E \quad (3-47)$$

The variation in  $M$  is

$$\begin{aligned} \delta M &= (n + \delta n) (t - t_0 - \delta t_0) - n (t - t_0) \\ &= (E + \delta E) - (e + \delta e) \sin (E + \delta E) \\ &\quad - E + e \sin E \end{aligned} \quad (3-48)$$

(3-48) is solved for  $\delta E$ .

$$\delta E = \frac{1}{1 - e \cos E} [(t - t_0) \delta n - n \delta t_0 + \sin E \delta e] \quad (3-49)$$

$\delta n$  can be expressed in terms of  $\delta a$  by means of Kepler's third law of planetary motion.

$$\mu = n^2 a^3 \quad (3-50)$$

Since  $\mu$  is invariant,

$$\delta \mu = 0 = 2 n a^3 \delta n + 3 n^2 a^2 \delta a \quad (3-51)$$

$$\delta n = -\frac{3}{2} n \frac{\delta a}{a} \quad (3-52)$$

Then  $\delta E$  becomes

$$\delta E = \frac{1 + e \cos f}{1 - e^2} \left( -\frac{3}{2} M \frac{\delta a}{a} - n \delta t_0 \right) + \frac{\sin f}{(1 - e^2)^{1/2}} \delta e \quad (3-53)$$

This expression is substituted into (3-45) and (3-46) to yield equations for  $\delta r$  and  $\delta s$  in terms of  $(\delta a/a)$ ,  $n \delta t_o$ ,  $\delta e$ , and  $\delta \phi$ , with the time-varying quantities being  $f$  and  $M$ . The parameters representing the variations of the orbital elements have been arranged such that they are all non-dimensional. The final equations for the components of  $\delta \underline{r}$  are

$$\delta r = a \left[ \left( \frac{1 - e^2}{1 + e \cos f} - \frac{3 M e \sin f}{2 (1 - e^2)^{1/2}} \right) \frac{\delta a}{a} - \frac{e \sin f}{(1 - e^2)^{1/2}} n \delta t_o - \cos f \delta e \right] \quad (3-54)$$

$$\delta s = a \left[ - \frac{3 M (1 + e \cos f)}{2 (1 - e^2)^{1/2}} \frac{\delta a}{a} - \frac{(1 + e \cos f)}{(1 - e^2)^{1/2}} n \delta t_o + \left( \frac{2 + e \cos f}{1 + e \cos f} \right) \sin f \delta e + \frac{(1 - e^2)}{(1 + e \cos f)} \delta \phi \right] \quad (3-55)$$

$$\delta z = \frac{a (1 - e^2)}{1 + e \cos f} (\sin f \delta i \cos \delta \Omega - \cos f \delta i \sin \delta \Omega) \quad (3-56)$$

It is shown in Section H.7 that the six constants of integration in (3-31), (3-32), and (3-33) can be written in terms of the variations in the orbital elements, and therefore the two methods of solution of the problem of the variant motion of the space vehicle are mathematically equivalent. The conclusion that can be drawn is that, in the solution for the deviation of the actual trajectory from the reference trajectory caused by small variations in initial conditions, the processes of integration and taking of first variations are commutative.

### 3.8 Variation in Position, Velocity, and Acceleration

The time-varying elements of Equations (3-54), (3-55), and (3-56) can be expressed in terms of the components of position and velocity along the reference trajectory by the use of the standard relations developed in Appendix B. The components of velocity variation  $\delta \underline{v}$  are obtained by differentiating  $\delta \underline{r}$ , and the components of variation in acceleration  $\delta \underline{a}$  are obtained by differentiating  $\delta \underline{v}$ . All of these results are contained in the following three vector equations, the details of which are developed in Appendix I.

$$\begin{aligned} \delta \underline{r} = & \left( \underline{r} \underline{u}_r - \frac{3}{2} \underline{v} t \underline{u}_q \right) \frac{\delta a}{a} + \frac{\underline{v}}{n} \underline{u}_q \delta M_o \\ & + \left( \frac{\underline{y}}{1 - e^2} \underline{u}_s - a \underline{u}_x \right) \delta e + r \underline{u}_s \delta \phi \\ & + r \sin (f - \delta \Omega) \delta i \underline{u}_z \end{aligned} \quad (3-57)$$

$$\begin{aligned} \delta \underline{v} = & \left( -\frac{\underline{v}}{2} \underline{u}_q - \frac{3}{2} a_r t \underline{u}_r \right) \frac{\delta a}{a} + \frac{a_r}{n} \underline{u}_r \delta M_o \\ & + \left( \frac{-\underline{v} \sin f \underline{u}_p + \underline{v}_s \cos f \underline{u}_s}{1 - e^2} \right) \delta e - \underline{v} \underline{u}_p \delta \phi \\ & + \underline{v} \cos (g - \delta \Omega) \delta i \underline{u}_z \end{aligned} \quad (3-58)$$

$$\begin{aligned} \delta \underline{a} = & \frac{\mu}{r^3} \left\{ \left[ (2r - 3\underline{v}_r t) \underline{u}_r + \frac{3}{2} \underline{v}_s t \underline{u}_s \right] \frac{\delta a}{a} \right. \\ & + \frac{1}{n} (2\underline{v}_r \underline{u}_r - \underline{v}_s \underline{u}_s) \delta M_o \\ & - \left[ 2a \cos f \underline{u}_r + \left( \frac{\underline{y}}{1 - e^2} + a \sin f \right) \underline{u}_s \right] \delta e \\ & \left. - r \underline{u}_s \delta \phi - r \sin (f - \delta \Omega) \delta i \underline{u}_z \right\} \end{aligned} \quad (3-59)$$

$$\begin{pmatrix} \delta r \\ \delta s \\ \delta z \\ \delta v_r \\ \delta v_s \\ \delta v_z \\ \delta a_r \\ \delta a_s \\ \delta a_z \end{pmatrix} = \begin{bmatrix} r - \frac{3}{2} v_r t & \frac{v_r}{n} & -a \cos f & 0 & 0 & 0 \\ -\frac{3}{2} v_s t & \frac{v_s}{n} & \frac{y}{1-e^2} + a \sin f & r & 0 & 0 \\ 0 & 0 & 0 & 0 & y & -x \\ -\frac{v_r}{2} - \frac{3}{2} a_r t & \frac{a_r}{n} & -\frac{v_s \sin f}{1-e^2} & -v_s & 0 & 0 \\ -\frac{v_s}{2} & 0 & \frac{v_y}{1-e^2} & v_r & 0 & 0 \\ 0 & 0 & 0 & 0 & v_y & -v_x \\ \left( \frac{\mu}{r^3} \right. & 2r - 3v_r t & -2a \cos f & 0 & 0 & 0 \\ \left. \frac{3}{2} v_s t \right) & -\frac{v_s}{n} & -\frac{y}{1-e^2} - a \sin f & -r & 0 & 0 \\ 0 & 0 & 0 & 0 & -y & x \end{bmatrix} \begin{pmatrix} \frac{\delta a}{a} \\ \delta M_0 \\ \delta e \\ \delta \phi \\ \delta i \cos \delta \Omega \\ \delta i \sin \delta \Omega \end{pmatrix}$$

(3-61)

In these equations  $\underline{u}$  represents a unit vector, with the appended subscript indicating its direction.  $v_r$  and  $v_s$  are the r-direction and s-direction components of the orbital velocity vector  $\underline{v}$ .  $a_r$  is the radial component of acceleration; it is equal to the magnitude of the acceleration vector  $\ddot{\underline{r}}$ .

$$a_r = -\frac{\mu}{r^2} \quad (3-60)$$

Equation (3-61) is a composite matrix equation presenting the components of  $\delta \underline{r}$ ,  $\delta \underline{v}$ , and  $\delta \underline{a}$  in the r s z coordinate system. The symbols  $v_x$  and  $v_y$ , introduced in this equation, are the components of  $\underline{v}$  in the x and y directions, respectively.

A comparison of the last three rows of (3-61) with the first three rows indicates that (3-7), in conjunction with (3-9), is satisfied by the solution obtained for  $\delta \underline{r}$ .

It may be noted that, of the fifty-four terms in the 9-by-6 matrix of (3-61), twenty-seven, half of the total number, are equal to zero.

### 3.9 Discussion of Effects of Variations in Orbital Elements

Some insight into the geometric and dynamic effects of variations of the orbital elements on the position and velocity of the space vehicle may be gained from Equations (3-57), (3-58), and (3-61), and Figures 3.1 to 3.5. The lack of coupling between the variant motion in the reference trajectory plane and the variant motion normal to that plane is indicated by the equations; position and velocity in the plane are affected only by variations in the elements  $a$ ,  $M_0$ ,  $e$ , and  $\phi$ , while position and velocity in the z direction are affected only by variations of the other two elements,  $\Omega$  and  $i$ .

In the following paragraphs the effect of a positive variation in each of the orbital elements will be investigated. Because of the linearity assumption, negative variations of the elements produce effects that are exactly opposite to their positive counterparts. (In this context, the out-of-plane "elements" are  $\delta i \cos \delta \Omega$  and  $\delta i \sin \delta \Omega$ .)

The effect of a positive ( $\delta a/a$ ) is illustrated in Figure 3.1. There are two distinct components, one geometric and the other dynamic in origin. The geometric effect is manifested by a change in size, but not in shape, of the elliptical trajectory. All linear dimensions on the actual trajectory are in the ratio  $1 + (\delta a/a)$  to the corresponding dimensions on the reference trajectory. The two trajectories are confocal rather than concentric, since the attractive focus (i.e., the center of the sun) is the only point directly related to the reference orbit that cannot be affected by any variations.

The geometric effect on position can be derived very simply from Equation (3-44). Since  $e$  and  $E$  are independent of  $\delta a$ ,

$$\frac{\delta r}{r} = \frac{\delta a}{a} \quad (3-62)$$

Then the ratio of the magnitude of  $r'$  to the magnitude of  $r$  is

$$\frac{r'}{r} = \frac{r + \delta r}{r} = 1 + \frac{\delta r}{r} = 1 + \frac{\delta a}{a} \quad (3-63)$$

The increased size of the elliptical trajectory reduces the magnitude of the velocity vector. This is readily seen from the vis viva integral.

$$v^2 = \mu \left( \frac{2}{r} - \frac{1}{a} \right) \quad (3-64)$$

$$= \frac{\mu}{a} \left( \frac{1 + e \cos E}{1 - e \cos E} \right) \quad (3-65)$$

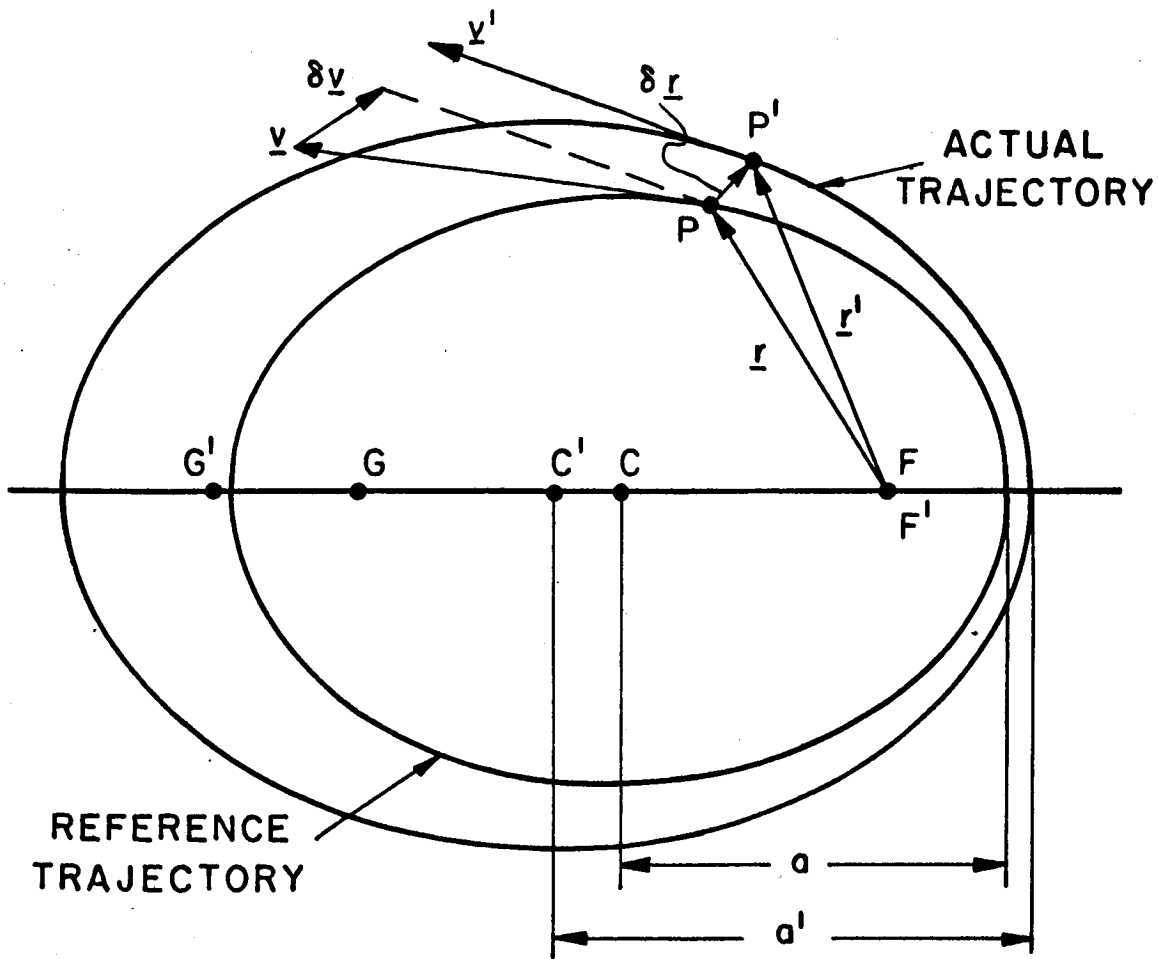
Since  $\mu$  is invariant and  $e$  and  $E$  are independent of  $\delta a$ ,

$$\left( \frac{v'}{v} \right)^2 = \left( \frac{v + \delta v}{v} \right)^2 = \frac{a}{a'} = \frac{a}{a + \delta a} \quad (3-66)$$

$$1 + 2 \frac{\delta v}{v} = \frac{1}{1 + \frac{\delta a}{a}} = 1 - \frac{\delta a}{a} \quad (3-67)$$

$$\frac{\delta v}{v} = -\frac{1}{2} \frac{\delta a}{a} \quad (3-68)$$





Unprimed capital letters apply to reference trajectory.

Primed capital letters apply to actual trajectory.

$F, F'$  — common attractive focus of two trajectories

$C, C'$  — centers of two trajectories

$G, G'$  — vacant foci of two trajectories

$P, P'$  — position on two trajectories at time  $t$

$\delta a = a' - a =$  variation in length of semi-major axis

$\delta \underline{r} = \underline{r}' - \underline{r} =$  variation in position

$\delta \underline{v} = \underline{v}' - \underline{v} =$  variation in velocity

Figure 3.1 Effect of  $\delta a$ , Variation in Length of Semi-Major Axis

The dynamic effect of  $(\delta a/a)$  is a consequence of Kepler's third law of planetary motion, which states that the squares of the periods of the planetary orbits are proportional to the cubes of their mean distances from the sun. Since the period  $P$  is inversely proportional to the mean angular motion  $n$ , the following expression for  $\delta P$  is obtained from (3-52):

$$\frac{\delta P}{P} = - \frac{\delta n}{n} = \frac{3}{2} \frac{\delta a}{a} \quad (3-69)$$

Thus, increasing the length of the semi-major axis increases the period of the elliptical motion and consequently causes a retardation in position. From (3-57), the position change is

$$- \frac{3}{2} v t \frac{\delta a}{a} \underline{u}_q = - v t \frac{\delta P}{P} \underline{u}_q \quad (3-70)$$

Unlike all the other variational effects, which are either periodic in time or constant, the dynamic effect of  $(\delta a/a)$  increases in magnitude continuously with elapsed time. If the space vehicle makes several circuits of the sun, the total change in position between two times that are exactly one period of the reference trajectory apart is

$$\begin{aligned} \delta \underline{r}(t + P) - \delta \underline{r}(t) &= - v \delta P \underline{u}_q \\ &= - 3 \pi \frac{v}{n} \frac{\delta a}{a} \underline{u}_q \end{aligned} \quad (3-71)$$

This position retardation is parallel to the local reference velocity vector  $\underline{v}$ .

The velocity change due to the dynamic effect is

$$- \frac{3}{2} a_r t \frac{\delta a}{a} \underline{u}_r = - a_r t \frac{\delta P}{P} \underline{u}_r \quad (3-72)$$

Since  $a_r$  is a negative quantity, a positive  $(\delta a/a)$  causes a change in  $\underline{v}$  in the positive  $r$  direction. This effect can be seen qualitatively in Figure 3.1. The position retardation due to  $(\delta a/a)$  causes  $\underline{v}'$  to be rotated clockwise relative to  $\underline{v}$ , thereby producing a positive component of  $\delta \underline{v}$  in the  $r$  direction. The velocity equation corresponding to (3-71) is

$$\begin{aligned}
\delta \underline{v}(t + P) - \delta \underline{v}(t) &= - a_r \delta P \underline{u}_r \\
&= - 3 \pi \frac{a_r}{n} \frac{\delta a}{a} \underline{u}_r = \frac{3 \pi \mu}{n r^2} \frac{\delta a}{a} \underline{u}_r
\end{aligned} \tag{3-73}$$

It may be noted that the geometric component of  $(\delta a/a)$  changes the magnitude of  $\underline{r}$  and  $\underline{v}$  but has no effect on their directions, while the dynamic component causes a position change in the direction of the reference velocity vector and a velocity change in the direction of the reference acceleration vector, which is also the direction of the reference position vector.

Figure 3.2 indicates the effect of a positive variation of mean anomaly at epoch. The actual trajectory coincides with the reference trajectory. The position and velocity of the vehicle on the actual trajectory at time  $t$  are those that it would have at a slightly later time if it were on the reference trajectory.

The mathematical explanation of this effect is straightforward. From (3-36), since  $n$  is independent of  $\delta M_o$ ,

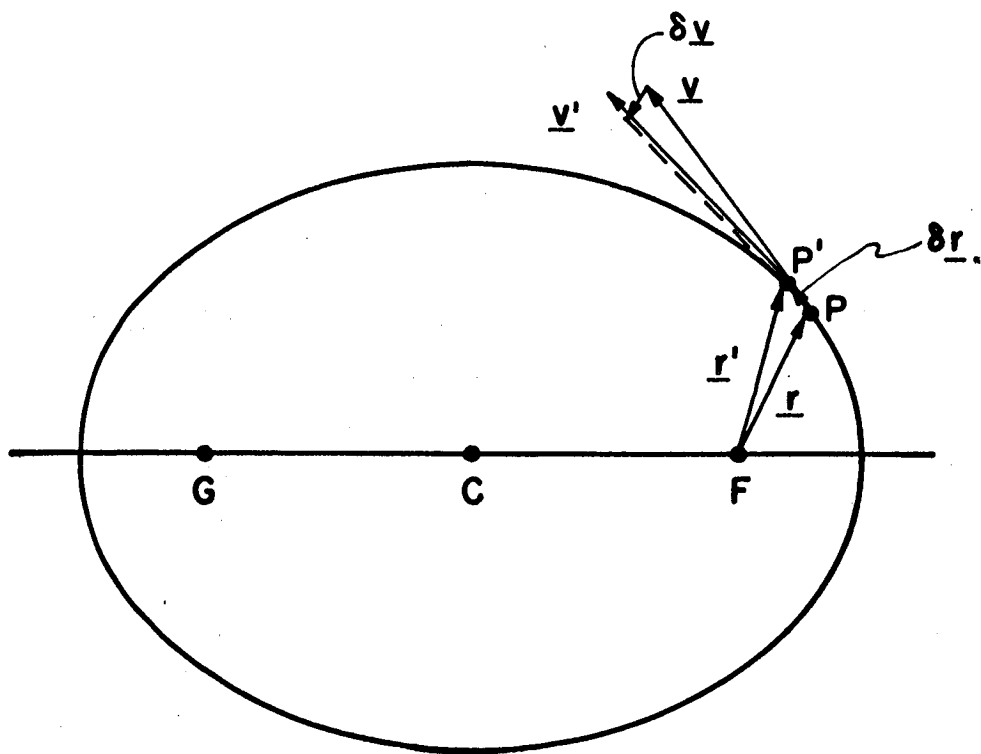
$$\frac{\partial t_o}{\partial M_o} = - \frac{1}{n} \tag{3-74}$$

Thus, when  $M_o$  is the only orbital element of those appearing in (3-57) and (3-58) to experience a variation, the variations in position and velocity are

$$\frac{\partial \underline{r}}{\partial M_o} \delta M_o = \frac{v}{n} \delta M_o \underline{u}_q = - v \delta t_o \underline{u}_q \tag{3-75}$$

$$\frac{\partial \underline{v}}{\partial M_o} \delta M_o = \frac{a_r}{n} \delta M_o \underline{u}_q = - a_r \delta t_o \underline{u}_q \tag{3-76}$$

The positive  $\delta M_o$  signifies that at epoch (i.e., at  $t = 0$ ) the actual mean anomaly is slightly more positive than the reference mean anomaly. Correspondingly, the vehicle actually passes perihelion ( $M = 0$ ) at a time slightly earlier than the time  $t_o$  at which it would have passed



Reference trajectory and actual trajectory coincide.

F – attractive focus

C – center

G – vacant focus

P – reference position at time t

P' – actual position at time t

$\delta M_0$  = variation in mean anomaly at epoch

$\delta \underline{r} = \underline{r}' - \underline{r}$  = variation in position

$\delta \underline{v} = \underline{v}' - \underline{v}$  = variation in velocity

Figure 3.2 Effect of  $\delta M_0$ , Variation in Mean Anomaly at Epoch

if it were on the reference trajectory. Therefore  $t_0'$ , the actual time of perihelion passage, is less positive than  $t_0$ , and  $\delta t_0$ , which is equal to  $(t_0' - t_0)$ , is negative, as indicated in (3-74). Since the time interval between the vehicle's actual state and its reference state is shown by (3-75) and (3-76) to remain fixed at  $\delta t_0$  for all values of elapsed time, the actual position and velocity vectors may be related to the reference vectors as follows:

$$\underline{r}'(t) = \underline{r}(t - \delta t_0) \quad (3-77)$$

$$\underline{v}'(t) = \underline{v}(t - \delta t_0) \quad (3-78)$$

The effect of an increase in eccentricity, shown in Figure 3.3, is somewhat more complex than the effect of variations of any of the other elements. The elliptical trajectory undergoes both a translation and a distortion. The translation is a shift parallel to the major axis in the direction of aphelion, with the attractive focus remaining fixed. This is indicated by the term  $-a \delta e \underline{u}_x$  in (3-57). Geometrically, it can be explained by the fact that the perihelion distance is changed from  $a(1 - e)$  to  $a(1 - e - \delta e)$  and the aphelion distance is changed from  $a(1 + e)$  to  $a(1 + e + \delta e)$ ; thus, both perihelion and aphelion are shifted an amount  $a \delta e$  in the negative  $x$  direction.

The distortion effect produces the reduction in the length of the ordinates of the ellipse that is required by the increase in eccentricity. The first term in the coefficient of  $\delta e$  in (3-57) is the mathematical expression for the distortion. Its physical meaning is clarified if it is expanded as follows:

$$\frac{y}{1 - e^2} \underline{u}_s \delta e = \left( -\frac{y \sin f}{1 - e^2} \underline{u}_x + \frac{y \cos f}{1 - e^2} \underline{u}_y \right) \delta e \quad (3-79)$$

Since  $y = 0$  at both perihelion and aphelion, neither point is affected by the distortion. Because  $y \sin f$  is non-negative, all other points on the reference trajectory are displaced in the negative  $x$  direction; this displacement is in addition to the fixed shift that has already been noted. The  $y$  coordinate is increased in magnitude on the perihelion side of the attractive focus and decreased in magnitude on the aphelion side.

The computation of the change in the length of the semi-minor axis  $b$  can be used to illustrate the way in which (3-79) provides the required distortion. The eccentric anomaly  $E$  corresponding to the positive semi-minor axis is  $90^\circ$ . The length of the semi-minor axis is

$$b = a (1 - e^2)^{1/2} \quad (3-80)$$

The variation of  $b$  due to a variation in  $e$  can be obtained quite simply from (3-80) without recourse to (3-79).

$$\frac{\partial b}{\partial e} \delta e = - \frac{a e}{(1 - e^2)^{1/2}} \delta e \quad (3-81)$$

The same result can be derived from (3-79) by first determining the variation of any value of  $y$  due to  $\delta e$  and making use of the relations in Section B.8.

$$\frac{\partial y}{\partial e} \delta e = \frac{y \cos f}{1 - e^2} \delta e = \frac{a \sin E (\cos E - e)}{(1 - e^2)^{1/2} (1 - e \cos E)} \delta e \quad (3-82)$$

The variation in  $b$  is then obtained by substituting  $E = 90^\circ$  into (3-82).

$$\frac{\partial b}{\partial e} \delta e = - \frac{a e}{(1 - e^2)^{1/2}} \delta e \quad (3-83)$$

As a final note on the effect of  $\delta e$  on  $\delta \underline{r}$ , the coefficient of  $\delta e$  in (3-57) will be derived directly from the relations for  $x$  and  $y$  in terms of  $E$  given in Section B.8. On the reference trajectory,

$$\begin{aligned} \underline{r} &= x \underline{u}_x + y \underline{u}_y \\ &= a (\cos E - e) \underline{u}_x + a (1 - e^2)^{1/2} \sin E \underline{u}_y \end{aligned} \quad (3-84)$$

The variation in  $\underline{r}$  due to  $\delta e$  is

$$\begin{aligned} \frac{\partial \underline{r}}{\partial e} \delta e = & a (-\sin E \delta E - \delta e) \underline{u}_x \\ & + a \left[ (1 - e^2)^{1/2} \cos E \delta E - \frac{e \sin E}{(1 - e^2)^{1/2}} \delta e \right] \underline{u}_y \end{aligned} \quad (3-85)$$

Equation (3-47) is used to relate  $\delta E$  to  $\delta e$ . Since  $t$  is the independent variable and  $n$  and  $t_0$  are unaffected by  $\delta e$ , the variation in  $M$  is zero.

$$\delta M = 0 = (1 - e \cos E) \delta E - \sin E \delta e \quad (3-86)$$

$$\delta E = \frac{\sin E}{1 - e \cos E} \delta e \quad (3-87)$$

(3-87) is substituted into (3-85). After simplification the result is

$$\begin{aligned} \frac{\partial \underline{r}}{\partial e} \delta e = & \left[ - \left( a + \frac{y \sin f}{1 - e^2} \right) \underline{u}_x + \frac{y \cos f}{1 - e^2} \underline{u}_y \right] \delta e \\ = & \left( \frac{y}{1 - e^2} \underline{u}_s - a \underline{u}_x \right) \delta e \end{aligned} \quad (3-88)$$

The coefficient of  $\delta e$  in (3-88) is identical with the coefficient of  $\delta e$  in (3-57).

Equation (3-58) indicates that the velocity change due to  $\delta e$  can be written as the vector sum of two components, one in the  $s$  direction and the other in the  $p$  direction. The  $s$ , or transverse, component can be explained in terms of Kepler's second and third laws of planetary motion. Since both the reference trajectory and the actual trajectory have the same major axis length, according to the third law both have the same period. From the second law, the "swept area" law, which can be deduced from (3-5), the rate at which the position vector sweeps through the area of an elliptical trajectory is constant. The constant is not the same for

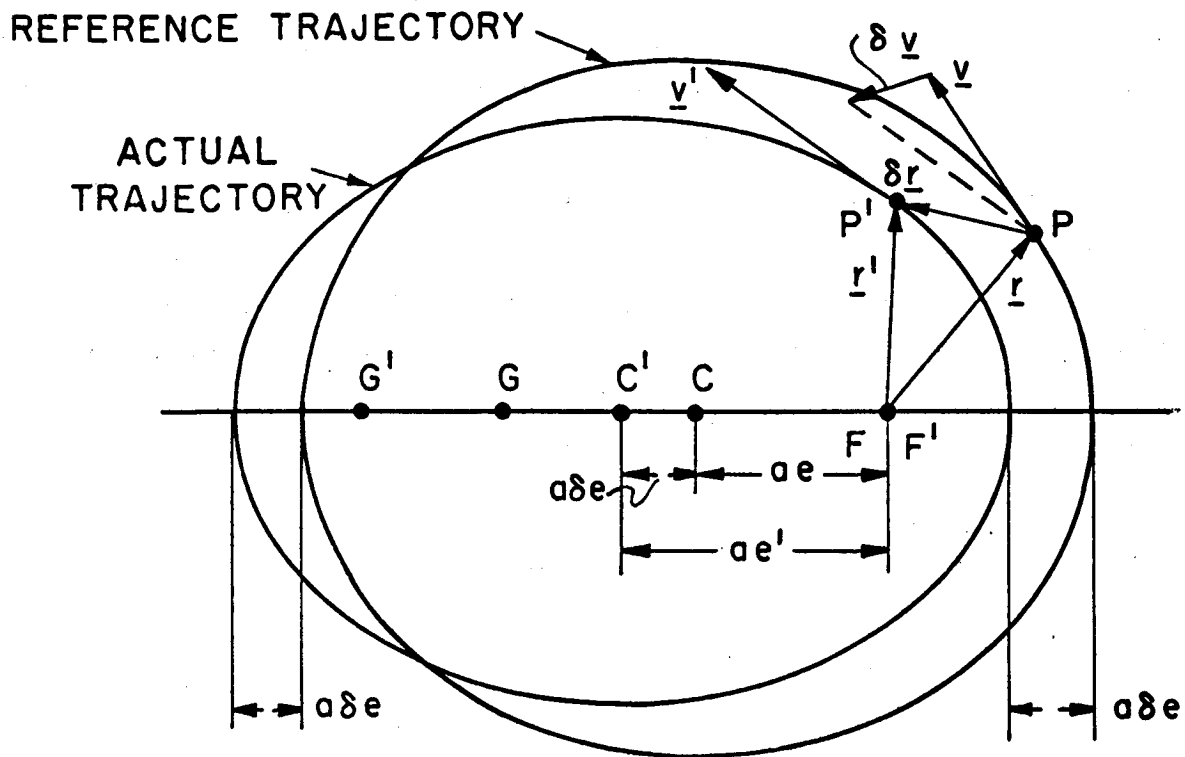
the reference and actual trajectories because, although they have the same period, the area of the former is larger than the area of the latter.

Figure 3.3 indicates that the percentage of the total area of the actual trajectory that is on the perihelion side of the attractive focus is smaller than the percentage of the total area of the reference trajectory on the perihelion side. Therefore,  $\underline{r}'$  must rotate more rapidly than  $\underline{r}$  on the perihelion side, and, since the periods are equal,  $\underline{r}'$  must rotate less rapidly than  $\underline{r}$  on the aphelion side. This line of reasoning is borne out by the fact that the time-varying part of the coefficient of  $\underline{u}_s \delta e$  in (3-58) is  $v_s \cos f$ . The direction of the rotation of  $\underline{r}$  is by definition the  $s$  direction. Since  $v_s$  is always positive, the sign of the coefficient of  $\underline{u}_s \delta e$  is the sign of  $\cos f$ ; consequently,  $\delta \underline{v}$  has a component in the  $s$  direction that is positive when  $\cos f$  is positive (i.e., on the perihelion side of the attractive focus) and negative when  $\cos f$  is negative (i.e., on the aphelion side of the attractive focus).

Since the  $y$  component of  $\delta \underline{r}$  is zero when  $\sin f$  is zero, vehicles on the actual and reference trajectories pass through their respective perihelions at the same time, and they also pass through their respective aphelions at the same time. In the journey from perihelion to aphelion the actual position vector leads the reference position vector (that is,  $f' > f$ ), while in the journey from aphelion to perihelion the actual position vector lags the reference position vector ( $f' < f$ ). The lead of  $\underline{r}'$  relative to  $\underline{r}$  in motion from perihelion toward aphelion causes  $\underline{v}'$  to be rotated toward the attractive focus (i.e., in the negative  $p$  direction) relative to  $\underline{v}$ . Conversely, the lag of  $\underline{r}'$  relative to  $\underline{r}$  in motion from aphelion toward perihelion causes a rotation of the velocity vector in the positive  $p$  direction. The rotation of the  $\underline{v}$  vector is one of the two sources of the  $p$  component of velocity variation due to  $\delta e$ .

The other source of the  $p$  component of velocity variation due to  $\delta e$  is the variation in the rate of change of the magnitude of  $\underline{r}$ . In flight from perihelion to aphelion, for which the time duration is one half the period on both trajectories, the magnitude of  $\underline{r}$  increases from  $a(1 - e)$  to  $a(1 + e)$ , the net change being  $2ae$ ; in a similar flight the net change in the magnitude of  $\underline{r}'$  is  $2a(e + \delta e)$ . Since the change in the magnitude





Unprimed capital letters apply to reference trajectory.

Primed capital letters apply to actual trajectory.

$F, F'$  — common attractive focus of two trajectories

$C, C'$  — centers of two trajectories

$G, G'$  — vacant foci of two trajectories

$P, P'$  — position on two trajectories at time  $t$

$\delta e = e' - e = \text{variation in eccentricity}$

$\delta \underline{r} = \underline{r}' - \underline{r} = \text{variation in position}$

$\delta \underline{v} = \underline{v}' - \underline{v} = \text{variation in velocity}$

Figure 3.3 Effect of  $\delta e$ , Variation in Eccentricity

of  $\underline{r}'$  is more positive than the change in the magnitude of  $\underline{r}$  and the same time is required for both journeys, the average value of  $\dot{r}'$  is more positive than the average value of  $\dot{r}$ . On the trip from aphelion to perihelion the reverse is true; the average value of  $\dot{r}'$  is more negative than the average value of  $\dot{r}$ .

The effect of the rotation of  $\underline{v}$  and the effect of the variation in  $\dot{r}$  tend to balance each other. On the basis of the qualitative discussion that has been presented, it is not possible to assign any relative weighting to the two factors. A mathematical analysis will now be made in order to relate the two quantitatively. The effect of both factors on  $\delta v_r$ , the component of  $\delta \underline{v}$  in the radial direction, will be determined.

From Figure 3.3 the effect of the rotation of  $\underline{v}$  on  $\delta v_r$  is

$$\delta v_r = -v \cos \gamma \sin \delta f = -v_s \delta f \quad (3-89)$$

The effect of the variation in  $\dot{r}$  is

$$\delta v_r = \dot{r}' \cos \delta f - \dot{r} = \dot{r}' - \dot{r} = \delta \dot{r} \quad (3-90)$$

From Equation (B-65),

$$\dot{r} = \frac{n a e \sin f}{(1 - e^2)^{1/2}} \quad (3-91)$$

The variation of  $\dot{r}$  is

$$\delta \dot{r} = \frac{n a}{(1 - e^2)^{3/2}} [\sin f \delta e + (1 - e^2) e \cos f \delta f] \quad (3-92)$$

The variation of the true anomaly can be obtained from the relation for  $\sin f$  in terms of  $e$  and  $E$ .

$$\sin f = \frac{(1 - e^2)^{1/2} \sin E}{1 - e \cos E} \quad (3-93)$$

The variation of  $\sin f$  is

$$\cos f \delta f = \frac{(\cos E - e) [\sin E \delta e + (1 - e^2) \delta E]}{(1 - e^2)^{1/2} (1 - e \cos E)^2} \quad (3-94)$$

But  $\cos f$  is given by

$$\cos f = \frac{\cos E - e}{1 - e \cos E} \quad (3-95)$$

so that

$$\delta f = \frac{\sin E \delta e + (1 - e^2) \delta E}{(1 - e^2)^{1/2} (1 - e \cos E)} \quad (3-96)$$

(3-87) is substituted into (3-96) in order to express  $\delta f$  in terms of the single variation  $\delta e$ .

$$\begin{aligned} \delta f &= \frac{[(1 - e \cos E) + (1 - e^2)] \sin E}{(1 - e^2)^{1/2} (1 - e \cos E)^2} \delta e \\ &= \frac{(2 + e \cos f) \sin f}{1 - e^2} \delta e \end{aligned} \quad (3-97)$$

(3-97) is substituted into (3-92), and the expression for  $v_s$  given by (B-66) is utilized.

$$\begin{aligned} \delta \dot{r} &= \frac{n a}{(1 - e^2)^{3/2}} (1 + e \cos f)^2 \sin f \delta e \\ &= \frac{(1 + e \cos f) v_s \sin f}{1 - e^2} \delta e \end{aligned} \quad (3-98)$$

From (3-89) and (3-97) the effect of the rotation of  $\underline{v}$  is

$$- v_s \delta f = - \frac{(2 + e \cos f) v_s \sin f}{1 - e^2} \delta e \quad (3-99)$$

The total effect of  $\delta e$  on  $\delta \underline{v}_r$  is

$$\begin{aligned}
 \frac{\partial \underline{v}_r}{\partial e} \delta e &= -v_s \delta f + \delta \dot{r} \\
 &= \left[ -(2 + e \cos f) + (1 + e \cos f) \right] \frac{v_s \sin f}{1 - e^2} \delta e \\
 &= -\frac{v_s \sin f}{1 - e^2} \delta e
 \end{aligned} \tag{3-100}$$

This equation is in agreement with the term in the fourth row, third column of the matrix in (3-61).

From (3-100) it is apparent that the rotation of  $\underline{v}$  is the dominant factor in determining the direction of the effect of  $\delta e$  on  $\delta \underline{v}_r$  (and also on  $\delta \underline{v}_p$ ).

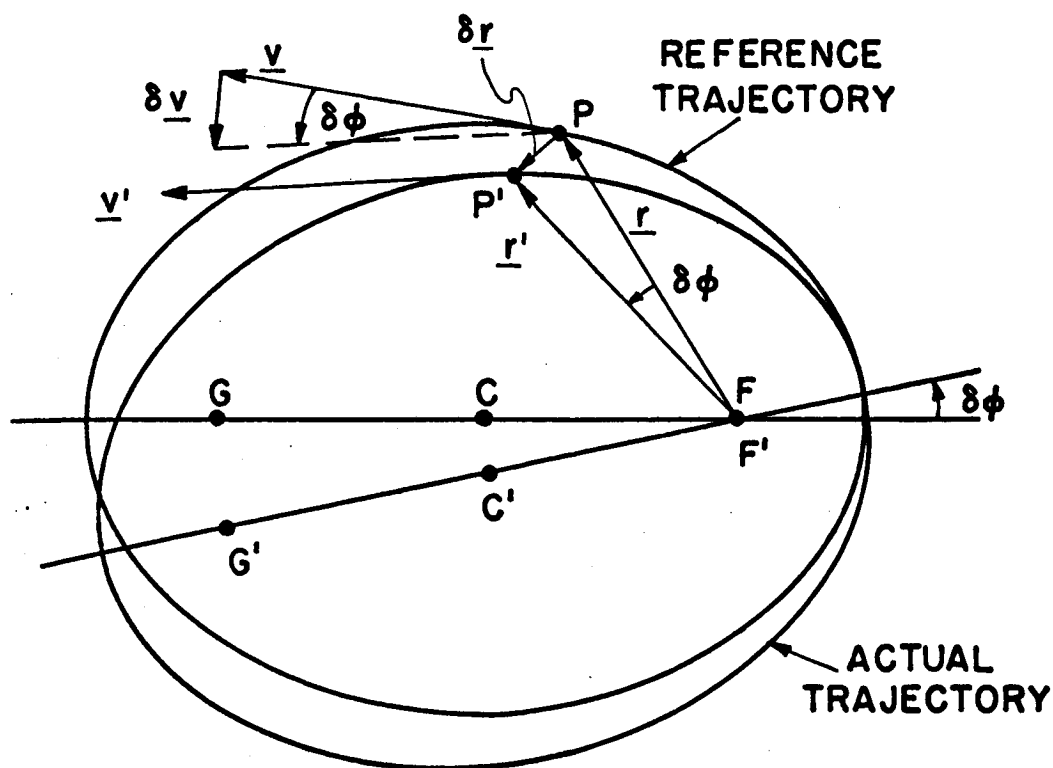
Equation (3-100) points up the analogy between the variational operator  $\delta$  and the derivative operator  $(d/dt)$  in the rotating  $r s z$  coordinate system. The radial component of the acceleration  $\underline{a}$  on the reference trajectory is

$$\underline{a}_r = \frac{d}{dt} (\underline{v}), \underline{u}_r = \frac{d}{dt} (\dot{r}) - v_s \frac{d}{dt} (f) \tag{3-101}$$

The radial component of the velocity variation  $\delta \underline{v}$  relative to the reference trajectory is

$$\delta \underline{v}_r = \delta \underline{v}, \underline{u}_r = \delta \dot{r} - v_s \delta f \tag{3-102}$$

Variation in  $\phi$ , the longitude of perihelion, causes a simple rotation, in the reference trajectory plane, of the actual trajectory relative to the reference trajectory. The angle of rotation is the fixed angle  $\delta \phi$ . The effect is to rotate both the position vector and the velocity vector through  $\delta \phi$  without affecting the magnitude of either.



Unprimed capital letters apply to reference trajectory.

Primed capital letters apply to actual trajectory.

$F, F'$  – common attractive focus of two trajectories

$C, C'$  – centers of two trajectories

$G, G'$  – vacant foci of two trajectories

$P, P'$  – position on two trajectories at time  $t$

$\delta\phi$  = variation in longitude of perihelion

$\delta\mathbf{r} = \mathbf{r}' - \mathbf{r}$  = variation in position

$\delta\mathbf{v} = \mathbf{v}' - \mathbf{v}$  = variation in velocity

Figure 3.4 Effect of  $\delta\phi$ , Variation in Longitude of Perihelion

$$\frac{\partial \underline{r}}{\partial \phi} \delta \phi = r \delta \phi \underline{u}_s \quad (3-103)$$

$$\frac{\partial \underline{v}}{\partial \phi} \delta \phi = -v \delta \phi \underline{u}_p \quad (3-104)$$

These relations are illustrated by Figure 3.4.

Because  $z$  and  $v_z$  are identically zero on the reference trajectory for all values of time,  $\delta z$  and  $\delta v_z$  are simply the projections on the  $z$ -axis of  $\underline{r}'$  and  $\underline{v}'$ , respectively, as shown in Figure 3.5. In the linear approximation, the magnitudes of  $\underline{r}$  and  $\underline{v}$  are not affected by the variations  $\delta z$  and  $\delta v_z$ . Also, the actual true anomaly  $f'$  is equal to the reference true anomaly  $f$ . Then,

$$\delta z = \underline{r}' \cdot \underline{u}_z = r \delta i \sin (f - \delta \Omega) \quad (3-105)$$

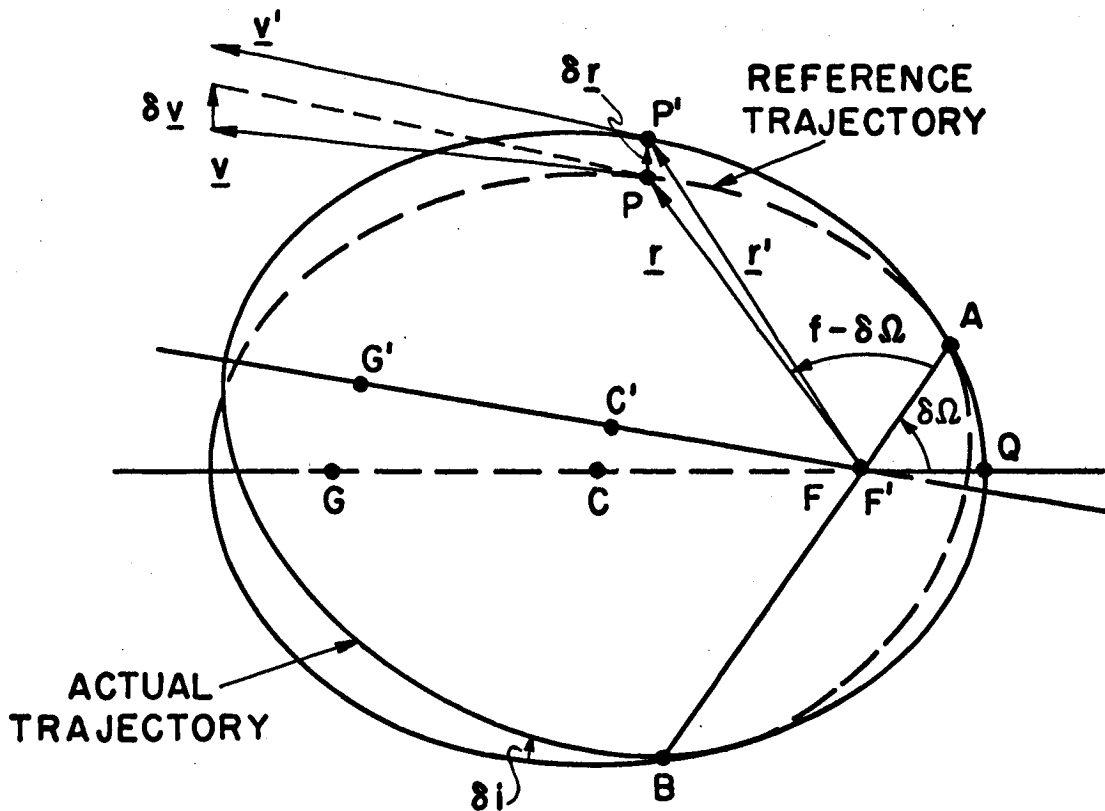
$$\delta v_z = \underline{v}' \cdot \underline{u}_z = v \delta i \cos (g - \delta \Omega) \quad (3-106)$$

Angles  $\delta \Omega$  and  $\delta i$  define the orientation of the actual trajectory plane relative to the reference trajectory plane. If  $\delta i$  is zero,  $\delta \Omega$  is undefined, and there are no variations in the  $z$  direction. Since  $\delta \Omega$  is defined as the variation (from zero) of the longitude of the ascending node,  $\delta i$  is always positive.  $\delta \Omega$  may have any value from  $0^\circ$  to  $360^\circ$ . The out-of-plane "elements" appearing in the six-component vector on the right-hand side of (3-61) are  $\delta i \cos \delta \Omega$  and  $\delta i \sin \delta \Omega$ , each of which is small and can take on either positive or negative values.

Because the force field is conservative, the variation in acceleration,  $\delta \underline{a}$ , depends only on  $\delta \underline{r}$  and is independent of  $\delta \underline{v}$ . The variation in the magnitude of  $\underline{a}$  comes directly from (3-60).

$$\delta a_r = \frac{2\mu}{r^3} \delta r \quad (3-107)$$

On the reference trajectory  $\underline{a}$  is collinear with  $\underline{r}$ ; on the actual trajectory  $\underline{a}'$  is collinear with  $\underline{r}'$ . Therefore, the small angle between



Unprimed capital letters apply to reference trajectory.

Primed capital letters apply to actual trajectory.

$F, F'$  – common attractive focus of two trajectories

$C, C'$  – centers of two trajectories

$G, G'$  – vacant foci of two trajectories

$P, P'$  – position on two trajectories at time  $t$

$AB$  – line of nodes

$f = \angle QFP$  = true anomaly of  $P$

$\delta\Omega$  = variation in longitude of ascending node

$\delta i$  = variation in inclination

$\delta \underline{r} = \underline{r}' - \underline{r}$  = variation in position

$\delta \underline{v} = \underline{v}' - \underline{v}$  = variation in velocity

Figure 3.5 Effect of  $\delta\Omega$ , Variation in Longitude of Ascending Node, and  $\delta i$ , Variation in Inclination

$\underline{a}$  and  $\underline{a}'$  is equal to the angle between  $\underline{r}$  and  $\underline{r}'$ . Then, since  $a_s$  and  $s$  are both zero on the reference trajectory, the acceleration variation component  $\delta a_s$  is

$$\begin{aligned}\delta a_s &= a_s' = \underline{a}' \cdot \underline{u}_s = \frac{a'}{r'} \underline{r}' \cdot \underline{u}_s \\ &= \frac{a_r \delta s}{r} = - \frac{\mu}{r^3} \delta s\end{aligned}\quad (3-108)$$

In similar fashion,

$$\delta a_z = a_z' = - \frac{\mu}{r^3} \delta z \quad (3-109)$$

Equations (3-107), (3-108), and (3-109) are the component equations of the matrix formulation given by (3-7) and (3-9).

### 3.10 Transition Matrix

Equation (3-61) can be used to find analytic expressions for the terms of the transition matrix  $\overset{*}{C}_{ji}$ , defined by Equations (2-8) and (2-9). The first six rows of (3-61) define a 6-by-6 matrix which relates the state vector  $\delta \underline{x}$  to the variations in the orbital elements. The inverse of this matrix provides an expression for the variations of the elements in terms of the components of  $\delta \underline{x}$ . If the subscript  $j$  is added to all the time-varying quantities in the first matrix, the state vector is  $\delta \underline{x}_j$ , corresponding to time  $t_j$ . If the subscript  $i$  is added to the time-varying quantities in the inverse matrix, the variations in the elements are expressed in terms of the components of  $\delta \underline{x}_i$ . The product of these two matrices is the transition matrix  $\overset{*}{C}_{ji}$ , relating  $\delta \underline{x}_j$  to  $\delta \underline{x}_i$ .

The algebraic manipulations required to perform the matrix inversion and the matrix multiplication are quite laborious. It is therefore worthwhile, before performing the indicated operations, to give careful consideration to the choice of a single time-varying parameter, the choice of a coordinate system, and the choice of a combination of variations in the six orbital elements. A discussion of these choices appears in the early sections of Appendix K. The amount of algebra is reduced (but is still by no means trivial) if the time-varying quantity is



the eccentric anomaly E, the coordinate system is the reference trajectory flight path (p q z) system, and the variations in the orbital elements are grouped as shown below in the path deviation vector  $\delta \underline{e}$ .

$$\delta \underline{e} = \left\{ \begin{array}{c} (1 - e^2)^{1/2} \delta \phi - n \delta t_o \\ \frac{\delta e}{(1 - e^2)^{1/2}} \\ \frac{1}{2} \frac{\delta a}{a} \\ e \delta \phi \\ (1 - e^2)^{1/2} \delta i \cos \delta \Omega \\ \delta i \sin \delta \Omega \end{array} \right\} \quad (3-110)$$

With these selections, the first six equations of (3-61) are transformed into the following:

$$\delta \underline{x}_j = \left\{ \begin{array}{c} \delta p_j \\ \delta q_j \\ \delta z_j \\ \delta v_{p_j} \\ \delta v_{q_j} \\ \delta v_{z_j} \end{array} \right\} = \left\{ \begin{array}{c} *F_j \\ *L_j \end{array} \right\} \left\{ \begin{array}{c} (1 - e^2)^{1/2} \delta \phi - n \delta t_o \\ \frac{\delta e}{(1 - e^2)^{1/2}} \\ \frac{1}{2} \frac{\delta a}{a} \\ e \delta \phi \\ (1 - e^2)^{1/2} \delta i \cos \delta \Omega \\ \delta i \sin \delta \Omega \end{array} \right\} \quad (3-111)$$

This equation is the same as Equation (K-30) of Appendix K. The 3-by-6 matrix  $\overset{*}{F}_j$  relates  $\delta \underline{r}_j$  to  $\delta \underline{e}$ ; the 3-by-6 matrix  $\overset{*}{L}_j$  relates  $\delta \underline{v}_j$  to  $\delta \underline{e}$ . Equations (K-31) and (K-32) express the elements of  $\overset{*}{F}_j$  and  $\overset{*}{L}_j$  in terms of  $a$ ,  $e$ ,  $n$ , and  $E_j$ .

The inverse of the 6-by-6 matrix  $\begin{Bmatrix} \overset{*}{F} \\ \overset{*}{L} \end{Bmatrix}$  is designated  $\begin{Bmatrix} \overset{*}{R} & \overset{*}{V} \end{Bmatrix}$ .

The equation relating the orbital element variations to state vector  $\delta \underline{x}_i$  is

$$\delta \underline{e} = \begin{Bmatrix} (1 - e^2)^{1/2} \delta \phi - n \delta t_o \\ \frac{\delta e}{(1 - e^2)^{1/2}} \\ \frac{1}{2} \frac{\delta a}{a} \\ e \delta \phi \\ (1 - e^2)^{1/2} \delta i \cos \delta \Omega \\ \delta i \sin \delta \Omega \end{Bmatrix} = \begin{Bmatrix} \overset{*}{R}_i & \overset{*}{V}_i \end{Bmatrix} \begin{Bmatrix} \delta p_i \\ \delta q_i \\ \delta z_i \\ \delta v_{p_i} \\ \delta v_{q_i} \\ \delta v_{z_i} \end{Bmatrix} \quad (3-112)$$

$\overset{*}{R}_i$  is a 6-by-3 matrix which gives the effect of  $\delta \underline{r}_i$  on  $\delta \underline{e}$ .  $\overset{*}{V}_i$  is a 6-by-3 matrix giving the effect of  $\delta \underline{v}_i$  on  $\delta \underline{e}$ . Equations (K-34) and (K-35) in Appendix K contain analytic expressions for the elements of  $\overset{*}{R}_i$  and  $\overset{*}{V}_i$ .

The transition matrix is obtained by substituting (3-112) into (3-111).

$$\begin{aligned} \delta \underline{x}_j &= \begin{Bmatrix} \overset{*}{F}_j \\ \overset{*}{L}_j \end{Bmatrix} \begin{Bmatrix} \overset{*}{R}_i & \overset{*}{V}_i \end{Bmatrix} \delta \underline{x}_i \\ &= \overset{*}{C}_{ji} \delta \underline{x}_i \end{aligned} \quad (3-113)$$



where 
$$\dot{C}_{ji}^* = \begin{Bmatrix} \dot{M}_{ji}^* & \dot{N}_{ji}^* \\ \dot{S}_{ji}^* & \dot{T}_{ji}^* \end{Bmatrix} \quad (3-114)$$

and

$$\dot{M}_{ji}^* = \dot{F}_j^* \dot{R}_i^* \quad (3-115)$$

$$\dot{N}_{ji}^* = \dot{F}_j^* \dot{V}_i^* \quad (3-116)$$

$$\dot{S}_{ji}^* = \dot{L}_j^* \dot{R}_i^* \quad (3-117)$$

$$\dot{T}_{ji}^* = \dot{L}_j^* \dot{V}_i^* \quad (3-118)$$

The matrix multiplications indicated by Equations (3-115) to (3-118) have been performed, and the analytic results are contained in Equations (K-39) to (K-42). The complete expression for  $\dot{C}_{ji}^*$  is Equation (3-119). The angles  $E_M$  and  $E_P$ , introduced in these equations for the purpose of simplification, are defined as follows:

$$E_M = \frac{1}{2} (E_j - E_i) \quad (3-120)$$

$$E_P = \frac{1}{2} (E_j + E_i) \quad (3-121)$$

Equation (3-119) expresses all the elements of  $\dot{C}_{ji}^*$  in terms of only four parameters, namely, the eccentricity  $e$  and the mean angular motion  $n$  of the reference trajectory, and the eccentric anomalies  $E_i$  and  $E_j$ .  $\dot{C}_{ji}^*$  is presented as the sum of two matrices. The first of the two is a diagonal matrix whose diagonal elements, reading from top to bottom, are equal, respectively, to

$$\frac{v_i}{v_j}, \quad \frac{v_j}{v_i}, \quad 1, \quad \frac{v_j}{v_i}, \quad \frac{v_i}{v_j}, \quad 1.$$

Every term in every element of the second of the two matrices contains either  $E_M$  or  $\sin E_M$ . From this information it is clear that when

$t_j = t_i$ , the first matrix becomes the identity matrix and the second matrix becomes the zero matrix. Thus,  $\tilde{C}_{ii}^*$  is the sixth-order identity matrix, as indicated in Chapter 2 by Equation (2-10).

For this special case in which the reference trajectory is an ellipse, a stronger statement can be made about the determinant of  $\tilde{C}_{ji}^*$  than that of Equation (2-13). Not only is the determinant of  $\tilde{C}_{ji}^*$  equal to unity, but there are two sub-matrices that can be formed, the determinant of each of which is equal to unity. The first sub-matrix consists of the sixteen in-plane elements of  $\tilde{C}_{ji}^*$ ; the second consists of the four out-of-plane elements of  $\tilde{C}_{ji}^*$ .

A visual check of the terms in (3-119) can be made by comparing  $\tilde{C}_{ji}^*$  with its inverse  $\tilde{C}_{ij}^*$  and noting that the inverse satisfies the relationship given by Equation (2-12).

If (3-119) is to be used for numerical computations performed on a digital computer, the accuracy with which the terms have been entered into the program can be effectively checked by the matrix multiplication of  $\tilde{C}_{ji}^*$  by  $\tilde{C}_{ij}^*$  for arbitrary values of  $E_i$  and  $E_j$ . If all terms have been entered correctly, the product matrix is the identity matrix. If the term in the  $m$ -th row and the  $n$ -th column is entered incorrectly, all the terms in the  $m$ -th row and all the terms in the  $n$ -th column of the product matrix will, in general, differ from the corresponding terms of the identity matrix.

### 3.11 Fixed-Time-of-Arrival Guidance

The two basic equations in FTA guidance are (2-33) and (2-35); the former relates the velocity correction  $\underline{c}_F$  to the predicted position variation at the target, the latter relates the state vector after the correction is applied to the state vector before it is applied. The two equations are repeated below for convenience.

$$\underline{c}_F = -K_{CD} \delta \underline{r}_D \quad (3-122)$$

$$\delta \underline{x}_D^+ = \begin{Bmatrix} {}^*0_3 & {}^*0_3 \\ -J_{DC}^* & I_3^* \end{Bmatrix} \delta \underline{x}_D^- \quad (3-123)$$

Analytic expressions for  $J_{DC}^*$  and  $K_{CD}^*$  can be determined directly from the sub-matrices of  $\tilde{C}_{DC}^*$  by the use of (2-27) and (2-28).

An alternate method of developing the terms of  $J_{DC}^*$  and  $K_{CD}^*$  is presented in Appendix K. This method involves the formulation of a path deviation vector consisting of the position variations at two times,  $t_i$  and  $t_j$ . First,  $\delta \underline{r}_i$  and  $\delta \underline{r}_j$  are expressed in terms of  $\delta \underline{e}$ .

$$\begin{Bmatrix} \delta \underline{r}_i \\ \delta \underline{r}_j \end{Bmatrix} = \begin{Bmatrix} {}^*F_i \\ {}^*F_j \end{Bmatrix} \delta \underline{e} = \tilde{A}_{ij}^* \delta \underline{e} \quad (3-124)$$

where  $\tilde{A}_{ij}^*$  is a 6-by-6 matrix whose first three rows depend only on  $t_i$  and whose last three rows depend only on  $t_j$ . The inverse of (3-124) is

$$\delta \underline{e} = \tilde{A}_{ij}^{*-1} \begin{Bmatrix} \delta \underline{r}_i \\ \delta \underline{r}_j \end{Bmatrix} = \begin{Bmatrix} {}^*H_{ij} & {}^*H_{ji} \end{Bmatrix} \begin{Bmatrix} \delta \underline{r}_i \\ \delta \underline{r}_j \end{Bmatrix} \quad (3-125)$$

${}^*H_{ij}$  is the 6-by-3 matrix relating  $\delta \underline{e}$  to  $\delta \underline{r}_i$  when  $\delta \underline{r}_j$  is held constant, and  ${}^*H_{ji}$  is the 6-by-3 matrix relating  $\delta \underline{e}$  to  $\delta \underline{r}_j$  when  $\delta \underline{r}_i$  is held constant. Equation (K-44) of Appendix K is an analytic expression for the elements of  ${}^*H_{ij}$ . The elements of  ${}^*H_{ji}$  are obtained by interchanging subscripts  $i$  and  $j$  in (K-44).

The state vector at any given time can now be related to the path deviation vector consisting of  $\delta \underline{r}_i$  and  $\delta \underline{r}_j$ . In particular, the state vector at  $t_i$  is

$$\delta \underline{x}_i = \begin{Bmatrix} {}^*F_i \\ {}^*L_i \end{Bmatrix} \delta \underline{e} = \begin{Bmatrix} {}^*F_i \\ {}^*L_i \end{Bmatrix} \begin{Bmatrix} {}^*H_{ij} & {}^*H_{ji} \end{Bmatrix} \begin{Bmatrix} \delta \underline{r}_i \\ \delta \underline{r}_j \end{Bmatrix} \quad (3-126)$$

Equation (3-126) can be sub-divided into two equations, one for position variation and the other for velocity variation.

$$\delta \underline{r}_i = \underline{F}_i^* (\underline{H}_{ij}^* \delta \underline{r}_i + \underline{H}_{ji}^* \delta \underline{r}_j) \quad (3-127)$$

$$\delta \underline{v}_i = \underline{L}_i^* (\underline{H}_{ij}^* \delta \underline{r}_i + \underline{H}_{ji}^* \delta \underline{r}_j) \quad (3-128)$$

The former equation indicates that

$$\underline{F}_i^* \underline{H}_{ij}^* = \underline{I}_3 \quad \underline{F}_i^* \underline{H}_{ji}^* = \underline{0}_3 \quad (3-129)$$

The equation for velocity variation is simplified as follows:

$$\delta \underline{v}_i = \underline{J}_{ij}^* \delta \underline{r}_i + \underline{K}_{ij}^* \delta \underline{r}_j \quad (3-130)$$

where

$$\underline{J}_{ij}^* = \underline{L}_i^* \underline{H}_{ij}^* \quad \underline{K}_{ij}^* = \underline{L}_i^* \underline{H}_{ji}^* \quad (3-131)$$

(3-130) is the same equation as (2-26). Equations (3-131) are the defining relations for the 3-by-3 matrices  $\underline{J}_{ij}^*$  and  $\underline{K}_{ij}^*$ , which are the fundamental matrices of linear guidance theory. With the proper substitution of subscripts they are the matrices appearing in (3-122) and (3-123). Analytic expressions for the elements of  $\underline{J}_{DC}^*$  are obtained by substituting D for i, C for j in Equation (K-47) of Appendix K. Since the subscript D precedes the subscript C in  $\underline{J}_{DC}^*$ , the angle  $E_M$  is given by

$$E_M = \frac{1}{2} (E_C - E_D) \quad (3-132)$$

The correction matrix  $\underline{K}_{CD}^*$  is obtained from (K-48) and because of its importance is reproduced here as Equation (3-133). In this equation, since the subscript C precedes the subscript D,

$$E_M = \frac{1}{2} (E_D - E_C) \quad (3-134)$$

$$\vec{k}_{CD} = \frac{n}{2}$$

76a

$$\left[ \frac{1}{(1 - e^2 \cos^2 E_C)^{1/2} (1 - e^2 \cos^2 E_D)^{1/2}} \times \right. \\ \left. \begin{aligned} & \left( (1 + e \cos E_C) (1 + e \cos E_D) \right. \\ & \quad \cdot \left( \frac{3 E_M}{\sin E_M} - e \cos E_P \right) \\ & \quad - 4(\cos E_M + e \cos E_P) \\ & \quad - 2(1 - e^2)^{1/2} (1 - e \cos E_C) \sin E_M \\ & \quad - (1 - e \cos E_C) (1 - e \cos E_D) \\ & \quad \cdot (\cos E_M + e \cos E_P) \end{aligned} \right. \\ \left. \begin{aligned} & 2(1 - e^2)^{1/2} (1 - e \cos E_D) \sin E_M \\ & 0 \end{aligned} \right) \end{aligned} \right. \\ \left. \begin{aligned} & 0 \\ & \frac{1}{\sin E_M (\cos E_M - e \cos E_P)} \end{aligned} \right) \quad (3-133)$$



The denominator factor  $X$  in the expressions for  $\overset{*}{J}_{DC}$  and  $\overset{*}{K}_{CD}$  is defined by

$$X = (3 E_M - e \sin E_M \cos E_P) (\cos E_M + e \cos E_P) - 4 \sin E_M \quad (3-135)$$

It is interesting and perhaps somewhat surprising to note that, of all the matrices considered in the last two sections,  $\overset{*}{K}_{CD}$ , the only one needed to compute the velocity correction, is one of the simplest.

### 3.12 Variable-Time-of-Arrival Guidance

The VTA velocity correction and the corresponding relation between  $\delta \underline{x}_D^+$  and  $\delta \underline{x}_D^-$  are determined from Equations (2-41) and (2-44), respectively. Aside from utilizing the analytic expressions for  $\overset{*}{K}_{CD}$  and  $\overset{*}{J}_{DC}$ , no further simplification of these two equations is afforded by the assumption of an elliptical reference trajectory.

When the expression for the VTA correction is formulated in the critical-plane coordinate system, there is an additional simplification for any two-body reference trajectory, whether it be elliptical, parabolic, or hyperbolic. From Equation (2-47) the correction may be written as

$$\underline{c}_W = \begin{Bmatrix} c_\xi \\ c_\eta \end{Bmatrix} = \overset{*}{Y} \begin{Bmatrix} \delta \xi_D^- \\ \delta \eta_D^- \end{Bmatrix} \quad (3-136)$$

It is shown in Section N. 8 of Appendix N that the upper right-hand term of the 2-by-2 matrix  $\overset{*}{Y}$  is equal to zero for two-body reference trajectories. Thus, only three quantities need be evaluated in order to compute the correction vector required at some time  $t_C$  for a given miss distance vector.

In Section O. 13 the following expression is derived for  $\bar{Y}^*$ :

$$\bar{Y}^* = n \left\{ \frac{\left( \frac{1}{4B} \quad 0 \right)}{\frac{K_{33}}{C} \left( \frac{D \cos i_D}{B} \quad -B \right)} \right\} \quad (3-137)$$

where

$$B = [(K_{11} \sin \Omega_D - K_{12} \cos \Omega_D)^2 + (K_{21} \sin \Omega_D - K_{22} \cos \Omega_D)^2]^{1/2}$$

$$C = [B^2 \sin^2 (f_D - f_C) \sin^2 i_D + K_{33}^2 X^2 \sin^2 E_M \cos^2 i_D]^{1/2} \quad (3-139)$$

$$D = (K_{11}^2 - K_{12}^2 + K_{21}^2 - K_{22}^2) \sin \Omega_D \cos \Omega_D \\ + (K_{11} K_{12} + K_{21} K_{22}) (\sin^2 \Omega_D - \cos^2 \Omega_D) \quad (3-140)$$

The K factors are functions of the eccentricity  $e$  and the two eccentric anomalies  $E_C$  and  $E_D$ ; they are defined in Equations (O-77) to (O-81).  $\Omega_D$  and  $i_D$  are the orientation angles of the relative velocity vector  $\underline{v}_R$  with respect to the  $p_D$ ,  $q_D$ ,  $z$  axes.

Equation (3-137) indicates that reducing the magnitude of  $K_{33}$  and  $D$  and increasing the magnitude of  $C$  all have the desirable effect of reducing the magnitude of  $\underline{c}_V$ . The role of the magnitude of  $B$  is more equivocal. If  $\delta \xi_D^-$  is much larger than  $\delta \eta_D^-$ ,  $B$  should be as large as possible; if  $\delta \eta_D^-$  is much larger than  $\delta \xi_D^-$ , the magnitude of  $B$  should be kept small. All of these factors are properly weighted in the determination of the optimum correction time in the manner indicated in Section 2. 16.

The physical significance of the zero element in  $\bar{Y}^*$  is that the component of the correction vector along the line of nodes between the critical plane at  $t = t_C$  and the reference trajectory plane is affected by only that component of the miss distance vector that lies along the line of nodes between the critical plane at  $t = t_D$  and the reference trajectory plane.

The nodal component of  $\underline{c}_W$  is completely independent of the variant motion along the z-axis; it depends only on  $\delta \xi_D^-$ , which by definition lies in the reference trajectory plane, on the in-plane elements of  $\underline{K}_{CD}^*$ , and on  $\Omega_D$ , the angle in the reference trajectory plane between the  $p_D$ -axis and the line of nodes. Therefore, the correction required for the out-of-plane component of the predicted position variation (i. e., for  $\delta z_D^-$ ) is contained entirely in the  $\eta_C$ -component of the correction.

### 3.13 General Discussion of Singularities in the Matrix Solution

The solution for the state vector at time  $t_j$  as a function of the state vector at time  $t_i$  has no singularities. Irrespective of the time selected for  $t_i$ , the six components of  $\delta \underline{x}_i$  are independent and therefore can be used to determine the components of the state vector  $\delta \underline{x}_j$  for any  $t_j$ . The mathematical validity of this statement is manifest from the fact that the determinant of  $\underline{C}_{ji}^*$  can never vanish; it is always equal to one.

However, if the path deviation vector  $\delta \underline{e}$  is expressed as a function of the path deviation vector consisting of two position variation vectors  $\delta \underline{r}_i$  and  $\delta \underline{r}_j$ , as in Equation (3-124), there may be singularities in the solution. There are certain combinations of  $t_i$  and  $t_j$  for which the components of  $\delta \underline{r}_j$  are not independent of the components of  $\delta \underline{r}_i$ . For these combinations the determinant of  $\underline{A}_{ij}^*$  vanishes, and hence matrices  $\underline{H}_{ij}^*$ ,  $\underline{H}_{ji}^*$ ,  $\underline{J}_{ij}^*$ , and  $\underline{K}_{ij}^*$  cannot be determined.

There are three different types of combinations of  $t_i$  and  $t_j$  for which  $\underline{A}_{ij}^*$  becomes singular. The first type occurs when the difference between  $t_i$  and  $t_j$  is an integer multiple of the reference period  $P$ ; the second type occurs when the difference in true anomaly ( $f_j - f_i$ ) is equal to  $(2N-1)\pi$  radians; the third type occurs when the factor  $X$ , defined by Equation (3-135), is equal to zero. These three types are discussed individually in the following three sections. A more comprehensive analysis appears in Appendix O.

A study of these singularities can be justified on academic grounds simply because they do exist, and an understanding of why they exist leads to a more thorough comprehension of the characteristics of elliptical motion. In addition, the study has practical significance if space

journeys are contemplated in which the total difference in true anomaly (between injection and arrival at the destination) is greater than  $\pi$  radians.

In order of increasing value of  $(f_j - f_i)$ , the first three singularities occur at  $(f_j - f_i) = 0, \pi$ , and  $2\pi$  radians. The first is a trivial case; if  $t_i = t_j$ , it is obvious that  $\delta \underline{r}_i = \delta \underline{r}_j$ , and hence the components of the six-vector composed of  $\delta \underline{r}_i$  and  $\delta \underline{r}_j$  are not independent. The singularities at  $\pi$  and  $2\pi$  radians are examples, respectively, of the second type and the first type. The first non-trivial case of a singularity at  $X = 0$  occurs at a value of  $(f_j - f_i)$  between  $2\pi$  and  $4\pi$  radians.

For manned interplanetary reconnaissance missions, minimization of total flight time is of prime importance because of logistic considerations. Such missions will normally involve a total change in true anomaly of approximately  $\pi$  radians for each of the two legs, outbound and return. The only singularity that need be considered on such missions is the one of the second type that occurs at  $(f_j - f_i) = \pi$  radians.

There are two types of space missions which involve considerably larger changes in true anomaly. The first is an unmanned nonstop round-trip reconnaissance of either Mars or Venus as described in Reference (2). The mission can be accomplished with relatively low expenditure of energy if the vehicle makes two circuits of the sun during the time that the earth makes three circuits, i. e., in three years. In one of the legs of such a journey, either outbound or return, the true anomaly difference must be greater than  $2\pi$  radians.

The second type of mission with large difference in true anomaly is that of a space vehicle in a temporary parking orbit about another planet. Such a trajectory may entail an appreciable number of complete circuits before the vehicle reaches its "destination", which is the point at which thrust is to be applied for the return trip to earth.

In both of these types of extended missions singularities of all three types can be encountered.

It is shown in the following sections that, in general, it is not possible to compute a finite FTA velocity correction when  $t_C$  and  $t_D$  are such that the conditions for any one of the three types of singularities are

satisfied. If VTA guidance is used, a finite correction can be computed under the conditions for the second and third types of singularities, but no finite VTA correction can be computed if the singularity is of the first type.

### 3.14 Singularities at $(t_j - t_i) = NP$

When  $t_i$  and  $t_j$  are an exact number of reference periods apart, the position variations  $\delta \underline{r}_i$  and  $\delta \underline{r}_j$  can differ from each other only due to the fact that the period  $P'$  of the actual trajectory differs slightly from  $P$ , the period of the reference trajectory.

$$\begin{Bmatrix} \delta p_j \\ \delta q_j \\ \delta z_j \end{Bmatrix} = \begin{Bmatrix} \delta p_i \\ \delta q_i \\ \delta z_i \end{Bmatrix} - \begin{Bmatrix} 0 \\ N v_i \delta P \\ 0 \end{Bmatrix} \quad (3-141)$$

In the path deviation vector consisting of  $\delta \underline{r}_i$  and  $\delta \underline{r}_j$ , only four of the six components are independent. Hence the rank of matrix  $\dot{A}_{ij}^*$  is reduced from six to four. Despite the fact that  $\dot{A}_{ij}^*$  is singular, (3-141) can be used to solve for  $\delta P$ , and by the use of Kepler's third law  $\frac{1}{2} \frac{\delta a}{a}$ , the third element of  $\delta \underline{e}$ , can be computed.

$$\frac{1}{2} \frac{\delta a}{a} = \frac{1}{3} \frac{\delta P}{P} = - \frac{(\delta q_j - \delta q_i)}{3 N P v_i} \quad (3-142)$$

The other five elements of  $\delta \underline{e}$  cannot be determined.

If correction time  $t_C$  and arrival time  $t_D$  are an exact number of reference periods apart, it is not possible to compute a small finite FTA velocity correction which will affect the predicted values of  $\delta p_D^-$  and  $\delta z_D^-$ . If either of these components of  $\delta \underline{r}_D^-$  is non-zero,  $\delta \underline{r}_D^+$  must be non-zero. The only condition under which it is possible to compute a finite  $\underline{c}_F$  that nulls  $\delta \underline{r}_D^-$  is when  $\delta \underline{r}_D^-$  is parallel to the velocity vector  $\underline{v}_D$ . Then the required correction changes the period of the motion in such a manner that  $\delta q_D$  is reduced to zero. The equation for the correction in this special case, developed as (O-13) in Appendix O, is

$$\underline{c}_F = \frac{\mu}{3 N P a v_D^2} (\delta q_D^-) \underline{u}_{q_D} \quad (3-143)$$

Equation (3-143) has little practical value inasmuch as it applies to a condition whose likelihood of occurrence is essentially zero. However, it does serve to illustrate a paradoxical characteristic of elliptical motion. A positive  $\delta q_D^-$  indicates that the predicted vehicle position at  $t_D$  is slightly ahead of the desired position. The correction therefore must slow the vehicle down somewhat in order to reduce  $\delta q_D$  to zero. But (3-143) indicates that for a positive  $\delta q_D^-$  the required velocity increment along the  $q_D$ -axis, which is also the  $q_C$ -axis, is positive, so that the vehicle experiences an instantaneous increase in orbital velocity. The question that arises is this: How can an initial increase in velocity cause an eventual retardation of the vehicle motion so that a positive  $\delta q_D$  is reduced to zero? The seeming contradiction is clarified by Kepler's third law. The initial increase in velocity increases the total energy of the path. An increase in total energy signifies an increase in the length of the semi-major axis  $a$ , which, from Kepler's third law, is accompanied by an increase in the period  $P$ . The increased period is so determined that after  $N$  circuits of the focus the vehicle arrives at the desired destination point at time  $t_D$ . Thus, the vehicle's position variation is initially increased by the correction but is eventually reduced to zero at  $t_D$ .

If VTA guidance rather than FTA guidance is used, it is still not possible in the general case to compute a finite velocity correction when  $(t_D - t_C) = N P$ . There are three special situations, however, in which a finite correction can be determined. The first is the trivial case when  $\delta \underline{r}_D^-$  is parallel to  $\underline{v}_R$  and no correction is required. The second is the same as the special case for FTA guidance; i. e.,  $\delta \underline{r}_D^-$  is parallel to  $\underline{v}_D$ ; in this case the VTA correction is the same as the FTA correction given by Equation (3-143). The third special case is the two-dimensional case, in which both  $\delta \underline{r}_D^-$  and  $\underline{v}_R$  lie in the reference trajectory plane; under these circumstances, the VTA correction is again given by the right-hand side of Equation (3-143).

A physical explanation of the inability to compute a finite FTA correction is based on the fact that the new path resulting from any correction must contain both the vehicle's actual position  $C'$  at the time of the correction and the desired destination point  $D$ . When  $C'$

and D are spatially close to each other but not coincident and the line C' D is not tangent to the reference trajectory, the difference between the required new trajectory and the reference trajectory is generally so great that it precludes the use of linear theory in computing the velocity correction. Even when the requirements on the correction are relaxed by the use of VTA navigation, it is not possible in the general case to compute a finite correction, because there is no path lying close to the reference path that passes through C' and some point on the line through D parallel to  $\underline{v}_R$ .

A more detailed analysis of the singularities at  $(t_D - t_C) = N P$  appears in Sections O.4, O.5, O.14, and O.17.

### 3.15 Singularities at $(f_j - f_i) = (2N-1)\pi$

If the difference in true anomaly  $(f_j - f_i)$  is an odd multiple of  $\pi$  radians, the in-plane components of  $\delta \underline{r}_i$  and  $\delta \underline{r}_j$  are independent of each other, but  $\delta z_i$  and  $\delta z_j$  are not independent. The relationship between the latter two can be derived from the z-component of (3-57), the vector equation for  $\delta \underline{r}$ .

$$\delta z_i = r_i \sin(f_i - \delta\Omega) \delta i \quad (3-144)$$

$$\begin{aligned} \delta z_j &= r_j \sin(f_j - \delta\Omega) \delta i \\ &= r_j \sin[f_i + (2N-1)\pi - \delta\Omega] \delta i \\ &= -r_j \sin(f_i - \delta\Omega) \delta i \\ &= -\frac{r_j}{r_i} \delta z_i \end{aligned} \quad (3-145)$$

Only five of the six elements of the two-position path deviation vector are independent, and the rank of  $\ddot{\mathbf{A}}_{ij}^*$  is reduced from six to five. The four in-plane components of  $\delta \underline{e}$  can be determined uniquely from measurements of  $\delta \underline{r}_i$  and  $\delta \underline{r}_j$ ; the two out-of-plane elements cannot.

If the correction time is such that  $(f_D - f_C) = (2N-1)\pi$ , no finite FTA velocity correction can in general be computed. If VTA guidance is used, a finite correction can be applied as long as  $\underline{v}_R$  has a non-zero component in the  $z$  direction. The computed VTA correction vector lies in the reference trajectory plane.

As in the case of the singularities at  $(t_D - t_C) = NP$ , the singularities at  $(f_D - f_C) = (2N-1)\pi$  can be interpreted physically by a consideration of the requirements imposed on the corrected path. If the actual correction point  $C'$  has a small position variation  $\delta z_C$  normal to the reference trajectory plane and if the difference in true anomaly between  $C'$  and  $D$  is an odd multiple of  $180^\circ$ , then the plane containing position vectors  $\underline{r}_{C'}$  and  $\underline{r}_D$  is perpendicular to the reference trajectory plane. But the plane containing  $\underline{r}_{C'}$  and  $\underline{r}_D$  is also the plane of the corrected trajectory computed by means of FTA guidance. Because the planes of the reference trajectory and the corrected trajectory are perpendicular to each other, a finite FTA velocity correction cannot be determined.

If VTA guidance is used, the destination point is changed from  $D$  to the point at which the line through  $D$  parallel to  $\underline{v}_R$  intersects the plane of the uncorrected trajectory. Thus the VTA correction does not alter the plane of the vehicle's motion; rather, it adjusts the trajectory so that the vehicle arrives at the destination planet at precisely that time when the planet is passing through the plane of the vehicle's actual trajectory.

This type of singularity is discussed further in Sections O.6, O.7, O.15, and O.17.

### 3.16 Singularities at $X = 0$

If  $t_i$  and  $t_j$  are such that  $X = 0$ ,  $\delta z_i$  and  $\delta z_j$  are independent of each other, but a linear relation exists among the components  $\delta p_i$ ,  $\delta q_i$ ,  $\delta p_j$ , and  $\delta q_j$ . This relation, as presented in Equation (O-30), is

$$p_j \delta q_j - p_i \delta q_i = -\frac{b}{2} (3E_M - e \sin E_M \cos E_P) \cdot (\cos \gamma_j \delta p_j + \cos \gamma_i \delta p_i) \quad (3-146)$$



where  $b$  is the length of the semi-minor axis of the reference ellipse. Only five of the six components of the two-position path deviation vector are independent; the rank of matrix  $\tilde{A}_{ij}^*$  is five. Observations of  $\delta \underline{r}_i$  and  $\delta \underline{r}_j$  can be used to determine the two out-of-plane elements of  $\delta \underline{e}$ , but the four in-plane elements are indeterminate.

The  $X = 0$  singularities differ from the other two types in that the singularity points depend on  $e$ , an orbital element of the reference ellipse. In the first two types the singularities occur at known values of the difference in true anomaly, irrespective of the characteristics of the reference trajectory.

Figure O.3 of Appendix O is a plot of  $X$  as a function of  $(E_j - E_i)$  for  $e = 0.25$  and  $E_j = 210^\circ$ ; these values are typical for outbound journeys from Earth to Mars or return trips from Venus to Earth. The singularity points in the plot are the points at which the curve crosses the abscissa axis. The graph indicates an  $X = 0$  point at  $(E_j - E_i) = 0^\circ$  and one additional  $X = 0$  point in the range  $2N\pi < (E_j - E_i) < 2(N+1)\pi$  for each positive value of  $N$ . It is shown in Section O.8 that as  $N$  gets very large, the singularity point associated with a given end point  $P_j$  is the point at which the line joining  $P_j$  and the vacant focus intersects the ellipse when extended through the vacant focus; this is illustrated in Figure O.4.

In the general case, when  $t_C$  and  $t_D$  are such that  $X = 0$  it is not possible to compute a finite FTA correction. A finite VTA correction can be computed as long as  $\underline{v}_R$  has a non-zero component in the reference trajectory plane.

A physical interpretation of the  $X = 0$  singularities can be obtained from an examination of a set of curves in which the time of flight  $t_F$  for a journey from a planet at distance  $r_1$  from the sun to a planet at distance  $r_2$  from the sun is plotted as a function of the length  $a$  of the semi-major axis of the elliptical path. Figure O.8 is such a plot for a journey from Earth to Mars. Each curve in the figure corresponds to a particular value of the transfer angle, which is defined as the total change in true anomaly.

The curves indicate that when  $N = 0$ , corresponding to a transfer angle smaller than  $360^\circ$ , there is no minimum value of  $t_F$  for a given transfer angle at any finite value of  $a$ . However, for  $N = 1$ , corresponding to a transfer angle between  $360^\circ$  and  $720^\circ$ , each curve has a distinct minimum value of  $t_F$ . The type of behavior indicated by the  $N = 1$  curves would also be present in curves for higher values of  $N$  if they were plotted.

In Section O. 11 it is proved that the slope of each time-of-flight curve in Figure O. 8 is proportional to the factor  $X$ , and thus the  $X = 0$  singularities occur at the points corresponding to the minimum time of flight on the various curves.

The physical meaning of the zero-slope points on the curves is that at such points if  $r_1$ ,  $r_2$ , and the transfer angle are held fixed, the time of flight is insensitive to small changes in  $a$ . It follows that if  $r_1$ ,  $r_2$ ,  $t_F$ , and the transfer angle are known at a zero-slope point, it is still not possible to solve for a unique value of  $a$ . This conclusion corroborates the earlier statement, at the beginning of this section, that the in-plane components of  $\delta \underline{e}$  cannot be found from  $\delta \underline{r}_i$  and  $\delta \underline{r}_j$  if  $X = 0$ .

In Section O. 12 the partial derivatives are manipulated to derive a relation that indicates that if  $\underline{r}_1$ ,  $t_F$ , and  $N$  are specified and if  $\underline{r}_2$  is such that  $X = 0$ , then  $\underline{r}_2$  is insensitive to small changes in the in-plane orbital elements. Therefore, it is not possible to compute a small FTA velocity correction which, if applied at  $t_1$ , can correct a predicted position variation at  $t_2$ .

The factor  $X$  is a function of the eccentricity  $e$  and the two eccentric anomalies  $E_C$  and  $E_D$ . When  $t_C$  and  $t_D$  are such that  $X = 0$  for a specified reference trajectory, any small finite change made in the time of arrival alters the effective value of  $E_D$ , so that  $X$  is no longer equal to zero and the singularity condition no longer exists. This, in essence, is what occurs when VTA guidance is utilized at a correction time for which  $X$  would be equal to zero if the arrival time were fixed. The VTA scheme changes the arrival time and computes the finite velocity correction required by the new arrival time.

The ramifications of the  $X = 0$  singularity, including a development of Lambert's theorem for the time of flight, are taken up in considerably greater detail in Sections O.8, O.9, O.10, O.11, O.12, O.16, and O.17.

### 3.17 The Noncritical Vector

The key to a more fundamental understanding of the physics of VTA guidance may lie in an intensive investigation of the rotation of the non-critical vector  $\underline{w}$  as a function of the time of correction  $t_C$ . Such an investigation has not been undertaken in the present study, but certain characteristics of the orientation of  $\underline{w}$  have been determined as a consequence of the analysis of singularities in Appendix O. These characteristics may be summarized as follows:

- (1) At  $t_C = t_D$  the  $\underline{w}$  vector is parallel to  $\underline{v}_R$ .
- (2) When  $(t_D - t_C) = NP$ ,  $\underline{w}$  lies in the plane perpendicular to  $\underline{v}_D$ ; i. e., the component of  $\underline{w}$  in the  $q_C$  direction is zero. The  $z$ -component of  $\underline{w}$  remains the same for all values of  $N$ ; the  $p_C$ -component alternates in sign for successive values of  $N$ . This behavior is indicated by Equation (O-107).
- (3) When  $(f_D - f_C) = (2N-1)\pi$ ,  $\underline{w}$  is parallel to the  $z$ -axis.
- (4) When  $X = 0$ ,  $\underline{w}$  lies in the reference trajectory plane, its direction in the plane being a function of the number of complete circuits between  $t_C$  and  $t_D$ . This is deduced from Equation (O-117).

### 3.18 Low-Eccentricity Reference Trajectories

It has already been pointed out in Section 3.7 that the analysis presented in that section is applicable to ellipses of "moderate" eccentricity and is not directly applicable when the reference trajectory is circular or nearly circular. In this section the effects of small variations of the elements of reference trajectories of low eccentricity are considered. It is shown that the relations already formulated for the transition matrix  $\tilde{C}_{ji}^*$  and the correction matrix  $\tilde{K}_{CD}^*$  are applicable to low-eccentricity two-body orbits.

The term "low eccentricity," as used here, indicates that the eccentricity of the reference trajectory is of the same order of magnitude as the non-dimensional orbital variations ( $\delta a/a$ ),  $\delta e$ , etc. Thus, a term involving the product of  $e$  and one of the small orbital variations is a second-order term in the "small" quantities.

The troublesome characteristic of low-eccentricity trajectories is the fact that large variations in the position of perhelion produce only small variations of the actual trajectory from the reference trajectory. Consequently  $\delta \phi$ , the variation in the longitude of perhelion, which is assumed to be small when  $e$  is appreciably greater than zero, need not be small when  $e$  is close to zero. Likewise, the variations in the anomalies,  $\delta f$ ,  $\delta E$ , and  $\delta M$ , need not be small when  $e$  is close to zero. However, the angles  $(\delta f + \delta \phi)$ ,  $(\delta E + \delta \phi)$ , and  $(\delta M + \delta \phi)$ , which define angular position on the actual trajectory relative to the well-defined and fixed x-axis of the reference trajectory, are small regardless of whether or not  $e$  is small.

With these factors taken into consideration, general relations (i.e., relations applicable for low  $e$  as well as moderate  $e$ ) for  $(\delta E + \delta \phi)$ ,  $\delta r$ , and  $\delta s$  are developed in Appendix H as Equations (H-25), (H-28), and (H-32), respectively.  $\delta z$  is unaffected by the fact that the eccentricity is low. In Appendix J equations specifically applicable when  $e$  is small are derived for  $\delta \underline{r}$ ,  $\delta \underline{v}$ , and  $\delta \underline{a}$ . The expressions for the components of  $\delta \underline{r}$  and  $\delta \underline{v}$  are contained in the matrix equation (J-20); the components of  $\delta \underline{a}$  are presented in (J-21). These equations can be compared with (3-61), which gives the corresponding relations for ellipses of moderate eccentricity.

In Section J.5 it is shown that the constants comprising the vector on the right-hand sides of (J-20) and (J-21) are linearly related to the constants of integration  $k_1$  through  $k_6$  developed in the integration procedure of Appendix G and described in Section 3.6. Therefore, the equations resulting from the integration, (3-31), (3-32), and (3-33), are applicable when the eccentricity is low. From this it can be deduced that the formulation for the transition matrix given by (3-119) and the formulations for  $\mathbf{J}_{DC}^*$  and  $\mathbf{K}_{CD}^*$  described in Section 3.11 are also applicable when  $e$  is small.

The equations for  $\dot{C}_{ji}^*$ ,  $\dot{J}_{DC}^*$ , and  $\dot{K}_{CD}^*$  are not applicable when the eccentricity is so close to unity that a small variation may cause  $e$  to equal or even exceed unity.

### 3.19 The Destination Point

In Section 2.18 it was pointed out that the magnitude of the truncation error due to linearization can be reduced by choosing as the nominal "destination" of the midcourse guidance system a point on the reference trajectory which the vehicle is scheduled to reach at some time earlier than the time of its closest approach to the destination planet. When the assumption of a two-body heliocentric reference trajectory is superimposed on the linearity assumption, there is an even more cogent reason for selecting an early nominal destination point. The two-body approximation neglects, in addition to all second-order and higher-order terms in the Taylor series expansion, the first-order terms associated with the gravitational forces due to the disturbing planets. Thus, the approximation deteriorates markedly as the vehicle approaches the vicinity of a planet.

It is now necessary to establish a criterion for selecting the early destination point. The point at which the reference trajectory intersects the sphere of influence of the destination planet is a reasonable destination point for the linear  $n$ -body analysis of Chapter 2. For the linear two-body analysis this point is too close to the planet; a more conservative selection is the point at which the reference trajectory intersects the sphere of perturbative relevance of the destination planet. This sphere is defined as the boundary along which the gravitational attraction due to the planet is equal to  $1/100$  of the gravitational attraction due to the sun.

Table 3-1 lists the radii of the spheres of influence and the spheres of perturbative relevance for all the planets. The data are derived from Table 9-1a of Ehricke, Vol. II<sup>(31)</sup>.

Table 3-1  
Planetary Data

Planet	Semi-major Axis (a. u.)	Planet Radius (mi.)	Radius of Sphere of Influence (mi.)	Radius of Sphere of Perturbative Relevance (mi.)
Mercury	0.387	1560	$0.694 \times 10^5$	$0.147 \times 10^6$
Venus	0.723	3860	$0.383 \times 10^6$	$1.055 \times 10^6$
Earth	1.0	3960	$0.575 \times 10^6$	$1.86 \times 10^6$
Mars	1.524	2060	$0.358 \times 10^6$	$0.824 \times 10^6$
Jupiter	5.203	43,500	$27.8 \times 10^6$	$154 \times 10^6$
Saturn	9.539	35,800	$26.6 \times 10^6$	$160 \times 10^6$
Uranus	19.182	15,900	$32.2 \times 10^6$	$122.5 \times 10^6$
Neptune	30.058	15,600	$54.0 \times 10^6$	$207 \times 10^6$
Pluto	39.518	(2080)	$21.1 \times 10^6$	$(21.5 \times 10^6)$

## CHAPTER 4

### ILLUSTRATIVE CALCULATIONS

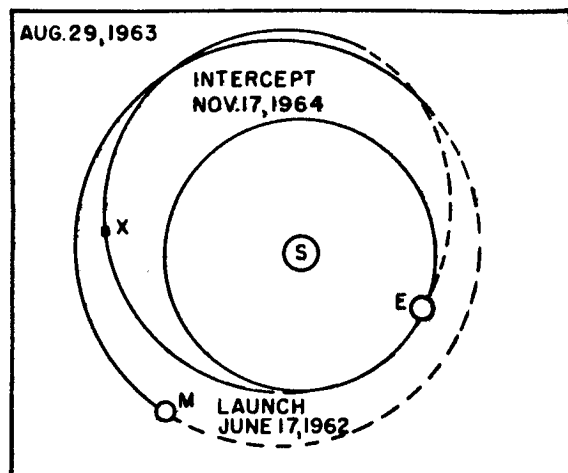
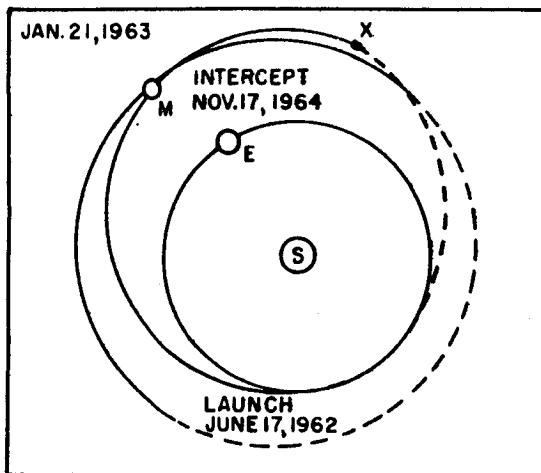
#### 4.1 Summary

Calculations are performed on an Earth-Mars reference trajectory to illustrate the method of determining the optimum time to apply a VTA velocity correction. Curves are obtained for FTA as well as VTA guidance. Additional computations show the effect of position variation and velocity variation at any intermediate time on position variation and velocity variation at the nominal time of arrival at the destination. The analytic formulations of the required matrices, as developed in Chapter 3, are used in the calculations. The physical significance of the curves is discussed.

#### 4.2 Introduction

The method of utilization of the guidance theory developed in Chapters 2 and 3 can best be demonstrated by numerical computations based on a specified interplanetary reference trajectory. In order to show the effects of all three types of singularities discussed in Chapter 3, a reference trajectory has been chosen in which the total transfer angle is greater than  $360^\circ$ . Such a trajectory is the outbound leg of Mars Trajectory No. 1034, described on Pages 102 and 103 of Reference (5). This trajectory is one of those generated by the staff of the M. I. T. Instrumentation Laboratory in connection with its study of the feasibility of an unmanned recoverable interplanetary space probe.

Figure 4-1, which illustrates the trajectory, is a reprint of a portion of Figure 4-8 of Reference (5). The orbits of Earth, Mars, and the space vehicle are shown, and their respective positions at three different times during the voyage are indicated. In the cases of Mars and the space vehicle, that part of the orbit which is represented by a solid line is the part for which the orbital plane is "above" the ecliptic (i. e.,  $z_E$  is positive), while the dashed lines indicate the parts of the orbital planes "below" the ecliptic. The last frame of the figure shows the vehicle's trajectory relative to Mars as it passes by the planet.



S - Sun

E - Earth

M - Mars

X - Space vehicle

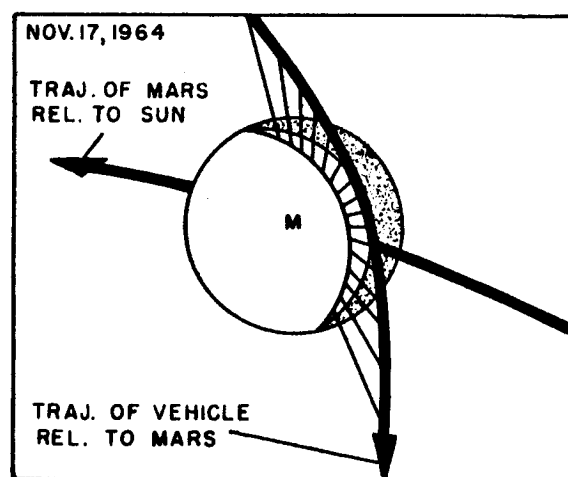
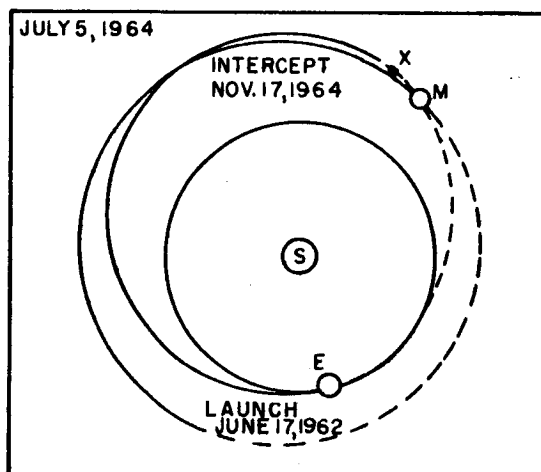


Figure 4.1 Outbound Leg of Trajectory No. 1034



For these illustrative calculations the destination point has been taken as the point of closest approach to Mars, and an elliptical reference trajectory between injection and arrival at the destination has been formulated. The perturbative effect of Mars on the vehicle has been ignored. Although this combination of conditions is not realistic for an accurate guidance analysis (as indicated in Section 3.19), it has the advantage of being more easily adapted to the data that were initially available, and it is adequate to demonstrate the techniques that have been formulated.

The programming of the computations and the plotting of the graphs in this chapter have been carried out by Captain Mack Mauldin, Jr. and Captain Robert G. Millard, both of the United States Air Force, and are described in detail in their Master of Science thesis. (32)

#### 4.3 Characteristics of the Reference Trajectory

The following data apply to Trajectory No. 1034:

Departure date from Earth	June 17, 1962
Arrival date in vicinity of Mars	November 17, 1964
Time of flight	2.422 years
Minimum distance of space vehicle from surface of Mars	4,693 miles

The orbital elements of the heliocentric elliptical trajectory are

$$a = 1.3242 \text{ a. u.}$$

$$e = 0.2432$$

$$t_o = 0.0545 \text{ years after epoch at injection into heliocentric orbit}$$

$$\Omega_E = 85.80^\circ$$

$$i_E = 3.130^\circ$$

$$\omega_E = -158.41^\circ$$

The alternate orbital elements are

$$M_O = -12.86^\circ = M_I$$

$$\phi_E = -72.61^\circ$$

The period and mean angular motion are

$$P = 1.524 \text{ years}$$

$$n = 4.123 \text{ radians/year}$$

At the time of injection,

$$t_I = 0$$

$$f_I = -21.59^\circ$$

$$E_I = -16.92^\circ$$

At the time of arrival at Mars,

$$t_D = 2.422 \text{ years}$$

$$f_D = 552.24^\circ$$

$$E_D = 555.66^\circ$$

$$M_D = 559.42^\circ$$

The total differences in the anomalies are

$$f_D - f_I = 573.83^\circ$$

$$E_D - E_I = 572.58^\circ$$

$$M_D - M_I = 572.28^\circ$$

The magnitude and orientation angles of the relative velocity  $\underline{v}_R$  are

$$v_R = 11,390 \text{ ft/sec}$$

$$\Omega_D = 123.25^\circ$$

$$i_D = 77.12^\circ$$

#### 4.4 Description of Data and Graphs

Figures 4.2 through 4.17 are graphs representing the guidance parameters that have been computed for Trajectory No. 1034. In this section the individual figures are described, and the methods of obtaining the plotted data are indicated. In some cases the equations used by Mauldin and Millard to obtain the data differ in form, but not in substance, from those that are suggested here. The difference is due to the fact that the final forms of some of the equations developed in this thesis were evolved subsequent to the time that the computations were made.

The unit of length used in the computations is the astronomical unit (a. u.), and the unit of time is the year.

In most of the plots the abscissa is  $(f_2 - f_1)$ .  $f_2$  is the same as  $f_D$ , the true anomaly at the destination point; it is equal to  $552.24^\circ$ . The variable part of the abscissa is  $f_1$ , the true anomaly at any earlier point of the trajectory.  $f_1$  is usually associated with the time of a midcourse correction. The value of  $f_1$  (and of time  $t_1$ ) increases from left to right in the graphs; the plotted value of  $(f_2 - f_1)$  increases from right to left. The choice of  $(f_2 - f_1)$  as the abscissa is motivated by the fact that two of the three types of singularities in FTA guidance occur when  $(f_2 - f_1)$  is an integer multiple of  $180^\circ$ .

The reciprocal of the velocity correction is plotted instead of the correction itself, in order to circumvent the scaling difficulty at the singular points, where the FTA correction becomes infinite.

Figure 4.2 is the basic plot for the determination of the optimum time of correction.  $1/c_V$  is plotted as a function of  $(f_2 - f_1)$  for several fixed values of  $\psi$ . The computation is normalized by computing  $c_V$  and  $1/c_V$  for a miss distance magnitude,  $\delta\rho^-$ , of one astronomical unit. The ordinate  $1/c_V$  in the graph has the dimensions of years/a. u. To give the ordinate more physical significance, it may be noted that a velocity of 1 a. u. /year is equivalent to 2.94 mi/sec or 15,540 ft/sec. Thus, if the value of  $1/c_V$  read from the graph is 1 year/a. u. and the miss distance is 9270 miles ( $10^{-4}$  a. u.), the magnitude of the correction is approximately  $1 \frac{1}{2}$  ft/sec.

Figures 4.3 and 4.4 are cross-plots of the data in Figure 4.2. In 4.3 the values of  $(f_2 - f_1)_{\text{opt}}$ , corresponding to the maxima of  $1/c_V$ , are plotted as a function of  $\psi$ ; in 4.4 the maxima of  $1/c_V$  are plotted as a function of  $\psi$ . The dotted portions of the curves, occurring at  $\psi$ 's between  $170^\circ$  and  $180^\circ$ , are caused by the fact that the constant- $\psi$  curves in this region (which are not shown in Figure 4.2) exhibit a high zero-slope plateau, with no definitive values of  $(f_2 - f_1)_{\text{opt}}$ .

Figures 4.5 and 4.6 are the FTA correction curves corresponding to the VTA curves of Figure 4.2. These curves are drawn for  $\delta\rho^- = 1$  a.u. and  $\delta\zeta_D^- = 0$ . It is necessary in the FTA case to assume a value of  $\delta\zeta_D^-$ , because this component of the position variation does affect the FTA correction, although it has no effect on the VTA correction.

The data for Figures 4.2, 4.5, and 4.6 are obtained by use of the equations of Appendix N.

$$(\underline{c}_F)_W = \underline{\dot{X}}_C \underline{c}_F = -\underline{\dot{X}}_C \underline{\dot{K}}_{CD} \underline{\dot{X}}_D^T (\delta \underline{r}_D^-)_W \quad (4-1)$$

Since  $\delta\zeta_D^-$  has been arbitrarily set at zero and  $\delta\rho^-$  has been arbitrarily set at 1 a.u.,

$$(\delta \underline{r}_D^-)_W = (\delta \rho^-) \begin{Bmatrix} \cos \psi \\ \sin \psi \\ 0 \end{Bmatrix} = \begin{Bmatrix} \cos \psi \\ \sin \psi \\ 0 \end{Bmatrix} \quad (4-2)$$

(4-2) is substituted into (4-1).

$$(\underline{c}_F)_W = -\underline{\dot{X}}_C \underline{\dot{K}}_{CD} \underline{\dot{X}}_D^T \begin{Bmatrix} 1 & 0 & 0 \\ 0 & 1 & 0 \\ 0 & 0 & 0 \end{Bmatrix} \begin{Bmatrix} \cos \psi \\ \sin \psi \end{Bmatrix} \quad (4-3)$$

The elements of  $\overset{*}{X}_C \overset{*}{K}_{CD} \overset{*}{X}_D^T$  are given by Equation (N-25). The non-zero element in the third row and third column is not used. The first two components of the solution for  $(\underline{c}_F)_W$  constitute the two-dimensional vector  $\underline{c}_W$ .

The computation is carried out by fixing  $E_1$ , determining the corresponding value of  $(f_2 - f_1)$ , then computing the components of  $(\underline{c}_F)_W$  for ten-degree increments in  $\psi$  between  $0^\circ$  and  $170^\circ$ . The process is repeated for a range of  $E_1$ 's between  $E_I$  ( $-16.92^\circ$ ) and  $E_D$  ( $555.66^\circ$ ).

Figures 4.2, 4.5 and 4.6 show the effect on the velocity correction of a position variation at the destination which lies in the critical plane. Figures 4.7 through 4.11 are the results of a similar study, the difference being that in these plots the position variation at the destination lies either normal to or in the reference trajectory plane. In the figures  $1/c_V$  and  $1/c_F$  are plotted as a function of  $(f_2 - f_1)$  for various orientations of a  $\delta \underline{r}_D$  vector whose magnitude is  $10^{-4}$  a.u. The basic equations used in the computations are

$$\underline{c}_F = - \overset{*}{K}_{CD} \delta \underline{r}_D \quad (4-4)$$

$$\underline{c}_V = \left( \overset{*}{I}_3 - \frac{\underline{w} \underline{w}^T}{\underline{w}^T \underline{w}} \right) \underline{c}_F \quad (4-5)$$

where

$$\underline{w} = \overset{*}{K}_{CD} \underline{v}_R \quad (4-6)$$

and Equation (3-133) contains analytic expressions for the elements of  $\overset{*}{K}_{CD}$ .

Figures 4.12 through 4.17 indicate the effect of a position variation or a velocity variation at time  $t_1$  on the magnitude of the position and velocity variations at time  $t_2$ . The data are obtained by use of the transition matrix, the elements of which are given in Equation (3-119).

$$\delta \underline{x}_2 = \begin{Bmatrix} \delta \underline{r}_2 \\ \delta \underline{v}_2 \end{Bmatrix} = \overset{*}{C}_{21} \begin{Bmatrix} \delta \underline{r}_1 \\ \delta \underline{v}_1 \end{Bmatrix} \quad (4-7)$$

#### 4.5 Analysis of Graphical Results

Figure 4.2 indicates that for the given reference trajectory there is a minimum value of  $c_V$  between  $0^\circ$  and  $180^\circ$  of true anomaly difference, another minimum between  $180^\circ$  and  $360^\circ$ , and a third between  $360^\circ$  and  $540^\circ$ . Except for the unusual behavior of the curves in the range of  $\psi$  close to  $175^\circ$ , the three minima of  $c_V$  for a given  $\psi$  are roughly equal; this is indicated by the cross-plot of Figure 4.4. The actual value of  $c_{V_{\min}}$  is strongly affected by the predicted  $\psi$ . When  $\psi$  is equal to  $90^\circ$ , the required correction is approximately an order of magnitude greater than it is when  $\psi$  is in the vicinity of  $0^\circ$  (or  $180^\circ$ ).

The optimum time of correction,  $t_{C_{\text{opt}}}$ , can be determined directly from the value of  $(f_2 - f_1)$  corresponding to  $c_{V_{\min}}$ . Figure 4.3 indicates that in the range of  $\psi$  between  $45^\circ$  and  $135^\circ$  there is little variation of  $t_{C_{\text{opt}}}$  with  $\psi$ , but in the  $\psi$  ranges  $0^\circ$  to  $45^\circ$  and  $135^\circ$  to  $180^\circ$  (particularly in the vicinity of  $\psi = 175^\circ$ ) the variation of  $t_{C_{\text{opt}}}$  with  $\psi$  is noticeable.

Curves similar to those of Figure 4.3, but with  $t_{C_{\text{opt}}}$  replacing  $(f_2 - f_1)_{\text{opt}}$  as the ordinate, can be built into the on-board computer of a space vehicle and used to determine the time of the next VTA velocity correction. The fact that there are three values of  $t_{C_{\text{opt}}}$  for each  $\psi$  requires that some type of simple strategy be designed to determine which of the three to choose if all three are subsequent to the time at which a reliable value of  $\psi$  has been computed. If the space mission is such that three or more midcourse corrections are to be made, an effective strategy is to apply the correction at the earliest  $t_{C_{\text{opt}}}$  following the time of determination of  $\psi$ . It is then possible to apply three corrections, each at the  $t_{C_{\text{opt}}}$  corresponding to the  $\psi$  computed for a particular segment of the actual trajectory. If only one midcourse correction is to be applied during the voyage, it is generally advantageous to select the last of the three values of  $t_{C_{\text{opt}}}$  in order to reduce the uncertainty in position at the time of arrival at the destination. Selection of the last  $t_{C_{\text{opt}}}$  tends to reduce position uncertainty in two ways: first, it allows more time for gathering data

from which  $\delta \underline{x}_D^-$  is estimated, and consequently the accuracy of the computation of  $\underline{c}_V$  is improved; secondly, uncertainty in the application of corrective thrust generally causes a smaller uncertainty in final position if the time of the correction is closer to the time of arrival.

The problem of which  $t_{C_{opt}}$  to select for a given  $\psi$  has no relevance for manned space missions. The primary consideration for such missions is minimization of the time of flight. The total transfer angle  $(f_D - f_I)$  for one leg of a manned flight is normally less than  $180^\circ$ ; consequently there is only one value of  $t_{C_{opt}}$  for each  $\psi$ . The portion of Figure 4.2 for the range of  $(f_2 - f_1)$  between  $0^\circ$  and  $180^\circ$  is typical of the curves that may be expected on an outbound manned trip to Mars.

Figure 4.3 indicates that the minimum value of  $(f_2 - f_1)_{opt}$  is  $80^\circ$ . If the vehicle is less than  $80^\circ$  away from its destination, there is no need to determine  $(f_2 - f_1)_{opt}$ , for it will have occurred at a point on the trajectory that the vehicle has already passed. The most economical time to correct is then the earliest feasible time (i. e., the earliest time at which a reliable estimate of  $\delta \underline{\rho}^-$  is available).

Figures 4.5 and 4.6 contain FTA curves corresponding to the VTA curves of Figure 4.2. It is difficult to make a direct comparison of the VTA and FTA velocity corrections, because the latter are dependent on the additional variable  $\delta \zeta_D^-$ ; the curves of Figures 4.5 and 4.6 are drawn for  $\delta \zeta_D^-$  equal to zero. For the non-singular points in the two figures, the effect of varying  $\delta \zeta_D^-$  at a given  $(f_2 - f_1)$  and a given  $\psi$  is to produce a variation in  $c_F$  from a minimum value which is equal to  $c_V$  under the given conditions to a maximum value which is at least as much greater than the plotted value of  $c_F$  as the plotted value is greater than  $c_V$ . At the singular points  $c_F$  is infinite regardless of the value of  $\delta \zeta_D^-$ .

The most immediately noticeable difference between the VTA and FTA curves is the difference in the number of singularities. Whereas the only singularities in  $c_V$  occur at  $(f_2 - f_1) = 0^\circ$  and  $360^\circ$ , there are singularities in  $c_F$  at  $(f_2 - f_1) = 0^\circ, 180^\circ, 360^\circ, 470^\circ$ , and  $540^\circ$ . The singularity at  $470^\circ$  is the  $X = 0$  singularity. These results are in agreement with the analysis of Appendix O. Although there is no singularity in the  $c_V$  curves

at true anomaly differences of  $180^\circ$  and  $540^\circ$ , the curves do exhibit minima of  $1/c_V$  (or maxima of  $c_V$ ) at these points; however, the effect of the  $X = 0$  singularity is completely obliterated by VTA guidance. This behavior is due in part to the fact that  $i_D = 77^\circ$ , and consequently  $\underline{v}_R$  is inclined only slightly to the reference trajectory plane. This orientation of  $\underline{v}_R$  tends to make the VTA system relatively more effective in counteracting the in-plane singularity at  $470^\circ$  and relatively less effective in counteracting the out-of-plane singularities at  $180^\circ$  and  $540^\circ$ .

When the vehicle is fairly close to its destination, i. e., for values of  $(f_2 - f_1)$  of  $20^\circ$  or less, the velocity correction is essentially independent of  $\psi$  and is the same for VTA as it is for FTA. The variation of  $1/c$  with  $(f_2 - f_1)$  is fairly linear in this range; the slope is approximately 0.0067 yr./a. u. per degree of true anomaly for a predicted miss distance of 1 a. u.

When  $(f_2 - f_1)$  increases from  $20^\circ$  toward  $45^\circ$ , the curves for the various values of  $\psi$  start to diverge from the common curve characterizing the region below  $20^\circ$ , but for a given  $\psi$  and a given  $(f_2 - f_1)$  the ordinate is still about the same in the FTA case as it is in the VTA case. Consequently, if a final vernier correction is to be made at a value of  $(f_2 - f_1)$  less than  $45^\circ$  and if  $\delta r_D^-$  is equal to  $\delta \rho^-$  (i. e., if the noncritical component  $\delta \zeta_D^-$  is small enough so that it does not appreciably affect the magnitude of  $\delta \underline{r}_D^-$ ), there is no fuel saving effected by the use of VTA for this correction. The really important consideration in making the vernier correction is to make it as early as possible.

The general shapes of the curves for VTA and FTA guidance are quite similar through the range  $0^\circ$  to  $180^\circ$  in  $(f_2 - f_1)$ , and there is still some similarity in the range  $180^\circ$  to  $360^\circ$ . The similarity is greatest for  $\psi$ 's near  $90^\circ$ . In the range of  $(f_2 - f_1)$  between  $360^\circ$  and  $540^\circ$  the VTA and FTA curves are decidedly different due to the effect of the  $X = 0$  singularity at  $(f_2 - f_1) = 470^\circ$ .

With the exception of the special case  $\psi = 0^\circ$ , each of the constant- $\psi$  curves for FTA guidance has four minimum values of  $c_F$  in the plotted range of  $(f_2 - f_1)$ . The minima occur at intermediate points between the singularities at  $(f_2 - f_1) = 540^\circ, 470^\circ, 360^\circ, 180^\circ$ , and  $0^\circ$ . For  $\psi$ 's near  $0^\circ$  (or  $180^\circ$ ) the minima tend to decrease in magnitude as the vehicle gets closer to the



destination. For  $\psi$ 's near  $90^\circ$ , the minima in the ranges  $470^\circ$  to  $360^\circ$ ,  $360^\circ$  to  $180^\circ$ , and  $180^\circ$  to  $0^\circ$  are roughly equal, and the minimum in the range  $540^\circ$  to  $470^\circ$  is somewhat higher than the other three. If FTA guidance is to be used and if the predicted  $\psi$  is near  $0^\circ$  or  $180^\circ$ , an appreciable amount of fuel can usually be saved by delaying the correction until the point corresponding to the last minimum of  $c_F$  has been reached.

When  $\psi = 0^\circ$ , there is no singularity in  $c_F$  at  $(f_2 - f_1) = 180^\circ$  or  $540^\circ$ . This is due to the fact that in this special case, with  $\delta \xi_D^-$  stipulated to be zero,  $\delta \underline{r}_D^-$  lies in the reference trajectory plane; consequently,  $\delta z_D^-$  is equal to zero, and the out-of-plane singularities have no effect. Instead of there being singularities at  $(f_2 - f_1) = 180^\circ$  and  $540^\circ$ , a comparison of Figure 4.5 with Figure 4.2 indicates that at each of these points  $c_F$  is equal to  $c_V$ . The two are equal because at these points the noncritical vector  $\underline{w}$  is parallel to the  $z$ -axis; therefore,  $\underline{c}_V$  is the component of  $\underline{c}_F$  in the reference trajectory plane. But since  $\delta z_D^-$  is zero,  $\underline{c}_F$  itself lies in the reference trajectory plane, and consequently  $\underline{c}_F$  and  $\underline{c}_V$  are identical.

When  $\psi = 0^\circ$ , the miss distance vector  $\delta \underline{\rho}^-$  lies in the reference trajectory plane. If the position variation vector  $\delta \underline{r}_D^-$  lies along the  $z$ -axis, the miss distance vector is parallel to the  $\eta_D$ -axis, and  $\psi = 90^\circ$ . Thus,  $\psi$ 's in the vicinity of  $0^\circ$  or  $180^\circ$  are associated primarily with position variations in the reference trajectory plane, while  $\psi$ 's close to  $90^\circ$  are associated with position variations normal to the reference trajectory plane. Additional insight into the guidance problem can be obtained by studying the way in which a position variation either in or normal to the reference trajectory plane affects the magnitude of  $\underline{c}_V$  and  $\underline{c}_F$ . Figures 4.7 through 4.11 present the results of such a study;  $1/c_V$  and  $1/c_F$  are plotted for various orientations of a position variation  $\delta \underline{r}_D^-$  whose magnitude is  $10^{-4}$  a.u. or 9270 miles.

A link may be established between the curves that have already been analyzed and the curves of Figures 4.7 through 4.11. The  $\psi = 90^\circ$  curve of Figure 4.2 is the same, except for a difference in the scale and the dimensions of the ordinate, as the VTA curve of Figure 4.7. The  $\psi = 0^\circ$  curve of Figure 4.2 would be the same as a curve for  $\mu_2 = \Omega_D = 123^\circ$  in Figure 4.9 if such a curve were drawn; the  $\mu_2 = 120^\circ$  curve of 4.9 closely

resembles the  $\psi = 0^\circ$  curve in 4.2.  $\mu_2$  is the angle between  $\delta \underline{r}_2^-$  and the  $p_2$ -axis. The FTA curve for  $\psi = 90^\circ$  in Figure 4.5 bears a close similarity to the FTA curve of Figure 4.7 for values of  $(f_2 - f_1)$  between  $0^\circ$  and  $360^\circ$ ; at higher values of  $(f_2 - f_1)$  the curves are no longer similar. The reason that these two curves are not completely equivalent, as is the case for their VTA counterparts, is that in the curve of 4.5 the position variation to be corrected is parallel to the  $\eta_D$ -axis, while in the curve of 4.7 the variation is parallel to the  $z_D$ -axis; the two axes are  $13^\circ$  apart. The in-plane singularity at  $(f_2 - f_1) = 470^\circ$  affects the curve of Figure 4.5 but has no effect on the curve of Figure 4.7. Finally, the FTA curve for  $\psi = 0^\circ$  in Figure 4.5 is quite similar to the  $\mu_2 = 120^\circ$  curve in Figure 4.11.

The curves of Figure 4.7 show that the maxima and minima of  $c_V$  occur at the same values of  $(f_2 - f_1)$  as the maxima and minima of  $c_F$  when  $\delta \underline{r}_D^-$  is parallel to the  $z$ -axis. At each of its maxima  $c_F$  goes to infinity, while  $c_V$  goes to infinity at  $(f_2 - f_1) = 0^\circ$  and  $360^\circ$  but reaches finite maxima at  $(f_2 - f_1) = 180^\circ$  and  $540^\circ$ . The minima of  $c_V$  are not materially lower than the corresponding minima of  $c_F$ . The variation of  $1/c_F$  with  $(f_2 - f_1)$  is periodic, repeating itself every  $360^\circ$  of  $(f_2 - f_1)$ . The periodicity becomes apparent if  $k_{33}$ , the only element in the correction matrix  $\mathbf{K}_{CD}^*$  that affects  $z$ -axis motion, is written as follows:

$$k_{33} = \frac{h}{r_C r_D \sin(f_D - f_C)} \quad (4-8)$$

The variation of  $1/c_V$  with  $(f_2 - f_1)$  does not repeat itself exactly every  $360^\circ$  of  $(f_2 - f_1)$  due to the presence of the secular term in  $k_{11}$ , which affects  $\underline{w}$ , which in turn affects  $\underline{c}_V$ . The fact that the FTA and VTA curves are so close to each other is a manifestation of a point that has already been made, namely that for this particular reference trajectory, with  $\underline{v}_R$  being situated close to the reference trajectory plane, VTA guidance is relatively ineffective in reducing the magnitude of the velocity correction if  $\delta \underline{r}_D^-$  is parallel to the  $z$ -axis.

Comparison of the VTA curves of Figures 4.8 and 4.9 with the FTA curves of Figures 4.10 and 4.11 indicates that VTA usually reduces the magnitude of the required correction by an appreciable percentage if  $\delta \underline{r}_2$  is in the reference trajectory plane. For any value of  $\mu_2$ , the VTA and

FTA curves are tangent to each other at  $(f_2 - f_1) = 180^\circ$  and  $540^\circ$ ; this is due to the fact that the noncritical vector  $\underline{w}$  is parallel to the z-axis at these two values of  $(f_2 - f_1)$ . Both  $c_V$  and  $c_F$  go to infinity at  $(f_2 - f_1) = 360^\circ$  for all values of  $\mu_2$  except  $\mu_2 = 90^\circ$ . For the special case  $(f_2 - f_1) = 360^\circ$  and  $\mu_2 = 90^\circ$ , the VTA and FTA curves are tangent to each other at a finite value of  $1/c$ . Sections O.4, O.5, and O.14 indicate the reason for the absence of the singularity at  $(f_2 - f_1) = 360^\circ$  when  $\mu_2 = 90^\circ$ , i. e., when  $\delta \underline{r}_2^-$  is parallel to  $\underline{v}_2$ .

The really striking feature of the curves of Figures 4.7 to 4.11 is the large difference in magnitude between an optimum VTA correction of a z-axis position variation and an optimum VTA correction of a position variation in the plane of the reference trajectory. To emphasize this point, the VTA curve of Figure 4.7 has been added to Figures 4.8 and 4.9, and the FTA curve of Figure 4.7 has been added to Figures 4.10 and 4.11. If only the range of  $(f_2 - f_1)$  between  $0^\circ$  and  $180^\circ$  is considered,  $c_{V_{opt}}$  for a z-axis position variation is at least three to four times as large as  $c_{V_{opt}}$  for a position variation of the same magnitude that lies in the reference trajectory plane. For the optimum points at larger values of  $(f_2 - f_1)$ , the ratio of out-of-plane  $c_{V_{opt}}$  to in-plane  $c_{V_{opt}}$  is at least as large and may be considerably larger, depending on the orientation of  $\delta \underline{r}_2^-$  in the reference trajectory plane; when  $\delta \underline{r}_2^-$  lies close to the  $q_2$ -axis,  $c_{V_{opt}}$  is much smaller than it is when  $\delta \underline{r}_2^-$  is close to the  $p_2$ -axis.

When FTA guidance is used, the disparity between out-of-plane  $c_{F_{opt}}$  and in-plane  $c_{F_{opt}}$  is significant but not nearly so great as in the VTA case. This is shown in Figures 4.10 and 4.11.

Figures 4.12 through 4.17 illustrate the contrast between in-plane motion and out-of-plane motion in a different way. The effect on  $\delta r_2$  and  $\delta v_2$  is shown for either a position variation of 927 miles  $= 10^{-5}$  a. u. at  $t_1$  or a velocity variation of one foot per second at  $t_1$ . The most significant curves from the guidance standpoint are the curves relating  $\delta r_2$  to  $\delta \underline{v}_1$  in Figures 4.13 and 4.16. When  $\delta \underline{v}_1$  is parallel to the  $q_1$ -axis,

$\delta r_2$  is usually several times as large as it is when  $\delta \underline{v}_1$  is parallel to the  $p_1$ -axis; in turn, when  $\delta \underline{v}_1$  is parallel to the  $p_1$ -axis,  $\delta r_2$  is usually several times as large as it is when  $\delta \underline{v}_1$  is parallel to the  $z$ -axis. If the concept of "sensitivity" is introduced, it may be stated that the magnitude of the position variation at the destination is most sensitive to a velocity variation in the  $q_1$  direction at time  $t_1$ , is less sensitive to a velocity variation in the  $p_1$  direction, and is least sensitive to a velocity variation in the  $z$  direction. Thus, for a given magnitude of  $\delta \underline{r}_2$ , the magnitude of the optimum FTA correction is generally smallest if the direction of the required correction is close to the  $q_C$ -axis, larger if its direction is close to the  $p_C$ -axis, and largest of all if its direction is close to the  $z$ -axis.

Figures 4.13 and 4.16 also show the effect of an error in injection velocity on position variation at the destination. For an injection velocity error of 1 ft/sec,  $\delta r_2$  is equal to almost 50,000 miles if the velocity error is in the  $q_1$  direction, about 5,000 miles if the velocity error is in the  $p_1$  direction, and slightly less than 1,000 miles if the velocity error is in the  $z$  direction. If the uncertainty in injection velocity is isotropic, it is probable that the vector  $\delta \underline{r}_2$ , before the first midcourse correction, will lie close to the reference trajectory plane.

It may be noted from Figure 4.16 that in this particular example the time of actual injection is worse than any later time from the standpoint of sensitivity of position variation at the destination to initial velocity error. For a Hohmann-type transfer, in which  $(f_D - f_I)$  is  $180^\circ$ , the sensitivity to an injection velocity error in the  $q_1$  direction would be less than half of the value shown for  $(f_D - f_I) = 574^\circ$ .

The effect of a position variation at  $t_1$  on position variation at  $t_2$  is indicated in Figures 4.12 and 4.14. Again the sensitivity in the  $z$  direction is very much less than the sensitivity in the  $p$ - $q$  plane. This time, however, the  $p_1$ -axis is the most sensitive axis. A position error of one mile in the  $p_1$  direction at injection causes a position variation of forty miles at the destination. For the  $q_1$  and  $z$  directions the sensitivity factor is approximately one mile of position variation at  $t_D$  per mile of position variation at  $t_I$ . The actual launch point at  $(f_D - f_I) = 574^\circ$  has a sensitivity factor in the critical  $p_1$  direction that is twice as large as the factor for a Hohmann transfer.

An isotropic distribution of the uncertainties in position and velocity at injection is not the most desirable distribution. It is preferable to design the injection guidance system in such a manner that the velocity uncertainty in the direction of the velocity vector is minimized even if this results in an increased velocity uncertainty along the other two axes of the  $p\ q\ z$  coordinate system. In the case of position variation, the uncertainty in the  $p_1$  direction should be reduced as much as possible.

A position variation  $\delta r_1$  of  $10^{-5}$  a.u. produces an effect on  $\delta r_2$  that is of the same order of magnitude as a velocity variation  $\delta v_1$  of 1 ft/sec. In the design of the injection guidance system it is relatively easy to keep the uncertainty in heliocentric position at injection below  $10^{-5}$  a.u., but it is virtually impossible to design a system in which the uncertainty in injection velocity is as low as 1 ft/sec. Therefore, the curves relating  $\delta r_2$  to  $\delta v_1$  are of considerably greater importance to the guidance system analyst than the curves relating  $\delta r_2$  to  $\delta r_1$ .

In the guidance concepts considered in this study,  $\delta \underline{r}_D$  is the controlled vector and hence is of paramount importance. The vector  $\delta \underline{v}_D$ , although not controlled, is monitored. It is of some interest, therefore, to examine the effects of  $\delta \underline{r}_1$  and  $\delta \underline{v}_1$  on the magnitude of  $\delta \underline{v}_2$ . These effects are shown in Figures 4.12, 4.13, 4.15, and 4.17. For  $\delta z_1 = 10^{-5}$  a.u., the maximum magnitude of  $\delta v_{z_2}$  is 0.57 ft/sec; for  $\delta v_{z_1} = 1$  ft/sec, the maximum magnitude of  $\delta v_{z_2}$  is 1 ft/sec. When  $\delta \underline{r}_1$  lies in the reference trajectory plane, its effect on  $\delta v_2$  is greatest if  $\delta \underline{r}_1$  is close to the  $p_1$ -axis, much smaller if  $\delta \underline{r}_1$  is close to the  $q_1$ -axis (but still considerably larger than the effect of  $\delta v_{z_1}$ ). The in-plane relationship between  $\delta \underline{v}_1$  and  $\delta v_2$  is such that  $\delta v_2$  is most sensitive to a  $\delta \underline{v}_1$  in the  $q_1$  direction and much less sensitive to a  $\delta \underline{v}_1$  in the  $p_1$  direction.

The shapes of the curves in Figure 4.14 are quite similar to the shapes of the curves in Figure 4.15 for like orientations of  $\delta \underline{r}_1$ ; also, the shapes of the curves in Figure 4.16 are similar to the shapes in Figure 4.17 for like orientations of  $\delta \underline{v}_1$ . Thus, in relating  $\delta \underline{r}_1$  to either  $\delta r_2$  or  $\delta v_2$ , the  $p_1$  direction is the critical direction; in relating  $\delta \underline{v}_1$  to either  $\delta r_2$  or  $\delta v_2$ , the  $q_1$  direction is the critical direction.

As in the case of the effects on  $\delta r_2$ , the effect on  $\delta v_2$  of a small error in injection position in the critical  $p_1$  direction or a small error in injection velocity in the critical  $q_1$  direction is greater at the actual injection point than at any subsequent point of the trajectory. For a Hohmann transfer the sensitivity of  $\delta v_2$  to injection errors in the critical directions would be halved.

To conclude this section, the effect on the magnitude of the required VTA velocity correction of using a pre-programmed correction time rather than one determined from the phase angle  $\psi$  will be investigated. The analysis is based on consideration of a manned flight; therefore, only the range of  $(f_2 - f_1)$  between  $0^\circ$  and  $180^\circ$  is studied.

The pre-programmed  $t_C$  can be chosen after an analysis of the curves of Figure 4.2. The fact that  $\delta \underline{r}_D^-$  is likely to be oriented close to the reference trajectory plane and the critical plane is inclined at an angle of  $77^\circ$  to the reference trajectory plane indicates that values of  $\psi$  close to  $0^\circ$  or  $180^\circ$  are more likely to occur than values in the vicinity of  $90^\circ$ ; this suggests that the curves for  $\psi = 0^\circ$ ,  $10^\circ$ , and  $170^\circ$  be favored in selecting a fixed value of  $t_C$ . On the other hand, if the unlikely does occur and  $\psi$  on a particular flight is computed to be close to  $90^\circ$ , the minimum correction for a given  $\delta \rho^-$  is much larger than it would be if  $\psi$  were  $0^\circ$ ; the pre-selected  $t_C$  should not have too adverse an effect on the magnitude of the correction when  $\psi = 90^\circ$ . Based on these considerations, a reasonable compromise is to apply the midcourse correction at a  $t_C$  corresponding to  $(f_2 - f_1) = 100^\circ$ .

The effect of the fixed correction time on the magnitude of the VTA correction is shown in Table 4-1 for four different  $\psi$ 's. The effect is most pronounced for  $\psi = 0^\circ$ , where the ratio of the correction at  $(f_2 - f_1) = 100^\circ$  to  $c_{V_{\min}}$  is 1.82; for the other values of  $\psi$  in the table the ratio is less than 1.1. At  $\psi = 90^\circ$   $c_{V_{\min}}$  is seven times the value at  $\psi = 0^\circ$ ; therefore, even though the ratio is only 1.08 at  $\psi = 90^\circ$ , the numerical increase in  $c_V$  is sizeable.

TABLE 4-1

Effect of Fixed Correction Time on Magnitude of VTA Correction

$\psi$	$c_{V \min}$ (a.u./yr.)	$c_{V(f_2 - f_1)} = 100^\circ$ (a.u./yr.)	$\left[ \frac{c_{V(f_2 - f_1)} - c_{V \min}}{c_{V \min}} \right]$ (a.u./yr.)	$\frac{c_{V(f_2 - f_1)} - c_{V \min}}{c_{V \min}}$
$0^\circ$	0.44	0.80	0.36	1.82
$10^\circ$	0.88	0.91	0.03	1.03
$170^\circ$	0.96	1.05	0.09	1.09
$90^\circ$	3.08	3.33	0.25	1.08

#### 4.6 Concluding Remarks

The salient points of the analysis in the last section may be summarized as follows:

1. The method presented for determining the optimum time of application of a VTA correction as a function of the phase angle of the miss distance vector is practical.
2. The same set of curves (Figure 4.2) used to determine the optimum correction time a posteriori can also be used alternatively for the determination of a pre-programmed correction time.
3. The variant motion along the z-axis is quantitatively quite different from the variant motion in the reference trajectory plane. The state of the vehicle at the time of arrival at the destination is relatively insensitive to changes in state along the z-axis at the initial or midcourse points. Conversely, the midcourse velocity correction required to produce a specified change in state along the z-axis at the time of arrival is relatively large.
4. The sensitivity of a Venus or Mars trajectory to a 1 ft/sec variation in velocity at a given time is roughly equivalent to the sensitivity of the trajectory to a 1,000 mile variation in position at the same time.
5. The sensitivity of the trajectory is greatest to that component of velocity variation which is parallel to the reference velocity vector and to that component of position variation which is perpendicular to the reference velocity vector and in the reference trajectory plane.
6. It is desirable to design the injection guidance system so that the uncertainty in the magnitude of the injection velocity vector is reduced to a minimum, even at the expense of some increase in the uncertainty of the direction of the injection velocity vector.
7. Although position uncertainty at injection is far less critical than velocity uncertainty, the injection guidance scheme is improved if the position variation component in the direction normal to the injection velocity vector and in the reference trajectory plane is minimized.
8. For "wrap-around" trajectories, in which the total transfer angle is greater than  $360^\circ$ , the sensitivity to injection errors is considerably greater than it is for Hohmann-type trajectories, in which the total transfer angle is  $180^\circ$ .



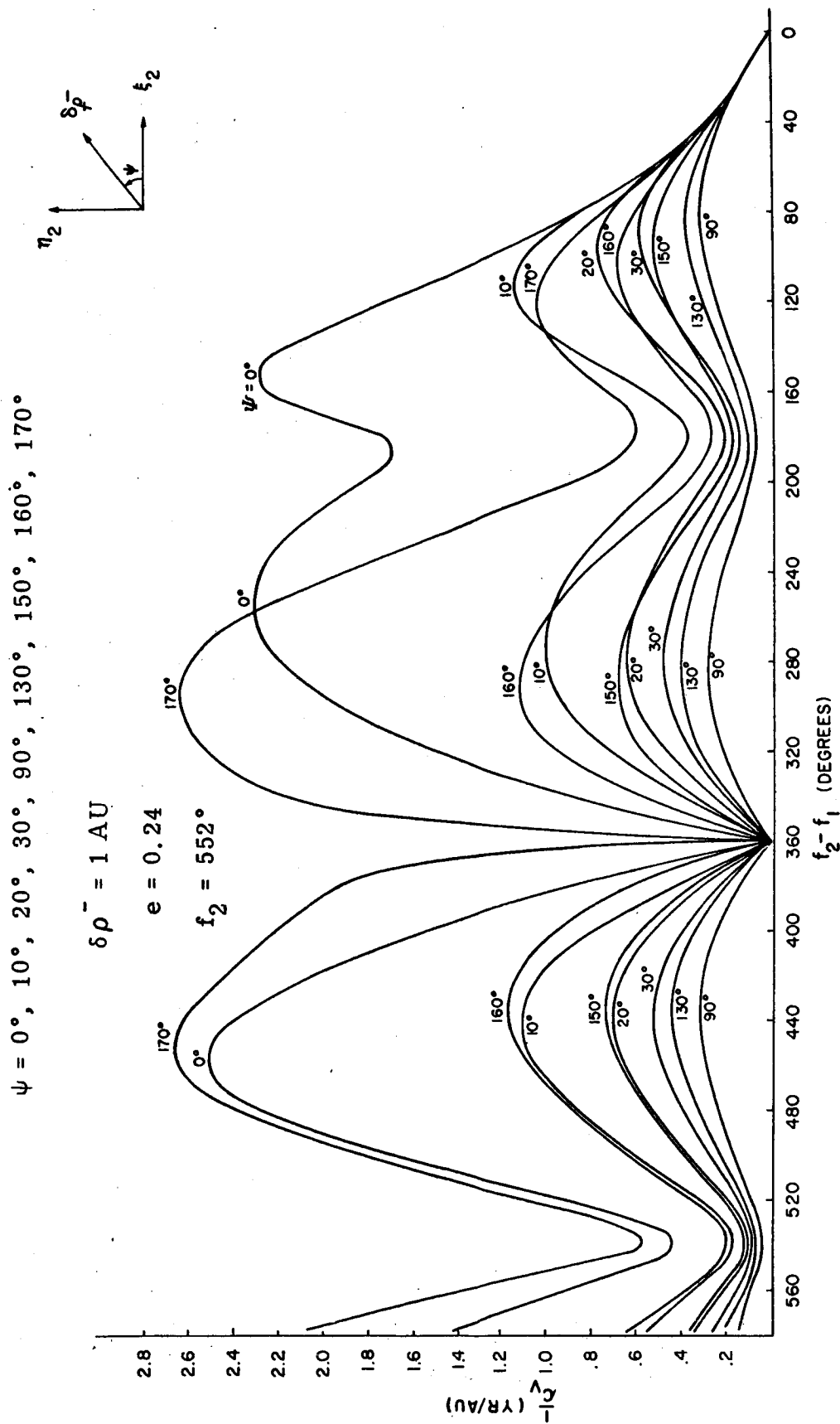


Figure 4.2 Reciprocal of Magnitude of VTA Velocity Correction,  $1/c_V$ ,  
 vs. Difference in True Anomaly,  $(f_2 - f_1)$ , for Constant  
 Values of Phase Angle  $\psi$ .

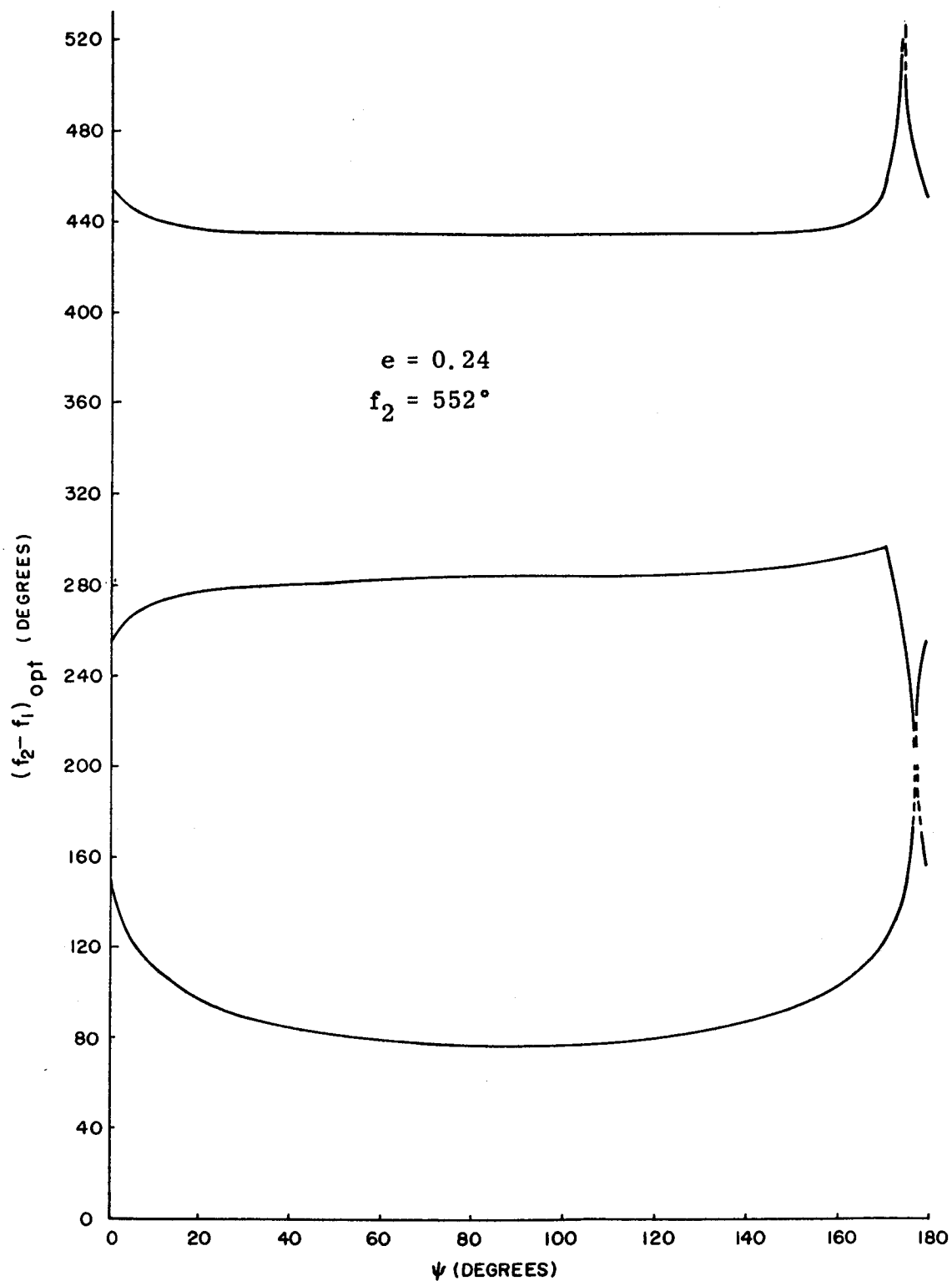


Figure 4.3 Optimum Value of True Anomaly Difference for Application of VTA Velocity Correction

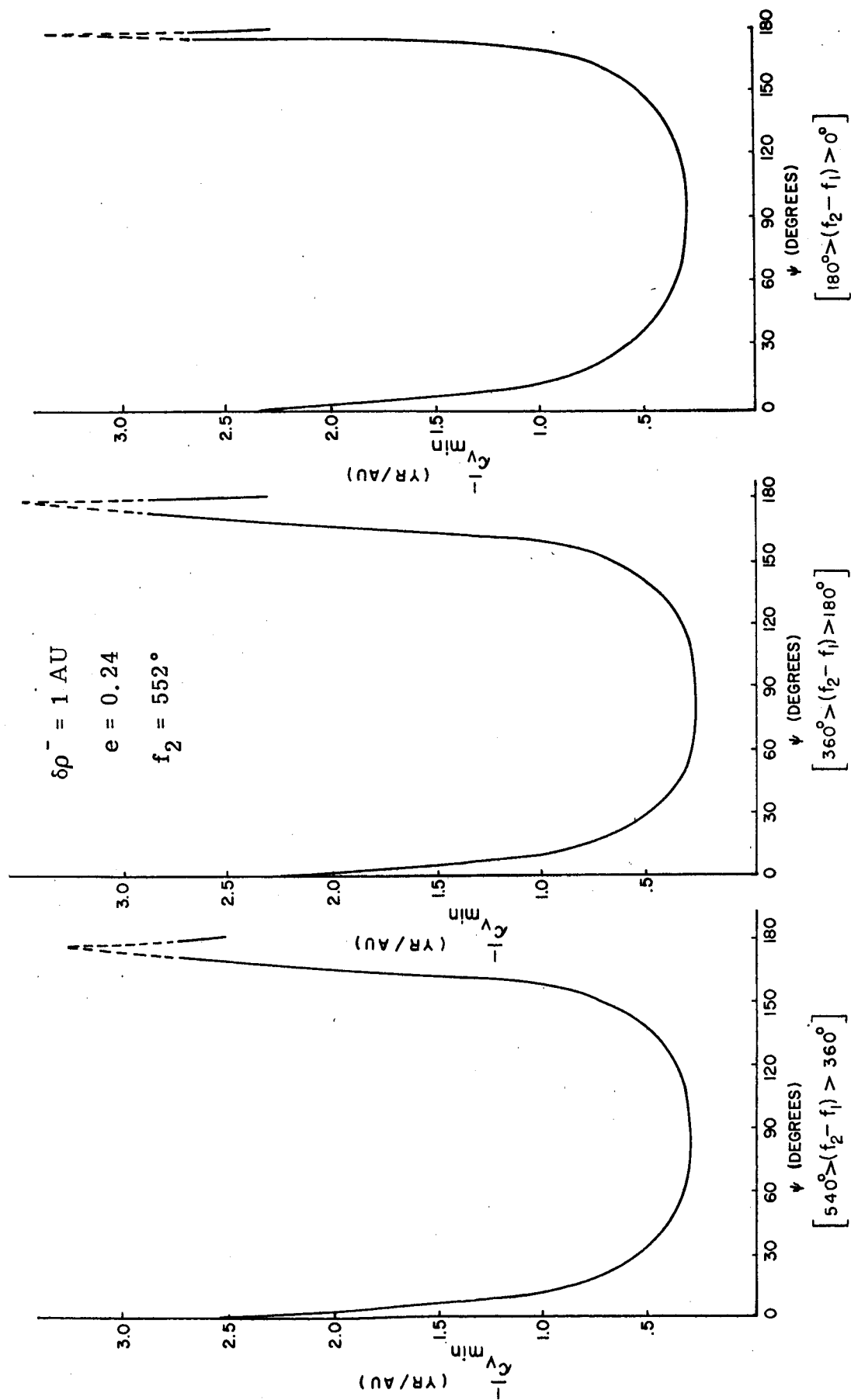


Figure 4.4 Reciprocal of Minimum Value of Magnitude of VTA Velocity

Correction,  $1/c_{v \min}$ , as a Function of Phase Angle  $\psi$ .

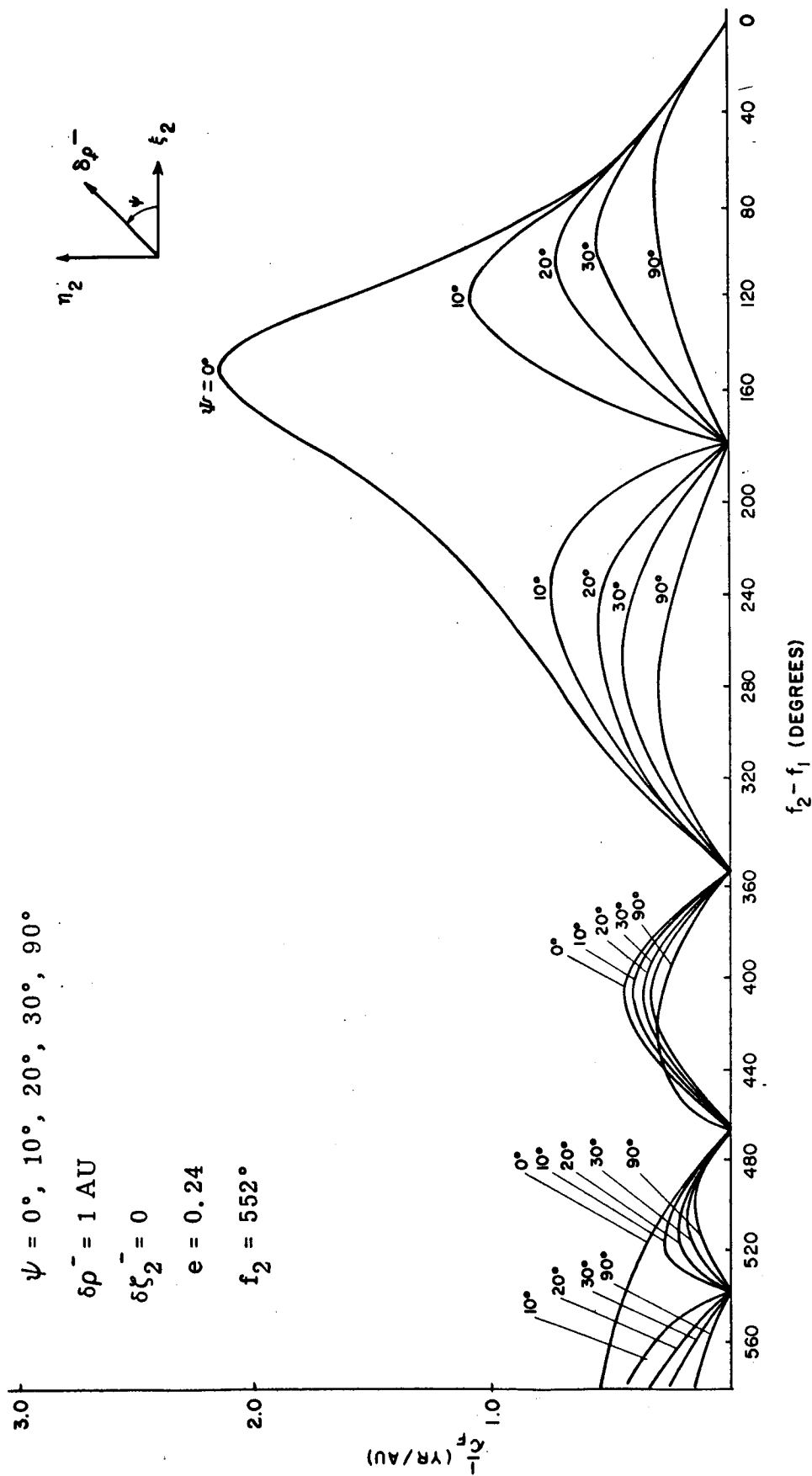


Figure 4.5 Reciprocal of Magnitude of FTA Velocity Correction,  $1/c_F$ , vs. Difference in True Anomaly,  $(f_2 - f_1)$ , for Constant Values of Phase Angle  $\psi$  between  $0^\circ$  and  $90^\circ$

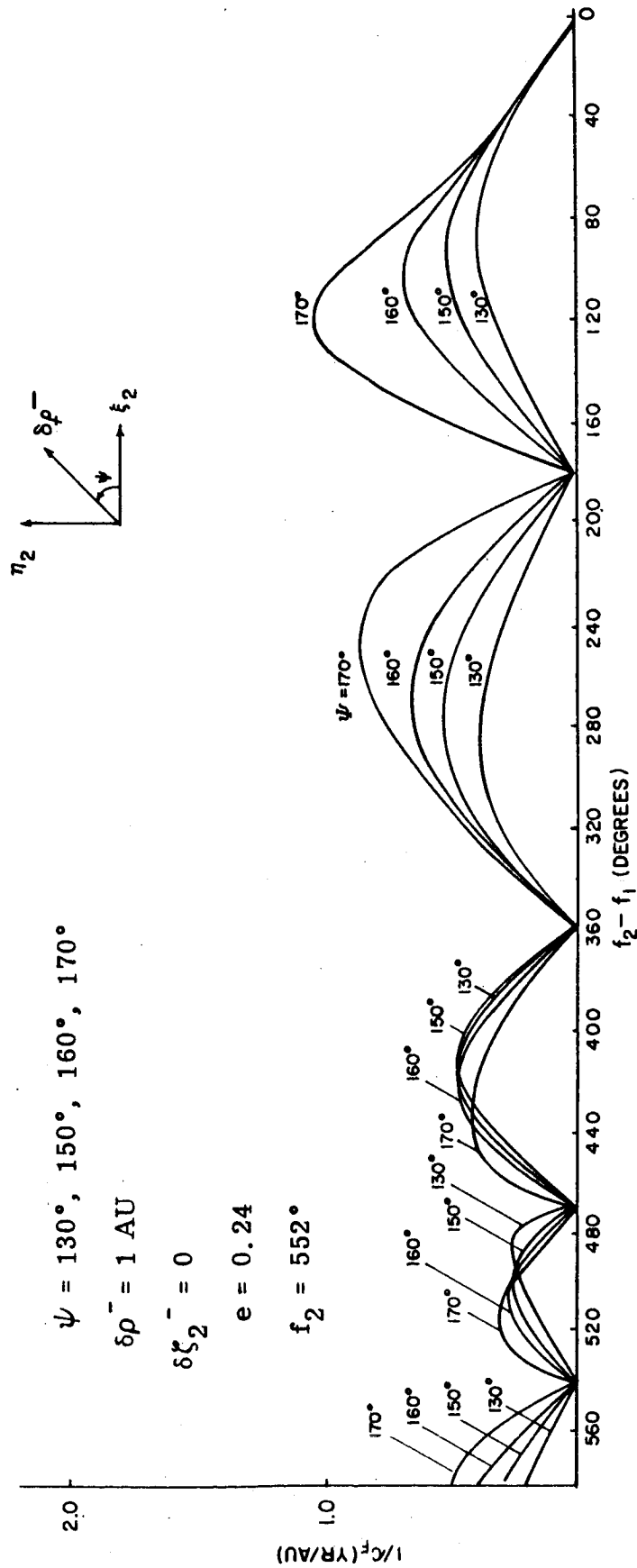


Figure 4.6 Reciprocal of Magnitude of FTA Velocity Correction,  $1/c_F$ , vs.  
 Difference in True Anomaly,  $(f_2 - f_1)$ , for Constant Values of  
 Phase Angle  $\psi$  between  $130^\circ$  and  $170^\circ$

$$\delta p_2^- = 0 = \delta q_2^-$$

$$\delta z_2^- = 9270 \text{ Miles} = 10^{-4} \text{ AU}$$

$$e = 0.24$$

$$f_2 = 552^\circ$$

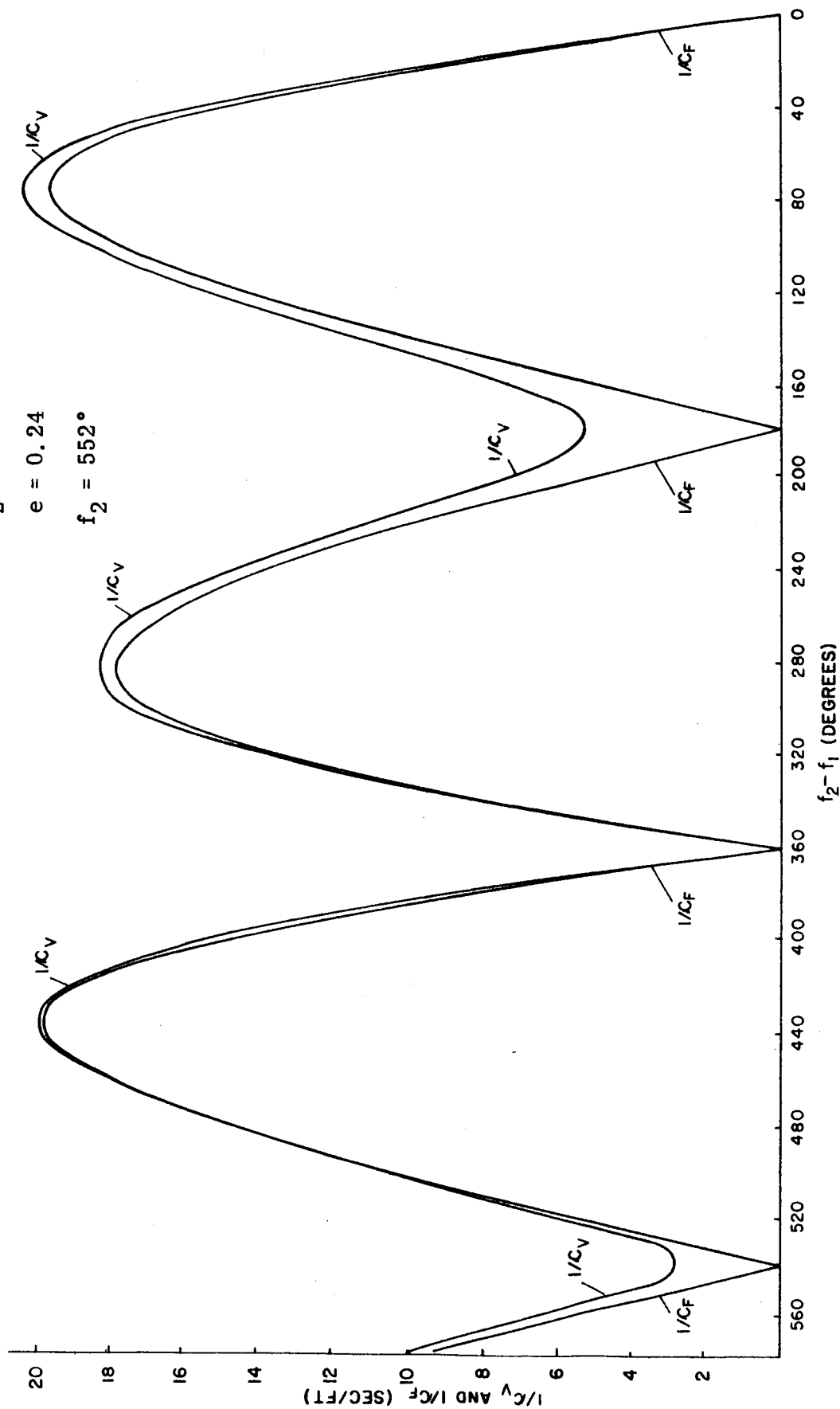


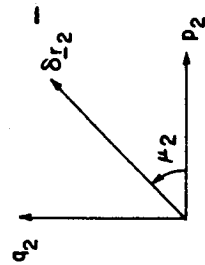
**Figure 4.7** Comparison of FTA and VTA Velocity Corrections When  
Position Variation at Destination is Normal to Reference  
Trajectory Plane

For all curves except 1,

$$\left\{ \begin{array}{l} \mu_2 = 0^\circ, 60^\circ, 70^\circ, 80^\circ, \text{ or } 90^\circ \\ \delta r_2^- = 9270 \text{ Miles} = 10^{-4} \text{ AU} \\ \delta z_2^- = 0 \end{array} \right.$$

For curve 1:

$$\left\{ \begin{array}{l} \delta p_2^- = 0 = \delta q_2^- \\ \delta z_2^- = 9270 \text{ Miles} = 10^{-4} \text{ AU} \end{array} \right.$$



$$e = 0.24$$

$$f_2 = 552^\circ$$

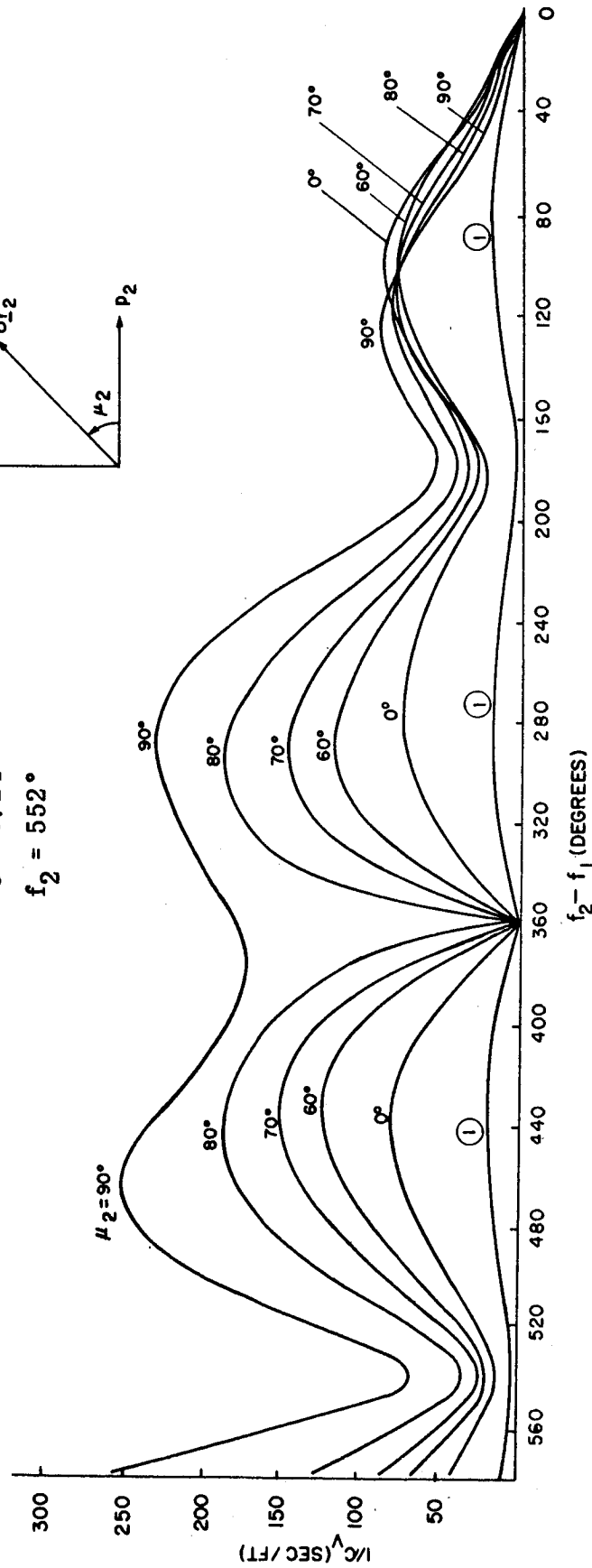


Figure 4.8 Reciprocal of Magnitude of VTA Velocity Correction,  $1/c_v$ , vs. Difference in True Anomaly,  $(f_2 - f_1)$ , for Constant Values of Phase Angle  $\mu_2$  between  $0^\circ$  and  $90^\circ$ .

For all curves except 1,

$$\left\{ \begin{array}{l} \mu_2 = 100^\circ, 110^\circ, 120^\circ, \text{ or } 170^\circ \\ \delta r_2^- = 9270 \text{ Miles} = 10^{-4} \text{ AU} \\ \delta z_2^- = 0 \end{array} \right.$$

For curve 1,

$$\left\{ \begin{array}{l} \delta p_2^- = 0 = \delta q_2^- \\ \delta z_2^- = 9270 \text{ Miles} = 10^{-4} \text{ AU} \end{array} \right.$$

$$e = 0.24$$

$$f_2 = 552^\circ$$

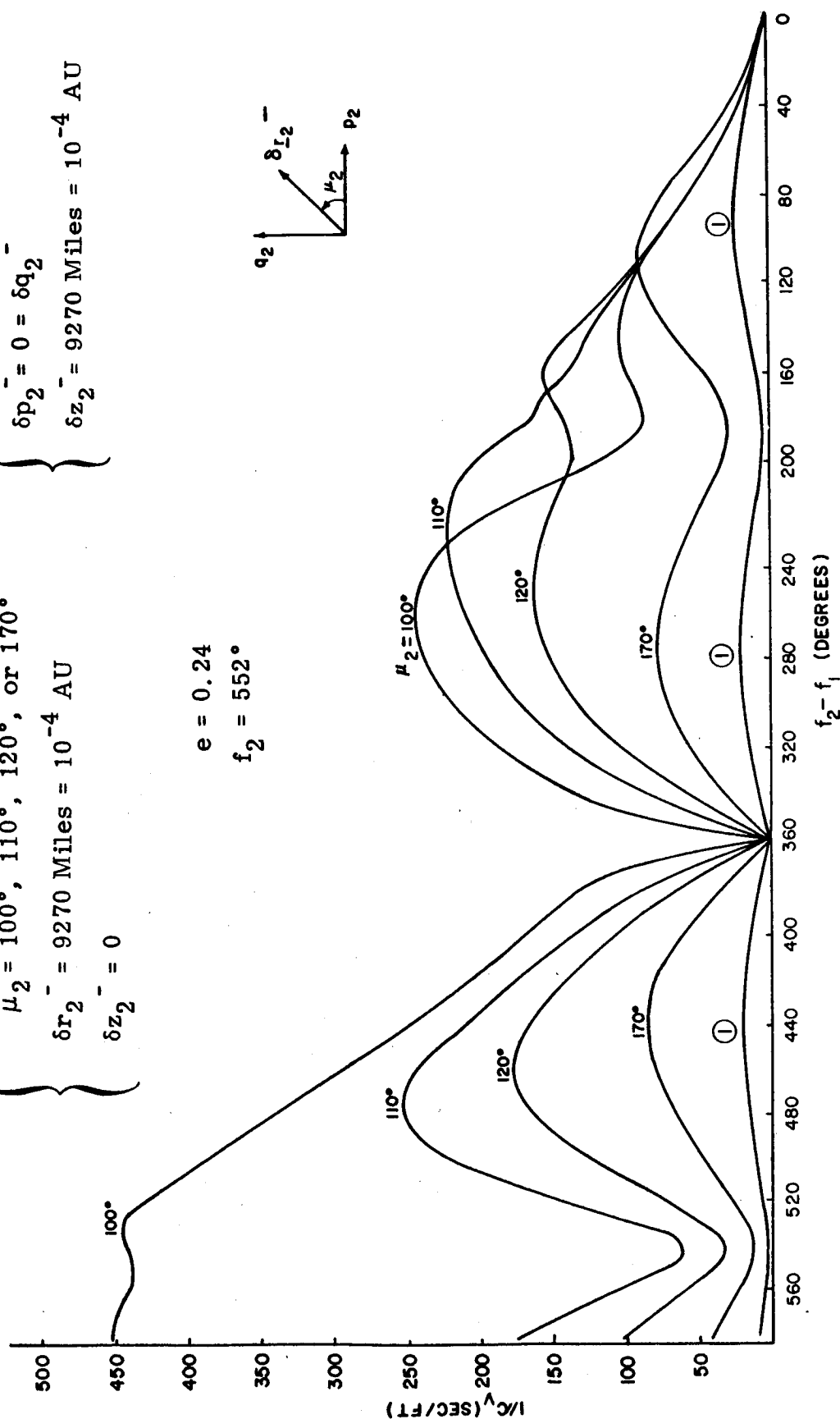
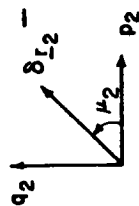
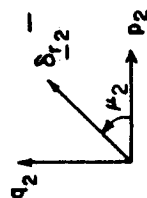


Figure 4.9 Reciprocal of Magnitude of VTA Velocity Correction,  $1/c_v$ , vs. Difference in True Anomaly,  $(f_2 - f_1)$ , for Constant Values of Phase Angle  $\mu_2$  between  $100^\circ$  and  $170^\circ$



For curve 1,

$$\begin{cases} \delta p_2^- = 0 = \delta q_2^- \\ \delta z_2^- = 9270 \text{ Miles} = 10^{-4} \text{ AU} \end{cases}$$



For all curves except 1,

$$\begin{cases} \mu_2 = 0^\circ, 60^\circ, 70^\circ, 80^\circ, \text{ or } 90^\circ \\ \delta r_2^- = 9270 \text{ Miles} = 10^{-4} \text{ AU} \\ \delta z_2^- = 0 \end{cases}$$

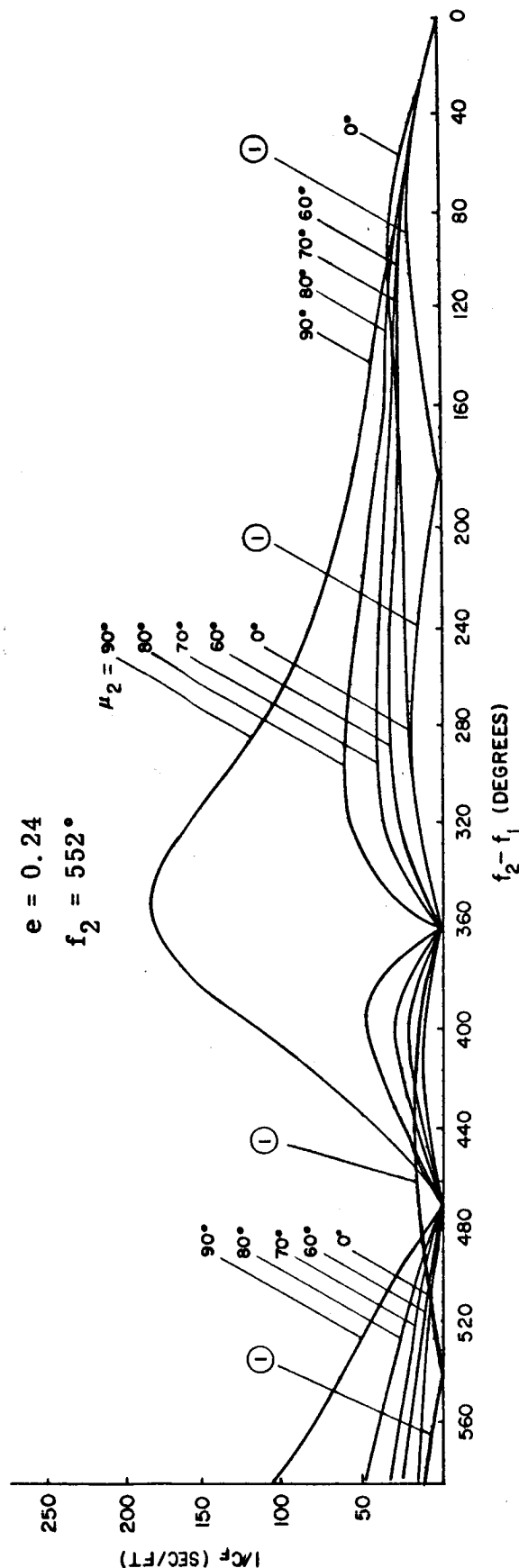


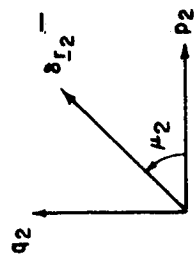
Figure 4.10 Reciprocal of Magnitude of FTA Velocity Correction,  $1/c_F$ , vs. Difference in True Anomaly,  $(f_2 - f_1)$ , for Constant Values of Phase Angle  $\mu_2$  between  $0^\circ$  and  $90^\circ$

For all curves except 1,

$$\left\{ \begin{array}{l} \mu_2 = 100^\circ, 110^\circ, 120^\circ, \text{ or } 170^\circ \\ \delta r_2^- = 9270 \text{ Miles} = 10^{-4} \text{ AU} \\ \delta z_2^- = 0 \end{array} \right.$$

For curve 1,

$$\left\{ \begin{array}{l} \delta p_2^- = 0 = \delta q_2^- \\ \delta z_2^- = 9270 \text{ Miles} = 10^{-4} \text{ AU} \end{array} \right.$$



$$e = 0.24$$

$$f_2 = 552^\circ$$

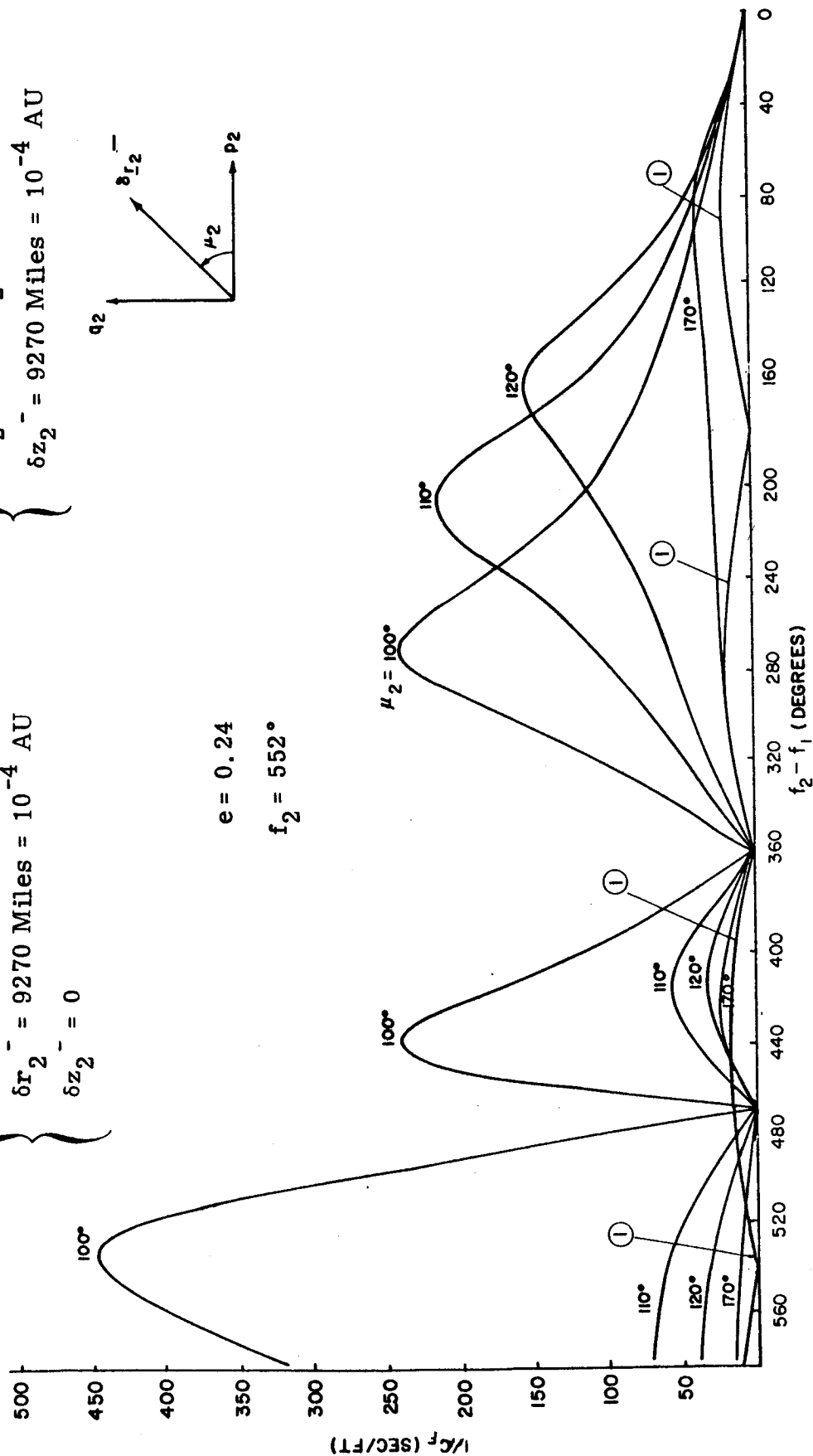


Figure 4.11 Reciprocal of Magnitude of FTA Velocity Correction,  $1/c_F$ , vs. Difference in True Anomaly,  $(f_2 - f_1)$ , for Constant Values of Phase Angle  $\mu_2$  between  $100^\circ$  and  $170^\circ$

$$\begin{aligned}\delta p_1 &= 0 = \delta q_1 \\ \delta z_1 &= 927 \text{ Miles} = 10^{-5} \text{ AU} \\ \delta v_{-1} &= 0 \\ e &= 0.24 \\ f_2 &= 552^\circ\end{aligned}$$

① -  $\delta r_2$   
② -  $\delta v_2$

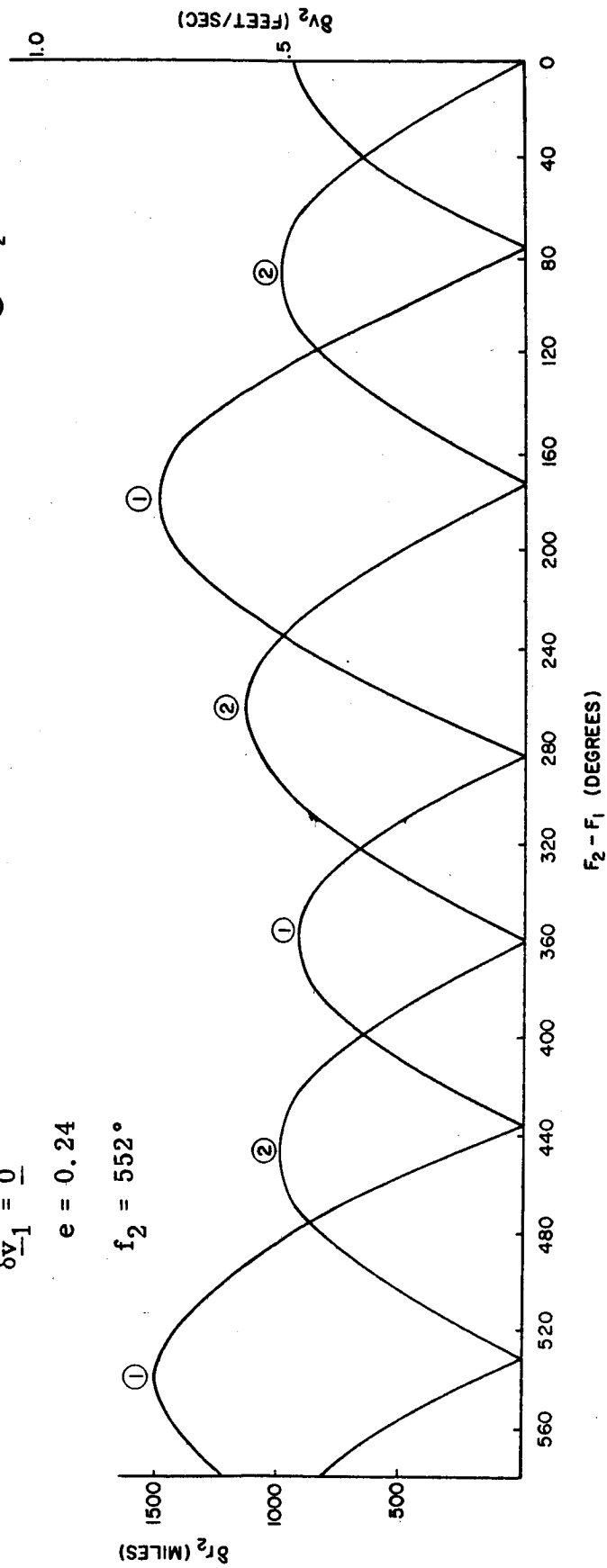


Figure 4.12 Effect of Position Variation Normal to Reference Trajectory  
Plane at Time  $t_1$  on Position Variation and Velocity Variation  
at Time  $t_2$

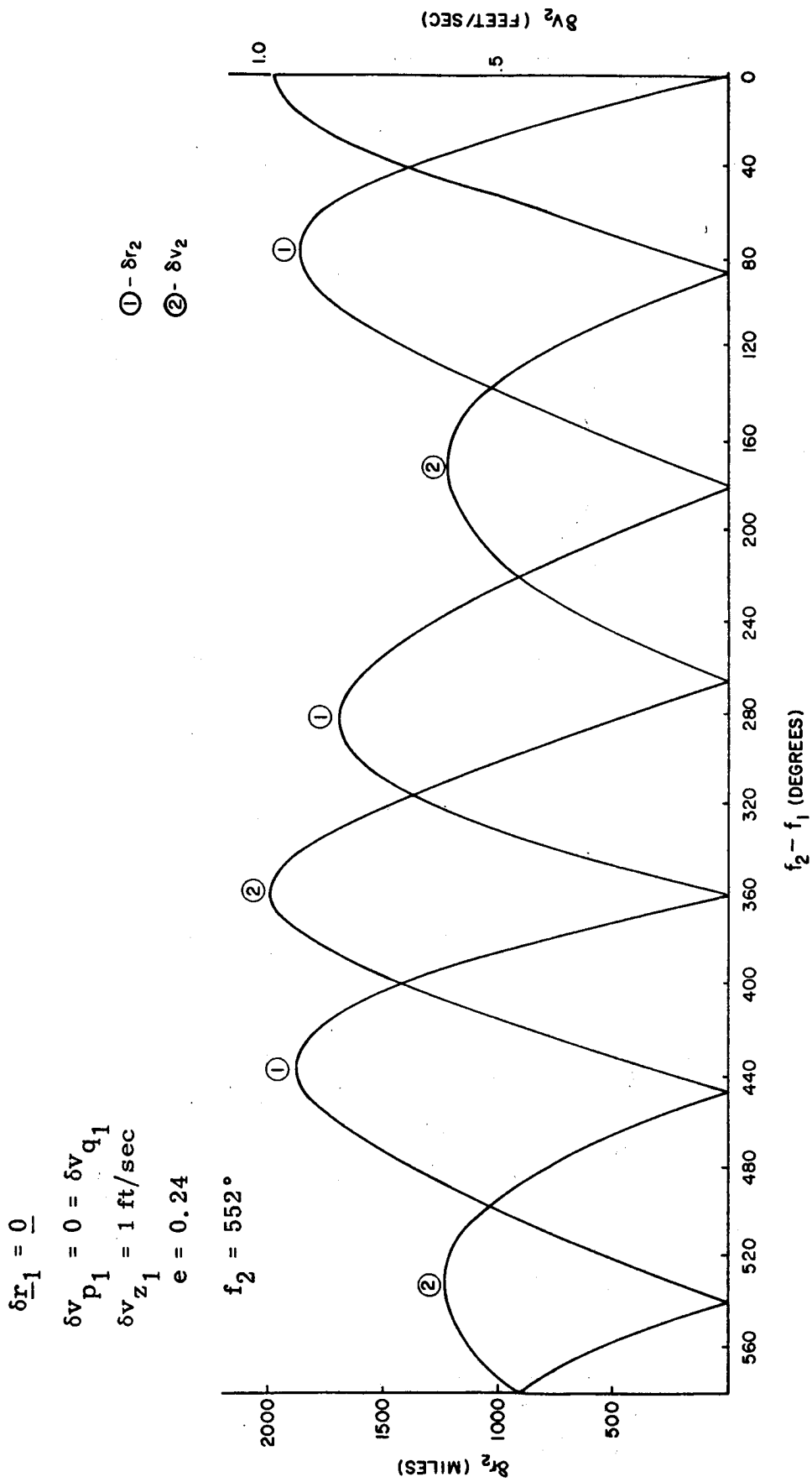


Figure 4.13 Effect of Velocity Variation Normal to Reference Trajectory Plane at Time  $t_1$  on Position Variation and Velocity Variation at Time  $t_2$

$$\delta r_1 = 927 \text{ Miles} = 10^{-5} \text{ AU}$$

$$\mu_1 = 0^\circ, 30^\circ, 60^\circ, 90^\circ, 100^\circ, 120^\circ, 170^\circ$$

$$\delta z_1 = 0$$

$$\delta v_1 = 0$$

$$e = 0.24$$

$$f_2 = 552^\circ$$

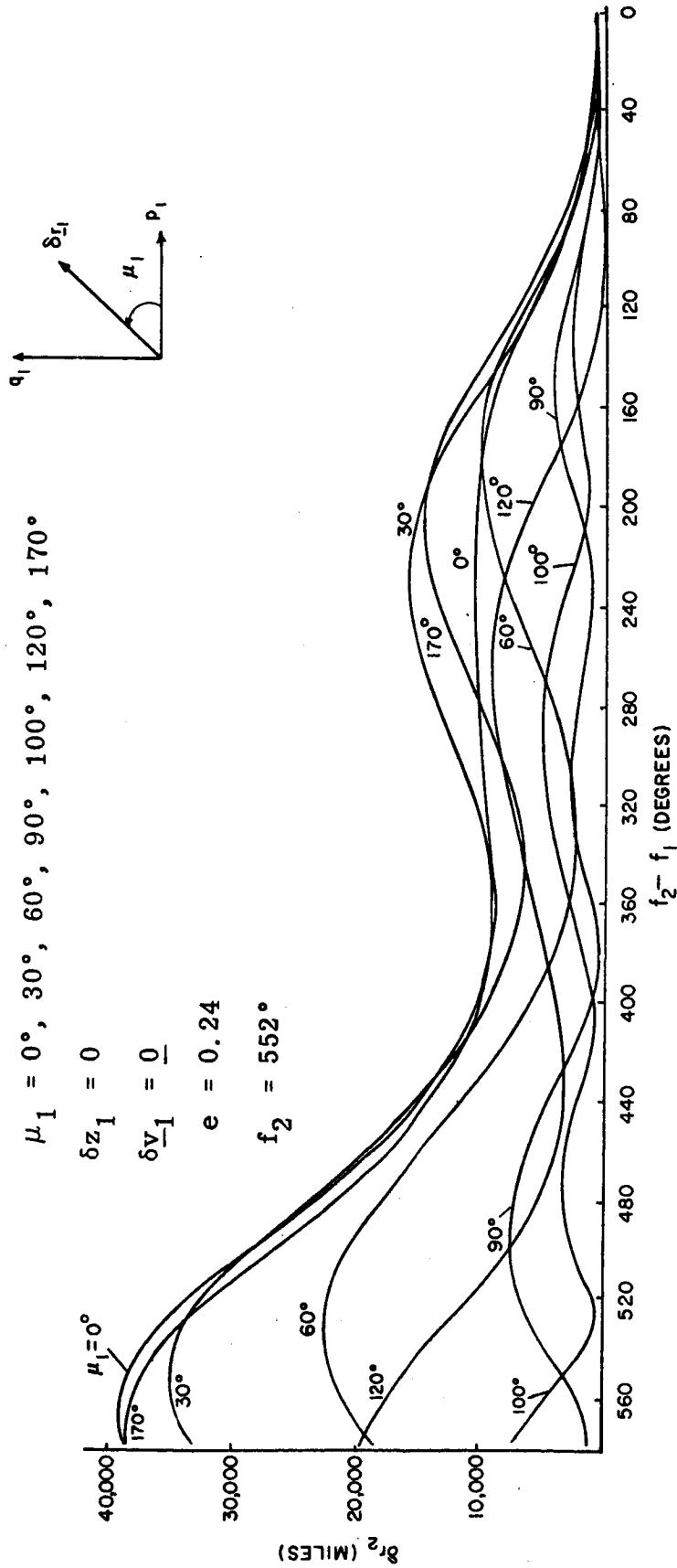


Figure 4.14 Effect of Position Variation in Reference Trajectory Plane at Time  $t_1$  on Position Variation at Time  $t_2$

$\delta r_1 = 927 \text{ Miles} = 10^{-5} \text{ AU}$

$\mu_1 = 0^\circ, 60^\circ, 90^\circ, 100^\circ, 120^\circ, 150^\circ, 170^\circ$

$\delta z_1 = 0$

$\delta v_1 = 0$

$e = 0.24$

$f_2 = 552^\circ$

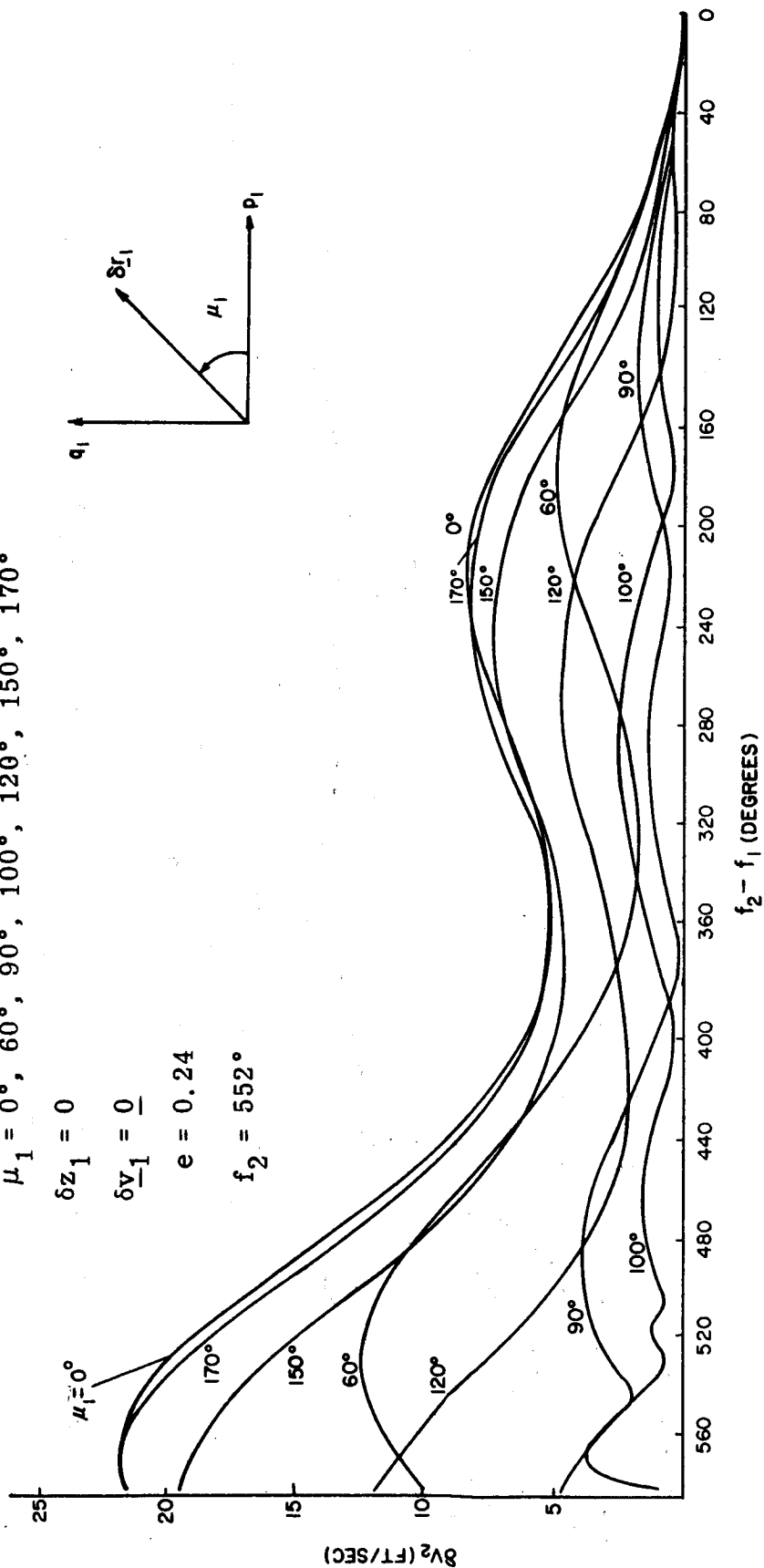


**Figure 4.15** Effect of Position Variation in Reference Trajectory Plane at Time  $t_1$   
on Velocity Variation at Time  $t_2$

$$\delta r_1 = 0$$

$$\delta v_1 = 1 \text{ ft/sec}$$

$$v_1 = 0^\circ, 30^\circ, 60^\circ, 90^\circ, 120^\circ, 150^\circ, 170^\circ$$

$$\delta v_{z1} = 0$$

$$e = 0.24$$

$$f_2 = 552^\circ$$

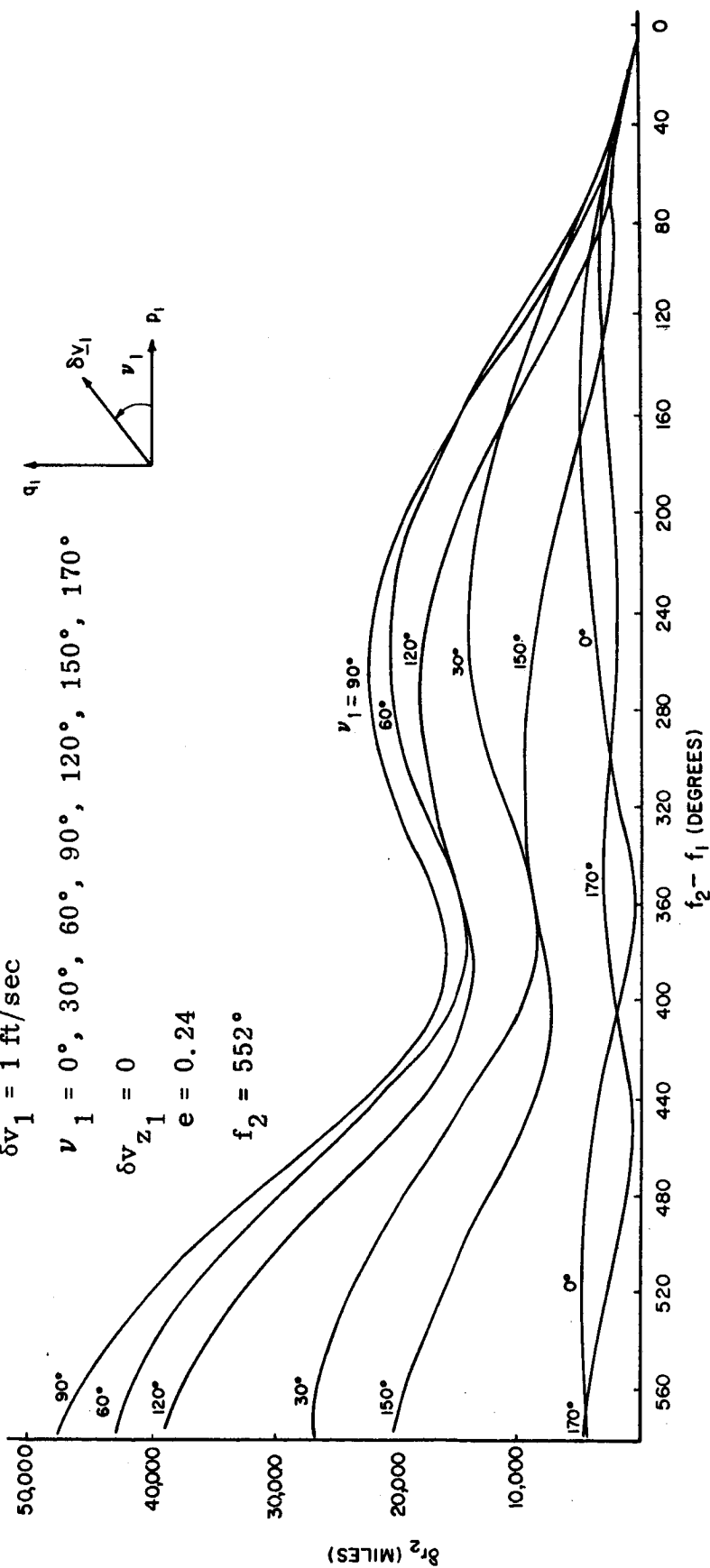


Figure 4.16 Effect of Velocity Variation in Reference Trajectory Plane at Time  $t_1$  on Position Variation at Time  $t_2$

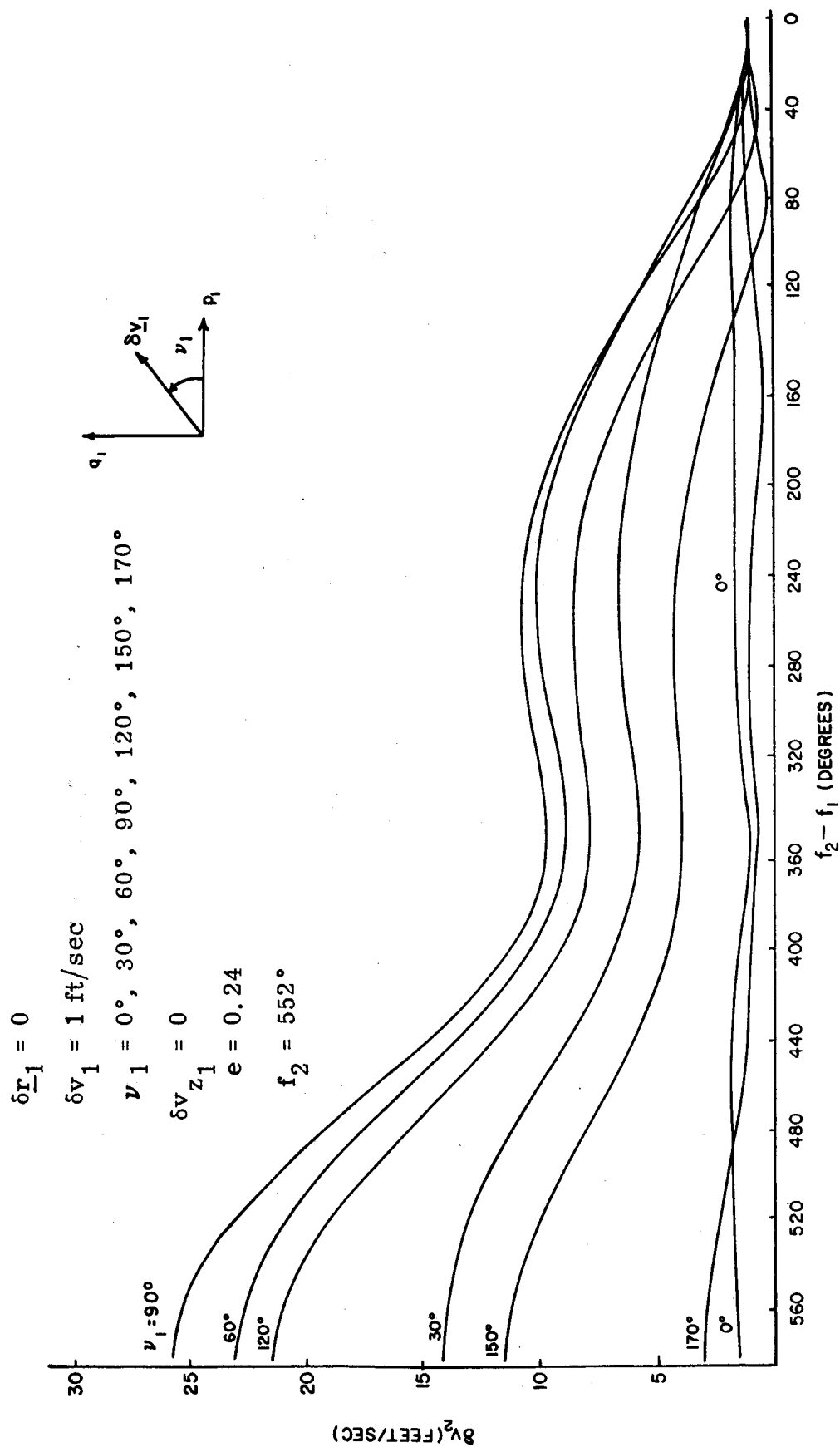


Figure 4.17 Effect of Velocity Variation in Reference Trajectory Plane at Time  $t_1$   
 on Velocity Variation at Time  $t_2$



## CHAPTER 5

### NAVIGATION THEORY

#### 5.1 Summary

The method of determining the space vehicle's variant path from measurements made during the voyage is developed. Earth-based radio-command and on-board self-contained measurement techniques are discussed. In both techniques there are redundant data which are processed statistically to obtain an estimate of the variant path.

In the radio-command system the variant path is estimated directly from the observed data. In the self-contained system there is an intermediate step; the vehicle's position is estimated from a set of simultaneous measurements, and the variant path is estimated after several position determinations, made at different times, have been obtained.

For the specific self-contained system in which the measured quantities are the angles between the lines of sight to pairs of celestial bodies, a simple method is proposed for selecting the stars to be used in the sightings.

#### 5.2 Introduction

In the guidance theory of Chapters 2 and 3 it is assumed that the vehicle's variant path is already known. The present chapter describes methods of determining the variant path from observed data; this determination is the objective of navigation theory. The chapter is primarily a review of previously proposed techniques for obtaining and processing measurements, with the addition of several suggested new features. It rounds out the analytic study of the midcourse guidance problem.

The number of independent measurements usually exceeds six, the number of parameters required to define the variant path. All measurements are subject to uncertainties and possibly to fixed biases as well. To estimate the parameters of the variant path from redundant measurements containing uncertainties, the method of maximum likelihood is used. The mathematical development of the method appears in Appendix P.

It is assumed that the distribution of the uncertainty in each measurement is normal with zero mean. The variance of each measurement is assumed to be known a priori.

Computations are based not on the observed value of each measured quantity but rather on the difference between the observed value and a pre-computed reference value. Since the difference is assumed to be small, linear theory is applicable.

The two types of navigation systems to be discussed are the Earth-based radio-command system developed by the Jet Propulsion Laboratory (JPL) at California Institute of Technology and the self-contained optical system of the M.I.T. Instrumentation Laboratory.

### 5.3 Earth-Based Radio-Command System

A general description of the Earth-based navigation system is presented in Reference (11). A detailed explanation of the method of computing the variant path appears in Reference (33).

Radio signals transmitted from the vehicle are received by a tracking station on Earth. To provide line-of-sight tracking of the vehicle at all times, three such stations are required. The observed quantities are the azimuth and elevation of the line of sight relative to the tracking station, range rate, and possibly range. Repeated measurements of any combination of these quantities are processed on a centrally located Earth-based computer by use of the method of maximum likelihood.

Many measurements can be made relatively easily during the early phase of an outbound interplanetary voyage. For this phase the two-body mathematical model does not accurately represent the physical situation; therefore, the more elaborate n-body model of Chapter 2, with the effect of earth oblateness included, is used.

In Reference (33) the solution for the variant path is obtained in terms of the six components of  $\delta \underline{x}_I$ , the state vector at the time of injection. The selection of  $\delta \underline{x}_I$  to define the variant path is motivated physically by the fact that, before any midcourse corrections are applied, the variations of the observed quantities from their reference values are due primarily to the variations in position and velocity at injection. However, it has been

shown in Chapter 2 that the really significant state vector for guidance analysis is not  $\delta \underline{x}_I$  but rather  $\delta \underline{x}_D$ , the state vector at the nominal time of arrival at the destination. With a caret superscript used to designate the maximum likelihood (ML) estimate of a quantity, the estimate of  $\delta \underline{x}_D$  is related to the estimate of  $\delta \underline{x}_I$  by the equation

$$\delta \hat{\underline{x}}_D = \hat{C}_{DI}^* \delta \hat{\underline{x}}_I \quad (5-1)$$

The tracking and orbit determination functions are sub-divisions of the larger problem of vehicle guidance. It would therefore be appropriate to solve the likelihood equations directly for an estimate of  $\delta \underline{x}_D$ , without going through the intermediate step of estimating  $\delta \underline{x}_I$ . An outline of the mathematical development of the modification of the JPL system being suggested here is presented in the next section of this chapter.

In addition to the components of the state vector  $\delta \underline{x}_I$ , the JPL computation yields estimates of the fixed bias of each type of measurement made at each tracking station. An iterative procedure is used to refine the estimates of the state vector and the biases beyond the results that are obtained from a single solution of the linearized equations.

The Earth-based navigation system makes use of virtually continuous computation throughout the period during which the vehicle is being tracked. According to Reference (10), measurements are made every ten seconds, so that in a tracking period of ten hours 3600 sets of input data are fed into the computer. The computer facility required is large, far beyond that which could be carried in any space vehicle. The fundamental advantage of this system is that it utilizes such a large volume of input data that, even if the individual measurements have fairly high uncertainties, the uncertainty in the estimated state vector, from which the velocity correction is computed, is quite low.

The system shows to best advantage when the vehicle is close to Earth. As the distance from Earth increases, the signal-to-noise ratio of the radio signals transmitted from vehicle to tracking station is reduced, with a consequent increase in the uncertainty of the measurements. In addition, the sensitivity of the predicted state vector to errors in angular measurements increases linearly with distance of vehicle from station.

The radio-command system is most useful in accurately determining when and how to apply the first midcourse correction on an outbound journey from Earth to another planet.

#### 5.4 Estimate of the State Vector from Earth-Based Measurements

In this simplified analysis it will be assumed that the measurements are unbiased, and consequently the likelihood equations are to be solved only for the components of  $\delta \underline{\hat{x}}_D$ .

At time  $t_S$  a set of measurements is obtained. The R-th type of measurement made at  $t_S$  is designated  $m_{SR}$ . The variation of the actual measurement from its reference value is  $\delta m_{SR}$ . This variation is a linear function of the components of the state vector  $\delta \underline{x}_S$ .

$$\delta m_{SR} = p_{SR}^T \delta \underline{x}_S \quad (5-2)$$

$p_{SR}$  is a six-component vector whose elements are the partial derivatives of  $m_{SR}$  with respect to the components of  $\underline{x}_S$ . Analytic expressions for the partial derivatives used by JPL are listed in Appendix A of Reference (33).

$\delta m_{SR}$  can be related to  $\delta \underline{x}_D$  by means of the transition matrix.

$$\delta m_{SR} = p_{SR}^T \bar{C}_{SD}^* \delta \underline{x}_D = q_{SR}^T \delta \underline{x}_D \quad (5-3)$$

where

$$q_{SR}^T = p_{SR}^T \bar{C}_{SD}^* \quad (5-4)$$

The method of computing the elements of  $\bar{C}_{SD}^*$  by numerical integration is described in Section 2.10.

If K different types of measurement are made at  $t_S$ , the K measurement variations can be combined in a vector designated  $\delta \underline{m}_S$ .

$$\delta \underline{m}_S = \begin{Bmatrix} \delta m_{S1} \\ \vdots \\ \delta m_{SK} \end{Bmatrix} = \begin{Bmatrix} q_{S1}^T \\ \vdots \\ q_{SK}^T \end{Bmatrix} \quad \delta \underline{x}_D = \underline{Q}_S^{*T} \delta \underline{x}_D \quad (5-5)$$

where

$$\underline{Q}_S^{*T} = \begin{Bmatrix} q_{S1}^T \\ \vdots \\ q_{SK}^T \end{Bmatrix} \quad (5-6)$$

Finally, if measurements have been made at times extending from  $t_1$  to  $t_L$ , the total measurement variation vector  $\delta \underline{m}$  is defined as follows:

$$\delta \underline{m} = \begin{Bmatrix} \delta \underline{m}_1 \\ \vdots \\ \delta \underline{m}_L \end{Bmatrix} = \begin{Bmatrix} \underline{Q}_1^{*T} \\ \vdots \\ \underline{Q}_L^{*T} \end{Bmatrix} \quad \delta \underline{x}_D = \underline{Q}^{*T} \delta \underline{x}_D \quad (5-7)$$

where

$$\underline{Q}^{*T} = \begin{Bmatrix} \underline{Q}_1^{*T} \\ \vdots \\ \underline{Q}_L^{*T} \end{Bmatrix} \quad (5-8)$$

$\underline{Q}^{*T}$  is an M-by-6 matrix, where M is the total number of individual measurements being processed.

A superscript tilde will be used to indicate the observed measurement, as distinguished from the true value of the observed quantity. The difference between the two is the random measurement error  $\underline{u}$ , which is normally distributed with zero mean and known standard deviation. For all M measurements,

$$\delta \underline{\tilde{m}} = \delta \underline{m} + \underline{u} \quad (5-9)$$

The covariance matrix of the uncertainty vector  $\underline{u}$  is defined as

$$\underline{\hat{U}} = \overline{\underline{u} \underline{u}^T} \quad (5-10)$$

A bar over a quantity signifies the average value of the quantity.  $\underline{\hat{U}}$  is a symmetrical M-by-M matrix.

The estimated state vector  $\delta \underline{\hat{x}}_D$  is computed from  $\underline{\hat{Q}}$ ,  $\underline{\hat{U}}$ , and  $\delta \underline{\hat{m}}$  by the use of Equation (P-20).

$$\delta \underline{\hat{x}}_D = (\underline{\hat{Q}} \underline{\hat{U}}^{-1} \underline{\hat{Q}}^T)^{-1} \underline{\hat{Q}} \underline{\hat{U}}^{-1} \delta \underline{\hat{m}} \quad (5-11)$$

If the error  $\underline{\epsilon}_D$  in the estimate is defined by

$$\underline{\epsilon}_D = \delta \underline{\hat{x}}_D - \delta \underline{x}_D \quad (5-12)$$

the covariance matrix  $\underline{\hat{E}}_D$  of  $\underline{\epsilon}_D$  is obtained from Equation (P-25).

$$\underline{\hat{E}}_D = \overline{\underline{\epsilon}_D \underline{\epsilon}_D^T} = (\underline{\hat{Q}} \underline{\hat{U}}^{-1} \underline{\hat{Q}}^T)^{-1} \quad (5-13)$$

The uncertainties in the individual measurements are assumed to be uncorrelated. Therefore, for measurements  $m_i$  and  $m_j$ ,

$$\overline{u_i u_j} = \delta_{ij} \sigma_i^2 \quad (5-14)$$

where  $\delta_{ij}$  is the Kronecker delta and  $\sigma_i^2$  is the variance of  $u_i$ . Then  $\underline{\hat{U}}$  is a diagonal matrix, the non-zero element in the k-th row being  $\sigma_k^2$ , and  $\underline{\hat{U}}^{-1}$  is also a diagonal matrix with  $\frac{1}{\sigma_k^2}$  being the non-zero element in its

k-th row. When all uncertainties are uncorrelated, the maximum likelihood estimate is the same as the least squares estimate.

The matrix  $\underline{\hat{Q}} \underline{\hat{U}}^{-1} \underline{\hat{Q}}^T$ , which must be inverted in order to solve for  $\delta \underline{\hat{x}}_D$ , is a symmetrical 6-by-6 matrix. This inversion is the most time-consuming operation in the computation process; it must be performed every time a new estimate is calculated from (5-11).

## 5.5 Self-Contained Optical System

The self-contained optical system for space navigation that is discussed in this section is the one that is described in Reference (5). The

mathematical development is given in Appendix B of that reference and also in Reference (3).

The first step in the procedure is the estimation of vehicle position relative to the reference trajectory at some specified time  $t_S$ . Position is estimated by making a set of measurements of the angles between the lines of sight to pairs of celestial bodies; all measurements are made within a short time interval centered at  $t_S$ . When more than three such measurements are made in the interval, the maximum likelihood technique is used to compute the estimated position variation  $\delta \tilde{\underline{r}}_S$  and the estimated clock error  $\delta \tilde{t}_S$ .

For each angular measurement at least one of the two celestial bodies involved must be a "near" body, i. e., one whose motion relative to the space vehicle is significant. The near bodies are confined to the solar system; either the sun or one of the planets is usually used. The second body involved in the measurement may be a "far" body (i. e., a star other than the sun), or it may be another near body.

The position estimation procedure is repeated for a number of different values of  $t_S$  during the flight. The final phase of the computation is the determination by means of maximum likelihood of  $\delta \hat{\underline{x}}_D$  from the estimates of  $\delta \underline{r}$  that have already been obtained.

The assumption is made that all angular measurements have zero bias. The uncertainty in each measurement is normally distributed with zero mean and known standard deviation.

When the self-contained system is compared with the Earth-based system, the following differences are noted:

1. All measurements in the self-contained system are of the same type; they are optical measurements of celestial angles. Measurements in the Earth-based system are of several types, including angular measurements, doppler measurement of range rate, and measurement of range.
2. Each on-board angular measurement requires an appreciable amount of time for adjustment of the two telescopes involved. The Earth-based tracking system allows measurements to be made very quickly.

3. The frequency of measurements is very much smaller for the self-contained system; the number of position determinations is limited by the capacity of the on-board computer. Since the Earth-based measurements are linked to a computer of large capacity, large numbers of measurements can be effectively processed.

4. The error in the measurement of time, if uncorrected, can be significant in the self-contained system; it is negligible in the Earth-based system.

5. The self-contained navigation system uses a two-step computation: first, position variation and clock error are determined; then  $\delta \hat{\underline{x}}_D$  is determined. The Earth-based system computes  $\delta \hat{\underline{x}}_D$  directly.

6. The accuracy obtainable from the self-contained system is improved when the vehicle is close to any planet. The accuracy of the Earth-based measurements depends on the vehicle's distance from Earth.

7. In the self-contained system the designer has the problem of selecting the angles to be measured at each measurement time. There are usually several near bodies that can be used, and there are always many bright stars from which a selection can be made. By contrast, there is no problem of selection in the Earth-based system. The types of measurement are limited, the number of tracking stations from which the vehicle is visible is limited, and the space vehicle is the only object being tracked.

#### 5.6 The Effect of Clock Error

Some justification is required for the two-step computation procedure called for in the self-contained system, as opposed to the single-step procedure in the Earth-based system. If the angular measurements were all made at times that were known accurately, all the data could be processed together to determine  $\delta \hat{\underline{x}}_D$  directly. Unfortunately the times of the measurements are not known accurately in the self-contained system, because the space vehicle's clock is itself subject to error. The maximum likelihood method is incapable of distinguishing a clock error from a variation in the trajectory parameters if the single-step computation is used. This problem is not present in the Earth-based system, because in that system the clock error is negligibly small.



When four or more angular measurements are made at the nominal time  $t_S$ , the solution of the resulting likelihood equations yields an estimate of the clock error  $\delta \tilde{t}_S$  as well as an estimate of the position variation  $\delta \tilde{\underline{r}}_S$ . Thus, the celestial bodies are used to determine the correct time. After every set of angular measurements has been completed and processed, a correction of  $\delta \tilde{t}_S$  seconds is applied to the vehicle's clock.

Two simple examples serve to illustrate the inability of the computer to detect a clock error when all the angular measurements are processed together. The first is the case in which the clock has a fixed bias; assume that it is  $\delta t_S$  seconds slow. Then every measurement is made at a later time than it is supposed to be, and the vehicle appears to be farther along the path than it should be. The computer interprets this situation as a variation in  $t_0$ , the time of perihelion passage.  $\delta t_0$  is computed to be the negative of  $\delta t_S$ ; that is, the trajectory appears to be such that the vehicle passed through perihelion  $\delta t_S$  seconds early. The computed FTA correction retards the motion so that the vehicle arrives at the destination at the correct time according to its clock, but actually  $\delta t_S$  seconds late.

The second example is that in which the vehicle's clock has a constant drift rate; assume that the clock reads correctly at injection and loses  $j$  days per day thereafter. The interval between the actual time of an angular measurement and the apparent time of the measurement gets progressively longer; a measurement apparently made  $t_S$  days after injection is actually made  $[(1 + j)t_S]$  days after injection. The computer interprets the data as indicating that the period of the actual trajectory is smaller than the reference period. The computed FTA correction increases the period so that the vehicle arrives at its destination at the correct time according to its clock, but actually  $[j(t_D - t_I)]$  seconds late, where  $(t_D - t_I)$  is expressed in seconds.

In general, a consistent clock error for which the clock reading will be  $t_D$  when the correct time is  $(t_D + \delta t_D)$  results in a computation that causes the vehicle to reach the destination at  $(t_D + \delta t_D)$  if FTA guidance is used. At time  $t_D$  the vehicle's position variation relative to the moving destination point is

$$(\delta \underline{r}_D)_R = - \underline{v}_R \delta t_D \quad (5-15)$$

where  $\underline{v}_R$  is the velocity of the vehicle relative to the destination planet.

When VTA guidance is used, a consistent clock error (either a fixed bias or a constant drift rate) requires no velocity correction. The vehicle achieves the objective of reaching the destination even though the time of arrival is not known accurately. If the clock is subject to random fluctuations, a velocity correction is computed even by the VTA system.

As a numerical illustration, consider a mission whose duration is 200 days, a clock whose drift rate is one second per day (roughly  $10^{-5}$ ), and a relative velocity vector whose magnitude is 3 mi/sec. When  $t$  is actually equal to  $t_D$ , the clock error is 200 seconds. With FTA guidance the magnitude of  $(\delta \underline{r}_D)_R$  is  $200 \times 3 = 600$  miles; with VTA guidance no corrections are applied, and the magnitude of the miss distance is zero.

It is apparent that the effect of an unknown clock error is reduced considerably by the VTA system. However, the two-step computation procedure is still felt to be justified for two reasons. First, even when it is permissible to vary the time of arrival, it is desirable on most missions to be able to predict accurately what that time will be; secondly, in the usual case the clock fluctuation is random, and some fuel will be expended unnecessarily for VTA corrections if the one-step procedure is used.

There is one final reason for the development of the two-step computation. In the event of a partial computer failure on a manned mission, despite the fact that the elaborate timing mechanism associated with the computer is inoperative, it may still be possible to navigate adequately with more conventional and simpler timepieces if the two-step procedure is utilized.

### 5.7 Estimate of the State Vector from Optical Measurements

The first step in the two-step computation is the determination of the position variation  $\delta \underline{r}_S$  at nominal time  $t_S$  from angular measurements made in a short time interval centered at  $t_S$ . The variation  $\delta A_{SR}$  of the  $R$ -th angle measurement made at  $t_S$  from its reference value is assumed to be a linear function of the position variation  $\delta \underline{r}_S$  and the clock error  $\delta t_S$ .

$$\delta A_{SR} = \underline{g}_{SR}^T \delta \underline{s}_S \quad (5-16)$$

where

$$\delta \underline{s}_S = \begin{Bmatrix} \delta t_S \\ \delta \underline{r}_S \end{Bmatrix} \quad (5-17)$$

and  $\underline{g}_{SR}$  is a four-component vector composed of the partial derivatives of  $A_{SR}$  with respect to  $\delta t_S$  and the components of  $\delta \underline{r}_S$ . Analytic expressions for the partial derivatives are developed in Reference (3).

The number of angles measured at  $t_S$  is  $K$ . Obviously, all these measurements cannot be made simultaneously, so that the angle  $A_{SR}$  is actually measured at time  $(t_S + \delta t_{SR})$ . The time increment  $\delta t_{SR}$  is small and can be accurately recorded. The observed value  $\delta \tilde{A}_{SR}$  used in the computation is compensated for the effect of  $\delta t_{SR}$ ; therefore,  $\delta \tilde{A}_{SR}$  is the "effective" angle variation that would have been observed if the measurement had taken place when the space vehicle's clock read  $t_S$ .

The measurement variation vector  $\delta \underline{m}_S$  consists of the variation in the clock reading in addition to the variations in the  $K$  angular measurements.

$$\delta \underline{m}_S = \begin{Bmatrix} \delta t_S \\ \delta A_{S1} \\ \vdots \\ \delta A_{SK} \end{Bmatrix} = \underline{G}_S^{*T} \delta \underline{s}_S \quad (5-18)$$

where

$$\underline{G}_S^{*T} = \begin{Bmatrix} \underline{g}_{S0}^T \\ \underline{g}_{S1}^T \\ \vdots \\ \underline{g}_{SK}^T \end{Bmatrix} \quad (5-19)$$

and

$$\underline{g}_{S0} = \begin{Bmatrix} 1 \\ 0 \\ 0 \\ 0 \end{Bmatrix} \quad (5-20)$$

The observed measurement vector  $\delta \underline{\tilde{m}}_S$ , the true measurement vector  $\delta \underline{m}_S$ , and the uncertainty vector  $\underline{u}_S$  are related by the equation

$$\delta \underline{\tilde{m}}_S = \delta \underline{m}_S + \underline{u}_S \quad (5-21)$$

In component form,

$$\begin{Bmatrix} 0 \\ \delta \tilde{A}_{S1} \\ \vdots \\ \delta \tilde{A}_{SK} \end{Bmatrix} = \begin{Bmatrix} \delta t_S \\ \delta A_{S1} \\ \vdots \\ \delta A_{SK} \end{Bmatrix} + \begin{Bmatrix} u_{S0} \\ u_{S1} \\ \vdots \\ u_{SK} \end{Bmatrix} \quad (5-22)$$

The "observed" value of  $\delta t_S$  is zero. The uncertainty in the time measurement is designated  $u_{S0}$ .

The covariance matrix of the uncertainty vector is

$$\underline{U}_S^* = \overline{\underline{u}_S \underline{u}_S^T} \quad (5-23)$$

Since the uncertainties in all the measurements are assumed to be independent with zero mean,  $\underline{U}_S^*$  is a diagonal matrix, and so is  $\underline{U}_S^{*-1}$ .

Then the ML estimate of the vector  $\delta \underline{s}_S$  is

$$\delta \underline{\tilde{s}}_S = \begin{Bmatrix} \delta \tilde{t}_S \\ \delta \tilde{\underline{r}}_S \end{Bmatrix} = (\underline{G}_S^* \underline{U}_S^{*-1} \underline{G}_S^T)^{-1} \underline{G}_S^* \underline{U}_S^{*-1} \delta \underline{\tilde{m}}_S \quad (5-24)$$

Vector  $\delta \underline{\tilde{s}}_S$  is an "inferred measurement" vector. Note that the inferred measurement of  $\delta t_S$  is not zero, even though the observed measurement is. The correction  $\delta \tilde{t}_S$  is applied to the clock.

The error vector  $\underline{\xi}_S$  is the difference between the inferred measured vector and the true measurement vector.

$$\underline{\xi}_S = \delta \underline{\tilde{s}}_S - \delta \underline{s}_S \quad (5-25)$$

or

$$\begin{Bmatrix} \nu_S \\ \underline{\beta}_S \end{Bmatrix} = \begin{Bmatrix} \delta \tilde{t}_S \\ \delta \tilde{\underline{r}}_S \end{Bmatrix} - \begin{Bmatrix} \delta t_S \\ \delta \underline{r}_S \end{Bmatrix} \quad (5-26)$$

The covariance matrix of  $\underline{\xi}_S$  is

$$\overline{\underline{\xi}_S \underline{\xi}_S^T} = (\underline{G}_S^* \underline{U}_S^{-1} \underline{G}_S^T)^{-1} \quad (5-27)$$

The variance in the inferred estimate of clock error is  $\overline{\nu_S^2}$ , the upper left-hand element of  $\overline{\underline{\xi}_S \underline{\xi}_S^T}$ .

In order to solve (5-24) for  $\delta \underline{\tilde{s}}_S$ , it is necessary to know the variances in the uncertainties of all measurements comprising  $\delta \underline{\tilde{m}}_S$ . For the angular measurements these variances are known a priori. For the clock measurement Reference (3) suggests a simple yet effective model that can be used to determine  $\overline{u_{S0}^2}$ .

Clock errors are important only during those short time intervals when measurements are being made or a velocity correction is being applied. It is therefore reasonable to assume that the clock has a constant drift rate between measurement time  $t_{S-1}$  and measurement time  $t_S$ . The variance

of this drift rate is  $\sigma_c^2$ , which is known a priori. Then  $\overline{u_{S0}^2}$  is given by

$$\overline{u_{S0}^2} = \sigma_c^2 (t_S - t_{S-1})^2 + \overline{v_{S-1}^2} \quad (5-28)$$

The recursive operation is started by stating that at injection  $\overline{u_{I0}^2}$  is known a priori.

The inferred measurements to be used in the determination of  $\delta \hat{\underline{x}}_D$  are the components of  $\delta \tilde{\underline{r}}_S$ . The covariance matrix of the uncertainties in  $\delta \tilde{\underline{r}}_S$  is

$$\begin{aligned} \underline{B}_S^* = \underline{\beta}_S \underline{\beta}_S^T &= \begin{Bmatrix} 0 & 1 & 0 & 0 \\ 0 & 0 & 1 & 0 \\ 0 & 0 & 0 & 1 \end{Bmatrix} (\underline{G}_S^* \underline{U}_S^{*-1} \underline{G}_S^{*T})^{-1} \begin{Bmatrix} 0 & 0 & 0 \\ 1 & 0 & 0 \\ 0 & 1 & 0 \\ 0 & 0 & 1 \end{Bmatrix} \\ &\quad (5-29) \end{aligned}$$

The second major step in the two-step method can now be carried out. At each of L measurement times an inferred position variation vector is obtained, and for each of these vectors the corresponding moment matrix is computed. The equation

$$\delta \tilde{\underline{m}} = \delta \underline{m} + \underline{u} \quad (5-30)$$

now takes the form

$$\begin{Bmatrix} \delta \tilde{\underline{r}}_1 \\ \vdots \\ \delta \tilde{\underline{r}}_L \end{Bmatrix} = \begin{Bmatrix} \delta \underline{r}_1 \\ \vdots \\ \delta \underline{r}_L \end{Bmatrix} + \begin{Bmatrix} \underline{\beta}_1 \\ \vdots \\ \underline{\beta}_L \end{Bmatrix} \quad (5-31)$$

The uncertainty in the inferred measurement vector  $\delta \tilde{\underline{r}}_S$  is assumed to be uncorrelated with the uncertainties in the other inferred measurement vectors. The covariance matrix  $\underline{U}^*$ , which is again defined as  $\underline{u} \underline{u}^T$ , is a

diagonal matrix of 3-by-3 sub-matrices. This is illustrated by the equations shown below for  $\bar{U}^*$  and  $\bar{U}^{*-1}$  when  $L = 3$ . The extension to higher values of  $L$  is obvious.

$$\bar{U}^* = \begin{Bmatrix} \bar{B}_1^* & \bar{O}_3^* & \bar{O}_3^* \\ \bar{O}_3^* & \bar{B}_2^* & \bar{O}_3^* \\ \bar{O}_3^* & \bar{O}_3^* & \bar{B}_3^* \end{Bmatrix} \quad (5-32)$$

$$\bar{U}^{*-1} = \begin{Bmatrix} \bar{B}_1^{*-1} & \bar{O}_3^* & \bar{O}_3^* \\ \bar{O}_3^* & \bar{B}_2^{*-1} & \bar{O}_3^* \\ \bar{O}_3^* & \bar{O}_3^* & \bar{B}_3^{*-1} \end{Bmatrix} \quad (5-33)$$

$\delta \underline{r}_S$  is related to  $\delta \underline{x}_D$  by the equation

$$\delta \underline{r}_S = \begin{Bmatrix} \bar{M}_{SD}^* & \bar{N}_{SD}^* \end{Bmatrix} \delta \underline{x}_D \quad (5-34)$$

The 3-by-3 matrices  $\bar{M}_{SD}^*$  and  $\bar{N}_{SD}^*$  are sub-matrices of the transition matrix  $\bar{C}_{SD}^*$ ; they are explained in Section 2.7. Then

$$\delta \underline{m} = \bar{Q}^{*T} \delta \underline{x}_D \quad (5-35)$$

where

$$\bar{Q}^{*T} = \begin{Bmatrix} \bar{M}_{1D}^* & \bar{N}_{1D}^* \\ \vdots & \vdots \\ \bar{M}_{LD}^* & \bar{N}_{LD}^* \end{Bmatrix} \quad (5-36)$$

With these definitions of  $\bar{Q}$ ,  $\bar{U}$ , and  $\delta \underline{\tilde{m}}$ , the ML estimate of  $\delta \underline{x}_D$  has the same form as (5-11).

$$\delta \hat{\underline{x}}_D = (\bar{Q}^* \bar{U}^{*-1} \bar{Q}^{*T})^{-1} \bar{Q}^* \bar{U}^{*-1} \delta \underline{\tilde{m}} \quad (5-37)$$

The error  $\underline{\epsilon}_D$  in the estimate and the covariance matrix  $\underline{E}_D^*$  are given by Equations (5-12) and (5-13), respectively.

### 5.8 The Initial Estimate

An improvement in the estimate of the variant path of the vehicle can be achieved by regarding as additional measurements the design value of the state vector at injection. This suggestion has been made in References (12) and (33).

The "pseudo-measurement" of the injection state vector is

$$\delta \underline{\tilde{x}}_I = \underline{0}_6 \quad (5-38)$$

This is the vector that would be achieved if there were no errors in the injection guidance system. Because such errors do exist, the actual vector  $\delta \underline{x}_I$  is not the zero vector. The injection error vector  $\underline{\epsilon}_I$  is defined as

$$\underline{\epsilon}_I = \delta \underline{\tilde{x}}_I - \delta \underline{x}_I \quad (5-39)$$

The corresponding covariance matrix is

$$\underline{U}_I^* = \overline{\underline{\epsilon}_I \underline{\epsilon}_I^T} \quad (5-40)$$

The elements of  $\underline{U}_I^*$  are assumed to be known a priori from the characteristics of the injection guidance system.

$\delta \underline{x}_I$  is related to  $\delta \underline{x}_D$  by the transition matrix  $\underline{C}_{ID}^*$ .

$$\delta \underline{x}_I = \underline{C}_{ID}^* \delta \underline{x}_D \quad (5-41)$$

To incorporate  $\delta \underline{\tilde{x}}_I$  into the computation for the ML estimate of  $\delta \underline{x}_D$ , the definitions of  $\underline{Q}^*$ ,  $\underline{U}$ , and  $\delta \underline{\tilde{m}}$  must be modified. The new  $\underline{Q}^*$  is given by

$$\underline{Q}^* = \left\{ \begin{array}{c} \underline{C}_{ID}^* \\ \underline{Q}_1^* \\ \vdots \\ \underline{Q}_L^* \end{array} \right\}^T \quad (5-42)$$



The new covariance matrix is

$$\underline{\underline{U}}^* = \begin{Bmatrix} \underline{\underline{U}}_I^* & \underline{\underline{O}}_{6 \times M}^* \\ \underline{\underline{O}}_{M \times 6}^* & \underline{\underline{U}}_{M \times M}^* \end{Bmatrix} \quad (5-43)$$

where  $\underline{\underline{U}}_{M \times M}^*$  is the original covariance matrix, obtained from the M measurements. It is assumed in (5-43) that uncertainties associated with the injection guidance system are uncorrelated with the later measurements. Finally, the new observed measurement variation vector is

$$\delta \underline{\underline{m}} = \begin{Bmatrix} \delta \underline{\underline{x}}_I \\ \delta \underline{\underline{m}}_1 \\ \vdots \\ \delta \underline{\underline{m}}_L \end{Bmatrix} = \begin{Bmatrix} \underline{\underline{O}}_6 \\ \delta \underline{\underline{m}}_1 \\ \vdots \\ \delta \underline{\underline{m}}_L \end{Bmatrix} \quad (5-44)$$

With these definitions Equation (5-11) can be solved for an improved estimate of  $\delta \underline{\underline{x}}_D$ .

### 5.9 The Estimate Immediately Following a Midcourse Correction

Whenever a midcourse correction is applied,  $\delta \underline{\underline{x}}_D$  is changed. Subsequent measurements are used to estimate the new  $\delta \underline{\underline{x}}_D$ . The concept of the initial estimate, as developed in the preceding section, can be adapted to provide a more accurate estimate of the new  $\delta \underline{\underline{x}}_D$ .

On the basis of measurements made prior to the correction time  $t_C$ , an estimate is obtained for the uncorrected  $\delta \underline{\underline{x}}_D$ , which is designated  $\delta \underline{\underline{x}}_D^-$ . The uncorrected state vector at the time of correction is  $\delta \underline{\underline{x}}_C^-$ .

$$\delta \underline{\underline{x}}_C^- = \underline{\underline{C}}_{CD}^* \delta \underline{\underline{x}}_D^- \quad (5-45)$$

Immediately after the correction  $\underline{c}$  is applied, the new state vector is

$$\delta \underline{x}_C^+ = \delta \underline{x}_C^- + \begin{Bmatrix} \underline{0}_3 \\ \underline{c} \end{Bmatrix} \quad (5-46)$$

$$= \hat{C}_{CD}^* \delta \underline{x}_D^+ \quad (5-47)$$

where  $\delta \underline{x}_D^+$  is the new state vector for which an estimate is required.

$\underline{c}$  is the velocity correction actually applied. Because of instrumentation inaccuracy it differs from  $\tilde{\underline{c}}$ , the "observed" or desired correction. The difference between the two is designated  $\underline{\eta}$ .

$$\underline{\eta} = \tilde{\underline{c}} - \underline{c} \quad (5-48)$$

The "observed" value of  $\delta \underline{x}_C^+$  is

$$\delta \tilde{\underline{x}}_C^+ = \delta \hat{\underline{x}}_C^- + \begin{Bmatrix} \underline{0}_3 \\ \tilde{\underline{c}} \end{Bmatrix} \quad (5-49)$$

The error in the observed value is

$$\begin{aligned} \underline{u}_C^+ &= \delta \tilde{\underline{x}}_C^+ - \delta \underline{x}_C^+ \\ &= (\delta \hat{\underline{x}}_C^- - \delta \underline{x}_C^-) + \begin{Bmatrix} \underline{0}_3 \\ \tilde{\underline{c}} - \underline{c} \end{Bmatrix} \\ &= \underline{\epsilon}_C^- + \begin{Bmatrix} \underline{0}_3 \\ \underline{\eta} \end{Bmatrix} \end{aligned} \quad (5-50)$$

where

$$\delta \hat{\underline{x}}_C = \hat{C}_{CD}^* \delta \hat{\underline{x}}_D \quad (5-51)$$

and

$$\underline{\epsilon}_C^- = \hat{C}_{CD}^* \underline{\epsilon}_D^- \quad (5-52)$$

The covariance matrix of  $\underline{\epsilon}_C^-$  is

$$\underline{\hat{E}}_C^- = \overline{(\underline{\epsilon}_C^-) (\underline{\epsilon}_C^-)^T} = \underline{\hat{C}}_{CD} \underline{\hat{E}}_D^- \underline{\hat{C}}_{CD}^T \quad (5-53)$$

The covariance matrix of  $\underline{u}_C^+$  is

$$\begin{aligned} \underline{\hat{U}}_C^+ &= \overline{(\underline{u}_C^+) (\underline{u}_C^+)^T} \\ &= \underline{\hat{E}}_C^- + \left\{ \begin{matrix} \underline{\hat{O}}_{6 \times 3} & \overline{\underline{\epsilon}_C^- \underline{\eta}^T} \end{matrix} \right\} + \left\{ \begin{matrix} \underline{\hat{O}}_3 & \underline{\hat{O}}_3 \\ \underline{\hat{O}}_3 & \overline{\underline{\eta} \underline{\eta}^T} \end{matrix} \right\} \end{aligned} \quad (5-54)$$

To evaluate  $\underline{\hat{U}}_C^+$ , it is necessary to formulate a model of the control system used to apply the midcourse correction and to analyze the errors in the contemplated system. One such analysis is given in Reference (13).

Equation (5-11) is used to solve for  $\delta \underline{\hat{x}}_D^+$  when the following are used for  $\underline{\hat{Q}}^T$ ,  $\underline{\hat{U}}$ , and  $\delta \underline{\hat{m}}$ :

$$\underline{\hat{Q}}^T = \left\{ \begin{matrix} \underline{\hat{C}}_{CD} \\ \underline{\hat{Q}}_1^T \\ \vdots \\ \underline{\hat{Q}}_L^T \end{matrix} \right\} \quad (5-55)$$

$$\underline{\hat{U}} = \left\{ \begin{matrix} \underline{\hat{U}}_C^+ & \underline{\hat{O}}_{6 \times M} \\ \underline{\hat{O}}_{M \times 6} & \underline{\hat{U}}_{M \times M} \end{matrix} \right\} \quad (5-56)$$

$$\delta \underline{\tilde{m}} = \begin{Bmatrix} \delta \underline{\tilde{x}}_C^+ \\ \delta \underline{\tilde{m}}_1 \\ \vdots \\ \delta \underline{\tilde{m}}_L \end{Bmatrix} \quad (5-57)$$

The M measurements referred to in these equations are the measurements made subsequent to the correction at  $t = t_C$ .

The inclusion of the initial observation vector  $\delta \underline{\tilde{x}}_C^+$  in the determination of  $\delta \underline{\hat{x}}_D^+$  enables all the observations made since injection to be utilized. It therefore has a much more significant effect on the accuracy of estimation than the inclusion of the initial estimate  $\delta \underline{x}_I$  has.

#### 5.10 Physical Considerations in the Selection of Optical Sightings

It has been pointed out in Section 5.5 that the designer of a self-contained navigation system has the problem of determining which angles should be measured at each measurement time  $t_S$  in order to determine the position variation  $\delta \underline{\tilde{r}}_S$ . Battin<sup>(6)</sup> has developed the mathematics for optimizing a set of three angular measurements, from which position is determined uniquely under the assumption that the clock error can be neglected. The analysis in this section is concerned with the optimization of a redundant set of angular measurements; the emphasis is on physical reasoning rather than mathematical rigor.

For the purpose of selecting the sightings, it is justifiable to simplify the problem by neglecting clock error. It is unlikely that the relatively small effect of the clock error on  $\delta \underline{\tilde{r}}_S$  can affect the selection, and neglecting this effect simplifies the analysis considerably. With this assumption, Equation (5-18) becomes

$$\delta \underline{m}_S = \begin{Bmatrix} \delta A_{S1} \\ \vdots \\ \delta A_{SK} \end{Bmatrix} = \underline{G}_S^*{}^T \delta \underline{r}_S \quad (5-58)$$

where

$${}^*_G S^T = \begin{Bmatrix} \mathbf{g}_{S1}^T \\ \vdots \\ \mathbf{g}_{SK}^T \end{Bmatrix} \quad (5-59)$$

K is greater than 3.

For a sighting of the angle between the line of sight to a near body and the line of sight to a star, a mathematical expression for the vector  $\mathbf{g}_{SR}$  can readily be derived from Figure 5-1. At time  $t_s$  the reference position of the planet is X; its actual position is X'. The position of the near body is P; its distance from X is  $z_P$ . The line of sight to the star from X is XY; from X' it is X'Y'. Since the star's distance is assumed to be infinite, XY and X'Y' are parallel. The reference value of the angle to be measured is

$$A_{SR} = \angle PXY \quad (5-60)$$

The actual angle measured is

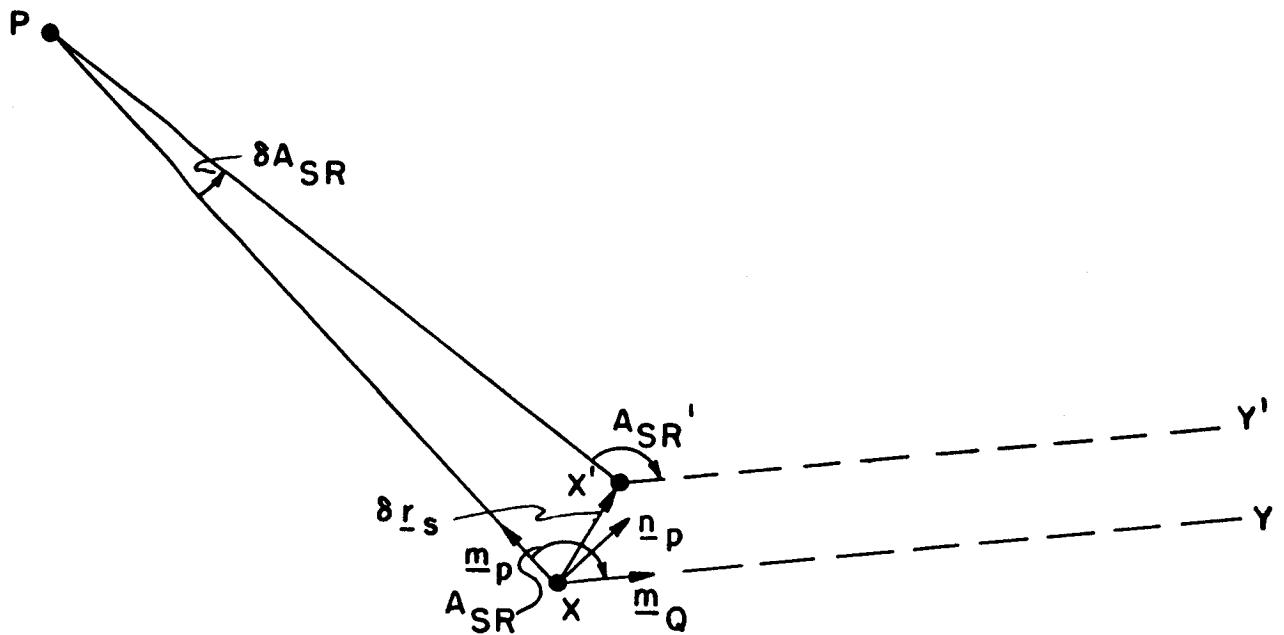
$$A_{SR}' = \angle PX'Y' \quad (5-61)$$

The difference between the two is  $\delta A_{SR}$ .

$$\delta A_{SR} = A_{SR}' - A_{SR} \quad (5-62)$$

Unit vectors  $\underline{m}_P$  and  $\underline{m}_Q$  lie along the lines from X to P and from X to the star, respectively. The unit vector  $\underline{n}_P$  is normal to  $\underline{m}_P$  and in the plane containing  $\underline{m}_P$  and  $\underline{m}_Q$ .

$$\underline{n}_P = \frac{1}{\sin A_{SR}} (\underline{m}_Q - \underline{m}_P \cos A_{SR}) \quad (5-63)$$



- X - vehicle's reference position
- X' - vehicle's actual position
- P - position of near body
- XY, X'Y' - line of sight to star
- $A_{SR} = \angle PXY =$  reference value of angle to be measured
- $A_{SR}' = \angle PX'Y' =$  actual angle to be measured
- $\delta A_{SR} = A_{SR}' - A_{SR}$
- $\delta \underline{r}_S$  - position variation of vehicle at time  $t_S$
- $\underline{m}_P$  - unit vector along nominal line of sight from vehicle to near body
- $\underline{m}_Q$  - unit vector along nominal line of sight from vehicle to star
- $\underline{n}_P$  - unit vector normal to nominal line of sight from vehicle to near body

Figure 5.1 Geometry of Angular Measurement

From the figure it is apparent that  $\delta A_{SR}$  is related to the component of  $\delta \underline{r}_S$  parallel to  $\underline{n}_P$ .

$$z_P \delta A_{SR} = \underline{n}_P^T \delta \underline{r}_S \quad (5-64)$$

Then

$$\underline{g}_{SR} = \frac{\underline{n}_P}{z_P} \quad (5-65)$$

The error in the computed component of  $\delta \underline{r}_S$  caused by an error  $u_{SR}$  in the observation of  $\delta A_{SR}$  is directly proportional to  $z_P$ . Thus, to minimize the error in the computed value of  $\delta \underline{r}_S$ , it is desirable to sight on the nearest of the near bodies in several of the measurements.

The plane containing the two lines of sight for a particular angular measurement will be designated the "measurement plane." If two stars are chosen such that the measurement plane of the angle between the nearest body and the first star is perpendicular to the measurement plane of the angle between the nearest body and the second star, two orthogonal components of  $\delta \underline{r}_S$  can be determined, both components lying in the plane normal to  $\underline{m}_P$ .

There still remains the problem of finding the component of  $\delta \underline{r}_S$  parallel to  $\underline{m}_P$ . This component cannot be found by measuring the angle between  $\underline{m}_P$  and the line of sight to any star. It is possible to make an estimate of  $(\underline{m}_P^T \delta \underline{r}_S)$  by measuring the angular diameter of the nearest body, but this measurement has little practical value in the midcourse phase of the flight, when the distance of the nearest planet from the vehicle is at least of the order of hundreds of planet diameters. Thus, at least one angular measurement involving another near body is required.

It would be ideal if there were a second near body whose distance from the vehicle is not much greater than that of the nearest body and whose line of sight is perpendicular to the line of sight to the nearest body. Then an angular measurement between the lines of sight to the second body and a star can be made such that the component of  $\delta \underline{r}_S$  along the line of sight to the nearest body can be determined. In practice this ideal is seldom, if ever, achieved. As a consequence, the third angular measurement gives the component of  $\delta \underline{r}_S$  in a direction different from

$\underline{m}_P$ . After three measurements have been made, there is greater uncertainty about the component of  $\delta \underline{r}_S$  along  $\underline{m}_P$  than there is about the components of  $\delta \underline{r}_S$  in the plane perpendicular to  $\underline{m}_P$ . The first objective of the redundant measurements is to reduce the uncertainty in the component of  $\delta \underline{r}_S$  along  $\underline{m}_P$ .

The near bodies for an interplanetary journey consist of the sun and the inner planets Mercury, Venus, Earth, and Mars. When the vehicle is not too distant from Earth, the moon may also be used. The fact that all the inner planets as well as the moon move in orbits that are inclined by only a few degrees to the ecliptic can be used to advantage in the selection of sightings, for, from considerations of energy required for injection into a heliocentric orbit, the vehicle's orbital plane is also close to the ecliptic.

A measurement of the angle between a near body and a star whose line of sight is inclined only slightly to the ecliptic plane (and hence inclined only slightly to the reference trajectory plane) leads to an estimate of a component of  $\delta \underline{r}_S$  which is roughly in the reference trajectory plane. Another measurement, involving a second near body and the same star, yields an estimate of the component of  $\delta \underline{r}_S$  in some other direction, also close to the reference trajectory plane. Additional measurements, between additional near bodies and the same star or between pairs of near bodies, refine the accuracy of the estimate of position variation in the reference trajectory plane.

To estimate position variation normal to the reference trajectory plane, a measurement is made of the angle between a near body and a star whose line of sight is normal to the reference trajectory plane, if a star of sufficient brightness for good visibility can be found in this direction. Additional measurements between other near bodies and the same star reduce the uncertainty in the estimate of position variation normal to the reference trajectory plane.

The measurement selection procedure being suggested is in reality another exploitation of the condition that was used to advantage in the guidance analysis of Chapter 3, namely that characteristics associated with the reference trajectory plane are virtually uncoupled from characteristics normal to that plane.



It has been mentioned that angular sightings between two near bodies may be used in addition to near body-star sightings to improve the estimate of position variation in the reference trajectory plane. Equations (5-64) and (5-65) are not applicable to this type of measurement. If the nearest body is P, at distance  $z_P$  from the vehicle, and if the other near body is Q, at distance  $z_Q$  from the vehicle, Equation (2-5) of Reference (3) indicates that, when clock errors are neglected,

$$\delta A_{SR} = \left( \frac{\underline{n}_P}{z_P} + \frac{\underline{n}_Q}{z_Q} \right) \cdot \delta \underline{r}_S \quad (5-66)$$

Thus

$$\underline{g}_{SR} = \frac{\underline{n}_P}{z_P} + \frac{\underline{n}_Q}{z_Q} \quad (5-67)$$

where  $\underline{n}_P$  is defined by Equation (5-62), and correspondingly,

$$\underline{n}_Q = \frac{1}{\sin A_{SR}} (\underline{m}_P - \underline{m}_Q \cos A_{SR}) \quad (5-68)$$

Measuring the angle between two near bodies yields an estimate of the component of  $\delta \underline{r}_S$  in a direction which is the weighted average of the normals to the lines of sight to the two bodies, the weighting being inversely proportional to the distance of the body from the vehicle.

The sensitivity factor S will be defined as the error in the relevant component of  $\delta \underline{r}_S$  caused by a unit error in the measurement of  $A_{SR}$ . S is the reciprocal of the magnitude of  $\underline{g}_{SR}$ . For a near body-star measurement,

$$S = z_P \quad (5-69)$$

For a measurement between two near bodies, the law of cosines is used to show that

$$S = \frac{z_P z_Q}{d} \quad (5-70)$$

where d is the distance of Q from P.

It is obviously desirable to keep  $S$  as low as possible. Equations (5-69) and (5-70) indicate that the value of  $S$  for a measurement between two near bodies is smaller than the value of  $S$  for a near body-star measurement only when the distance of  $Q$  from the vehicle is less than the distance of  $Q$  from  $P$ . This sensitivity criterion applies only to the magnitude of the inferred position error. It is occasionally desirable to use a measurement with a higher  $S$  in order to obtain an estimate of  $\delta \underline{r}_S$  in a direction in which the uncertainty is relatively high.

#### 5.11 Mathematical Criterion for the Selection of Optical Sightings

A useful mathematical criterion for selecting a redundant number of angular measurements for position determination is the minimization of the volume of the equi-probability ellipsoid, subject to the constraint that the three axes of the ellipsoid be kept approximately equal in length.

The concept of the equi-probability ellipsoid is discussed in Appendix P. The equation for the ellipsoid corresponding to measurements made at time  $t_S$  is the quadratic form

$$\underline{\beta}_S^T \underline{B}_S^{*-1} \underline{\beta}_S = k^2 \quad (5-71)$$

where  $k$  is a constant. The center of the ellipsoid is at the point

$$\underline{\beta}_S = \underline{O}_3 \quad (5-72)$$

The volume of the ellipsoid is

$$V = \frac{4}{3} \pi k^3 \left| \underline{B}_S^* \right|^{1/2} \quad (5-73)$$

where  $\left| \underline{B}_S^* \right|$  is the determinant of the covariance matrix  $\underline{B}_S^*$ .

For any specified value of  $k$ , the probability that the error vector  $\underline{\beta}_S$  will lie totally within the ellipsoid is a constant. Thus it is desirable to reduce the volume of the ellipsoid for the given  $k$ , and this can be accomplished only by reducing  $\left| \underline{B}_S^* \right|$ . Maintaining the axes of the ellipsoid roughly equal in length ensures that the reduction in volume is not achieved by means of a reduction in uncertainty in one direction at the expense of a relatively large uncertainty in another direction.

Since clock errors are being neglected,

$$\mathbf{B}_S^* = (\mathbf{G}_S^* \mathbf{U}_S^{*-1} \mathbf{G}_S^{*T})^{-1} \quad (5-74)$$

If it is assumed that the standard deviation of the uncertainty in each of the K angular measurements is  $\sigma$ ,

$$\mathbf{U}_S^{*-1} = \frac{1}{\sigma^2} \mathbf{I}_K \quad (5-75)$$

Then,

$$\mathbf{B}_S^* = \sigma^2 (\mathbf{G}_S^* \mathbf{G}_S^{*T})^{-1} \quad (5-76)$$

Reducing the determinant of  $\mathbf{B}_S^*$  for a given  $\sigma^2$  is equivalent to increasing the determinant of  $(\mathbf{G}_S^* \mathbf{G}_S^{*T})$ .  $\mathbf{G}_S^*$  is a 3-by-K matrix.

$$\mathbf{G}_S^* = \begin{Bmatrix} \mathbf{g}_{S1} & \cdot & \cdot & \cdot & \mathbf{g}_{SK} \end{Bmatrix} \quad (5-77)$$

$$\mathbf{G}_S^* \mathbf{G}_S^{*T} = \sum_{R=1}^K \mathbf{g}_{SR} \mathbf{g}_{SR}^T \quad (5-78)$$

It is convenient to express the components of the  $\mathbf{g}_S$  vectors in one of the reference trajectory coordinate systems of Appendix A. In any of these systems the third component of  $\mathbf{g}_S$  is zero for an in-plane measurement (a measurement of the angle between two lines of sight, both of which lie in the reference trajectory plane). For an out-of-plane measurement (one in which the angle measured is between the line of sight to a near body in the reference trajectory plane and the line of sight to a star normal to the reference trajectory plane), the first two components of  $\mathbf{g}_S$  are zero.

If several measurements of each of the two types are made, the resulting matrix  $(\mathbf{G}_S^* \mathbf{G}_S^{*T})$  has the same uncoupled feature as all of the matrices of Chapter 3; that is, the first two elements of the third row and the first two elements of the third column are all zero. In practice

this condition cannot be achieved precisely, because the lines of sight to the celestial bodies used in the measurements do not lie exactly in or perpendicular to the reference trajectory plane. Moreover, if the lines of sight to two near bodies are roughly perpendicular to each other, the in-plane measurements can be so chosen that  $(\overset{*}{G}_S \overset{*}{G}_S^T)$  closely resembles a diagonal matrix.

The procedure to be used in selecting measurements is straightforward. If six angles are to be used, four will be in-plane and two out-of-plane. Let P, Q, and R represent three near bodies in order of increasing distance from the vehicle. Let  $B_1$  and  $B_2$  be "in-plane" stars, and let  $C_1$  and  $C_2$  be "out-of-plane" stars, the line of sight to  $C_1$  being closer to the normal to the reference trajectory plane than the line of sight to  $C_2$ .

The first two measurements are the obvious ones. P and  $B_1$  are used for an in-plane measurement, and P and  $C_1$  are used for an out-of-plane measurement. These two provide estimates of the components of  $\delta \underline{r}_S$  in the plane normal to the line of sight from the vehicle to P. Next, a second out-of-plane measurement can be made; this involves either P and  $C_2$  or Q and  $C_1$ , whichever combination gives the larger value of the lower right-hand element of  $(\overset{*}{G}_S \overset{*}{G}_S^T)$ .

The remaining three in-plane measurements depend on the positions of Q and R relative to P and the vehicle. The primary problem is to obtain a reasonably accurate estimate of the component of  $\delta \underline{r}_S$  along the line of sight to P. The pairs of bodies used in the measurements are normally chosen from among the following:

1. P and Q
2. Q and  $B_1$
3. Q and R
4. Q and  $B_2$
5. R and  $B_1$
6. P and R

Those three are chosen for which the diagonal elements of the resulting 2-by-2 sub-matrix of  $(\overset{*}{G}_S \overset{*}{G}_S^T)$  are most nearly equal. A simple graphical method of making the selection is discussed in Section 5.13.

It may be noted that six distinctly different angles are measured even though theoretically greater accuracy can be obtained by repeating some of the original measurements. The reason for using all different angles is to minimize the effect of any unknown non-random errors in the instrumentation system.

## 5.12 Survey of First Magnitude Stars

The optical system for acquiring and tracking celestial bodies is simplified if only the relatively bright bodies are used for the angular measurements. The apparent brightness of the other planets as seen from Earth varies with time, but all those that are to be used as "near bodies" (except Mars during a short portion of its cycle relative to Earth) are at least as bright as first-magnitude stars. Jupiter and Saturn, although they are not used as near bodies, are also at least as bright as first-magnitude stars. The variations in planet brightness are illustrated in the chart on Pages 34 and 35 of Reference (34). A discussion of the meaning of the "magnitude" of a star may be found in Reference (35), Pages 329 et seq.

There are 22 stars whose brightness as seen from the solar system is greater than that of a star with apparent visual magnitude of 1.5. These stars have been investigated to determine which, if any, are suitable as "in-plane" stars and which are suitable as "out-of-plane" stars. The resulting data are contained in Table 5-1. The stars are listed in order of decreasing brightness. The order and the apparent visual magnitude are taken from Table 11.II of Reference (35).

The computed data for each star consist of celestial longitude, celestial latitude, and the components of the line-of-sight unit vector along the  $x_E$ ,  $y_E$ ,  $z_E$  axes of the heliocentric ecliptic coordinate system. The computations are based on values of right ascension and declination obtained from the section entitled "Mean Places of Stars, 1962.0" in Reference (36).

If  $\alpha$  and  $\delta$  are, respectively, the right ascension and declination, the components of the line-of-sight unit vector  $\underline{m}$  are

$$m_{x_E} = \cos \delta \cos \alpha \quad (5-79)$$

TABLE 5-1 Characteristics of First Magnitude Stars

Star Number	Star Name	Apparent Visual Magnitude	$m_{x_E}$	$m_{y_E}$	$m_{z_E}$	Celestial Longitude (degrees)	Celestial Latitude (degrees)
1	Sirius	-1.43	-0.1806	0.7491	-0.6374	103.56	-39.60
2	Canopus	-0.73	-0.0610	0.2371	-0.9696	104.44	-75.83
3	$\alpha$ Centauri	-0.27	-0.3792	-0.6311	-0.6766	239.00	-42.58
4	Arcturus	-0.06	-0.7868	-0.3454	0.5115	203.70	30.76
5	Vega	0.04	0.1208	-0.4579	0.8808	284.78	61.73
6	Capella	0.09	0.1390	0.9109	0.3885	81.33	22.86
7	Rigel	0.15	0.2028	0.8317	-0.5169	76.30	-31.13
8	Procyon	0.37	-0.4102	0.8693	-0.2758	115.26	-16.01
9	Achernar	0.53	0.4915	-0.1338	-0.8605	344.77	-59.38
10	$\beta$ Centauri	0.66	-0.4293	-0.5752	-0.6963	233.26	-44.13
11	Betelgeuse	0.4 to 1.0	0.0298	0.9606	-0.2762	88.22	-16.03
12	Altair	0.80	0.4522	-0.7456	0.4895	301.24	29.30
13	Aldebaran	0.75 to 0.95	0.3525	0.9309	-0.0953	69.26	-5.47
14	$\alpha$ Crucis	0.87	-0.4531	-0.3987	-0.7973	221.34	-52.88
15	Antares	0.90 to 1.06	-0.3535	-0.9321	-0.0796	249.23	-4.57
16	Spica	1.00	-0.9178	-0.3955	-0.0358	203.31	-2.05
17	Fomalhaut	1.16	0.8335	-0.4187	-0.3605	333.32	-21.13
18	Pollux	1.16	-0.3831	0.9163	0.1163	112.69	6.68
19	Deneb	1.26	0.4537	-0.2134	0.8652	334.81	59.91
20	$\beta$ Crucis	1.31	-0.4978	-0.4346	-0.7505	221.12	-48.63
21	Regulus	1.36	-0.8598	0.5105	0.0081	149.30	0.46
22	$\epsilon$ Canis Majoris	1.49	-0.2159	0.5858	-0.7811	110.23	-51.36

$$m_{y_E} = \cos \delta \sin \alpha \cos \epsilon + \sin \delta \sin \epsilon \quad (5-80)$$

$$m_{z_E} = -\cos \delta \sin \alpha \sin \epsilon + \sin \delta \cos \epsilon \quad (5-81)$$

$\epsilon$ , the obliquity of the ecliptic, is equal to  $23.444^\circ$ . The celestial longitude  $\lambda$  and the celestial latitude  $\beta$  are given by

$$\lambda = \arctan \left[ \frac{m_{y_E}}{m_{x_E}} \right] \quad (5-82)$$

$$\beta = \arctan \left[ \frac{m_{z_E}}{(m_{x_E}^2 + m_{y_E}^2)^{1/2}} \right] \quad (5-83)$$

Figure 5.2 is a polar plot of the star locations on the celestial sphere.

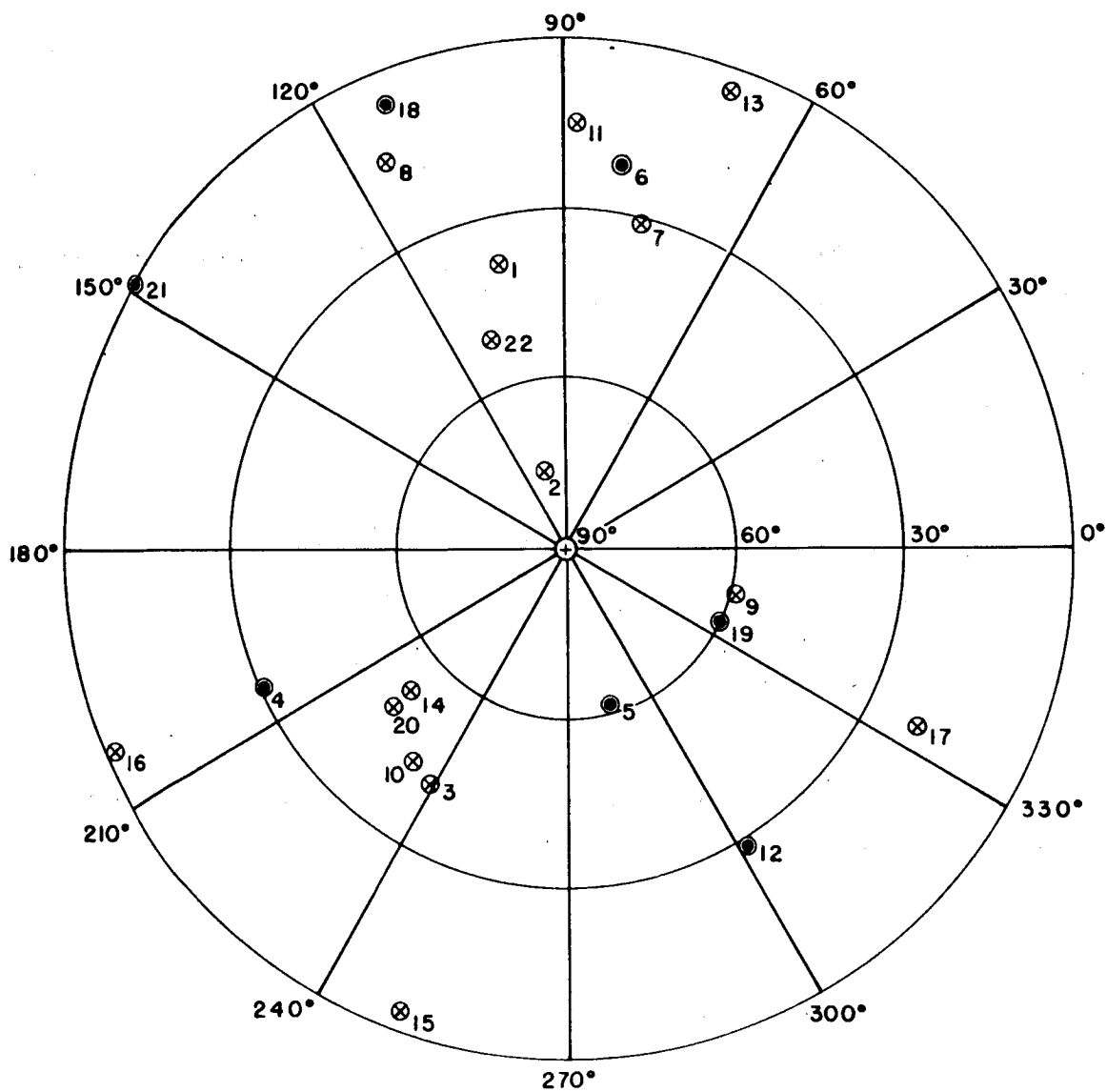
The data indicate that five of the stars are at celestial latitudes between  $-10^\circ$  and  $+10^\circ$  and thus may be used as in-plane stars. In order of increasing magnitude of latitude, they are

- 21. Regulus
- 16. Spica
- 15. Antares
- 13. Aldebaran
- 18. Pollux

In addition, either Jupiter or Saturn may be used as far bodies for in-plane measurements.

Canopus, the second brightest star, is the best situated for out-of-plane measurements. Other stars that may be used for out-of-plane measurements, in order of decreasing magnitude of latitude, are

- 5. Vega
- 19. Deneb
- 9. Achernar



Numbers refer to stars listed in Table 5-1.

⊙ Star in positive celestial latitude.

⊗ Star in negative celestial latitude.

$\lambda$  = Celestial longitude

$\beta$  = Celestial latitude

Figure 5.2 Celestial Longitude and Latitude of First Magnitude Stars



### 5.13 Illustration of Procedure for Selection of Angular Measurements

An illustrative example serves to demonstrate the method of selecting the sightings to be used for position determination. Figure 5.3 shows the nominal position of the space vehicle and the positions of the near bodies one year after launch on Trajectory 1034, which was also used for illustrative purposes in Chapter 4. The lines of sight to the in-plane stars are indicated in the figure. All positions shown are projections of the true positions into the plane of the reference trajectory.

The distances of the near bodies from the vehicle are

for Mars,  $z_M = 1.57$  a.u.

for the sun,  $z_S = 1.59$  a.u.

for Venus,  $z_V = 1.83$  a.u.

for Earth,  $z_E = 2.38$  a.u.

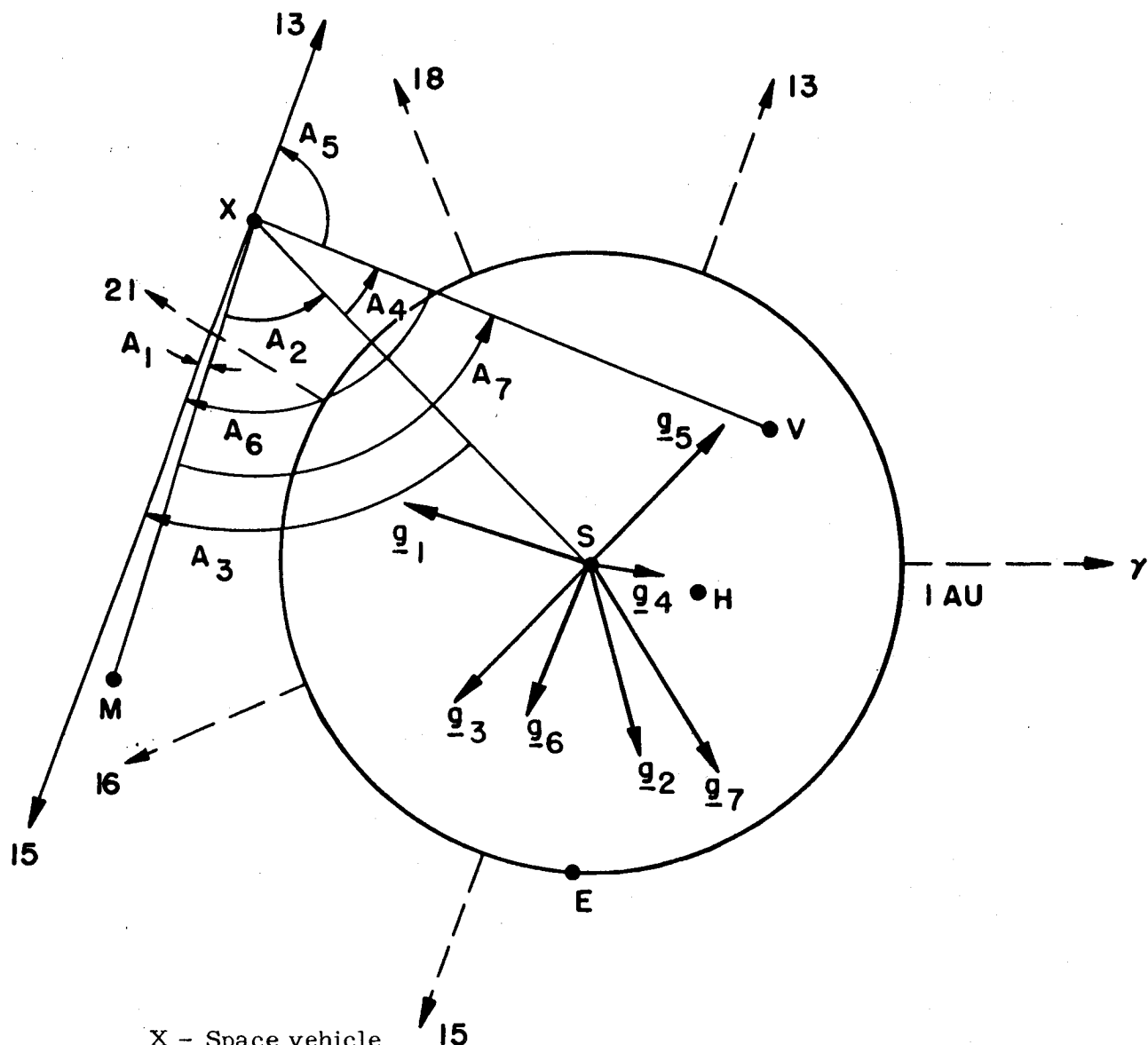
Mercury, the other near body, is not used for measurements in this case, because its line of sight is too close to that of the sun. In Reference (5) it is stated that bodies whose lines of sight are within  $15^\circ$  of that of the sun are optically undesirable for measurement purposes.

The configuration shown, which was picked at random, is somewhat unusual in that the vehicle, Mars, and the sun form roughly an equilateral triangle. In manned missions the distance of the vehicle from the launch planet, or from the destination planet, or sometimes from both, is considerably smaller than its distance from the sun.

Six measurements are to be selected, two out-of-plane and four in-plane. The near bodies to be used are Mars, the sun, and Venus.

Since Mars and the sun are virtually equidistant from the vehicle, the two best out-of-plane measurements are the angles that the line of sight to each makes with the line of sight to Canopus, the first-magnitude star situated closest to the celestial polar axis.

The four in-plane measurements are to be selected from the seven shown in Figure 5.3. For simplicity the double-subscript notation of previous sections has been replaced by a set of single numerical



X - Space vehicle

S - Sun

H - Mercury

V - Venus

E - Earth

M - Mars

Dotted lines indicate directions to points on celestial sphere.

$\gamma$  - First point of Aries

13, 15, 16, 18, 21 - Stars from Table 5-1

$A_1, \dots, A_7$  - Possible measurement angles

$\underline{g}_1, \dots, \underline{g}_7$  - Corresponding geometry vectors

Positions and vectors shown are projections of actual quantities into plane of reference trajectory.

Figure 5.3 Selection of Measurement Angles

subscripts. The celestial bodies involved in the seven possible angular measurements are

$A_1$  : Mars - Antares

$A_2$  : Mars - Sun

$A_3$  : Sun - Antares

$A_4$  : Sun - Venus

$A_5$  : Sun - Aldebaran

$A_6$  : Venus - Antares

$A_7$  : Mars - Venus

Antares is used in all except one of the possible measurements involving stars, because its line of sight forms the smallest angles with the lines of sight to the near bodies. Because there are practical limitations on the maximum angle that the vehicle's tracking system can measure, it is desirable, when other factors are equal, to select the smallest possible angles. All the angles listed above are smaller than  $120^\circ$ .

The geometry vectors  $\underline{g}_1$  through  $\underline{g}_7$  are also shown in Figure 5.3. The final selection of four in-plane measurements is based on the magnitude and direction of these vectors. The selection can be made visually if any pair of orthogonal axes can be found in the reference trajectory plane such that the sums of the squares of the components of the selected vectors along each of these axes can be seen to be maximized and roughly equal to each other.

Axes parallel and normal to  $\underline{g}_1$  are convenient. The first vector selected is  $\underline{g}_1$ .  $\underline{g}_4$  is immediately ruled out because of its small magnitude. The other three vectors to be chosen should have large components normal to  $\underline{g}_1$ . In this particular example,  $\underline{g}_2$ ,  $\underline{g}_3$ ,  $\underline{g}_5$ ,  $\underline{g}_6$ , and  $\underline{g}_7$  all have components normal to  $\underline{g}_1$  that are approximately equal in magnitude, so that the position uncertainty normal to  $\underline{g}_1$  is not appreciably affected by the selection. In this circumstance, the three vectors of largest magnitude are selected, because they will cause the largest reduction in position uncertainty parallel to  $\underline{g}_1$ . The selected vectors are

$g_7$ ,  $g_2$ , and  $g_3$ . Although  $g_3$  and  $g_5$  are equal in magnitude,  $g_3$  is selected because the measurement angle  $A_3$  is smaller than  $A_5$ .

The six angles selected involve the following pairs of celestial bodies:

1. Mars - Canopus
2. Sun - Canopus
3. Mars - Antares
4. Mars - Venus
5. Mars - Sun
6. Sun - Antares

These angles, although selected without need for computation, satisfy the mathematical criterion of producing a large value of the determinant of  $(G_S^* G_S^{*T})$ . Regardless of which of the reference trajectory coordinate systems is used, the diagonal elements of  $(G_S^* G_S^{*T})$  are large compared to the off-diagonal elements, and the diagonal elements are of the same order of magnitude.

#### 5.14 Physical Considerations

In all of the preceding analysis the navigational problem has been treated from a geometric viewpoint; in this section physical factors that tend to affect the utilization of the measurements are briefly outlined.

In the Earth-based system corrections are applied to the data for the effect of refraction of the radio signals emanating from the vehicle as they pass through the earth's atmosphere, for the difference between the apparent vertical at the tracking station (as measured by a plumb line) and the geocentric vertical, and for the effect of aberration due to the transverse velocity of the vehicle relative to the tracking station. Reference (33) contains an analysis of the first two effects.

Larmore<sup>(37)</sup> presents a discussion of a number of physical phenomena that affect the angular measurements in the self-contained system. Larmore's analysis is based on the assumption that it is possible to achieve an ultimate accuracy of 0.2 seconds of arc or 1 microradian in the measurement of celestial angles; in the present study the far more conservative

figures of 10 seconds of arc or 50 microradians are regarded as reasonable for the accuracy of on-board angular measurements made with instrumentation systems consistent with the present state of the art. As a consequence, some of the effects that are regarded as significant by Larmore as assumed to be negligible in this study.

One effect that is significant is the aberration of starlight due to the component of vehicle velocity that is normal to the line of sight to the star. This effect may cause an apparent shift of the line of sight to the star of as much as 100 microradians. A related effect is the apparent shift in the line of sight to a planet due to the finite velocity of light. If Mars is being viewed from a distance of 1 a. u., the planet will have moved approximately 7,000 miles in the time that it takes a light ray to travel from it to the vehicle.

The phasing of the planets also presents some difficulty. The optical apparatus is assumed to seek the point of maximum light intensity when the body being tracked is not a point source. When the illuminated portion of a planet is crescent-shaped, the point of maximum light intensity is removed from the center of the planet by an amount which may be significant. The difficulty is compounded by the fact that cloud formations and other variations in planetary atmospheres are not predictable, and their effects on the center of light intensity is not known precisely. For Venus at inferior conjunction the difference between the center of light intensity and the center of the planet could cause an angular measurement error of as much as 100 microradians for a sighting made from the surface of the earth.

Other sources of error mentioned by Larmore which are not considered significant in the present analysis include the small inaccuracies in the planetary position data of Reference (36), the parallax effect due to the fact that the star distances are not truly infinite, the effect of the proper motion of the stars, and the fact that in a double star system the center of light intensity does not coincide with the center of mass of the system.

The inexact knowledge of the size of the astronomical unit in terms of standard lengths used in the laboratory does not directly affect the angular measurements, since the angles are really ratios of lengths rather than lengths themselves. However, this uncertainty does affect the accuracy of

the prediction of vehicle position relative to the destination point. As a result of recent tests in which radar signals have been reflected from Venus, the uncertainty in the ratio of the astronomical unit to a laboratory unit such as the kilometer or the mile has been reduced from one part in  $10^4$  to three parts in  $10^6$ . The results of the radar investigation are reported in Reference (38). The uncertainty of three parts in  $10^6$  is equivalent to an uncertainty of 300 miles in the length of the astronomical unit.

The effect of relativity on instrumentation in the space vehicle is discussed in Reference (39). The primary effect is an induced drift rate in the vehicle's clock relative to a standard clock on the surface of the earth. Due to special relativity the vehicle's clock tends to run fast; due to general relativity it tends to run slow. For travel within the solar system both effects are at least two orders of magnitude smaller than the random drift rate of one part in  $10^6$  which is assumed to be feasible for the clock in the vehicle.

The systematic effects that are significant include the aberration of starlight, the finite velocity of light, and the phasing of the planets. All three can be taken into account in pre-computing the reference value of a space angle that is to be measured at a specified time.

## CHAPTER 6

### APPLICATIONS OF THE THEORY

#### 6.1 Summary

As an application of the guidance and navigation concepts developed in previous chapters, a midcourse guidance system is proposed for a manned flight from Earth to Mars. Other possible uses of the theory on an interplanetary flight are discussed.

#### 6.2 Introduction

The objective of this chapter is to show how the analytic approach to guidance theory can be effectively utilized in the design of the guidance system for a specific interplanetary mission. The type of mission that is to be discussed is an outbound manned mission from Earth to Mars.

For a practical mission of this type the total transfer angle,  $(f_D - f_I)$ , is equal to or less than  $180^\circ$ . Both radio-command and self-contained navigation systems are to be used. The nature of the mission is assumed to be such that VTA guidance is permissible.

The system that is to be described is felt to offer the combined advantages of simplicity, reliability, and low cost without any reduction in accuracy relative to previously proposed systems. These advantages are a direct consequence of the analytic solution of the guidance equations.

#### 6.3 Reference Trajectory

The reference trajectory for the interplanetary flight is pre-computed. All known perturbative effects of any significance are included in the formulation of the equations of motion. These equations are integrated numerically on a large-scale digital computer. The method of computation is described in considerable detail in Reference (40).

If several reference trajectories have been computed, all of which are approximately equally advantageous from the standpoint of time of flight and fuel requirements for launch and injection, midcourse guidance characteristics may affect the final choice of a trajectory. Computations such as those embodied in Figures 4.2, 4.13, and 4.16 are use-

ful in comparing trajectories. The latter two indicate the sensitivity of position variation at the destination to error in injection velocity; the first is a composite picture of the effect of the orientation of the relative velocity vector  $\underline{v}_R$  on the magnitude of the VTA correction.

#### 6.4 Injection Guidance

Although this study is not directly concerned with the problem of injection guidance, the illustrative example of Chapter 4 indicates clearly where the emphasis should be placed in the design of the injection guidance system. It is of primary importance to control the magnitude of the velocity vector at injection into the heliocentric orbit. In terms of hardware, the emphasis is to be placed on the accuracy of the integrating accelerometer system and on achieving fast, reliable cut-off of the propulsion system.

#### 6.5 Midcourse Guidance

Both the radio-command navigation system and the self-contained navigation system are to be used for midcourse guidance. Each of the two is used as the primary measurement source in the region of its greatest accuracy, and each is used as a stand-by measurement source when the other is the primary source. The vehicle's on-board computer and its control system are designed so that inputs can be accepted from either source at any time.

#### 6.6 Radio-Command Guidance

The Earth-based tracking system is the primary measurement source during the early stages of the heliocentric ballistic trajectory. It remains the primary source at least until the vehicle leaves Earth's sphere of perturbative relevance, at a distance of roughly two million miles from Earth.

The radio measurements, made several times a minute as long as the vehicle is visible to a tracking station, are combined with the initial estimate of the state vector at injection and used to determine the maximum likelihood estimate of the state vector at the nominal time of arrival at the destination.

Within Earth's sphere of perturbative relevance numerical integration is used to compute the elements of the required transition matrices. The computation is most simply accomplished in the non-rotating  $x y z$



coordinate system. The estimate obtained for  $\delta \underline{x}_D$  is transformed from  $x y z$  coordinates to  $p q z$  coordinates and then transmitted to the vehicle's computer by means of radio signals from one of the tracking stations.

The destination point used in the computation is the point at which the reference trajectory intersects the sphere of perturbative relevance of Mars, at a distance of approximately one million miles from the planet.

The first midcourse correction is to be made at the optimum time  $t_{C_{opt}}$ . As explained in the next section, the determination of this time is accomplished by the computer on board the space vehicle.

Because it corrects for the effects of errors in injection guidance, the first midcourse velocity correction is normally much larger in magnitude than any succeeding corrections. It is therefore quite fortunate that the Earth-based tracking system, with its thousands of individual measurements, can be used to obtain an accurate estimate of  $\delta \underline{x}_D^-$ , and it is likewise fortunate that the correction can be applied at the time when its magnitude is a minimum.

## 6.7 Self-Contained Guidance

Although the point at which the self-contained system replaces the radio-command system as the primary source of input data will depend on hardware development in the two types of systems, a reasonable point for the change-over is assumed to be at the surface of the sphere of perturbative relevance. Since the first correction, at  $t_{C_{opt}}$ , is made at a point considerably beyond this sphere, measurements from both systems are used in the computation of this correction. At the change-over point the final estimate of  $\delta \underline{x}_D^-$  made by the Earth-based system serves as an "initial estimate" for the vehicle's computer, to be used in conjunction with subsequent position measurements to compute a more accurate  $\delta \hat{\underline{x}}_D^-$ , from which  $t_{C_{opt}}$  and  $\underline{c}_V$  can be determined.

Since all of the computations performed by the vehicle's computer are related to that portion of the flight in which the vehicle is outside the sphere of perturbative relevance of any planet, the analytic forms of the guidance matrices can be used. No numerical integration is required of the computer even though the time  $t_{C_{opt}}$  is determined a posteriori.

In addition to being used for making the final determination of the first midcourse correction, the self-contained system is used for computing any subsequent corrections that may be required. The accuracy of subsequent corrections is improved by utilizing the concept of the initial estimate immediately after the last correction, as explained in Section 5.9.

Because of the presence of clock errors, the two-step procedure of Chapter 5, involving first determination of both present position and clock error and then determination of the estimated state vector at the destination, is used in all on-board computations.

For a voyage of roughly six months' duration a position determination once a week is deemed reasonable. The nominal time of each position determination and the specific angular measurements to be made at that time are pre-programmed. The graphical procedure illustrated in Section 5.13 is used to select six angles to be observed.

For each sighting at each measurement time the reference value of the angle is stored in the computer. This value includes the effects of the significant physical phenomena mentioned in Section 5.14. In addition, one number per measurement must be stored in the computer to account for the fact that the angular measurement is not made precisely at the time when the space ship clock reads  $t_S$ , the nominal time of the measurement; this number is a function of the velocity of the vehicle relative to the two bodies involved in the sighting.

Finally, in order to solve Equation (5-24) for the inferred values of clock error and position variation at time  $t_S$ , sufficient information must be stored so that the matrix product  $(\dot{G}_S^* \dot{U}^{-1} \dot{G}_S^* T)^{-1} \dot{G}_S^* \dot{U}_S^{-1}$  can be determined. All the data required are known a priori with one exception, the variance of the clock error  $u_{S0}^2$ . Normally this variance is small enough to justify an a priori estimate of its value at each  $t_S$ . Then the 24 elements of the matrix product may be pre-computed and stored in the memory of the on-board computer.

The intervals between times of position measurement need not be equally spaced. Occasionally improved position accuracy can be achieved by taking advantage of a favorable configuration of the planets at a particular time. For example, it is deemed inadvisable to sight on a planet

whose line of sight makes an angle of less than  $15^\circ$  with the line of sight to the sun. If a planet relatively close to the vehicle lies near the vehicle-sun line at a weekly measurement time, the measurement time is changed so that the planet's proximity can be exploited in improving the accuracy of vehicle position determination.

In the analysis of Chapter 5 only celestial bodies of first magnitude or brighter are considered for the optical sightings. Because the number of such bodies is quite limited, the possibility of ambiguities (i.e., of measuring the angle between an incorrect pair of celestial bodies) is remote. Nevertheless, this possibility should be kept in mind when the angular sightings are being selected.

Another consideration in selecting the sightings is the magnitude of the angle being measured. From practical considerations in the design of the on-board sextants, it is not possible to measure space angles in the vicinity of  $180^\circ$ . A practical limit of  $120^\circ$  in the angle to be measured is felt to be reasonable; this constraint is to be taken into consideration in utilizing the graphical method of selecting the measurements.

After the computation of clock error and position variation is completed at a measurement time, the clock is corrected, and a revised maximum likelihood estimate of  $\delta \underline{x}_D$  is determined from Equation (5-37). The determination of the revised  $\delta \hat{\underline{x}}_D$  is the most complicated operation required of the on-board computer, because, each time it is performed, a new matrix of the form  $(\hat{Q} \hat{U}^{-1} \hat{Q}^T)$  must be inverted. The inversion cannot be carried out before the flight due to the fact that the uncertainty matrix  $\hat{U}$  in (5-37) depends on the actual measured values of the angles.

After the first correction has been applied, there is no further need for determining  $t_{C_{opt}}$ , because it will have occurred prior to the time of the most recent set of measurements. The time at which any required additional correction is applied is discussed in the next section. Each correction vector  $\underline{c}_V$  is computed analytically from the matrix forms of Chapter 3.

## 6.8 Strategy for Determining Whether to Make a Correction

After the first correction has been made, the necessity for making additional corrections is determined by the predicted miss distance at

the destination. The specification for the mission defines a permissible miss distance. If the predicted miss distance is computed to be well within the permissible value, it is obviously unnecessary to make any additional corrections.

In order to give these statements quantitative significance, the miss distance will be re-defined, and the concept of circular probable error will be introduced. As indicated in Section 2.14, the miss distance vector  $\delta \underline{\rho}$  is that component of the position variation  $\delta \underline{r}_D$  which lies in the plane normal to the relative velocity vector  $\underline{v}_R$ . The estimated miss distance vector,  $\delta \hat{\underline{\rho}}$ , can be computed by transforming the maximum likelihood estimate  $\delta \hat{\underline{x}}_D$  into the critical-plane coordinate system. The first two elements of the transformed vector are the components of the two-dimensional vector  $\delta \hat{\underline{\rho}}$ . The transformation is accomplished mathematically by modifying the equations of Section 5.4 as follows:

$$\delta \underline{m} = \underline{Q}^{*T} \underline{Y}_D^{*T} (\delta \underline{x}_D)_W \quad (6-1)$$

where

$$\underline{Y}_D^* = \begin{Bmatrix} \underline{X}_D^* & \underline{O}_3^* \\ \underline{O}_3^* & \underline{X}_D^* \end{Bmatrix} \quad (6-2)$$

and  $\underline{X}^*$  is the standard transformation matrix for transforming a three-dimensional vector into the critical-plane coordinate system.

$$(\delta \hat{\underline{x}}_D)_W = (\underline{Y}_D^* \underline{Q}^* \underline{U}^{*-1} \underline{Q}^{*T} \underline{Y}_D^{*T})^{-1} \underline{Y}_D^* \underline{Q}^* \underline{U}^{*-1} \delta \underline{\tilde{m}} \quad (6-3)$$

$$(\underline{\tilde{E}}_D^*)_W = \overline{(\underline{\epsilon}_D)_W (\underline{\epsilon}_D^T)_W} = (\underline{Y}_D^* \underline{Q}^* \underline{U}^{*-1} \underline{Q}^{*T} \underline{Y}_D^{*T})^{-1} \quad (6-4)$$

The first two elements of the first two rows of  $(\underline{\tilde{E}}_D^*)_W$  constitute the 2-by-2 covariance matrix of the uncertainty in  $\delta \hat{\underline{\rho}}$ . This matrix is designated  $\underline{\tilde{E}}_\rho^*$ . The equi-probability ellipse associated with the uncertainty in  $\delta \hat{\underline{\rho}}$  has the form

$$\left\{ \begin{matrix} \epsilon_{D\xi} & \epsilon_{D\eta} \end{matrix} \right\} \bar{E}_{\rho}^{*-1} \left\{ \begin{matrix} \epsilon_{D\xi} \\ \epsilon_{D\eta} \end{matrix} \right\} = k^2 \quad (6-5)$$

where  $\epsilon_{D\xi}$  and  $\epsilon_{D\eta}$  are the first two components of the uncertainty vector  $(\underline{\epsilon}_D)_W$ . If  $k = 1.1774$ , the probability that the uncertainty vector of  $\delta \hat{\rho}$  lies within the boundaries of the ellipse is 0.5. When the measurements are properly chosen, the axes of the ellipse are approximately equal in length, so that the ellipse closely resembles a circle. The radius of the circle whose area is the same as that of the ellipse is known as the "circular probable error" (CPE). The CPE is a convenient measure of the accuracy of the prediction of the miss distance. The equation relating CPE to the determinant of  $\bar{E}_{\rho}^*$  is

$$\text{CPE} = 1.1774 \left| \bar{E}_{\rho}^* \right|^{1/4} \quad (6-6)$$

Appendix P contains a more detailed treatment of CPE.

Every time a measurement is made, the CPE is reduced slightly. Every time a velocity correction is applied, the CPE is increased due to the uncertainty  $\eta$  associated with the correction.

Before a correction is applied, the predicted miss distance is  $\delta \hat{\rho}^-$ , and the circular probable error is  $(\text{CPE})^-$ . Immediately after application of a VTA correction, the predicted miss distance  $\delta \hat{\rho}^+$  is zero, and the circular probable error  $(\text{CPE})^+$  is greater than  $(\text{CPE})^-$ .

If the sum of the magnitude of  $\delta \hat{\rho}^-$  and  $(\text{CPE})^-$  is smaller than the required position accuracy at the destination, no further correction is necessary.

If the sum of the magnitude of  $\delta \hat{\rho}^-$  and  $(\text{CPE})^-$  exceeds the required position accuracy, an additional correction should be made. The time of additional correction is determined by the computed value of  $(\text{CPE})^+$ . As the vehicle gets closer to the destination, the magnitude of  $(\text{CPE})^+$  gets smaller, but the magnitude of the required correction gets larger. Therefore, the correction is made at the earliest time at which  $(\text{CPE})^+$  falls within the specification for position accuracy at the destination.

With the high accuracy obtained from the Earth-based tracking system for the first correction and with a reasonably accurate midcourse thrust application, it is felt that three midcourse corrections, and possibly only two, are sufficient to meet the requirements of a typical manned interplanetary mission.

### 6.9 Other Applications

The theory developed in the preceding chapters has several applications in addition to those already illustrated by the proposed guidance system for the manned interplanetary mission. The additional applications include the following:

1. Direct calculation of the midcourse velocity correction by crew members on an interplanetary mission.
2. Calculation of abort guidance requirements by crew members on an interplanetary mission.
3. Systematic study of the effect of parameters associated with the reference trajectory on midcourse guidance requirements for an interplanetary mission.

Equation (3-133), the analytic expression for the elements of the correction matrix  $\overset{*}{K}_{CD}$ , is sufficiently simple that a hand calculation of the velocity correction is feasible when the correction time  $t_C$  is specified and the on-board digital computer has provided an estimate of  $\delta \underline{r}_D$ . Such a calculation serves as a check of the on-board digital computer. On a mission of many months' duration the psychological value of the calculation in providing a useful outlet for the energies of the flight crew may be significant.

Hand calculations for abort guidance are also feasible. If the mission has to be aborted while the vehicle is outbound from Earth and if the on-board computer is incapacitated, it is possible that sufficient tabular data can be supplied to the flight crew so that measurements of angular deviations relative to a special abort reference trajectory can be processed by hand calculation to determine the required velocity corrections.

The use of the analytic forms of the guidance matrices to make a parametric study of reference trajectories is an extension of the type of

analysis presented in Chapter 4, in which only one reference trajectory was studied. There are relatively few parameters involved, and the range of some of these is quite limited for a specified type of mission. Consequently, the amount of computation required falls within reasonable bounds.

#### 6.10 Concluding Remarks

The fundamental difference between the midcourse guidance system proposed in this chapter and those that have been previously suggested is that the correction times in the proposed system are not pre-programmed, but rather are determined as a function of the variations measured during the flight. This degree of flexibility is made practical by the development of the analytic form of the correction matrix  $K_{CD}^*$ . With this development the velocity correction vector at any correction time  $t_C$  can be readily determined by an on-board digital computer of modest capacity.

The flexibility in the selection of time of correction is combined with the empirical method developed for determining the optimum time of correction to ensure that the first midcourse correction, which is much larger than any succeeding correction, is made at the time when its magnitude is minimized. The times of the remaining corrections are adjusted to achieve the best compromise between magnitude of the correction and position accuracy at the destination.

The proposed system also differs from previous systems in that it accounts for clock errors and at the same time utilizes all the measurement data in predicting the vehicle's state at the nominal time of arrival at the destination.

Finally, the uncoupling between in-plane and out-of-plane motion is exploited to provide a method of selecting those optical sightings which provide the most accurate estimate of present position. The method is graphical; no elaborate computer program is required.

## CHAPTER 7

### CONCLUSIONS AND RECOMMENDATIONS

#### 7.1 Summary

The subject matter of the thesis is briefly reviewed. The features of the analysis that are felt to be original are listed. Those areas in which further study appears desirable are indicated.

#### 7.2 Résumé of Guidance Theory

The problem of midcourse guidance of an interplanetary vehicle has been linearized by assuming that the vehicle's actual trajectory experiences only small departures from a known pre-computed reference trajectory. Matrix forms have been used to obtain a compact set of guidance equations for the vehicle's motion in an n-body gravitational field.

The difference between the actual trajectory and the reference trajectory is expressed mathematically as a six-component vector consisting of the three components of position variation and the three components of velocity variation at some specified time. This vector is known as the state vector. The most useful state vector for guidance analysis is the one for which the specified time is the nominal time of arrival at the destination.

The state vector at one time is related to the state vector at some other time by means of a 6-by-6 matrix known as the transition matrix.

If the time of arrival is fixed, the midcourse velocity correction required at some time  $t_C$  is a function of the predicted position variation at the destination. The negative of the 3-by-3 matrix relating the velocity correction vector to the position variation vector is called the correction matrix.

When the time of arrival is not critical and small variations in arrival time are permissible, the velocity correction of minimum magnitude at time  $t_C$  is a function of that component of the position variation at the destination which lies in the plane perpendicular to the relative velocity



of the vehicle with respect to the destination planet. This component of position variation is the miss distance. For this type of velocity correction the form of the guidance equations can be simplified by introducing the rotating coordinate system known as the critical-plane coordinate system; in this system both the velocity correction vector and the miss distance vector are two-dimensional vectors.

The magnitude of the velocity correction is a function of the time at which the correction is applied. For the case of variable arrival time, the correction time for which the magnitude of the correction is a minimum is determined empirically as a function of the angular orientation of the miss distance vector in the plane perpendicular to the relative velocity vector.

For the n-body problem the elements of the transition matrix are computed by numerical integration. The correction matrix is the inverse of one of the four 3-by-3 sub-matrices constituting the transition matrix.

For the midcourse phase of an interplanetary journey, when the vehicle is outside the sphere of perturbative relevance of any planet, the n-body problem can be reduced to a two-body problem without any significant loss of accuracy. The reference trajectory is then a conic section. The plane containing the reference trajectory is the reference trajectory plane. The actual trajectory is also a conic section; its plane normally differs slightly from the reference trajectory plane.

The two-body assumption simplifies the equations of motion of the vehicle. The variant motion in the plane of the reference trajectory is uncoupled from the variant motion normal to the reference trajectory plane. By proper choice of a coordinate system the sixth-order system is sub-divided into two independent systems, one of fourth order and the other of second order. These two systems have been integrated analytically for the case when the conic section is an ellipse.

The same analytic solution is also obtained in a different manner, namely by applying the techniques of the calculus of variations to a set of six orbital elements which define the reference trajectory.

The analytic solution is used to obtain analytic expressions for all the elements of the transition matrix, the correction matrix, and several other matrices that are useful in the development of guidance theory.

There are three types of combinations of the correction time  $t_C$  and the arrival time  $t_D$  in which the matrix that must be inverted in order to evaluate the correction matrix becomes singular. When any of these singularity conditions occurs, the correction matrix is indeterminate, and no finite velocity correction can be computed by means of fixed-time-of-arrival guidance. If variable-time-of-arrival guidance is used, the effects of two of the singularity types are obliterated, and finite velocity corrections can be computed even when the conditions for these singularity types occur.

### 7.3 Résumé of Navigation Theory

As used in this thesis, the term navigation refers to the obtaining and processing of measurements made during the space voyage in order to compute the predicted state vector at the nominal time of arrival at the destination. This predicted state vector is the one utilized in the guidance theory to determine when and how to make a midcourse velocity correction.

Two types of navigation systems are described, the Earth-based radio-command system and the self-contained optical system. A linear theory is developed to process the measurements made in either system. Since redundant measurements are made, the method of maximum likelihood is used to estimate the predicted state vector at the destination.

The Earth-based system uses radio antennas to track the vehicle. Large amounts of data are processed by a centrally located digital computer facility. The system is most effective when the vehicle is relatively close to Earth.

The self-contained system utilizes two telescopes to measure the angles between lines of sight to pairs of celestial bodies. Relatively few measurements are made and are processed by the computer on board the space craft.

Clock error is a negligible factor in the Earth-based system. However, it can be significant in the self-contained system. To account for clock error and to correct for it, the self-contained system's computation is a two-step process. First, a group of measurements is made at a single

nominal measurement time. From this information estimates are made of the position variation at the nominal measurement time and of the clock error. The clock is corrected immediately. The process is repeated at other measurement times, and from the group of estimates of position variation, an estimate is made of the state vector at the time of arrival at the destination.

A graphical procedure, based on the lack of coupling between in-plane and out-of-plane variant motion, is developed for selecting those optical sightings which give the greatest accuracy of position determination at a given measurement time.

A set of pseudo-measurements, consisting of the components of the state vector at launch or immediately following a midcourse correction, is used to improve the accuracy of the predicted state vector at the time of arrival.

#### 7.4 Novel Features of the Analysis

It is the author's conviction that, in an analytic study of the type that has been presented, he is under some obligation to indicate clearly those results which he considers original. This is a risky undertaking, particularly in a field in which so many investigations are currently being carried on. It is therefore with considerable trepidation that the list appearing below has been prepared. The following features of the analysis are thought to be novel:

1. The relatively simple and straightforward analytic solution of the variant equations of motion by two different methods for the case of an elliptical reference trajectory.
2. The exploitation of the analytic solution to obtain closed-form expressions for the elements of the fundamental guidance matrices.
3. The discovery of the type of singularity called the  $X = 0$  singularity in Chapter 3, and the relation between singularities of the  $X = 0$  type and the minima of the time-of-flight curves obtained from Lambert's theorem.

4. The utilization of the critical-plane coordinate system in clarifying the equations of variable-time-of-arrival guidance, and the proof that in this coordinate system one of the four elements of the matrix relating the velocity correction vector to the miss distance vector is identically zero if the reference trajectory is a two-body trajectory.

5. The deterministic method of finding the optimum time to apply a variable-time-of-arrival velocity correction.

6. The proof that two of the three types of singularities that characterize fixed-time-of-arrival guidance are effectively removed when variable-time-of-arrival guidance is used.

7. The selection of "in-plane" and "out-of-plane" stars for use in position determination from optical sightings, and the graphical method of determining a combination of sightings that yields high position accuracy.

8. The physical explanation of the effect of clock error on navigational accuracy, including an explanation of why clock errors cannot be filtered if individual measurements are made at widely separated time intervals.

#### 7.5 The Analytic Approach

Most of the features mentioned in the last section are either manifestations of or consequences of the analytic approach to guidance theory. If they are novel, it is only because this approach has never before been intensively investigated.

The approach has yielded results that are valuable both academically and practically. From the academic viewpoint it has led to a deeper insight into the physical characteristics of elliptical motion. From the practical viewpoint it materially reduces the amount of computation required for guidance studies and applications, and the results obtained are more accurate because the round-off error is negligible.

If the author is permitted the liberty of expressing an opinion that may be controversial, he would like to suggest that the reason why the

analytic approach has not been more actively pursued is closely associated with the present availability of high-speed digital computers. It is difficult for a human being to generate the motivation for obtaining an analytic solution involving weeks, or even months, of algebraic drudgery when the computer offers the tantalizing prospect of providing any desired amount of numerical data with a relatively insignificant amount of human effort. It is felt that in the present case, at least, the drudgery has proved to be justified.

#### 7.6 Recommendations for Further Study

The following topics, related to the subject matter of this thesis, are suggested as possibly fruitful subjects of future investigations:

1. Analytic solution of the variant equations of motion for hyperbolic reference trajectories.
2. Empirical approach to the problem of finding closed-form expressions for the elements of the guidance matrices when the reference trajectory is a three-body trajectory.
3. Further investigation of the critical-plane coordinate system for use in variable-time-of-arrival guidance.
4. Parametric study of reference trajectories for specific types of missions.

The analytic solution for hyperbolic reference trajectories is based on the same approach as that presented in Chapter 3 for elliptical reference trajectories. The solution will be used for obtaining a new set of closed-form expressions for the elements of the guidance matrices.

When a closed-form solution is available for hyperbolic as well as elliptical reference trajectories, there is a distinct possibility that the two solutions can be combined and properly weighted, so that an empirical closed-form solution of the guidance equations can be obtained for an interplanetary vehicle when it is within the sphere of perturbative relevance of the destination planet. If such a solution is achieved, the destination point of the midcourse guidance system can be moved up to the point of closest approach to the planet, and the midcourse and terminal guidance systems can effectively be merged.

It is felt by the author that more can be learned about variable-time-of-arrival guidance by investigation of the variation in orientation of the noncritical vector  $\underline{w}$  as a function of the time of correction. A physical explanation should be sought for the fact that one of the four elements relating the velocity correction to the miss distance vector in the critical-plane coordinate system is identically zero.

The analytic solution for elliptical reference trajectories reduces the parameters affecting the guidance equations to a relatively small number. It should be a relatively simple matter to make a systematic numerical study of the effect of variations in these parameters on guidance requirements and thus to determine which reference trajectories are, from a guidance viewpoint, most desirable for a specified mission.

## REFERENCES

1. Battin, R.H., "The Determination of Round-Trip Planetary Reconnaissance Trajectories," *Journal of the Aero/Space Sciences*, Sept. 1959, pp. 545 - 567.
2. Laning, J.H., Jr., Frey, E.J., and Trageser, M.B., "Preliminary Considerations on the Instrumentation of a Photographic Reconnaissance of Mars," Vistas in Astronautics, Vol. II, Pergamon Press, New York, 1959, pp. 63 - 94.
3. Battin, R.H. and Laning, J.H., Jr., "A Navigation Theory for Round-Trip Reconnaissance Missions to Venus and Mars," Planetary and Space Science, Vol. 7, Pergamon Press, Inc., New York, 1961, pp. 40 - 56.
4. Battin, R.H., "A Comparison of Fixed and Variable Time of Arrival Navigation for Interplanetary Flight," Ballistic Missile and Space Technology, Vol. III, Academic Press, New York, 1960, pp. 3 - 31.
5. "A Recoverable Interplanetary Space Probe," M.I.T. Instrumentation Laboratory Report R-235, prepared by M.I.T. Instrumentation Laboratory in collaboration with AVCO Corporation, M.I.T. Lincoln Laboratory, and Reaction Motors Division of Thiokol Chemical Corporation, July 1959.
6. Battin, R.H., "Lecture Notes on Computational Procedures for the Navigational Fix," (unpublished), March 1961.
7. Battin, R.H., "Lecture Notes on Optimum Operations with Celestial Fix Data," (unpublished), March 1961.
8. Battin, R.H., "A Statistical Optimizing Navigation Procedure for Space Flight," ARS Journal, Vol. 32 No. 11, Nov. 1962, pp. 1681 - 1696.
9. Noton, A.R.M., "Interplanetary Post-Injection Guidance," JPL External Publication No. 653, June 1959.
10. Noton, A.R.M., Cutting, E., and Barnes, F.L., "Analysis of Radio-Command Mid-Course Guidance," JPL Technical Report No. 32 - 28, Sept. 1960.

## REFERENCES (Cont.)

11. Gates, C.R., Scull, J.R., and Watkins, K.S., "Space Guidance," *Astronautics*, Vol. 6 No. 11, Nov. 1961, pp. 24 - 27, 64 - 72.
12. Smith, G.L., Schmidt, S.F., and McGee, L.A., "Application of Statistical Filter Theory to the Optimal Estimation of Position and Velocity on board a Circumlunar Vehicle," NASA Tech. Rept. R-135, 1962.
13. McLean, J.D., Schmidt, S.F., and McGee, L.A., "Optimal Filtering and Linear Prediction Applied to a Midcourse Navigation System for the Circumlunar Mission," NASA Tech. Note D-1208, 1962.
14. Porter, J.G., "Navigation without Gravity," *Journal of the British Interplanetary Society*, Vol. 13 No. 2, March 1954, pp. 68 - 74.
15. Lawden, D.F., "Correction of Interplanetary Orbits," *Journal of the British Interplanetary Society*, Vol. 13 No. 4, July 1954, pp. 215 - 223.
16. Baker, R.M.L., Jr., "Note on Interplanetary Navigation," *Jet Propulsion*, Vol. 28, December 1958, pp. 834 - 835.
17. Wheelon, A.D., "Midcourse and Terminal Guidance," Chapter 26 of Space Technology, H.S. Seifert editor, John Wiley and Sons, Inc. N.Y., 1959.
18. Magness, T.A., McGuire, J.B., and Smith, O.K., "Accuracy Requirements for Interplanetary Ballistic Trajectories," Proceedings of Ninth International Astronautical Congress, Amsterdam 1958, Vol. I, Springer-Verlag, Vienna, 1959, pp. 286 - 306.
19. Gunkel, R.J., Lascody, D.N., and Merrilees, D.S., "Impulsive Midcourse Correction of an Interplanetary Transfer," Proceedings of Tenth International Astronautical Congress, London 1959, Vol. II, Springer-Verlag, Vienna, 1960, pp. 650 - 670.
20. Kierstead, F.H., Jr., "Guidance Requirements for Interplanetary Flight," Advances in the Astronautical Sciences, Vol. 5, Plenum Press, Inc., N.Y., 1960, pp. 66 - 81.



## REFERENCES (Cont.)

21. Kierstead, F.H., Jr., "Midcourse Guidance Requirements for Mars and Venus Probes," ARS Preprint 914 - 59, Nov. 1959.
22. Breakwell, J.V., "Fuel Requirements for Crude Interplanetary Guidance," Advances in the Astronautical Sciences, Vol. 5, Plenum Press, Inc., N.Y., 1960, pp. 53 - 65.
23. Breakwell, J.V., "The Spacing of Corrective Thrusts in Interplanetary Navigation," Advances in the Astronautical Sciences, Vol. 7, Plenum Press, Inc., N.Y., 1961, pp. 219 - 235.
24. Bock, C.D. and Mundo, C.J., "Guidance Techniques for Interplanetary Travel," ARS Journal, Vol. 29 No. 12, Dec. 1959, pp. 931 - 940.
25. Safren, H.G., "Differential Correction Method of Interplanetary Navigation," Proceedings of the National Specialists Meeting on Guidance of Aerospace Vehicles, published by IAS, N.Y., 1960, pp. 184 - 190.
26. Haake, H.B. and Welch, J.D., "A Self-Contained Interplanetary Navigator," IRE Transactions on Aerospace and Navigational Electronics, Vol. ANE-8 No. 1, March 1961, pp. 28 - 41.
27. Dunn, J.C. and Giannetto, C., "Lunar Trajectory Perturbations Analysis - Some Computational Results via the Adjoint Method," ARS Preprint 2072 - 61, Oct. 1961.
28. Smart, W.M., Celestial Mechanics, Longmans, Green and Co. Inc., New York, 1953.
29. Plummer, H.C., An Introductory Treatise on Dynamical Astronomy, Dover Publications, Inc., New York, 1960. (Originally published by Cambridge University Press, 1918).
30. Ehricke, K.A., Space Flight, Volume I, Environment and Celestial Mechanics, D. Van Nostrand Company, Inc., Princeton, N.J., 1960.

## REFERENCES (Cont.)

31. Ehricke, K. A., Space Flight, Volume II, Dynamics, D. Van Nostrand Company, Inc., Princeton, N.J., 1962.
32. Mauldin, M., Jr. and Millard, R. G., "Optimization of Interplanetary Mid-Course Velocity Corrections," M.I.T. Master of Science Thesis T-299, May 1962.
33. Carr, R. E. and Hudson, R. H., "Tracking and Orbit Determination Program of the Jet Propulsion Laboratory," JPL Technical Report No. 32-7, Feb. 1960.
34. Zim, H. S. and Baker, R. H., Stars, Golden Press, Inc., New York, 1956.
35. Baker, R. H., Astronomy, Seventh Edition, D. Van Nostrand Company, Inc., Princeton, N.J., 1959.
36. The American Ephemeris and Nautical Almanac for the Year 1962, U.S. Government Printing Office, Washington, 1960.
37. Larmore, L., "Celestial Observations for Space Navigation," Aero/Space Engineering, Vol. 18 No. 1, Jan. 1959, pp. 37 - 42.
38. Victor, W. K., Stevens, R., and Golomb, S. W., "Radar Exploration of Venus: Goldstone Observatory Report for March - May 1961," JPL Technical Report No. 32 - 132, Aug. 1961.
39. Corben, H. C., "Time Dilatation Effects in Space Travel," Chapter 11 of Space Technology, H. S. Seifert editor, John Wiley and Sons, Inc., N. Y., 1959.
40. Holdridge, D. B., "Space Trajectories Program for the IBM 7090 Computer," JPL Technical Report No. 32 - 223, Revision No. 1, Sept. 1962.
41. Hildebrand, F. B., Advanced Calculus for Engineers, Prentice-Hall, Inc., Englewood Cliffs, N.J., 1949
42. Weyl, H., The Classical Groups, Their Invariants and Representations, Princeton University Press, Princeton, N.J., 1946.

## REFERENCES (Cont.)

43. Shapiro, I.I., The Prediction of Ballistic Missile Trajectories from Radar Observations, McGraw-Hill Book Company, Inc., N.Y., 1957.
44. Cramér, H., Mathematical Methods of Statistics, Princeton University Press, N.J., 1946.
45. Burington, R.S. and May, D.C., Handbook of Probability and Statistics with Tables, Handbook Publishers, Inc., Sandusky, Ohio, 1953.
46. Locke, A.S. and collaborators from the Naval Research Laboratory, Guidance, D. Van Nostrand Company, Inc., Princeton, N.J., 1955.

## BIOGRAPHICAL SKETCH

Robert Gottlieb Stern was born in New York, N. Y. on June 11, 1920. He was raised in Bethlehem, Pa. and graduated from Bethlehem High School in 1936. He was awarded a scholarship to Lehigh University and in 1941 received the degree of Bachelor of Science in Engineering Physics.

After a short period of employment at Bethlehem Steel Corporation, Mr. Stern became a junior engineer at the Airplane Division of Curtiss-Wright Corporation in 1942. He spent a year in wind tunnel testing, a second year in flight testing, and then two years in the Stability and Control Analysis section of the Aerodynamics department. Late in 1945 he became project aerodynamicist on the XF15C-1, an experimental Navy carrier-based fighter aircraft which at the time was being wind tunnel tested and flight tested.

In the fall of 1946 Mr. Stern was transferred to the Propeller Division of Curtiss-Wright in order to participate in the design of an electronic flight simulator for the Boeing B-377 Stratocruiser. He carried out the aerodynamic and power plant analysis for the simulator and also designed the electro-mechanical analog computer system.

When the simulator activity achieved division status as the Curtiss-Wright Electronics Division in 1951, Mr. Stern was named head of the Aerodynamics Department. In this capacity he was responsible for the aerodynamic simulation of such aircraft as the Boeing B-50 and B-52, Convair CV-340 and B-36, Douglas DC-7 and C-124, Fairchild C-119, Lockheed Constellation and C-130, and McDonnell F2H-1. For his work on the design of analog computer systems for flight simulators he has been awarded seventeen patents, some in collaboration with other members of the Curtiss-Wright staff.

While working on flight simulators in northern New Jersey, Mr. Stern continued his technical education by attending night classes at engineering schools in the area. In 1950 he received the degree of Master of Science in Mathematics and Physics from Stevens Institute of Technology.

In 1956 he left Curtiss-Wright to become a full-time graduate student at M.I.T. For the academic year 1957 - 1958 he held a Sperry Gyroscope Company fellowship at M.I.T. For the academic years since 1958 he has been a research assistant at the M.I.T. Instrumentation Laboratory.

During the summer of 1957 Mr. Stern returned to Curtiss-Wright as a research specialist. He was employed in a similar capacity by the Autonetics Division of North American Aviation, Inc. during the summer of 1959. He has also served briefly as a consultant to Curtiss-Wright in a patent infringement lawsuit involving flight simulator patents.

Mr. Stern is a member of Tau Beta Pi, Sigma Xi, Sigma Gamma Tau, and Phi Eta Sigma. His professional affiliations include the American Association for the Advancement of Science, the American Institute of Aeronautics and Astronautics, and the Institute of Electrical and Electronic Engineers.